CORA Cork Open Research Archive
Cartlann Taighde Oscailte Chorcaí

Title	Investigation of micro-devices for neurobiological applications
Authors	Grygoryev, Konstantin
Publication date	2013
Original Citation	Grygoryev, K. 2013. Investigation of micro-devices for neurobiological applications. PhD Thesis, University College Cork.
Type of publication	Doctoral thesis
Rights	© 2013, Konstantin Grygoryev - http://creativecommons.org/licenses/by-nc-nd/3.0/
Download date	2026-11-02 08:07:40
Item downloaded from	https://hdl.handle.net/10468/1249



UCC
University College Cork, Ireland
Coláiste na hOllscoile Corcaigh

Department of Anatomy



ucc
Coláiste na hOllscoile Corcaigh, Éire
University College Cork, Ireland

Life Science Interface



Investigation of micro-devices for neurobiological applications

Konstantin Grygoryev
B.Sc.

A Thesis Submitted for the Degree of Doctor of Philosophy of the National University of Ireland

Research supervisors: Dr. Kieran McDermott, Dr. Grégoire Herzog, Dr. Paul Galvin, Dr. Damien Arrigan

July 2013

DECLARATION

The author hereby declares that, except where duly acknowledged, this thesis is entirely his own work and has not been submitted for any degree in the National University of Ireland, or in any other University.

Table of contents

Table of contents ii

Abstract 1

1.0 Introduction 3

1.1 HISTORICAL OVERVIEW 3
1.2 PATTERNED CELL GROWTH 7
1.2.1 Surface modification techniques 8
1.2.2 Surface chemistry density and topography 8
1.2.3 Laser ablation and selective silane removal (SSR) 9
1.2.4 Micro-moulding in capillaries (MIMIC) 11
1.2.5 Ink-jet printing 11
1.2.6 Substrate silanization and micro-contact printing 12
1.3 ELECTROPHYSIOLOGY 14
1.3.1 The action potentials 14
1.3.2 Voltage clamp 15
1.3.3 Patch clamp 17
1.3.4 Microelectrode arrays, their development and uses 21
1.3.5 MEA patterning and electrophysiology 23
1.4 MICROFLUIDICS 24
1.4.1 Microfluidic devices 26
1.4.2 µF device perfusion techniques 28
1.4.3 Application of microfluidics to neuronal cell culture 32
1.4.4 µF devices and MEAs 34
1.5 PLANNED NEURO TEST PLATFORM ARCHITECTURE 34
1.5.1 Proposed method of MEA patterning 35
1.5.2 The originality of proposed research 36

2.0 General experimental methods 39

2.1 MATERIALS & CHEMICAL REAGENTS 39
2.2 THE ASSEMBLY AND INTEGRATION 40
2.2.1 Threaded polystyrene and glass culture chambers 40
2.2.2 Modification of screw-on lids 41
2.2.3 Machined PMMA/Nylon culture chambers 41
2.2.4 PMMA media reservoirs 42
2.3 SILICON MASTER FABRICATION AND PDMS CASTING 43
2.3.1 Design of micro-stamps and microfluidic devices 43
2.3.2 Silicon master fabrication and specifications 46
2.3.3 Coating masters with release agents 46
2.3.4 PDMS micro-stamp fabrication 47
2.3.5 Fabrication of thin PDMS stamps 47
2.3.6 Master post treatment 49
2.4 FABRICATION AND ASSEMBLY OF MICROFLUIDIC DEVICES 49
2.4.1 The replica molding of µF device 49
2.4.2 Flat top µF devices 50
2.4.3 Fabrication of µF devices from µCP silicon masters 51
2.4.4 Aligning µF devices to the substrates 53
2.4.5 Methods of bonding the µF device to the surface 55
2.5 GRAVITY DRIVEN PASSIVE PERFUSION DEVICE 56
2.6 PASSIVE, VACUUM DRIVEN FILLING OF THE µF CHANNELS 58
2.7 CELL CULTURE PROTOCOLS 58
2.7.1 Culturing of rat embryo cortical and spinal cord neurons 58
2.7.2 Culturing protocol modification 60

2.8 ELECTROPHYSIOLOGY 61
2.9 MEA SURFACE CLEANING 62
2.9.1 Post tissue culture clean 62
2.9.2 Removing PDMS residue from MEA surface 62
2.9.3 Removing silica (SiO_2) from MEA surface 62
2.9.4 Updated and simplified MEA cleaning protocol 63
2.10 IMAGING 63
2.10.1 Image acquisition 63
2.10.2 Image processing 64

3.0 Micro-contact printing and microfluidic devices 67

3.1 MATERIALS AND METHODS 68
3.1.1 Chemical reagents 68
3.1.2 Silicon masters 69
3.1.3 Surface chemistry modifications 69
3.1.4 Micro-printing techniques 69
3.1.5 Surface patterning using µF devises 73
3.1.6 µF gradients 73
3.1.7 Gravity driven passive perfusion 76
3.1.8 Surface tension driven perfusion 76
3.2 RESULTS 77
3.2.1 µCP patterns generated using the drill stand. 77
3.2.2 µCP patterns generated using the flip-chip bonder 78
3.2.3 Defects and inconsistency of µCP 85
3.2.4 Effects of soak on quality of printed pattern 87
3.2.5 Observed surface contamination with PDMS 90
3.2.6 Patterning substrates using microfluidics 91
3.2.7 Microfluidic gradients 94
3.3 DISCUSSION 101
3.3.1 Fabrication of µCP stamps 101
3.3.2 Generation of good quality µCP patterns 101
3.3.3 Surface patterning using µF devices 102
3.3.4 Microfluidic perfusion and gradients 103
3.4 CONCLUSION 104

4.0 Electrophysiology and patterned neuronal networks 108

4.1 MATERIALS AND METHODS 110
4.1.1 Chemical reagents and equipment 110
4.1.2 Fabrication of micro-electrode arrays 111
4.1.3 Surface pre-treatment and chemical modification 113
4.1.4 MEA surface coating 114
4.1.5 Substrate patterning 115
4.1.6 Substrate silanization 115
4.1.7 Neuronal culture and electrophysiology 116
4.2 RESULTS 117
4.2.1 Neuronal culture optimization and patterning 117
4.2.2 Electrochemical impedance spectroscopy 124
4.2.3 Electrophysiology of un-patterned neurons 128
4.3 DISCUSSION 133
4.3.1 Neuronal patterning 133
4.3.2 Substrate recycling 134
4.3.3 Practical issues 135
4.3.4 Neuronal electrophysiology and electrode characterization 136
4.4 CONCLUSION 137

5.0 Integration of MEA with neuronal patterning and microfluidics 140

5.1 MATERIALS AND METHODS 142
5.1.1 Materials 142
5.1.2 Substrates and cell types 142
5.1.3 Microfluidic assembly 143
5.1.4 Fabrication of the reservoir plates 144
5.1.5 Surface modification for cell adhesion 145
5.1.6 Cell culture 146
5.1.7 Electroporation using MEAs 147
5.1.8 Biocompatibility testing 148
5.2 RESULTS 150
5.2.1 Biocompatibility trends of integrated MEAs 150
5.2.2 Biocompatibility test 151
5.2.3 Electroporation and cell staining 152
5.2.4 Neurons cultured inside microfluidic device 156
5.2.5 Aggregate migration 160
5.2.6 Controlled distribution of cells in µF channels 161
5.2.7 The neurobiological test platform 163
5.3 DISCUSSION 164
5.3.1 Biocompatibility and device recycling 164
5.3.2 Neuronal electrophysiology and electroporation 165
5.3.3 Integration of the µF device 166
5.3.4 Cell cultures using µF devices 167
5.3.5 Control of cell distribution with dynamic µF gradients 167
5.3.6 Integrated platform for neurobiological applications 168
5.4 CONCLUSION 169

6.0 Conclusion 171

6.1 SURFACE PATTERNING 171
6.2 INTEGRATION OF MICROFLUIDICS 173
6.3 PDMS ALTERNATIVES 174
6.4 PRIMARY NEURONAL CELL CULTURES 174
6.5 BIOCOMPATIBILITY AND INTEGRATION 175
6.6 CULTURING PATTERNED NEURONS IN THE NEURO TEST PLATFORM 176
6.7 FUTURE WORK 177

7.0 Acknowledgements 179

8.0 References 180

List of Abbreviations

AP - Action Potential

APTES - (3-Aminopropyl) triethoxysilane

APTMS - (3-aminopropyl) trimethoxysilane

CSPG - Chondroitin sulphate proteoglycan

C4S - Chondroitin 4 sulphate

DCE - Dichloroethane

DI - Deionized (water)

DMEM - Dulbecco's Modified Eagles Medium

DMF - Dimethylformamide

ECS - Extra cellular space

EtOH - Ethanol

EIS - Electrical impedance spectroscopy

FBS - Fetal Bovine Serum

FCS - Fetal Calf Serum

FITC - Fluorescein isothiocyanate

HBSS - Hanks Balances Salt Solution

MEA - Micro-electrode array

MeOH - Methanol

MEMS – Micro-electro mechanical systems

µF - Micro-fluidic (device/channel/gradient)

µCP - Micro-contact printing

PBS - Phosphate buffered saline

PDL - Poly-D-Lysine

PDMS - Polydimethylsiloxane

PDITC - p-Phenylene diisothiocyanate

PLL - Poly-L-Lysine

PMMA - Poly(methyl methacrylate)

RGD - Arginine-Glycine-Aspartic acid

SAM – Self assembled monolayer

S/N - Signal to noise ratio

TBAF - Tetra-n-butylammonium fluoride

TFOCS - Tridecafluoro-1,1,2,2-tetrahydrooctyl-1-trichlorosilane

Abstract

The aim of this project is to integrate neuronal cell culture with commercial or in-house built micro-electrode arrays and MEMS devices. The resulting device is intended to support neuronal cell culture on its surface, expose specific portions of a neuronal population to different environments using microfluidic gradients and stimulate/record neuronal electrical activity using micro-electrode arrays. Additionally, through integration of chemical surface patterning, such device can be used to build neuronal cell networks of specific size, conformation and composition.

The design of this device takes inspiration from the nervous system because its development and regeneration are heavily influenced by surface chemistry and fluidic gradients. Hence, this device is intended to be a step forward in neuroscience research because it utilizes similar concepts to those found in nature.

The large part of this research revolved around solving technical issues associated with integration of biology, surface chemistry, electrophysiology and microfluidics. Commercially available microelectrode arrays (MEAs) are mechanically and chemically brittle making them unsuitable for certain surface modification and micro-fluidic integration techniques described in the literature. In order to successfully integrate all the aspects into one device, some techniques were heavily modified to ensure that their effects on MEA were minimal.

In terms of experimental work, this thesis consists of 3 parts. The first part dealt with characterization and optimization of surface patterning and micro-fluidic perfusion. Through extensive image analysis, the optimal conditions required for micro-contact printing and micro-fluidic perfusion were determined.

The second part used a number of optimized techniques and successfully applied these to culturing patterned neural cells on a range of substrates including: Pyrex, cyclo-olefin and SiN coated Pyrex. The second part also described culturing neurons on MEAs and recording electrophysiological activity.

The third part of the thesis described integration of MEAs with patterned neuronal culture and microfluidic devices. Although integration of all methodologies proved difficult, a large amount of data relating to biocompatibility, neuronal patterning, electrophysiology and integration was collected. Original solutions were successfully applied to solve a number of issues relating to consistency of micro printing and microfluidic integration leading to successful integration of techniques and device components.

Chapter 1

1.0 Introduction

The central theme of this thesis is integration of biological cells with multifunctional, micro-scale devices, commonly referred to as micro-electro mechanical systems or MEMS. The above theme falls under a broad category of "Lab on a chip" which deals with miniaturization of experiments and methods of collecting data (Darby, 2013).

The specific aim of the research presented in this thesis is to grow neuronal cells on the surface of the multi-functional neurobiological test platform (neuro test platform) with two primary capabilities: controlling neuronal development and recording neuronal electrical activity *in vitro*. The control of network development is intended to be achieved by combining appropriate surface chemistry with defined microfluidic environment. This approach takes inspiration from the development of central nervous system (CNS) where neurons are guided to their targets via a set of surface cues and diffused chemical gradients (for extensive review see: Canty and Murphy, 2008, Ngalim et al., 2010). The final assembled device is intended to have following capabilities:

1) Sustain a viable neuronal culture.

2) Sustain a patterned neuronal cell culture.

3) Record the electrical activity of both patterned and non-patterned neuronal cultures.

4) Produce microfluidic gradients and expose defined parts of cell culture to these gradients.

5) Using the combination of patterned substrate and micro-fluidic gradients, control the growth and final shape of the patterned neuronal network while it is still confined to the printed pattern.

There are a vast number of documented methods of surface chemistry patterning, generating micro-fluidic gradients and collecting electrophysiological data. The most suitable methods and their relevance to neuroscience research will be overviewed in the proceeding sections. The last section of this chapter will discuss the novelty aspects of this research.

1.1 Historical overview

From the very beginning, neuroscience research concentrated on the most fundamental building blocks of the brain and the nervous system, the neuronal cells. With the invention of the microscope it became possible to examine neuronal tissue in closer

detail. However, due to lack of good staining techniques at the time, there were multiple theories regarding anatomical structure of the nervous system. During late 1800's, Cammilo Golgi found that treating neuronal tissue with potassium dichromate and impregnating with silver nitrate stained entire neurons black, making it possible to distinguish neuronal anatomical features (Dröscher, 1998). During the same period, a Spanish histologist Ramon y Cajal studied the structures of various anatomical areas of the nervous system using the Golgi staining method. Ramon y Cajal was the first researcher to intricately describe the structure of cerebral cortex through extremely elaborate drawings. Cajal's drawings greatly contributed to the establishment of the "neuron theory" (Andres-Barquin, 2001). The neuron theory describes the structure of the brain and the entire nervous system as a functional composition of anatomically defined neuronal cells. This theory, however, was constructed from 12 less inclusive theories which were based on empirical data collected during studies of specific anatomical and functional features of neuronal cells. The neuron theory has been in development since mid-1600's and is still considered incomplete to this day. This theory will be deemed complete and undisputed only if it accounts for all directly and indirectly observable phenomena (Jacobson, 1993). When the neuron theory was accepted as a preferred model for organisation of the nervous system, there still were a large number of questions with regard to how exactly neurons sent and received information. It was suspected that neurons interacted using a complex system of chemical messengers and electric potentials, these theories remained untested until the 1950's (Getting, 1989).

The basic principles of signal transduction were determined through pioneering studies of squid giant axon membrane, neuromuscular junctions and spinal motor neurons (for original publications see: Hodgkin and Huxley, 1952, Katz, 1966, Eccles, 1964, for review see: Stuart et al., 1997). These studies predicted exactly how the electrical signals might travel within and between neurons. The above studies also contributed to the notion that the function of neural networks largely depended on monosynaptic connections between neurons. It was also theorized that because of such dependency, the neuronal networks would not exhibit any "redundant" connections (Getting, 1989).

The early theories and predictions were far too simplistic with regards to neuronal connectivity, function and network anatomy.

The current accepted model describes neuronal networks as having a number of levels of organization. The anatomical level of organisation specifies the monosynaptic, physical connectivity of the neurons that define the network. This level of organisation resembles an electronic circuit where voltage generators connect with specific parts of the circuit to produce a desired output. The next level of organisation is the functional connectivity. This level describes the effects of one part of the network on another. The functional connectivity is not limited to direct monosynaptic connections between two neurons. Functional connectivity takes into account the types of neurons involved in signalling and any modulatory interconnections that may exist "in parallel" with the primary signal transduction route. Essentially, the functional organisation describes the activity pattern of the network (for review see: Getting, 1989). Importantly, the functional connectivity does not limit the network to a single function or single output pattern. Instead, the output is subject to dynamic modulation to suit external environmental conditions or internal hormonal levels for example. Essentially, a particular hardwired neuronal structure can perform a variety of tasks or produce different outputs.

One of the first studies to demonstrate modulation of functional connectivity was performed by Getting and Deking on *Tritonia's* escape swimming behaviour (Getting, 1989). The anatomical structure responsible for the escape behaviour of *Tritonia* consists of seven neurons: cortical neuron "C2", inhibitory "I-cell", three Dorsal Swim Interneurons (DSI) and two Ventral Swim Interneurons (VSI A and B).

The monosynaptic connections between the three DSI cells are excitatory (blue arrows in Figure 1.1a). However, the activity in any of the DSI will be inhibited by the I-cell (red lines in Figure 1.1a). The circuit will only become excitatory (change mode) and allow excitation of both VSI's when the cortical neuron "C2" becomes active and inhibits the I-cell (Getting and Dekin, 1985). This study showed that while networks are under anatomical constraints, the functional network within, can be reorganized in such a way as to provide the required output and behaviour (Figure 1.1).

The functional reorganization of neural networks is also evident in more complex systems such as the somato-sensory cortex of vertebrates, non-human primates and humans. The evidence for functional reorganisation comes from lesion studies that observed partial recovery of motor function. Corroborating evidence also comes from

non-lesion studies that involved mapping of motor cortex through focal electrical stimulation.

a) b)

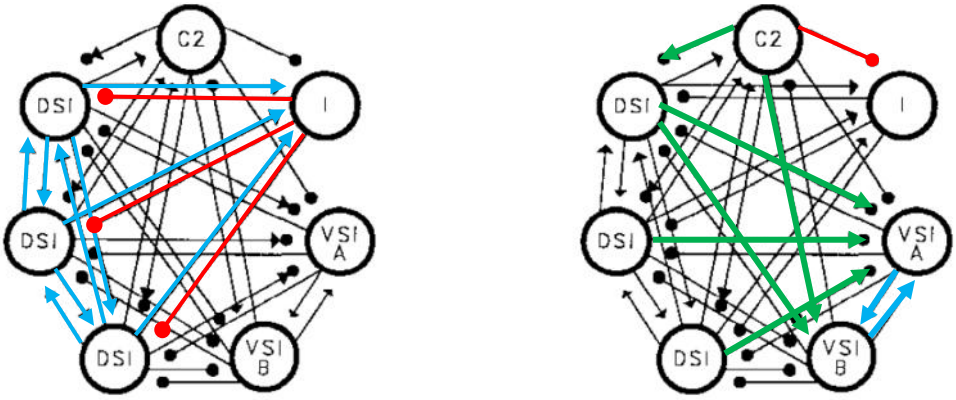


Figure 1.1: Diagram of anatomical connections made by neurons comprising the Tritonia's escape swimming behavior network. a) Schematic showing the excitatory DSI connections (blue arrows) and reciprocal, inhibitory I-cell connections (red line and circle). b) Schematic showing the inhibition of I-cell and excitation of VSI cells (Getting, 1989).

These studies indicated that repetition of specific a physical movement resulted in the expansion of associated cortical area. In addition, it was observed that the existing neuronal circuits around the damaged area can take on the functionality of the damaged area and restore function to a degree (Asanuma and Rosen, 1972, Castro-Alamancos and Borrell, 1995). These observations are some of the reasons why patients with acute brain injury are prescribed physical therapy exercises. It is claimed that coupling the cortical reorganization with physical training results in 85% functional recovery of the cortical area. However the cortical recovery does not guarantee equal degree of physical recovery. The physical recovery is a lot less complete and usually results in compensation involving other parts of the body, such as an altered position of the trunk for example (Nudo et al., 2001).

Interestingly, the complexity of neural networks bestows the nervous system with high degree of fault/damage tolerance. Damage to small number of neuron will not result in a total network dysfunction. The severe network dysfunction will only result following damage to a large proportion of constituent neurons (Haykin, 2008). This is very evident in patients suffering from Alzheimer's or Parkinson's Diseases. In fact, the early stages of these disorders show no symptoms at all even though neurons have started to die. The symptoms appear and progressively get worse only after a substantial

percentage of neurons have died (for review see: Vickers et al., 2000, Langston et al., 1999). Other examples include acute spinal cord injury. The extent of damage to the neurons of grey matter has a disproportionately small effect on the extent of loss of function. The spinal cord also shows similar trends of functional reorganization (Edgerton et al., 2004). Unfortunately, surrounding white matter and spinal cord tracts comprise a relatively simple network where individual neurons carry more "weight" with respect to circuit function. Thus, damage to white matter impacts the loss of network and motor function more severely.

Despite the documented neuronal reorganization, complete recovery of patients suffering from the progressive and acute disorders mentioned above is still impossible. The neuronal tissue in damaged regions of the CNS fails to regenerate due to persistent genetic factor, presence of physical barrier such as a glial scar, chemical barriers such as growth inhibiting proteins associated with myelin and oligodendrocytes and growth inhibitors in the extracellular space (Fawcett and Asher, 1999b). To try and address the issues of neuronal re-growth inhibition and gain a better understanding of neural circuit development, researchers have concentrated on studying neuronal growth on chemically modified surfaces and in microfluidically defined microenvironments. In addition, researchers have also attempted to investigate the effects of various pharmacological compounds on the global electrical activity of neuronal networks (Chung et al., 2005, Taylor et al., 2005, Taylor et al., 2003, Vahidi et al., 2008, Xiang et al., 2007). The next section will review a range of experiments dealing with the neuronal growth on chemically modified substrates and microfluidically defined environments. Additionally this chapter will review the fundamental techniques of gathering electrophysiological data and their integration with surface chemistry and microfluidics.

1.2 Patterned Cell Growth

One of the aims of this project is to attain a degree of control over neuronal network development. Specifically, geometrically patterning neuronal cells on substrates will yield cultures that are easier to study in terms of direction of neuronal process growth, cell-cell interactions, cell-substrate interaction and neuronal electrophysiology. The neuronal cell body placement is particularly important for electrophysiological experiments that utilise the micro-electrode arrays (MEAs) for recording neuronal

electrical activity. Thus, the following section will review some of the techniques that can be used for generating neuronal cell patterns.

1.2.1 Surface modification techniques

Cellular adhesion to surfaces is highly dependent on the surface chemistry. Often, this chemistry must be modified to render the surface bio-compatible (for review see: Folch and Toner, 2000).

There are a number of ways to chemically modify the cell culture surface. For instance, using air plasma, glass substrates can be made hydrophilic through introduction of $-OH^-$ functional groups to the surface. However, this is not an ideal long term solution as the surface will slowly revert to the hydrophobic state when exposed to ambient air (Cech et al., 2002, Harrick-Plasma, 2011).

Alternative modification techniques such as silanization and thiol deposition may also be used to achieve longer term surface modification (for review see: Chang and Wheeler, 2006). The most relevant surface modification reviewed by Chang and Wheeler is the silane chemistry. Silanes are useful because they tend to form self-assembled monolayers (SAM's) with specific functional groups. Unlike the temporary surface modification with oxygen plasma, the silanized surface tends to keep its properties long term. The silanization makes it possible to choose the required functional group. For example: alkylsilanes present a CH_3 on the surface which is cell repellent, aminosilanes on the other hand present an NH_3^+ group which is well suited for cell surface adhesion either by itself or when coupled with other polymers (Corey et al., 1996, Flink et al., 2001, Chang and Wheeler, 2006).

1.2.2 Surface chemistry density and topography

The cells in vivo, including neurons, are anchored to the extracellular matrix (ECM). The ECM, broadly referred to as connective tissue, is composed of large variety of proteins (Hay, 1991). The structure of the ECM is dictated by the presence of collagen and elastin proteins. However, the cell attachment to the matrix is achieved via the interaction of the cell membrane integrins with laminin and fibronectin proteins (Squire et al., 2008). For example, the ECM bound fibronectin, possesses the Arginine-Glycine-Aspartame (RGD) amino-acid sequence which binds to the glycine residues of integrins via hydrogen bonds thus anchoring the cell. Hence, to take advantage of the natural cell adhesive properties of the ECM, it was extensively used for surface chemistry

modification (Thompson et al., 2013). Further research revealed that the cell attachment is very much dependent on the concentration of cell adhesive structures, such as RGD, per unit area. For example, it has been demonstrated that by varying the distances between the hexagonally arranged, RGD grafted gold particles on the surface, it was possible to control the number of surface adherent MC3T3-E1 osteoblasts (Huang et al., 2009). Interestingly, similar observations were made on *rough* surfaces modified with different concentrations or RGD per unit area. It was observed, that regardless of the degree of roughness, the 44 nm spacing between the RGD motifs resulted in the highest number surface adherent endothelial cells (Le Saux et al., 2011). The secondary observation was that regardless of the surface chemistry, increasing surface roughness had a negative effect on the number of adherent endothelial cells. Without the adhesive RGD, the highest number of adherent endothelial cells was found on the polished (Ra 1.1 nm) surface. However, this effect was considered to be cell specific. For example, the neurons seeded on the surface of the patterned silicon wafer showed preference for the rough (Ra=25nm) pattern versus the polished (Ra=3nm) surface (Fan et al., 2002). These observations indicate that the cellular growth on the surfaces can be *tuned* using the combination of spatially controlled surface chemistry and surface roughness. Importantly, the degree of surface roughness has the potential to have a negative effect on the integration of the neuronal cultures with the micro-electrodes, designed for recording the electrical potentials. For the purposes of increased sensitivity and reduces impedance, the micro-electrodes are coated with TiN which results in an increased surface area and roughness (see section 1.3.4). This increase in roughness may have a negative effect on cell attachment to the electrodes.

1.2.3 Laser ablation and selective silane removal (SSR)

Laser ablation is a technique that utilises light amplified by stimulated emission of radiation (LASER) to degrade organic materials through photo-excitation (Srinivasan and Braren, 1989). The selective silane removal (SSR) is a conceptually similar technique to laser ablation, but this technique requires additional steps and uses oxygen plasma for silane removal. Corey et al. compared these two techniques via studying the compliance of rat embryo hippocampus neurons to the patterns of Poly-L-Lysine (PLL) produced via laser ablation and SSR.

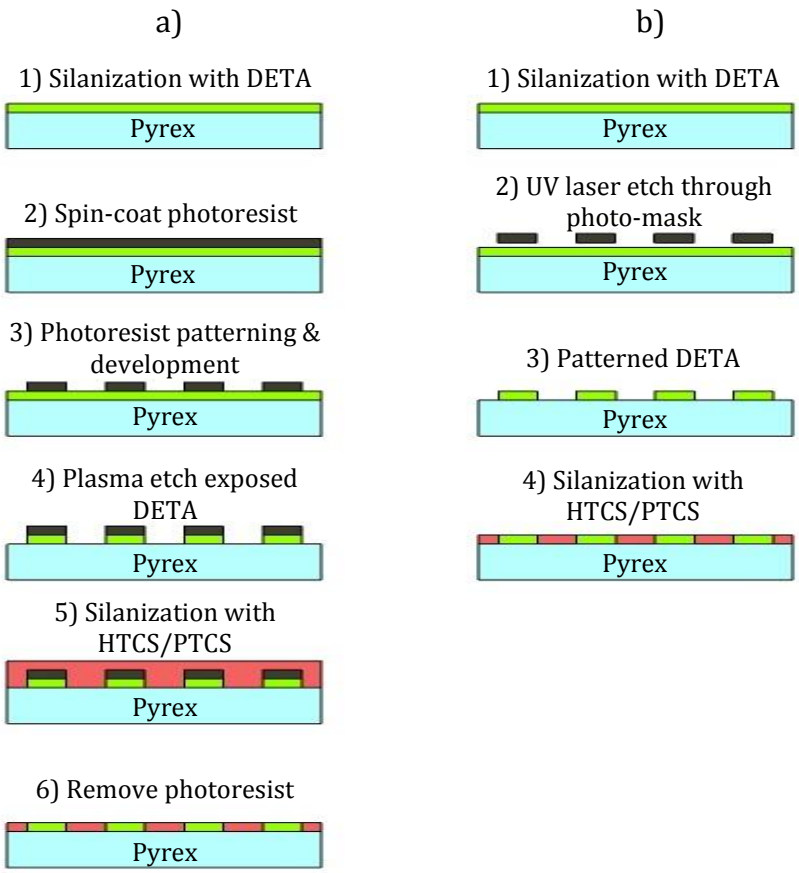


Figure 1.2: Schematic representing the basic steps of a) SSR and b) laser ablation surface patterning techniques.

Both tested techniques involved patterning of cytophilic diethylenetriamine-propyltriethoxysilane (DETA) and cytophobic hexadecyltrichlorosilane (HTCS) or phenyltrichlorosilane (PTCS) on glass surface. The basic steps for SSR and laser ablation procedures are summarized in Figure 1.2.

In terms of work load, the laser ablation technique is superior to SSR because it involves smaller number of steps. The silane patterning can be achieved in three steps as opposed to five in case of SSR. However, this method of surface patterning may be less accurate than SSR because it presumes that the cytophobic HTCS or PTCS silanes will not bind to areas occupied by DETA. Corey et al. (1996) found that both techniques produced patterned neuronal growth, however the SSR produced a much more pattern compliant hippocampal networks compared to the laser ablation technique.

A big advantage of these types of patterning techniques is the ability to precisely control the surface chemistry. The silanized surfaces can be further modified with crosslinkers and specific proteins. Using a similar method to SSR, Sorribas et al. patterned

aminopropyl-triethoxysilane (APTES) on silicon substrate. Using Sulfo-GMBS crosslinker they were able to covalently bind axonin-1 protein to patterned silane (Sorribas et al., 2002).

1.2.4 Micro-moulding in capillaries (MIMIC)

MIMIC is a surface patterning technique that results in a surface relief made from a specific polymer. This process begins with the design and fabrication of a mask, silicon processing and fabrication of the master for replica moulding of elastomeric, transparent, thermosetting poly-dimethyl siloxane (PDMS). The replica moulded PDMS features the open channels which will serve to pattern the substrate.

In order to pattern the desired substrate the replica moulded PDMS is temporarily attached to the surface. Then a low viscosity pre-polymer is injected into the open channels and cured either thermally or with UV. Once the pre-polymer is cured, the PDMS master is removed. The resultant moulded structure remains in the surface (Beh et al., 1999). This technique can be used to pattern cell populations by combining physical constraints in combination with cytophilic surface chemistry. For example, Shim et al. successfully patterned *E. Coli* and NIH3T3 fibroblast using a layer by layer surface deposition of cationic polyallylamine hydrochloride (PAH) and anionic polystyrene sulfonate (PSS). The PAH and PSS polyelectrolyte multi-layers served to bind bovine serum albumin (BSA) to the surface mainly through electrostatic interactions. The BSA on the polyelectrolyte surface combined with PEG structures proved an effective method for patterning cell cultures (Shim et al., 2007).

1.2.5 Ink-jet printing

Inkjet printing using commercially available photo-printers presents a relatively easy, inexpensive and most importantly repeatable method of printing bio-molecules. With some modifications this method can be adapted to create three dimensional polymer structures. This method uses existing hardware, imaging and design software such as CAD (Computer Aided Design) to design and print substances of interest onto an array of substrates such as glass or plastic such as printed circuit board (PCB) for example. The substances that can be printed include: extra-cellular matrix proteins and collagens, DNA, nano-particles and many more (for review see: Calvert, 2001).

There have been a number of studies utilizing inkjet printing for patterning of cells. Roth et al. were able to achieve patterned growth of smooth muscle cells (SMC) and

dorsal root ganglion cells (DRG) on coverslips ink-jet printed with collagen I (Roth et al., 2004).

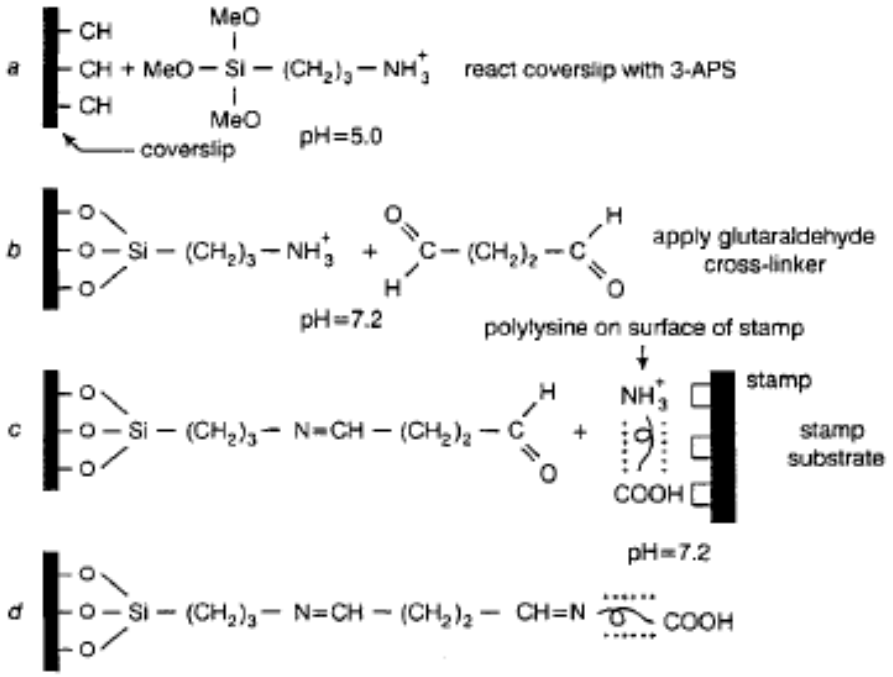
1.2.6 Substrate silanization and micro-contact printing

Micro-contact printing (μCP) is a part of a group of techniques collectively called "soft lithography". This process originated from the semiconductor industry where photolithography is used to create structures on micrometre scale. The soft lithography refers to the use of an elastomer, such as PDMS, during the surface patterning step (Xia and Whitesides, 1998, Bernard et al., 1998).

One of the first studies that used aminosilane chemistry and μCP was performed by Branch et al in 1998. The aim of this study was to investigate the effectiveness of biomolecule transfer during μCP (Branch et al., 1998). This study showed that surface patterning and patterned cell growth can be achieved without the use of such techniques as laser abolition (Corey et al., 1996).

Using the above method, Branch et al. were able to achieve well defined patterned cellular growth on a glass surface (Figure 1.3). A number of other studies researched the use of other silanes and crosslinkers in combination with μCP of PLL to try and produce better quality SAMs and patterns (for review see: Chang and Wheeler, 2006). A study by Scholl et al. in 2000 is an example of use of different silanes, crosslinkers and cell adhesion molecules to achieve patterned neuronal growth. In this study 3-aminopropyldimethylethoxysilane (APDMES) was used to silanized the entire surface.

a)



b) c)

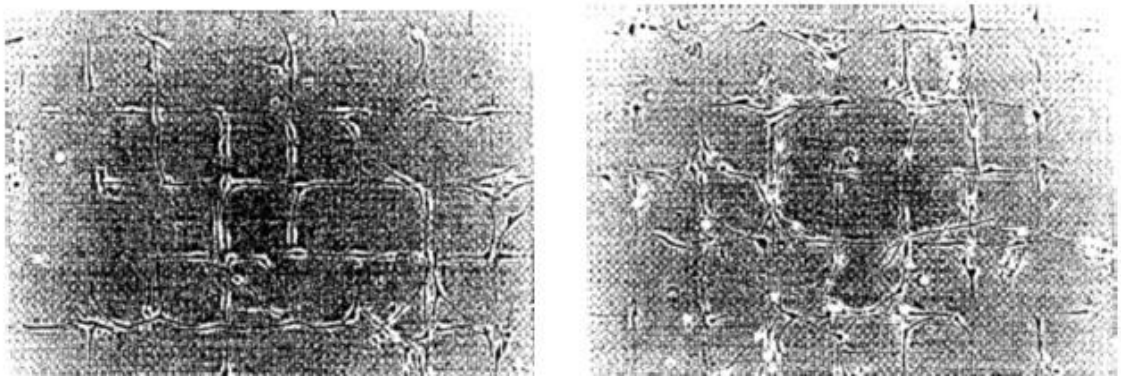


Figure 1.3: a) Schematic of chemical surface modification steps. b-c) Micrographs showing the comparison between patterned growth generated by b) μCP and c) physiosorption and laser ablation (Branch et al., 1998).

The N-γ-maleimidobutyryloxysulfosuccinimide ester (Sulfo-GMBS) was attached to the silanized surface. A synthetic peptide PA22-2 was then micro-printed onto Sulfo-GMBS as promoter of cell adhesion (Scholl et al., 2000). In addition to patterning of cytophilic areas and to further increase the cellular compliance to the pattern, selective cytophobic surface treatment may need to be applied. It is especially important in experiments where aminosalines have been used because bare aminosilane is an effective cell adhesion promoter (Corey et al., 1996).

The areas of silane un-occupied by the cytophilic pattern are referred to as "the background". To enhance neuronal compliance with the printed pattern, the background can be modified with proteoglycans (PG). Specifically, Chondroitin Sulphate Proteoglycan (CSPG) has been shown to be an excellent neuronal growth retardant and implicated as one of the major factors in prevention of axonal regeneration in spinal cord injury (Milev et al., 1994, Fawcett and Asher, 1999a, Bradbury et al., 2002, Massey et al., 2008).

1.3 Electrophysiology

The following section will describe some of the fundamental techniques used for collecting electrophysiological recordings from neuronal tissue. This section will also outline the ideas behind integration of surface patterning with MEAs.

1.3.1 The action potentials

The action potential can be described as a short, bio-electrical event largely caused by the movement of K^+, Na^+ and Cl^- ions through the cell membrane using the trans-membrane ion channels (Figure 1.4). These events can be initiated spontaneously by the cells, as is the case with cardiomyocytes for example, or as a response to a chemical signal such as the binding of the acetylcholine with its receptor in the neuronal synapse (Squire et al., 2008). At rest, the ion channels are closed, keeping the interior of the cell negatively charged as compared to the cell's exterior. This difference in charge is termed the membrane resting potential. The magnitude of the resting potential is dependent on the difference in charge and ionic concentrations between the cell interior and exterior. The concentration of the K^+ ions is higher within the cell as compared to the extra cellular space (ECS). The concentration of the Na^+ and Cl^- on the other hand is higher in the ECS resulting in the net negative charge. Interestingly, the K^+ and Cl^- ions show some limited movement through the cell membrane termed the leaking current. It is largely caused by the difference in the ionic concentration. However, due to the relative negative charge inside the cell, the concentration driven ionic current is offset by the motion-opposing charge thus establishing resting potential (Malmivuo and Plonsey, 1995).

The Na^+ and K^+ channels are voltage sensitive and increase the conductance of their respective ions with the arrival of the voltage pulse. The Na^+ conductance reaches its

maximum rate very quickly leading to a sharp depolarization. The conductance of the K^+ ions on the other hand only reaches its maximum after the Na^+ channels have closed.

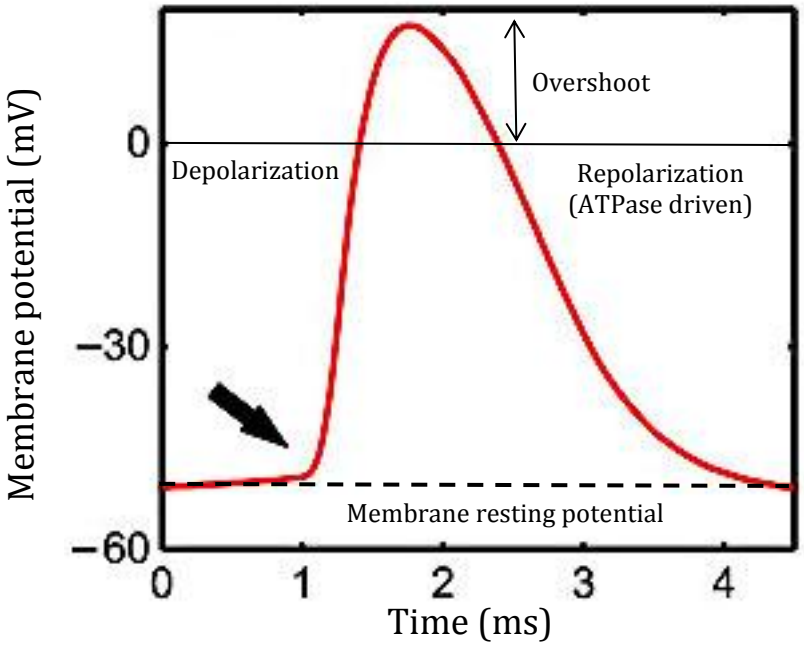


Figure 1.4: An example of an action potential recorded in vitro from a cat visual cortex slice (modified from: Naundorf et al., 2006).

This latency leads to the distinct potential overshoot where it rises above zero. Finally the K^+ conductance is reduced and the active, ATP driven ion transport occurs. The Na^+ is transported out of the cell, while K^+ is transported into the cell by the Na^+ and K^+-ATPases respectively thus restoring the resting membrane potential and the respective ionic concentrations (Squire et al., 2008).

1.3.2 Voltage clamp

The aim of the voltage clamp is to selectively measure the ionic currents that flow through the axon membrane (Hodgkin et al., 1952a, Malmivuo and Plonsey, 1995). As briefly mentioned above, Hodgkin and Huxley utilised this technique on the giant axon of the squid and developed a mathematical model that was able to describe the ion conductance during an action potential (AP) event (Hodgkin et al., 1952a). The essence of the voltage clamp experiments is the control of membrane voltage with electrodes and feedback amplifiers.

The experimental set up involves inserting stimulating and recording electrodes of predetermined lengths into an axon bathed in physiological salt solution inside a chamber of defined proportions. The predetermined dimensions of the electrodes and

the chamber ensure that the axial currents, which occur due to point stimulation, are eliminated. This feature of the voltage clam set up is called “the space clamp”. Figure 1.3 shows an illustration of voltage clamp set up as seen in Malmiviuo and Plosney (1995). To regulate the voltage across the axon membrane, current of specific magnitude is fed to the axon through one of the electrodes. As the electric current flows through the electrode, the membrane voltage is changed to the required level. However, the new voltage across the membrane opens some of the voltage gated ion channels, causing ionic currents. The new ionic currents will induce a voltage variation and deviation from set value. Hence, in order to offset the voltage variation, a feedback amplifier is used.

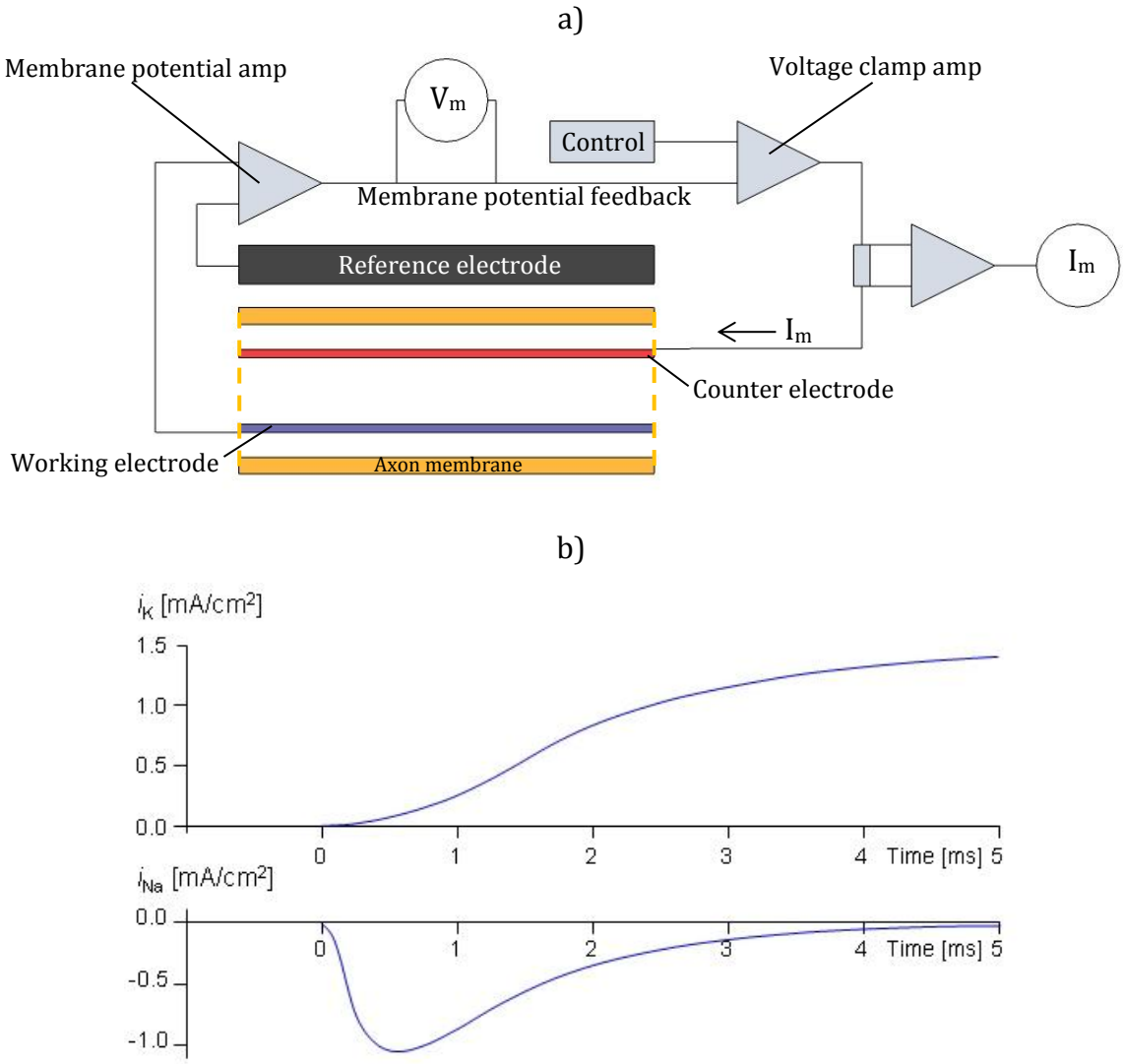


Figure 1.5: a) Schematic representation of voltage clamp experiment. b) Idealised voltage clamp recordings of sodium and potassium ion movement (Malmivuo and Plonsey, 1995).

The feedback amplifier generates an exact negative copy of the variable membrane voltage, sends this signal to the signal generator, which in turn feeds the modified signal

back into the axon to keep the membrane voltage at a pre-set value (Malmivuo and Plonsey, 1995, Hodgkin et al., 1952a). Since the feedback current is inversely proportional to the ion currents flowing through the membrane, by recording the feedback current, it is possible to extrapolate the magnitude of trans-membrane ion currents (Figure 1.5b).

1.3.3 Patch clamp

The patch clamp technique is similar to the voltage clamp because it also measures the membrane ionic currents. However, the patch clamp only measures the currents through a tiny number of channels due to the micrometer dimensions of the pipette tip. This technique was successfully applied to cell membrane by Neher and Sakmann in 1978 (Neher et al., 1978).

The patch clamp technique involves pressing an electrolyte filled, fire-polished micro-pipette (1-3 μm diameter) against a cell membrane. The pipette tip forms an electrical seal and has a direct correlation to the amplitude of the background noise. Hence, to achieve a good signal to noise ratio (S/N), a seal of 10-100GΩ (gigaseal) is desirable. Additional benefit of a gigaseal is its mechanical stability which is extremely important when measuring ionic currents in pA range (Neher et al., 1978, Hamill et al., 1981, Malmivuo and Plonsey, 1995).

The patch clamp pipettes can be made either from flint glass or borosilicate (Pyrex) glass. The flint glass is claimed to be easier to work with, and pipettes are less prone to defects. The borosilicate glass on the other hand is more difficult to work with as it tends to produce uneven and poorly broken tips. However, the borosilicate glass is claimed to have superior electrical properties due to thicker walls, resulting better seal and higher S/N. The drawback of a thick walled pipette tip is the occurrence of ionic currents right under the interface of pipette wall resulting in unsteady baseline and non-uniform current signals (Hamill et al., 1981).

The pipettes are made in three stages. The first stage involves heating and pulling the pipettes using an automated pipette puller, a bench-top device that uses combination of heat and mechanical force to stretch a pre-heated glass tubes. The pipette pulling step itself can have 2-3 steps depending on the type of glass and device used. The next step in pipette manufacture is coating the shank with PDMS. The purpose of this step is to reduce the capacitance of the pipette bath which further serves to reduce the

background noise. Due to hydrophobic nature of the PDMS surface, these pipettes cannot be filled via capillary action and need to be filled by sucking up a small amount of electrolyte and the backfilling the pipette. The third and final step of pipette manufacture is the heat polishing of the tip in the microforge. The polished pipette seals very well against the cell membrane and contributes the formation of gigaseal.

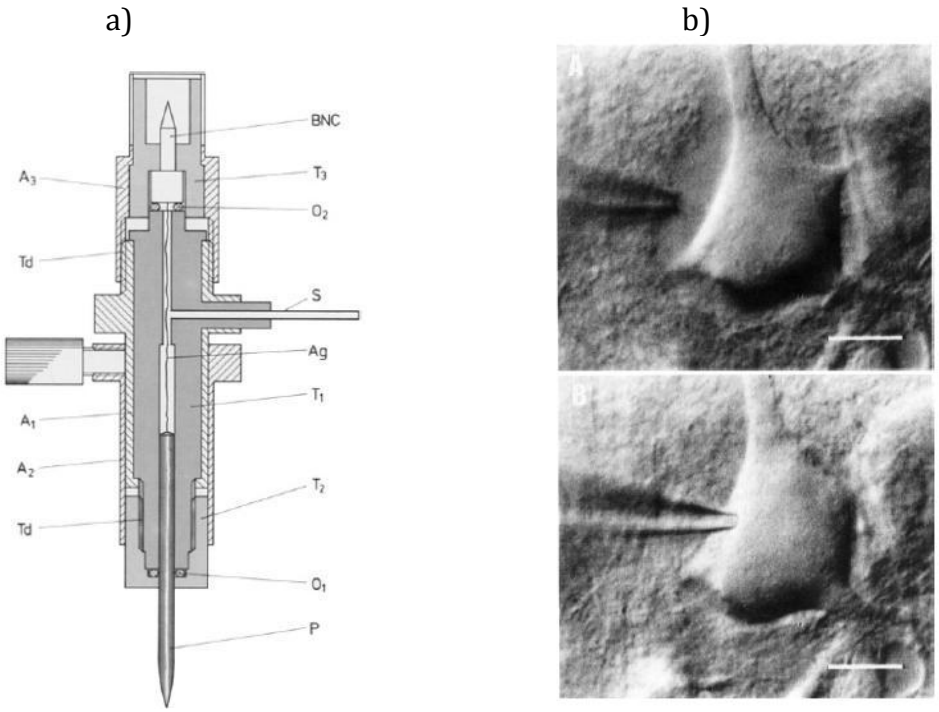


Figure 1.6: a) Schematic diagram of patch clamp pipette holder. The pipette (P) is held inside a Teflon body (T1) and secured by the means of Teflon screw-on cap (T2) and the rubber O-ring (O1). The Teflon support structures (T1-3) are secured inside aluminum body (A1-3). The Ag electrode is connected to an external electronics via a BNC connector. The suction/pressure is applied to the pipette through a designated port (S) (Hamill et al., 1981). b) A micrograph of a micropipette approaching the neuronal cell membrane (top) and in contact with the cell membrane (bottom) (Stuart et al., 1993).

The physical set up of the patch-clamp is a complex system consisting of a microscope, micro-manipulators, vacuum source and an array of electrophysiological equipment designed to amplify, filter and modify the recorded signal as needed. Figure 1.6(a) shows a schematic of a suction pipette holder. The primary function of the pipette holder is to provide the electrical connection between the electrolyte solution inside the pipette and the signal recording equipment. The pipette holder also allows application of suction or pressure to the pipette to create a seal or release the membrane.

Additionally to the complex hardware set up, a patch clamp experiment may require a parallel voltage clamp to be applied, so that the current can be measured at the pre-set membrane voltage. Apart from a carefully designed hardware setup, a good quality, high S/N current recording also might require enzymatic treatment, especially when dealing with muscle fibers since these are covered with collagen (Neher et al., 1978, Hamill et al., 1981).

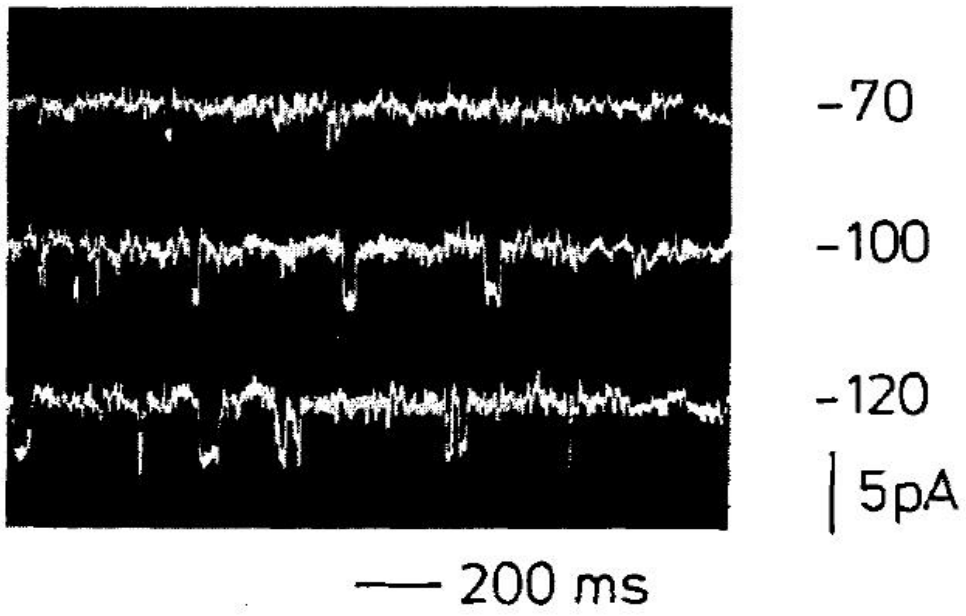


Figure 1.7: A patch clamp recording of rat diaphragm muscle membrane. During the patch clamp, the membrane was voltage clamped at -70,-100 and -120mV and 12 °C.

Neher and Sakmann applied patch clamp technique to the membranes of frog cutaneous pectoris muscles as well as rat diaphragm and omohyoid muscles (Figure 1.7). To avoid recordings from multiple ion channels and to reduce the chances of trapping ion channels under the tip wall, the pipettes were sealed against the muscle membrane regions with a relatively low concentration of acetylcholine receptor channels (AChR). Since the AChR channels are triggered via chemical interaction rather than voltage, the electrolyte solution was supplemented with a low concentration of acetylcholine.

The recordings of currents through the AChRs channels consisted of square pulses indicating that the transition between closed and open states was very quick with respect to the pulse duration. Once the channel was open, the current level remained uniform. The non-square and higher than normal pulses of ion currents were theorized to occur when a number of channels opened simultaneously. As mentioned above, the cell membrane can be voltage clamped simultaneously with the patch clamp. Hence the

voltage clamp can be used to depolarize the cell membrane and induce the inter-membrane ionic currents which can be recorded by the patch clamp.

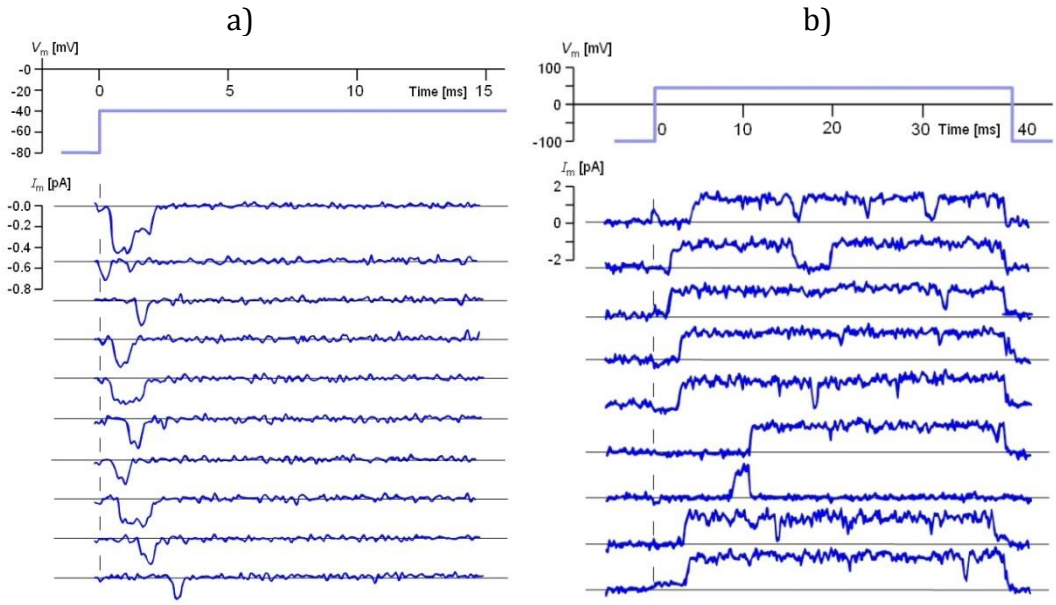


Figure 1.8: A series of patch clamp recordings of single a) Na^+ and b) K^+ ion channels. The ion channels were opened using a voltage clamp (top of a and b) (Malmivuo and Plonsey, 1995).

The shape of the recorded ionic current induced by the voltage clamp can be said to be the same as the currents induced via chemical interaction where the transition between open and closed states is relatively instantaneous. Figure 1.8 shows a series of patch clamp recordings of (a) sodium and (b) potassium ions (Neher et al., 1978, Hamill et al., 1981). A direct comparison of the Na^+ and K^+ ion currents recorded via the patch clamp to the ones recorded via the voltage clamp described in the previous sections shows a marked difference in the shape of the signal. The voltage clamp indicates that the ionic current reaches the maximum values gradually, while the patch clamp indicates that the transition between zero current and the maximum value is instantaneous. This can be directly linked to the number of membrane channels that are involved in the recordings. The voltage clamp recordings made by Hodgkin and Huxley represented a relatively large membrane area, housing a very large number of ionic channels. Hence, the recorded current signal is a combination of many channels opening at various intervals after the initiation of the voltage clamp. This can be confirmed by averaging the multiple patch clamp recordings of one ion channel as shown in Figure 1.8 (Hamill et al., 1981, Malmivuo and Plonsey, 1995).

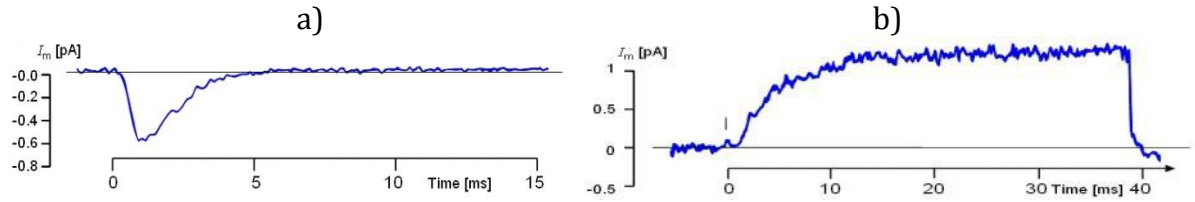


Figure 1.9: Averaged recordings of ion currents through a) Na^+ and b) K^+ channels.

1.3.4 Microelectrode arrays, their development and uses

The first report on a micro-electrode array (MEA) appeared in 1972. It was fabricated by Thomas et al. and consisted of 2x15 array spaced 100µm apart (Thomas Jr et al., 1972, Pine, 2006). This array was built on glass and the electrodes and the connecting tracks were made from gold. The entire MEA, except the electrodes, was insulated with photoresist. The surface of the gold electrodes was covered with platinum black to reduce impedance. The modern MEAs are quite similar to the original with regard to its construction. However, additional materials, such as indium tin oxide (ITO) and titanium nitride (TiN), are regularly used to form the microelectrodes of the MEA. ITO provides completely transparent microelectrodes and connecting tracks. ITO is mainly used on MEA where inverted microscopy is of high priority (Figure 1.10).

The MEA has an advantage over the patch clamp because it can record multiple signals simultaneously over an extended period of time with virtually no change in the position of recording electrodes. This is hard to achieve using the patch clamp because it cannot be left in culture during the culture period due to cumbersome and fragile nature of the set up. Thus, the apparatus has to be set up anew each time a recording is required. Since, it is practically impossible to set the patch clamp probe in exactly the same spot on a neuron, the change in recording positions results in variation of the recorded signals (Claverol-Tinture and Pine, 2002).

Thus, it becomes impossible to attribute a change in signal amplitude or frequency to anything other than change of position of the patch clamp probe.

The MEAs also have drawbacks. Due to the small size, the electrodes have very low sensitivity to change in potential (Fejtl et al., 2006). In order to record an AP of a neuron, the neuron has to be positioned right on top of the electrode. In addition to low sensitivity, the MEAs have high impedance directly related to the micrometre dimensions of the electrodes (Weber, 1989).

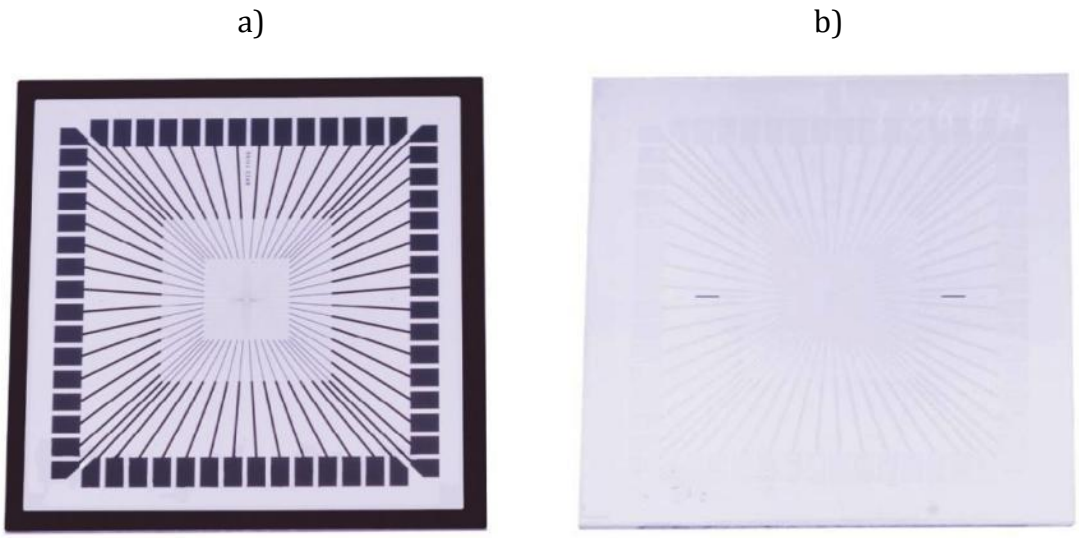


Figure 1.10: a) A commercial MEA with TiN tracks contact pads and electrodes. b) An MEA with contact pads and tracks made from ITO.

In order to generate a current in the small microelectrodes, a higher voltage is needed as compared to larger electrodes. This poses a problem when dealing with neuronal cells because neurons produce AP of fixed voltage irrespective of the amplitude of stimulating potential (Brodal, 2004, see: Bullock et al., 1965). The magnitude of impedance is also directly related to micro-electrode noise. Noise occurs due to random motion of the electrons within the conducting material (Leach, 1994). Interestingly, because of high impedance and low S/N it was thought that sub-threshold neuronal events such as excitatory post-synaptic potentials (EPSP) could not be detected using an MEA. It was theorized that the EPSP would simply be lost in the noise. This was shown not to be the case. The measured noise from an empty MEA was found to have smaller amplitude in comparison to the noise recorded from an MEA used to culture a very dense neuronal culture. When tetrodotoxin, a sodium channel blocker, was added to the culture, the noise level fell, indicating that sub-threshold events contribute to the overall noise of the MEA (Potter et al., 2006). Thus, if the MEA noise, produced by the electronic circuits is substantially reduced, it could be possible to detect the sub-threshold events such as EPSP's and IPSP's.

The electrode impedance is frequency dependant and usually measured between 100Hz-100kHz (Cogan, 2008). Impedance is also inversely proportional to the electrode surface area where larger electrodes have lower impedance. (Gesteland et al., 1959, Ross et al., 2004, Keefer et al., 2008). Since the impedance and the resulting noise is a

function of the microelectrode surface area, increasing the surface area, without increasing the physical size of an electrode also reduces the impedance and noise. The increase in surface area can be achieved through deposition of such materials as platinum black, titanium nitride (TiN) or carbon nano-tubes (CNTs) on to the surface of the electrode (Keefer et al., 2008). These deposits are good conductors and form a rough porous surface (Gesteland et al., 1959, Robinson, 1968, Leach, 1994, Ross et al., 2004, Pine, 2006). The noise produced by the microelectrodes can be further amplified by high temperature. This increase in noise due to heat is termed the thermal noise. Thus, one of the strategies of noise management is to try and keep the circuit at as low a temperature as possible. However, such a measure is applied only when all other noise minimization strategies have been implemented but prove insufficient. Additionally, this measure would be difficult to apply to an MEA housing a neuronal cell culture since decreasing the temperature too far can result in neuronal death (Leach, 1994).

1.3.5 MEA patterning and electrophysiology

The efficiency of recording an AP from a single cell using an MEA is directly linked to the area of the electrode that is in contact with the cell membrane (Fejtl et al., 2006, Tank, 1989). Hence, the larger the electrode area covered by the cell membrane the higher the amplitude of the recorded AP. Similarly to patch clamp, a good seal between the cell membrane and the electrode is crucial for high S/N electrophysiological recordings (Tank, 1989). Thus, one of the primary roles of patterning an MEA is to be able to position the neuronal cells on top of the microelectrodes. To date a number of studies investigated aligned patterning of neuronal cell cultures on the surfaces of microelectrode arrays and were able to record electrical activity of the patterned network (for review see: Chang and Wheeler, 2006).

One of the early studies of patterning neuronal cells on the surface of the MEA was performed by Chang et al. in 2000. The MEA was covered with photoresist, which was then exposed to UV through a custom photo-mask. After UV exposure the photoresist was developed. The development step strategically removed the photoresist from the surfaces of the microelectrodes, leaving a pattern of bare exposed MEA surface in-between the islands of photoresist. Following the resist development, poly-lysine was adsorbed to the free MEA surface and the photoresist. Poly-lysine was then patterned by removing the remaining photoresist with an appropriate solvent (Chang et al., 2000).

Using this technique, Chang et al. were able to record AP spikes of up to 200μV peak to peak generated by patterned rat embryonic hippocampal neurons.

Another study by Nam et al. in 2003 used aligned μCP to generate patterned cultures of rat embryo hippocampal neurons on the surface of an MEA. Using this technique Nam et al. were also able to record AP's from patterned neuronal network. In this study the reported AP amplitudes were up to 400μV peak to peak. This study also showed that it is possible to culture neurons long term on the surface of patterned MEA (Nam et al., 2003).

1.4 Microfluidics

Microfluidics is a technology and field of research where relatively small volumes of fluids are pumped through channels of micro-meter scale. Flow of fluids of such low volumes is dominated by surface tension, viscosity, surface area to volume ratio and diffusion. These micro-scale systems do not exhibit any random or turbulent flows or convectional mixing as seen on the macro scale. Instead the flow is laminar (Beebe et al., 2002).

According to a 2006 review article by George Whitesides, the development of microfluidics stemmed from the need for miniature devices capable of performing specific tasks such as chemical analysis. Even though chemical analysis systems such as gas phase chromatography (GPC) and high pressure liquid chromatography (HPLC) used minimum amounts of samples, they provided high sensitivity and resolution of chemical composition. Size limited these systems for laboratory use only; hence, in the attempt to perform the similar analysis on a micro-scale, the research and development of microfluidic technology came about. Additional needs for these miniature chemical analysis devices included field chemical and biological threats detectors commissioned in the US by Defence Advanced Research Projects Agency (DARPA) after the cold war. Molecular biology was another field that saw a need in developing microfluidic technology for increasing throughput of DNA sequencing and Polymerase Chain Reaction (PCR) (Whitesides, 2006, Beebe et al., 2002).

Microfluidic devices (μF) are essentially fluidic channel networks of microscopic dimensions. These channels can be etched into glass (e.g. Mellors et al., 2008), silicon (e.g. Chandrasekaran et al., 2007) or moulded into a block of structural polymer such as

Zeonor (Illa et al., 2010). The design and dimensions of these devices as well as choice of base material is governed by the experimental requirements and cost. For example, specific to experiments involving biological cell cultures and this project is the requirement that the μF device and the substrate are compatible with light and fluorescent microscopy. Hence the μF device and the substrate must be optically transparent. Materials such as Polydimethylsiloxane (PDMS) and Pyrex fit these criteria. PDMS is by far the most common material used for fabrication of μF devices. The common listed attributes of PDMS are its low cost, high transparency, good surface conformity, gas permeability, solvent resistance and bio-compatibility to list a few (Makamba et al., 2003, Zhou et al., 2010). Using PDMS, a new μF device can be made within 1.5 h provided the masters are available.

In order for the μF device to function as intended, the micro-channel network moulded into the surface of PDMS must be sealed by bonding the PDMS to another surface. The channels may be sealed by aligning and bonding one μF device with a second μF device with complimentary channel network there by creating a 3D μF device (Anderson et al., 2000, Flachsbart et al., 2006). The most common approach is to bond the μF device to a planar flat glass substrate such as a Pyrex slide or coverslip. Usually the bond is permanent and achieved by oxidizing both surfaces through exposure to plasma (Bhattacharya et al., 2005).

1.4.1 Microfluidic devices

The fundamental part of μF device is generation of laminar flow. Laminar flow occurs in fluids of small volume and low flow speeds. It is characterized by absence of mixing (Beebe et al., 2002). The molecules of the fluid that is in the state of laminar flow are still free to diffuse within the volume provided by the microfluidic device (Kamholz et al., 1999). Rate of diffusion is proportional to the surface area and can be controlled by introducing microfluidic mixers into the device design. These features do not introduce any turbulent currents, but rather increase the surface area between the two diffusing liquids (Beebe et al., 2002). Diffusion generates concentration gradients between two solutions that flow side by side in a state of laminar flow. These gradient profiles with in a microfluidic device can be made steep or shallow by controlling the flow velocity and concentrations of solutes. Although the true rate of diffusion is directly related to diffusion coefficients of the solutes.

An example of a simple device to demonstrate this control over laminar flow and gradients was built by Cheng et al. (2008) and illustrated in Figure 1.11. This device was built from a number of components. The base of the device is made from Pyrex glass. The actual microfluidic device is built from Poly(methyl-methacrylate) (PMMA) which is a transparent thermoplastic. Finally indium tin oxide (ITO) was used as a transparent cover for the device. In this case the ITO was also used as a heater for the culture chamber.

The working principle of this device is very simple; the culture media is supplied to the cell culture through a medium inlet. The “gate” ensures that media supply and flow is uniform over the entire cell culture surface. The culture media is then collected by another “gate” and then carried away to waste through the media outlet. The effusion inlet makes it possible to supply modified culture media into the main media flow resulting in a microfluidic gradient.

Figure 1.12 shows that the speed of the flow plays a crucial role in controlling the slope of the gradient. Slow flow speeds allow the dye to diffuse into the bulk of the flow before it is collected as waste. However, once the speed of the flow is increased, the gradient profile becomes steeper (Cheng et al., 2008). This device enables the user to control the gradient slope as well as the area that is exposed to the effluent flow.

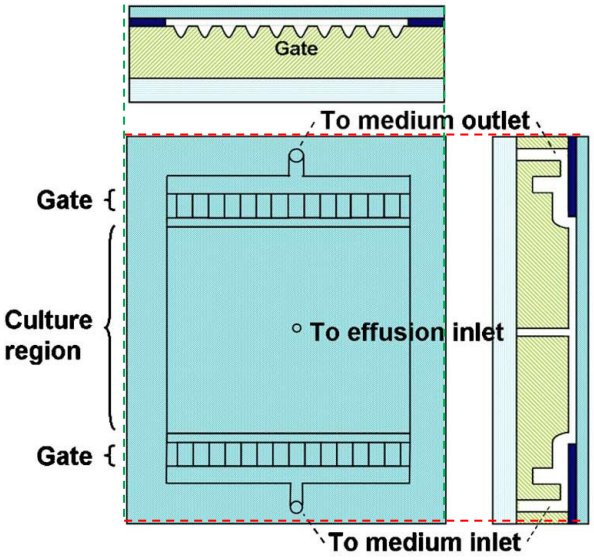


Figure 1.11: Schematic of a cell culture device as seen in (Cheng et al., 2008).

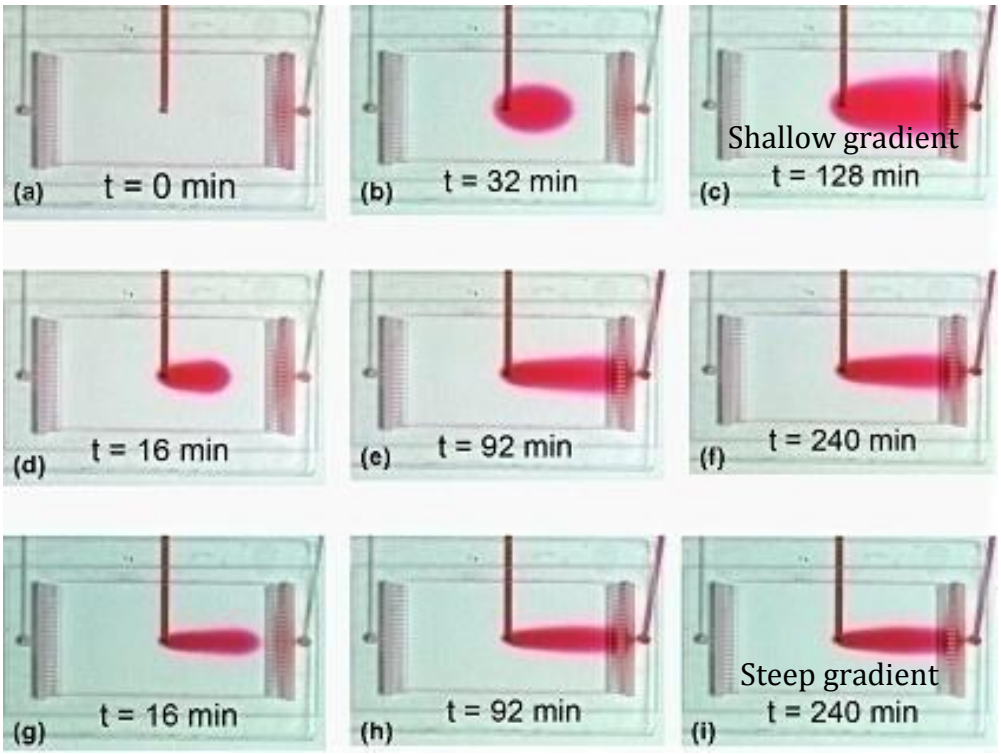


Figure 1.12: Generation of microfluidic gradients of varying slope using variation on flow velocity. (a-c): Bulk media flow at 10μL/h, dye supply through the effusion inlet is also at 10μL/h. (d-f): Bulk media flow at 30μL/h. (g-i): Bulk media flow at 50μL/h (Cheng et al., 2008).

1.4.2 µF device perfusion techniques

Culturing cell populations inside µF devices means that relative to the standard culture methods, the cell population is exposed to significantly smaller volumes of culture media. The smaller volumes are beneficial with regards to reduced waste of media, which combined with various supplements can be financially costly. However, feeding cells with smaller media volumes results in much faster nutrient depletion (due to low volume rather than cell response) and increased rate of waste build up. Hence to circumvent these issues, these devices need a system that efficiently introduces new nutrients and removes waste products (Kim et al., 2007). This can be achieved in a number of ways; simplest method is direct culture perfusion while more sophisticated methods involve diffusion of nutrients and waste through a thin membrane (Wong et al., 2010).

The direct perfusion can be achieved by pumping the media through the µF device using a mechanical pump. The mechanical pumps provide a good degree of control with regards to volumetric rates and media volumes that these machines can hold. The main disadvantage of the mechanical micro-fluidic pumps it that they are relatively large devices since they need to be able to hold up to 100ml (or 2 x 50ml syringe) of liquid. Additionally, external power supplies of these pumps can be a problem since most tissue culture incubators do not allow external lead access into the incubator due to risk of infection as well as maintaining the incubator environment.

The size of the setup can be reduced by using passive perfusion techniques such as gravity driven pumps or surface tension driven flows. Another option is incorporation of on-chip peristaltic or electro-osmotic pumps.

Gravity driven perfusion is conceptually the simplest solution. This method relies on difference in hydrostatic pressure between two or more fluidically connected reservoirs containing different fluid volumes or placed at different heights. The reservoir containing a larger volume of fluid will exert a higher hydrostatic pressure relative to the other reservoir. The higher pressure will induce fluid to flow into the other reservoir in order to equilibrate the pressure. The volumetric rate of such system is dependent on the volume difference or the height difference between the two reservoirs and the dimension of channel connecting the two reservoirs together (Kim et al., 2005).

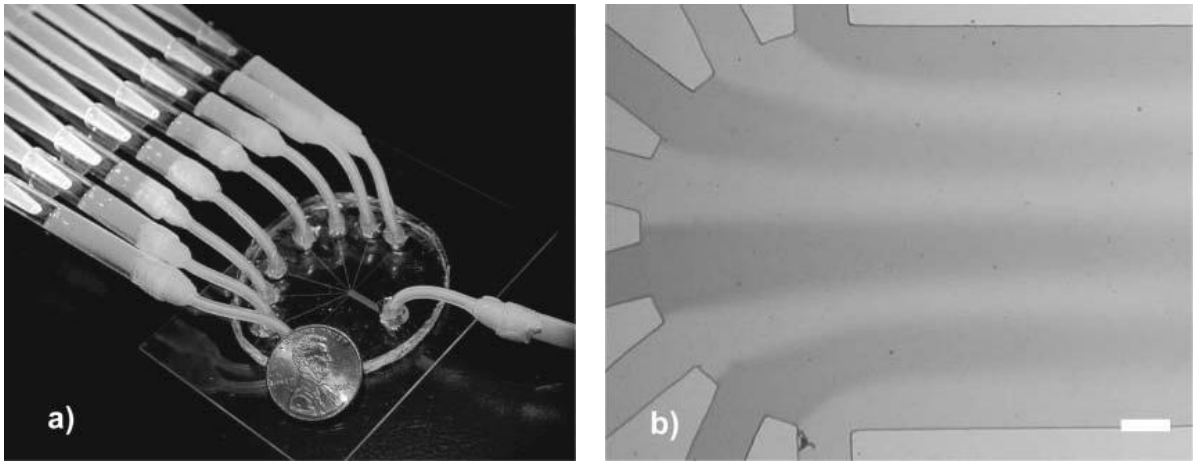


Figure 1.13: a) The gravity driven perfusion set up consisting of 8 source reservoirs draining into 1 waste reservoir through a replica moulded microfluidic device. b) An example of gradients generated by gravity driven perfusion (Zhu et al., 2004).

A good example of the gravity driven passive perfusion system was published by Zhu et al. in 2004 (Figure 1.13). Unlike the conventional, gravity driven devices, their device eliminates the dependence of the volumetric rate on the fluid volumes in the reservoirs. Eliminating such dependence is important for ensuring steady volumetric rate. The dependence on volume is eliminated by redesigning the system such that the reservoirs are arranged horizontally (long and narrow). The long and narrow reservoirs ensure that the fluid surface tension stops it from flowing out, while horizontal orientation and height difference between the source and sink reservoirs maintains constant difference in hydrostatic force irrespective of volume in each reservoir. Using this design Zhu et al. were able to sustain passive perfusion for prolonged periods of time as well as introducing microfluidic gradients into the μF device (Zhu et al., 2004).

Surface tension can also be used to drive fluidic flow. This method involves placing a large drop on one channel inlet and a relatively smaller drop on the opposite inlet (Figure 1.14). Provided that the two drops are fluidically connected, the liquid will start flowing from the small drop into the larger one. This physical phenomenon can be explained by a Young-Laplace Equation. This equation states that the difference in pressure (p) of a liquid with a given surface tension is inversely proportional to the radius of surface curvature:

$$\Delta p = \gamma \left(1/R_1 + 1/R_2\right)$$

where Δp is the pressure difference between liquid drops, γ is the surface tension of the liquid, R_1 and R_2 are liquid surface curvature radii (Berthier and Beebe, 2007).

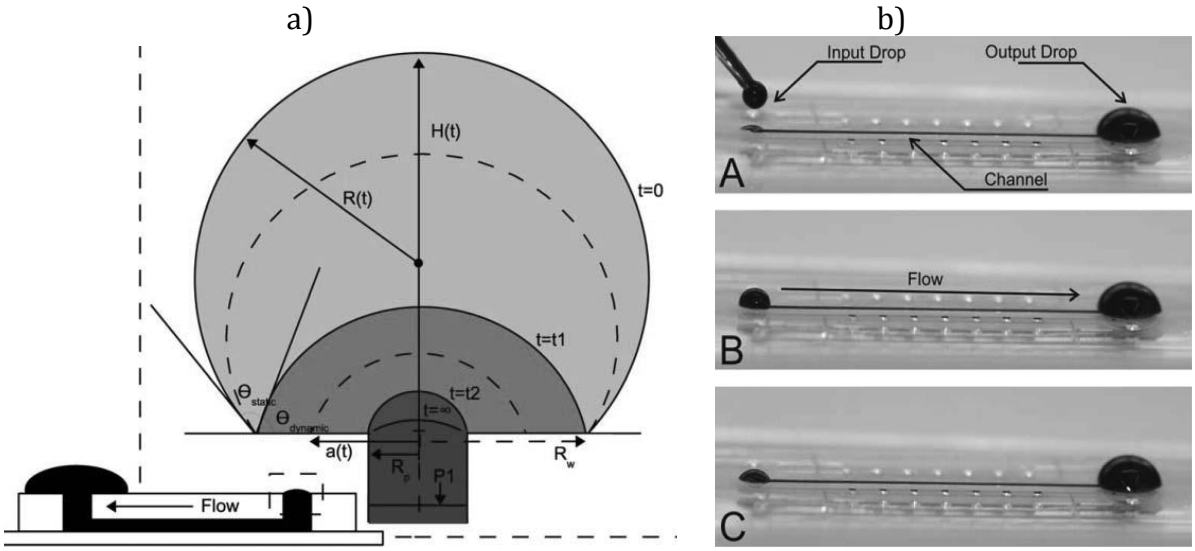


Figure 1.14: a) A schematic of a drop of liquid placed onto a fluidic inlet. b) A practical example of surface tension driven flow. The flow occurs from the small volume drop into the bigger volume drop (Berthier and Beebe, 2007).

Similar perfusion technique can be used on a patterned super-hydrophobic surface without the system of microchannels (Figure 1.15). The liquid in this case is confined by the surface chemical properties rather than mechanically by channel walls (Xing et al., 2011). This study also points out that it is possible to achieve bi-directional flow, rather than just the traditional flow from small volume drop into the larger one. The directionality of the flow relies not only on the volume and circumference of the drop but also on the radius of the contact patch or the fluidic inlet (Xing et al., 2011).

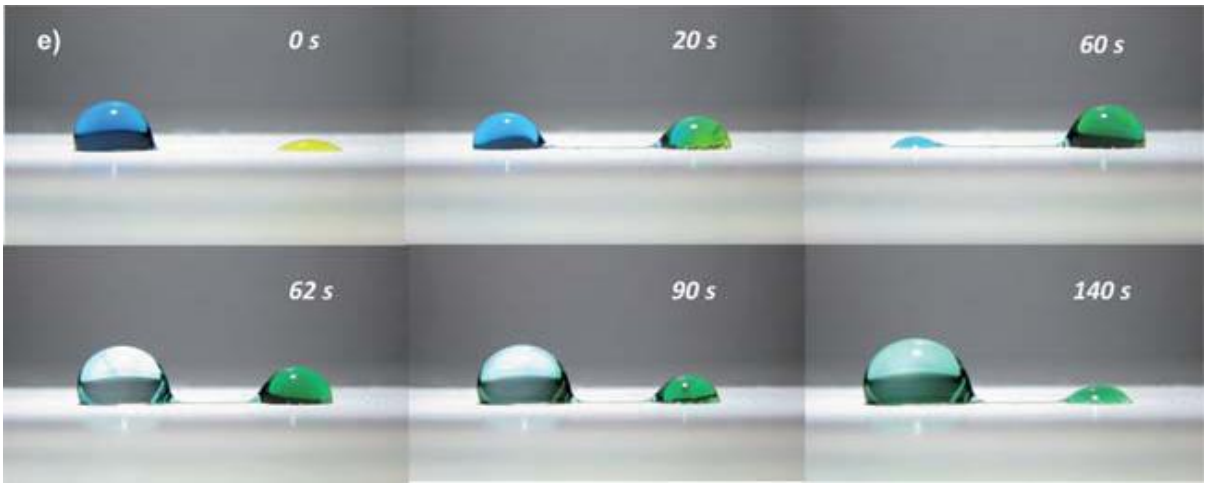


Figure 1.15: Bi-directional perfusion of a surface microfluidic channel. 0s-60s image sequence shows the fluid being transported from a larger drop into a smaller one. 62s-140s image sequence shows the opposite effect where transport occurs from a smaller volume into a larger volume drop (Xing et al., 2011).

The third example of μF perfusion involves the use of a peristaltic pump. This method of perfusion relies on sequentially closing and opening specially designed valves inside the μF channel. The closing of valves pinches a section of the channel, reduces channel volume and creates hydraulic pressure which then forces fluid flow (Figure 1.16).

One interesting example of peristaltic perfusion of μF device involved an integrated commercial Braille display. Braille displays are devices that enable the visually impaired to read text from a computer. It consists of an array of pins which can be raised or lowered depending on the text displayed.

By integrating a specifically designed μF device, made of an elastomer such as PDMS, onto the Braille display and aligning the μF channel with the pins it is possible to generate peristaltic flow by programming the Braille display to raise and lower the pins in specific order. The μF channel is separated from the pins via a thin membrane of PDMS permanently bonded to the μF device (Gu et al., 2004). Similarly peristaltic flow can be achieved by integration of pneumatic chambers within the μF device. Running the pneumatic chambers perpendicularly to the μF channels it is possible to generate peristaltic flow by sequentially controlling the pressure the chambers (Unger et al., 2000, Wu et al., 2008).

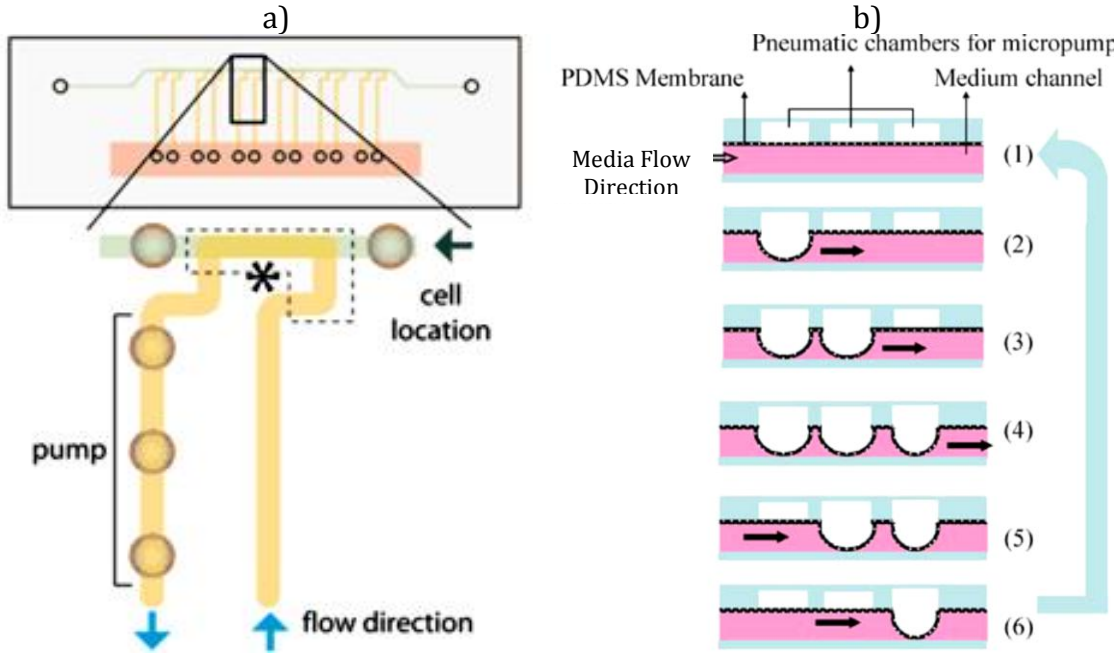


Figure 1.16: a) A schematic representing cell culture perfusion using Braille display peristaltic pump. The circles in the schematic represent the pins of the Braille display. b) A schematic representing the pneumatic peristaltic pump and the sequence or pressure increase in each pneumatic chamber (Gu et al., 2004, Wu et al., 2008, Unger et al., 2000).

1.4.3 Application of microfluidics to neuronal cell culture

One of the simplest examples of μF devices being used for neural cell culture is a study by Taylor et al. (2003). The purpose of this study was to physically localize and contain chemical insult to the neuronal culture. The μF device consisted of two parts: i) a substrate, such as a polystyrene culture plate or a Pyrex cover slip and ii) a replica moulded microfluidic device made from PDMS (Taylor et al., 2003). More complex multi-layered microfluidic devices can also be constructed (Taylor et al., 2005, Wang et al., 2008). In order to promote neural adhesion both types of substrates were first treated with oxygen plasma and then with a solution of PLL. The oxygen plasma treatment serves two roles. First, it removes any organic residues that might be present on the surface of substrates. Second, it turns glass surface hydrophilic.

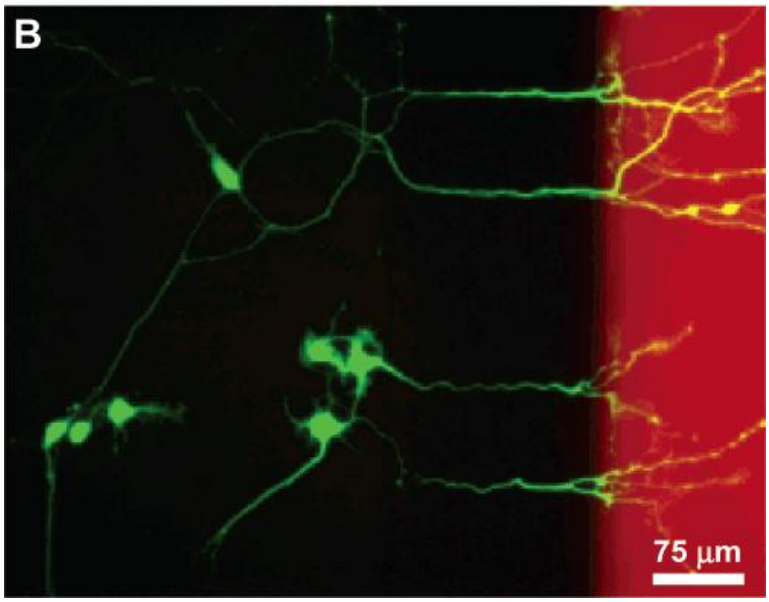


Figure 1.17: A micrograph showing neurons (Green) growing inside the microfluidic device. The efficiency of containment of different fluidic environments is demonstrated by confinement of Texas Red stain to the axonal chamber (Taylor et al., 2003).

The bare hydrophilic surface is much more favourable for neuronal attachment and growth as well as adsorption of polymers such as cell adhesive PLL. Hydrophilic surface also provides better adhesion with PDMS creating a better seal (Bhattacharya et al., 2005, Taylor et al., 2003).

The functional features of this microfluidic device consisted of two large parallel chambers interconnected by a number of small microchannels. This design made it possible to confine the neural cell bodies in one chamber (cell body chamber) while

allowing the axons and processes of neural cells to grow into the neighbouring chamber (axonal chamber) through the interconnecting microchannels (Figure 1.17).

Taylor et al. showed that it was possible to confine the chemical insult to the axonal chamber by regulating the hydrostatic pressure difference between the two chambers. By ensuring that the axonal chamber contained a slightly higher volume of media, they generated a net media flow from chamber housing cell bodies into axonal chamber. The effectiveness of fluidic containment is illustrated in Figure 1.17 (Taylor et al., 2003).

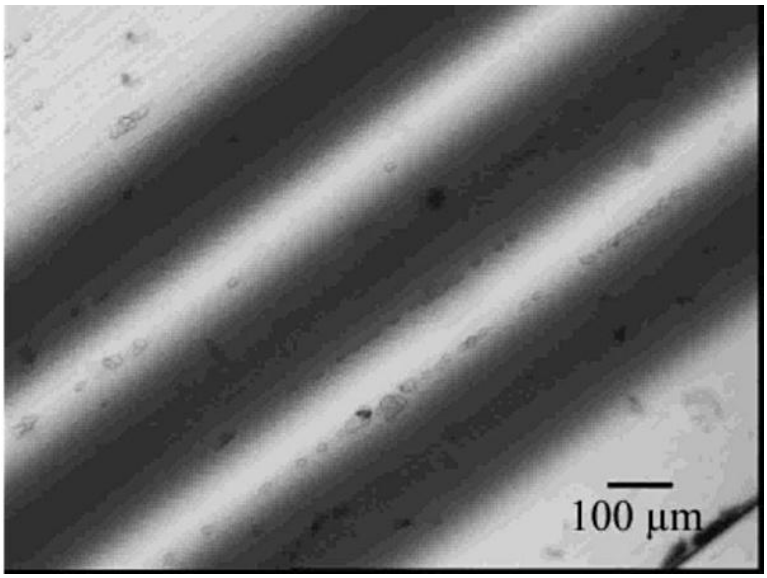


Figure 1.18: An example of laminar flow. The three dark diagonal lines are separate streams of culture media containing tryptan blue. Each stream has originated from one of eight inlet channels upstream (Thiébaud et al., 2002).

Another example of a device capable of confined and controlled exposure of neuronal culture to specific environments was built by Thiebaud et al (Figure 1.18). This device is much more complex and incorporates selective chemical surface modifications and growth media perfusion (Thiébaud et al., 2002). The purpose of this device was to localized delivery of chemicals and pharmaceutical compound to selected areas of cell culture.

Like Taylor's device, this device consisted of a glass substrate and a micro-fabricated PDMS microfluidic device. Rather than utilizing passive difference in hydrostatic pressure, this device uses hydrodynamics and laminar flow to generate chemical gradients as described above (Thiébaud et al., 2002).

PLL was used as a means for cellular attachment to the substrate; however, unlike in Taylor's device, here the substrate was patterned with PLL using μCP. The printed pattern was aligned with the position of the eight perfusion inlets.

This device shows that it is possible to dynamically supply the same cell culture on a common surface with an array of chemical compounds. It is also a good example of integration of surface patterning, micro-fluidics and neuronal cell culture.

1.4.4 μF devices and MEAs

The μF devices can be integrated with other devices such as MEAs to build lab on a chip devices. These devices are capable of performing such functions as: drug delivery (Ziaie et al., 2004), cell culture chambers (Cheng et al., 2008) or cell electroporation and transfections (Odorizzi et al., 2010). The most relevant example of integrating μF devices and MEAs was published by Morin et al. (2006). The aim of their study was to investigate surface patterning of neurons using the channels of μF devices to physically constrain the neurons in a close proximity to the micro-electrodes. Morin et al. were able to record neuronal activity in a number of micro-electrodes and more importantly were able to maintain the viable neuronal cell culture inside the device up to four weeks (Morin et al., 2006).

The integration of the μF device and MEA can also be used for a different purpose. For example Varshney et al. (2007) used μF device integrated MEA for detection of *Escherichia Coli* O157:H7, a leading bacterial pathogen responsible for food borne illnesses. The microelectrodes in this study were used to measure the difference in impedance associated with presence of *E. Coli* in suspension media. The impedance measurements were statistically significant for the *E. Coli* concentrations of over $1.6x10^2$ cfu mL^{-1} in pure culture samples and $1.3x10^3$ cfu mL^{-1} in ground beef samples as compared to controls (Varshney et al., 2007).

1.5 Planned neuro test platform architecture

This chapter has reviewed a number of experiments dealing with surface chemistry, microfluidics and electrophysiology as well integration of these methods with one another. This section will outline the proposed architecture of the neuro test platform which will be used for neuronal cell culture and associated experiments.

The simplest way to construct a multifunctional platform with capability to record electrophysiological data was to use an MEA as the foundation. MEAs, discussed in section 1.3, provided a flat transparent surface suitable for cell culture as well as light microscopy. The flat surface also allowed for integration of other components such as microfluidic devices discussed in section 1.4.

The primary level of control over neuronal network formation can be achieved by patterning the surface of the MEA with cytophilic polymers or proteins. In addition, the surface patterning was also aimed at increasing the amount of electrophysiological data collected by placing the neurons on top of the micro-electrodes. The secondary level of control over the formation of neuronal network was intended to be achieved with the integrated µF device. The µF device perfused with neuronal growth media containing e.g. varying amounts of growth factor supplements was intended allow neuronal growth on select portions of cytophilic surface pattern.

1.5.1 Proposed method of MEA patterning

The compatibility of surface patterning methods with MEAs and µF devices is crucial. The surface patterning technique must have minimal effects on the functionality of other integrated components. Therefore, below is a brief overview of compatibility of reviewed patterning methods with the MEA.

The MEAs are relatively expensive and are designed to be reused after each experiment. Laser ablation or SSR patterning methods are poorly suited to this substrate due to permanency of surface modification. Even though, the top layers of silane can probably be removed with a strong corrosive/oxidizing agent such as hydrofluoric acid (HF) this will likely compromise the fragile micro-electrodes.

The MIMIC technique potentially poses a different problem for the functionality of the proposed device. MIMIC introduces 3D polymer structures onto the surface of the MEA. This method may be incompatible because the 3D structures may disrupt proper functionality or surface adhesion of the microfluidic device.

With regards to inkjet printing, there are two problems with application of this method to printing on the MEAs. First, the minimum feature size achieved by Roth et al. in their study was 350µm. The maximum resolution of this method is limited to 20-50 µm because of statistical limitation posed by variation of droplet trajectory and spreading on the substrate. The higher resolution can be achieved only when additional substrate

modifications are performed (Sirringhaus et al., 2000). Since the MEA dimensions are in order of 10-50 μm, this method would be too imprecise for generating aligned patterned neuronal networks. The second problem is a mechanical one. The commercial MEAs come with a glass culture ring bonded to the circuit board. The dimensions of the culture well are too small to allow the printer head to reach the MEA surface and the electrodes. Ordering the MEAs without a culture ring introduces other problems such as accelerated wear and higher risk of damage due to repeated gluing and removal of the culture ring every time the surface needs to be patterned.

Taking these factors into consideration, the μCP was chosen as the primary surface patterning method. The major advantage of μCP is that it is a relatively simple technique. Once all the silicone processing has been performed the actual patterning of substrates is flexible with regards to printable surface modifiers and if needed can be combined with silane chemistry in order to achieve a more permanent pattern.

1.5.2 The originality of proposed research

To date there has been a large number of devices built through integration of any two of the following: patterned surface chemistry, MEAs or microfluidics. However, there are limited numbers of studies attempting to integrate all three techniques into one device. The study by Morin et al. (2005) does incorporate all three aspects; but, this device had certain problems with regards to even cell distribution and cell nutrient supply. Importantly, the surface patterning was achieved through the physically constraining neuronal growth using the walls of μF device rather than chemical surface patterning (Morin et al., 2005).

This project describes experiments and methodology that were used for integration of patterned neuronal networks, microfluidics and MEAs to fabricate an integrated neurobiological test platform (referred to as “neuro test platform” in the proceeding text). The combination of micro-fluidic gradients and surface patterning potentially provides an additional level of control over the formation of the neuronal network. The integrated MEA provides the means for monitoring the electrical activity (Figure 1.19). This project attempted to improve upon the existing devices by building a multifunctional platform able to perform a combination of experiments related to electrophysiology, electroporation, surface chemistry, microfluidics and tissue culture. As an additional improvement it was attempted to engineer this platform to be re-

usable and compatible with multiple cell types, surface chemistry modification methods and microfluidic device designs.

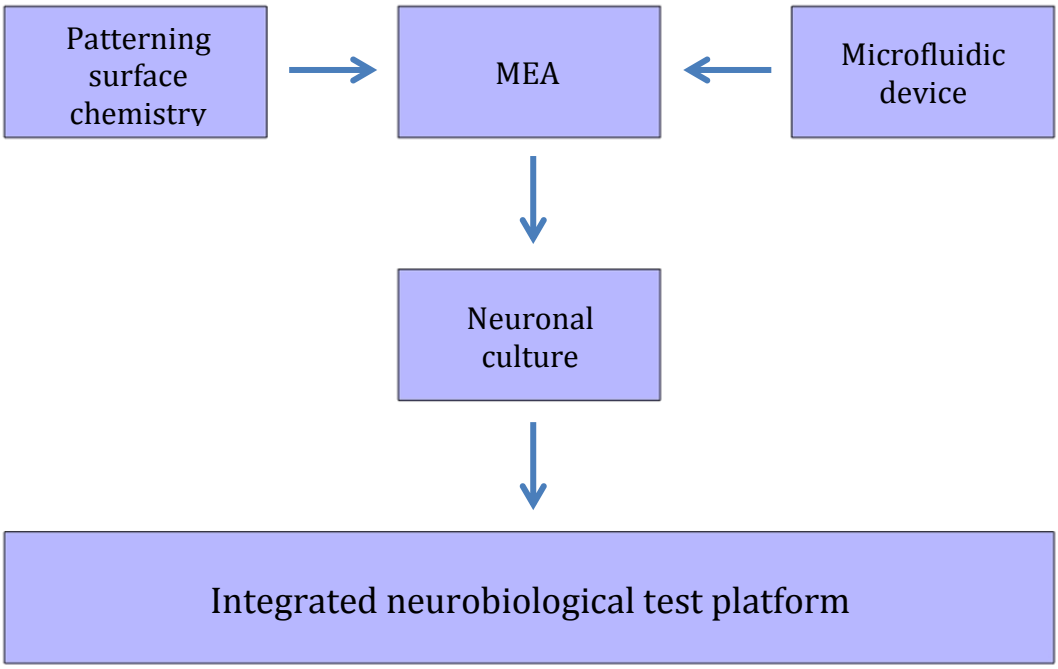


Figure 1.19: Schematic of the relationship between the parts and techniques that make up the integrated test platform. The MEA serves as a foundation for the entire assembly. The patterning of the MEA surface controls the growth of neuronal culture. The addition of the μF device to the MEA serves a dual purpose. First, this allows for perfusion with fresh cell culture media thus ensuring cell survival. Second, the fluidic gradients have the potential to further control the neuronal growth through inhibition or stimulation.

Chapter 2

2.0 General experimental methods

During the course of this research, integration and testing of protocols involving cell culture, surface patterning and microfluidics required in house component fabrication as well as modifications of various existing lab ware. To solve various problems and incompatibilities some protocols were modified or substituted.

The aim of this chapter is to describe the fabrication of various components, associated protocols and protocol modifications. Although the protocols described in this chapter have been previously published, they were used as stepping stones to achieve certain goals. It was also necessary to perform them in order to gain practical experience, understanding of the advantages or shortcomings and an idea of how these protocols can be modified to improve or integrate them with other protocols and devices.

This chapter will also be referenced to in the subsequent chapters.

2.1 Materials & chemical reagents

Tridecafluoro-1,1,2,2-tetrahydrooctyl-1-trichlorosilane (TFOCS) was purchased from Flurochem Ltd. Acetone, Cy3-streptavidin, 1,2 dichloroethane (DCE), hydrogen peroxide solution (30%), isopropanol (IPO), laminin, methanol (MeOH) p-Phenylene diisothiocyanate (PDITC), poly-L-Lysine (PLL), poly-L-lysine FITC (PLL-FITC), sodium dodecyl sulphate (SDS), sodium hydroxide pellets and Tetra-n-butylammonium fluoride (TBAF) were all purchased from Sigma-Aldrich, UK. Chondroitin 4 sulphate (C4S) and polyethylene(imine) (PEI), were all branded "Fluka Analytical" however, purchased from Sigma-Aldrich UK. Dimethylformamide (DMF) was purchased from Fischer Scientific, Ireland. Dymax UV curing adhesive was purchased from ECT Adhesive Solutions, Ireland. Biocompatible double-sided pressure sensitive adhesive tape was purchased from Orafol, Germany. B-27 supplement, Dulbecco's modified eagle medium (DMEM), GlutaMAX, Hank's Balanced Salt Solution (HBSS), L-Glutamine, Neurobasal media were purchased from Invitrogen. NOA 68 UV curing adhesive was purchased from Norland, NJ, USA. Polydimethylsiloxane (PDMS) was purchased from Dow Corning Europe under trademark Sylgard 184. De-ionised water was purified using Elga water purification system (Veolia Water Systems, Ireland). The de-ionised water used throughout had resistivity of 18.2 MΩ·cm. Pyrex substrates and six well polystyrene culture plates were purchased from Corning via Sigma-Aldrich, UK.

Halogenated Ether/Isoflow used for rodent anesthesia was purchased from a veterinary clinic with permission from UCC. To ensure personal safety, the rat anesthesia was carried out inside a glass bell jar located in a biological fume hood in the designated laboratory with permission from the Dept. of Anatomy.

Other hardware required for fabrication of micro-stamps, cell culture and micro-contact printing were machined from poly(methylmethacrylate) (PMMA), polytetrafluoroethylene (PTFE), Nylon or Aluminium in Tyndall mechanical workshop. Greiner 20mL polystyrene sample tubes were used to make the polystyrene culture chambers with a screw on top. The etched silicon masters were fabricated in Tyndall wafer fabrication facility. The micro-electrode arrays (MEAs) used for neuronal electrophysiology and the associated hardware (MEA Kit) were purchased from Multi-Channel Systems GmbH, Reutlingen, Germany. The biocompatible two part epoxy system Epo-Tek 353 ND was purchased from Epoxy Technology Inc. USA. Teflon tubing 0.8 mm inner diameter and 1.6 mm outer diameter was purchased from Dolomite Microfluidics, UK.

2.2 The assembly and integration

The neuro test platform consisted of the following: an MEA, a culture chamber, the reservoir plate and the μF device. Prior to surface patterning or cell culture, the MEAs or other substrates (e.g. Pyrex or Zeonor slides) were modified by attaching a culture chamber. The following section describes the fabrication of these chambers and other associated hardware.

2.2.1 Threaded polystyrene and glass culture chambers

The culture chambers were made from polystyrene or glass. Both types of chambers were threaded and could be sealed using a screw-on lid. The polystyrene culture rings were made by cutting a 2 cm section from the 20 mL sample tube using a saw. Smaller sized glass chambers were made by cutting top sections of small glass bottles using a mini-tome. The polystyrene chambers were 2 cm deep with inner diameter (ID) of 2.1 cm. The glass chambers were smaller and measured 1.8 cm deep with ID of 1.7 cm (Figure 2.1).

The chambers were secured to the substrate using two part bio-compatible epoxy. When using the glass chambers, the epoxy was cured at 90 °C for 30 min. When attaching the plastic chambers, the epoxy cure temperature was lowered to 40 °C and

cure time increased to 1.5 h. The cure temperature was decreased because the difference in thermal expansion between polystyrene and glass caused bond failure during cooling. Note: To avoid having to mix up new batches of epoxy each time, the syringe with uncured epoxy was stored in a freezer at -20 °C for up to three weeks.

The substrates with these chambers were primarily used for experiments that did not specifically require an integrated µF device.

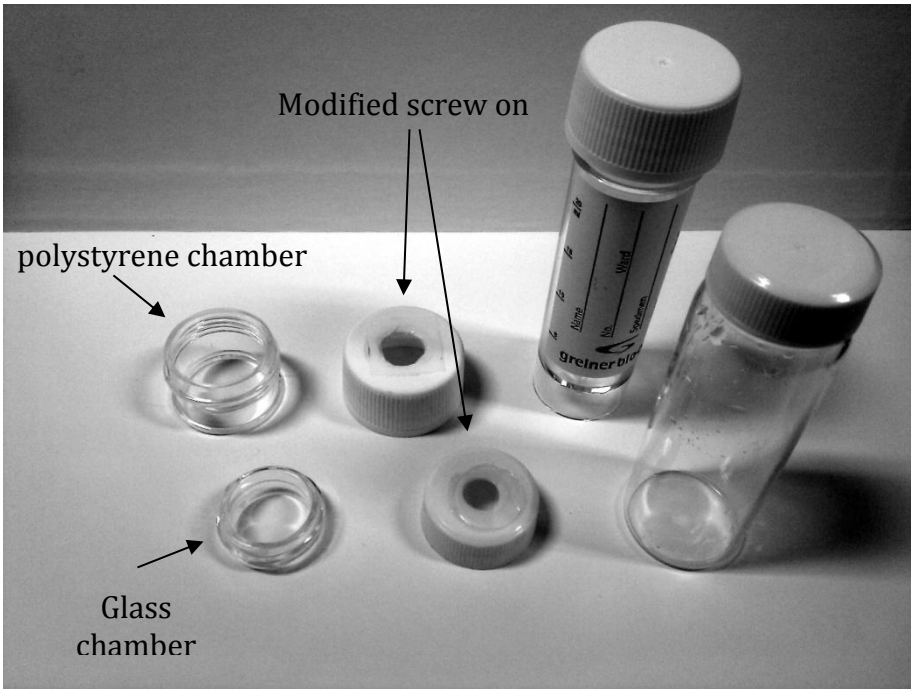


Figure 2.1: Photograph showing the lab-ware used to make the substrate culture chambers.

2.2.2 Modification of screw-on lids

The screw-on lids for the glass and polystyrene chambers were modified to allow phase contrast imaging of the surface when the chambers are sealed (Figure 2.1). A hole of ~5 mm was drilled in the center of the plastic screw on lid. Then a Pyrex coverslip was glued onto the lid using epoxy. The epoxy was cured as described above.

2.2.3 Machined PMMA/Nylon culture chambers

The polystyrene culture chambers described above sometimes had issues with bonding to substrate even after the epoxy cure temperature was reduced. Additionally both types of chambers (Polystyrene/glass) were found to be brittle and were prone to cracking and springing leaks. Hence, using a computer numerical control (CNC) machine, tougher culture rings were fabricated from PMMA or Nylon by a qualified engineer. The custom rings were 5 mm deep with ID of 1.7 cm and OD of 2.3 cm. The

contact patch of the culture ring was calculated to be 1.9 cm^2. The outer dimensions of the custom culture rings were similar to commercial culture rings that were supplied with Multi-Channel Systems MEAs. This similarity ensured that an MEA integrated with these rings could still be used with the MEA kit. Each custom ring featured four equally spaced, threaded openings. These openings allowed other parts to be securely attached to the culture rings via screws. The newly fabricated chambers were first degreased by washing with detergent and DI water. The clean chambers were then lightly sanded with P100 abrasive sheet and exposed to oxygen plasma for 5 min at 900 mTorr and 32 W. Using epoxy or double sided pressure sensitive adhesive tape, the chambers were aligned and attached to the substrate. Note: the plasma treatment step helped with wetting of the surface with epoxy. Without this step the epoxy tended to bead on both surfaces. The epoxy was cured as described above. The substrates with the machined culture chamber could be used for experiments with or without the attached µF device.

a) b)

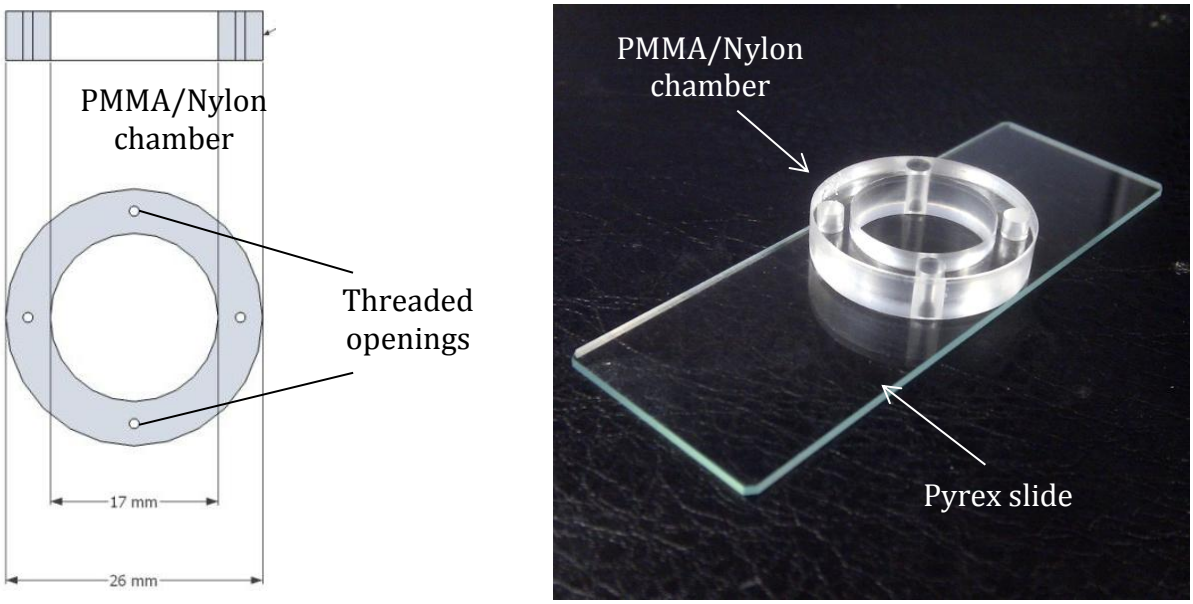


Figure 2.2: a) Schematic showing the basic dimentions of PMMA/Nylong culture chamber.The threaded opening provide a means for securing other parts to the culture chamber and the MEA (see setion 2.2.4).b) The photograph of the PMMA culture chamber bonded to a Pyrex microscope slide.

2.2.4 PMMA media reservoirs

The PMMA media reservoirs were designed to fit the PMMA culture rings shown in Figure 2.1 above. The reservoirs were fabricated by drilling the openings in a square block of PMMA. Their main function was to provide extra volume for culture media

when the µF device was attached (see section 2.4.5.4). The three reservoirs (marked R_{1-3} in Figure 2.3) were 5 mm deep with ID of 7 mm and resultant volume of ~192 µL. The combined volume of all 3 reservoirs adds up to ~576 µL. Additionally this part was also used to clamp the µF device to the substrate. To prevent any liquid leaking from the reservoirs through the joints, adhesive PCR film was used as a gasket.

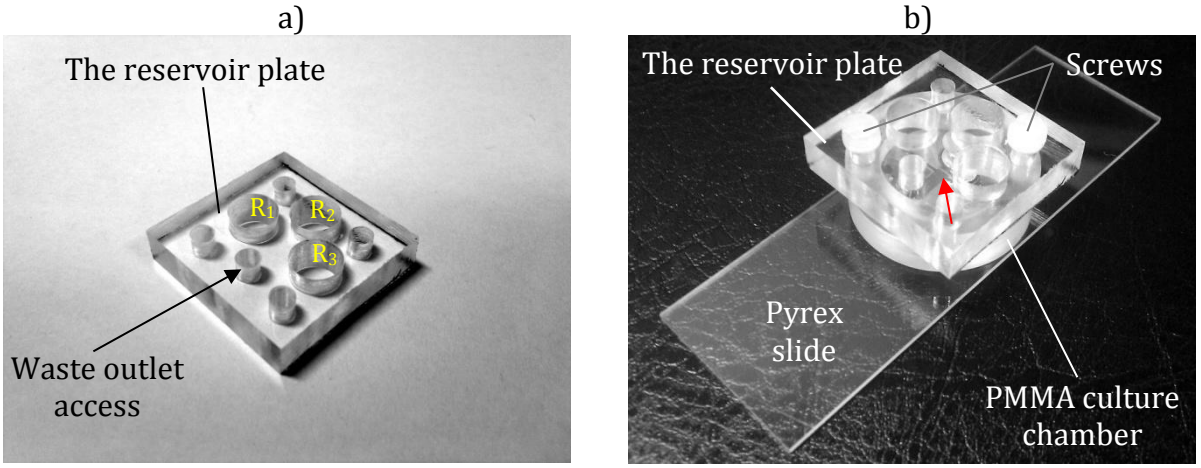


Figure 2.3: a) The PMMA block with drilled reservoirs (R_{1-3}) and waste outlet access. The volume of each reservoir is 192 µL (5 mm deep, 7 mm diameter). b) The reservoir block attached to the PMMA culture chamber (Figure 2.2) on Pyrex substrate. The channels of µF device under the reservoir plate are indicated by the red arrow (see section 2.4.5.4).

2.3 Silicon master fabrication and PDMS Casting

2.3.1 Design of micro-stamps and microfluidic devices

2.3.1.1 Micro-stamps

Four variations of the micro-stamps were designed (Figure 2.4). The basic micro-stamp layout is a square grid of circles interconnected with narrow paths. The dimensions and spacing of micro-stamp features were matched to the 8x8 electrode grid of the commercial MEA. The circles or nodes have a radius of 60µm and are spaced 200 µm centre to centre. The interconnecting lines or paths are of two widths: in Figure 2.4 (a) and (b) they are 10 µm wide, while in (c) and (d) they are 20 µm wide. The main difference between the designs is the additional diagonal paths incorporated into designs (a) and (c). Table 2.1 summarizes the differences between the four stamp layouts. The circular area around the grid was intended to provide additional area for neuronal attachment. The neurons attached to this area were intended to increase the

neuronal population to achieve better conditioning of the culture media (Brewer et al., 1993).

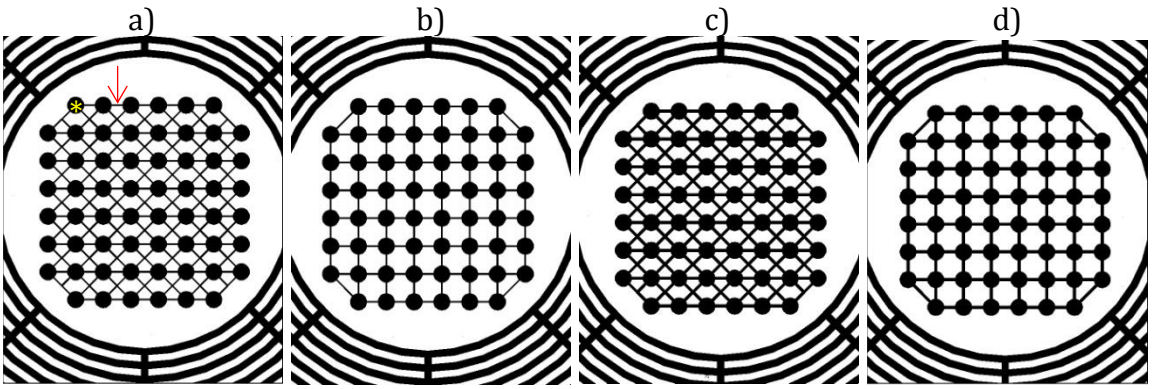


Figure 2.4: The 4 variations of µCP stamp. The designs in (a) and (b) have 60 µm nodes and 10 µm wide paths. The yellow star in (a) indicates the node, the red arrow indicates the path. The designs in (c) and (d) have 60 µm node and 20 µm wide paths. The circular paths around the grid are 50 µm wide. See Table 2.1

Table 2.1: Table listing the design and layout specifications of the µCP stamps.

	Design 1 (a)	**Design 2 (b)**	**Design 3 (c)**	**Design 4 (d)**
Design Layout	Diamond	Square	Diamond	Square
Node diameter	60 µm	60 µm	60 µm	60 µm
Distance between nodes	200 µm	200 µm	200 µm	200 µm
Paths width	10 µm	10 µm	20 µm	20 µm

2.3.1.2 The micro-fluidic device

The µF device was designed to fit the dimensions of the MEA and it features one main channel and two additional inlets (Figure 2.5(a)). The purpose of the main channel is to supply the neuronal culture with culture media. Also this channel provides the volume for generation of the fluidic gradient over the MEA and the neuronal culture. The purpose of side inlets is to introduce media carrying various supplements such as growth factors or inhibitors for example (Massey et al., 2008).

The micro-fluidic device was designed in three variations. The differences in design can be seen in the Figure 2.5(b). Two out of three designs feature a row of square and round pillars extending the width of the main channel. These pillars are as tall as the channels,

hanging from the channel ceiling. The purpose of these pillars was to restrict the neuronal cell bodies to one area of the device while still permitting the axonal growth past these pillars to the rest of the device and over the micro-electrodes. The culture chamber is the area intended for delivery and culture of bulk of the neuronal population. This area will also contain one media supply inlet.

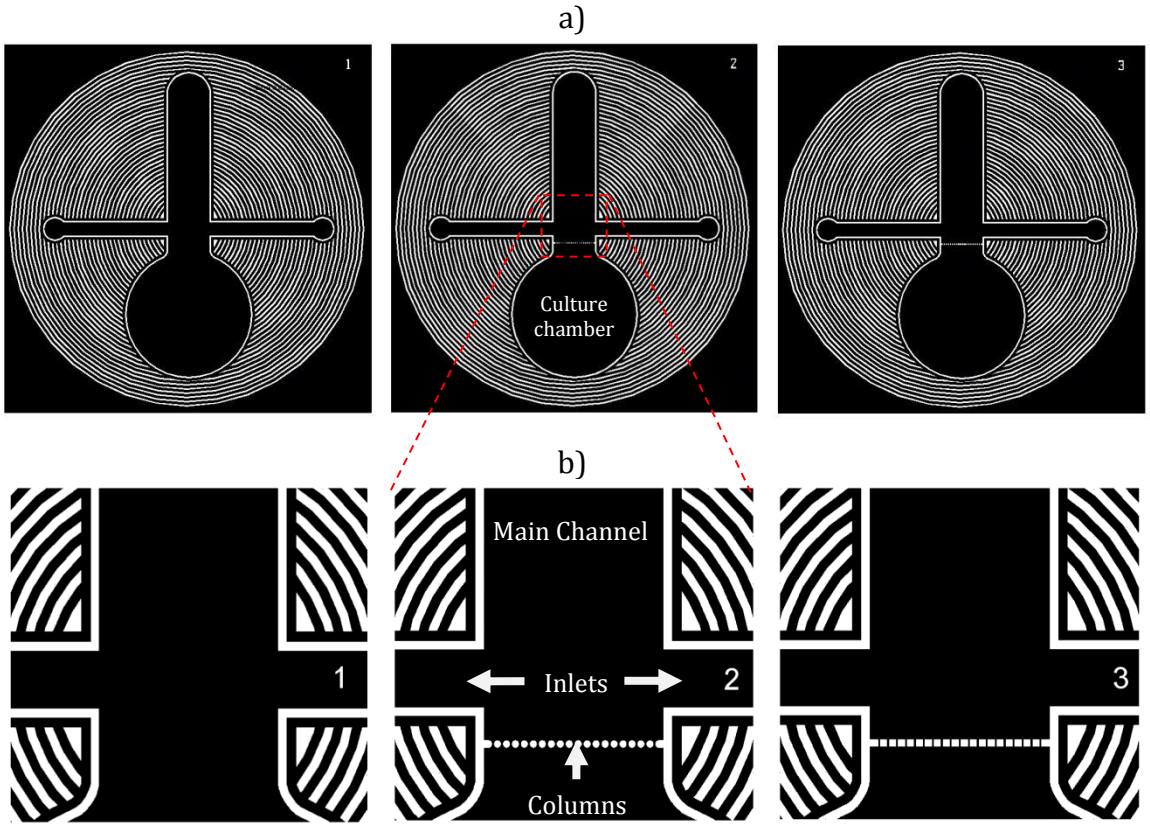


Figure 2.5: a) Three variations of microfluidic device. The main channel is 2000 µm wide. The inlet channels are 600 µm wide. The red dashed square represents the area of the device shown in (b). b) Close-up of the three different design features. The circular columns of design 2 are 100 µm tall and have a diameter of 85 µm. The dimensions of square columns in design 3 are 85 x 85 µm and 100 µm tall. The device is perfused through the two inlet channels as well as through the inlet punched into the ceiling of the culture chamber.

Table 2.2: Table listing the specifications of the three µF device designs seen in Figure 2.5

	µF Design 1	**µF Design 2**	**µF Design 3**
Main channel width	2000 µm	2000 µm	2000 µm
Inlet width	600 µm	600 µm	600 µm
Channel height	100 µm	100 µm	100 µm
Pillars	None	Circular (ø 85 µm)	Square (85 µm^2)

2.3.2 Silicon master fabrication and specifications

The silicon masters for μCP stamps and the microfluidic devices were fabricated in-house fabrication facility. The very first step in this process was the drawing of the concept sketch using Google Sketch Up software. This stage outlined basic dimensions and features of masters to be manufactured. The sketch was then redrawn into a precise set of mask blueprints in AutoCAD by a qualified computer aided design (CAD) technician. The fabrication of masks was outsourced to Compugraphics, UK. Once the masks were fabricated, the silicon masters were fabricated by a qualified engineer via the following steps. A blank, new wafer was cleaned using the standard Radio Corporation of America (RCA) cleaning method. The RCA clean was designed to remove organic, inorganic and metal contaminants from the wafer surface without attacking the silicon itself (Kern, 1970). To define the master features, AZ 9260 resist was applied to the wafer and exposed through a photo-mask. The exposed photoresist was developed using HPRD 402 developer. Using the Bosch process, the wafers were etched to the depth of 10 and 15 μm for the μCP stamps and 100μm for the μF devices. The Bosch process involves a sequence of etch and passivation steps (Laermer and Schilp, 2003). The etch steps were 5 sec long utilizing sulfur hexafluoride (SF_6) plasma followed immediately by 2 sec. passivation with Octafluorocyclobutane (C_4F_8). The depth is controlled by the number of etch-passivation cycles performed. This method allows for creation of high aspect features in silicon crystal. After etch, the remaining photoresist was stripped by a combination of plasma and Piranha solution. All the steps above were performed by a trained silicon fabrication engineers.

2.3.3 Coating masters with release agents

Prior to replica molding of PDMS, the silicon masters were treated with release agent. Two release agents were tested. This procedure ensured clean separation of PDMS from the master.

2.3.3.1 SDS

The coating procedure with SDS was carried out as per protocol described previously (Lauer et al., 2001). SDS proved to be an unreliable release agent because cured PDMS often tore during separation.

2.3.3.2 TFOCS

An alternative treatment of masters involved silanization using TFOCS. This trichlorosilane served as an effective release agent and ensured effortless separation of PDMS from silicon masters of any size. The procedure was carried out as described previously (Li et al., 2007, Qin et al., 2010). Briefly, prior to silanization with TFOCS, the silicon masters were treated with oxygen plasma for 1 min at 32 W and 600-700 mTorr. The masters were then placed into a desiccator that contained lint-free tissue soaked with a drop of TFOCS. The desiccator was evacuated and sealed. The masters were kept in vacuum for 40 min and then used for casting PDMS without any further treatment.

2.3.4 PDMS micro-stamp fabrication

Micro-stamps for μCP were fabricated by casting PDMS against a silicon master as previously described (Lauer et al., 2001). Briefly, a drop of PDMS/hardener mix (10:1) was placed onto one end of a small metal rod inside the plastic holder (Figure 2.6(a)). The masters were then secured above the rod and the PDMS drop. The screw below the metal rod was tightened until the PDMS drop came into contact with the overhanging master. The protocol for PDMS curing was modified to improve the stamp quality. The curing temperature was increased from 70 to 100 °C. The curing time was also increased from 30 min to 1 h as previously reported (Thibault et al., 2007). The fabricated stamps were 3 mm in diameter with surface area of 0.3 cm^2. To increase the number of stamps that can be made by this method, an alternative casting holder was designed and machined from PMMA (Figure 2.6(b)). This holder was used to fabricate six μCP stamps simultaneously.

2.3.5 Fabrication of thin PDMS stamps

The μCP stamps fabricated in section 2.3.4 were relatively thick (~1mm) and prone to excessive deformation when under load. To attempt and solve this issue, thin PDMS stamps were fabricated as follows. First, Pyrex coverslips were glued onto the narrowed end of a machined aluminium cylinder using epoxy. The epoxy was cured in an oven at 80 °C for 1 h. After the epoxy cured, a drop of pre-polymerized PDMS was placed onto the surface of the master. The master was then placed into a desiccator to remove any air bubbles from PDMS. The aluminium cylinder with the Pyrex coverslip was then gently pressed down onto the PDMS and silicon master ensuring that no air bubbles got trapped between the two surfaces. The assembly was then transferred into an oven. The

PDMS was cured at 100 °C for 1 h. Once cured, a scalpel blade was used to carefully separate the silicon master from the thin μCP stamp (Figure 2.7).

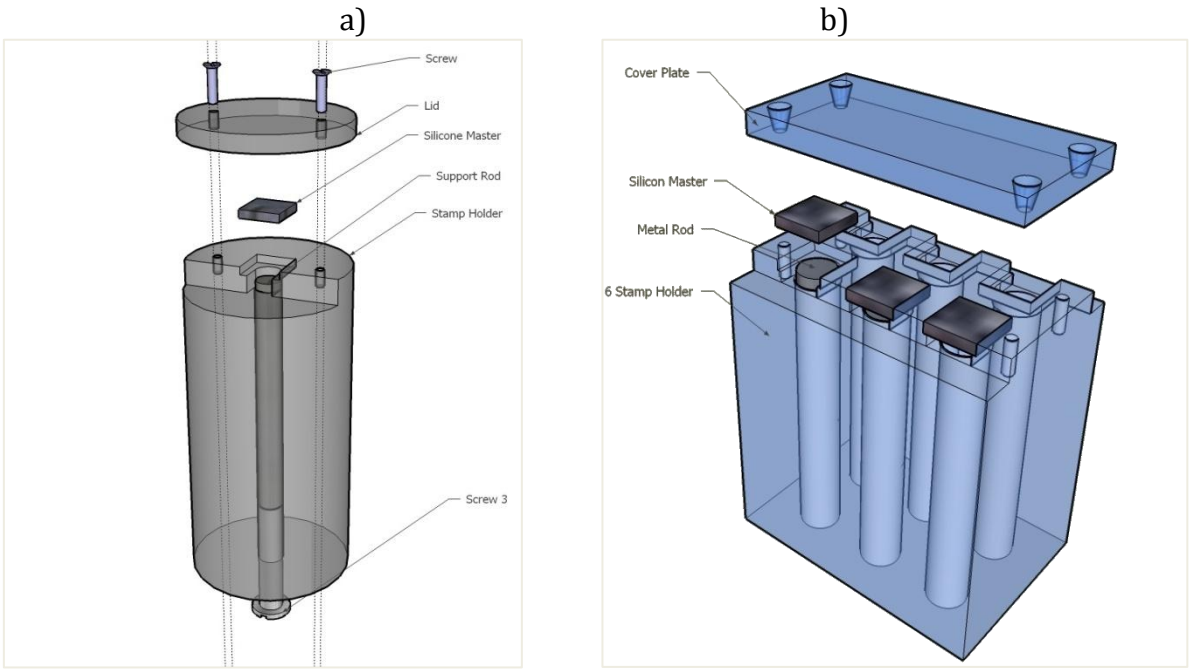


Figure 2.6: The parts used to cast the PDMS against the master to produce a micro-stamp. a) The old, single stamp casting holder as described in (Lauer et al., 2001). b) The newer 6 stamp casting holder. This machined device significantly reduced the amount of time required for making multiple micro-stamps. (Note: Silicon masters are 5 mm² x 1 mm).

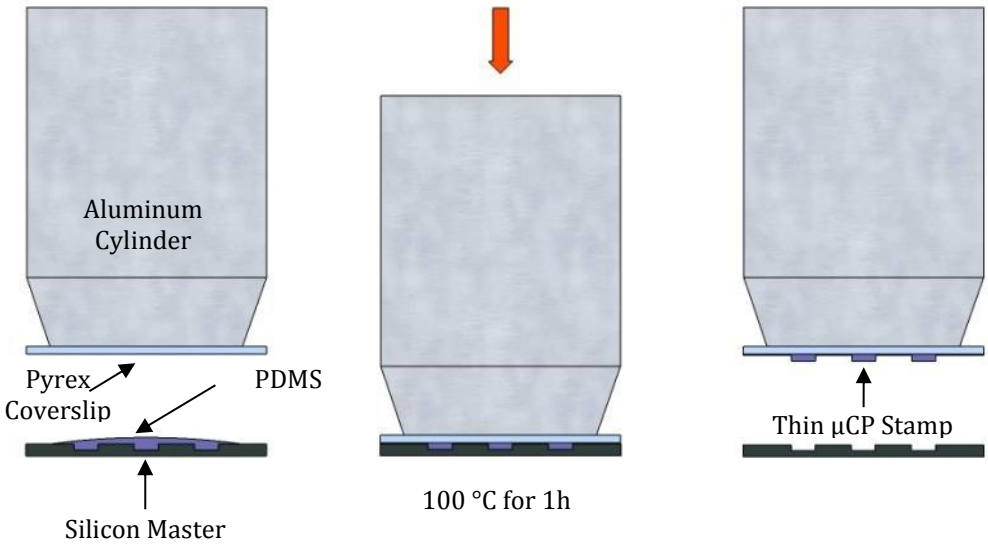


Figure 2.7: Schematic diagram showing the basic steps of fabrication of thin PDMS stamps.

2.3.6 Master post treatment

On occasion, PDMS debris needed to be removed from the silicon master after a failed casting step. The masters were simply soaked in 1:14 solution of TBAF and DMF for approximately 1 h. Then, the masters were rinsed three times with fresh DMF followed by rinse with methanol. If PDMS debris remained, the procedure was repeated (Lee et al., 2003).

2.4 Fabrication and assembly of microfluidic devices

2.4.1 The replica molding of µF device

The masters for the µF devices were designed and fabricated in house using photolithography (See section 2.2 above). The silicon wafer was etched to the depth of 100 µm. After silicon wafer processing, the wafer was diced in-house into individual 2cm^2 silicon masters. Similarly to fabrication of µCP stamps, prior to replica molding, the silicon masters were silanized with TFOCS as described in section 2.2.1. Following the silanization, the master was glued onto a microscope slide using a drop of PDMS. A hollow metal cylinder of 1.7 cm ID was then visually aligned and carefully placed on the silicon master. The cylinder was secured to the master and the glass slide using the metal stationery clamps (Figure 2.8). Once the casting cylinder was secured to the master, a small volume of pre-polymer PDMS mix was poured onto the surface of the master. The entire assembly was then degassed. Care was taken to control the degree of vacuum in the chamber to avoid PDMS boiling over the rim of the casting cylinder into the vacuum chamber. Once the PDMS was degassed, PDMS was cured at 100 °C for 1 h. The assembly was then removed from the oven and cooled using an air gun. Using a scalpel, the cured PDMS was carefully separated from the wall of the metal cylinder. The cylinder was then removed, and the µF device peeled off the silicon master. Note: the diameter of the metal cylinder ensured that the µF device could fit inside the culture chambers if required. The µF devices fabricated via this method were used for characterization of µF gradients (section 3.2.6).

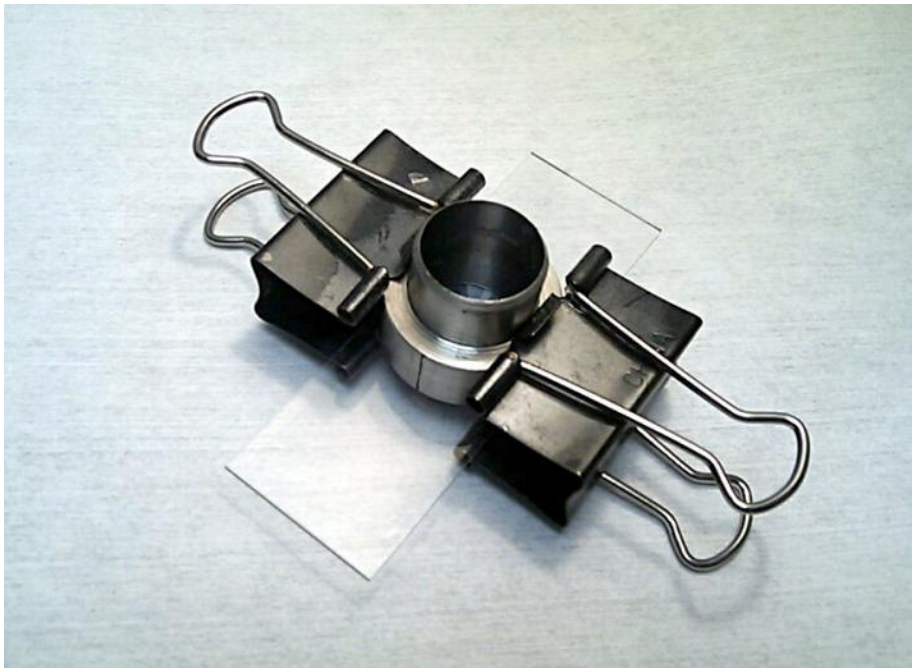


Figure 2.8: An image of μF device replica molding assembly. Assembly consists of a Pyrex microscope slide, two metal clamps, a silicon master and the metal cylinder.

2.4.2 Flat top μF devices

The μF devices fabricated as described in the above section had a number of undesirable features. First, the μF devices ranged in mass and dimensions; some were too thick and were prone to tearing when punching the channel inlets. The other fault was the meniscus created by PDMS surface tension. The curved surface created problems when filling the μF devices with solutions. The concave caused the drops of liquid to pool in the center of the μF device rather than remain over the channel inlets.

Thus, to solve the above problems, the metal cylinder was replaced with a PMMA or Nylon culture chambers shown in Figure 2.2. The flat μF device was cast in two stages (Figure 2.9 (1-6)). The first stage was similar to the method described in section 2.4.1. However, in this case the PMMA/Nylon culture chambers were used instead of the metal cylinder. The PMMA culture chamber was clamped to the master using metal clamps; a small volume of PDMS was then poured onto the master and degassed. The volume of PDMS poured onto the master was just enough to cover the entire master inside the PMMA ring borders. Once PDMS was free from air bubbles, the assembly was placed in the oven at 90 °C for 1 h. The temperature was reduced in these casting experiments to avoid the PMMA reaching its glass transition temperature.

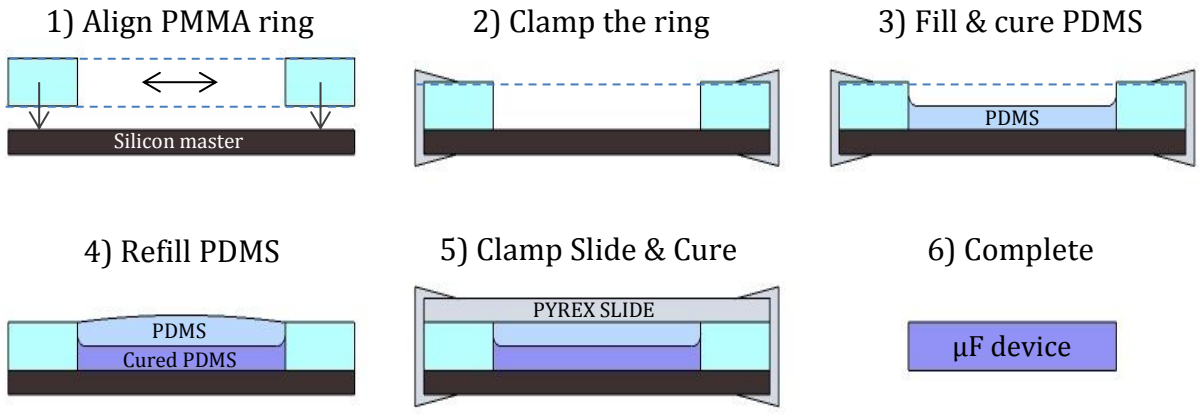


Figure 2.9: The schematic representing the basic steps involved in fabrication of flat µF devices. The fabrication involves two stages. Stage #1 is represented by steps 1-3. Stage #2 is represented by steps 4-6.

After 1 h at 90 °C, the assembly was removed from the oven and cooled on a bench. Once cool, the metal clamps were carefully removed and put aside. The degassing often resulted in PDMS boiling over onto the rim of the PMMA ring. Using an edge of the glass slide, cured PDMS was removed from the rim of the culture chamber. Care was taken not to separate the cured PDMS from the master at this stage. Following this, pre-polymerized PDMS was poured on top of cured PDMS inside the PMMA ring and degassed again. It was important to ensure that the PDMS meniscus rose slightly over the PMMA rim as this prevented trapping of air bubbles during the next stage of fabrication. After degassing, the PDMS volume was topped up if required. A clean Pyrex slide was then carefully placed on top of the PMMA ring by lowering it from one side. It was critical to ensure that no air bubbles got trapped in PDMS when lowering the slide. The Pyrex slide was let settle for a few minutes and then clamped onto the assembly using the metal clamps. The entire assembly was then placed back into the oven for 1 h at 90 °C. After the PDMS cured, the assembly was cooled and disassembled. To ensure adequate PDMS cure, the µF device was post-cured at 100 °C for 1 h on a hotplate (Figure 2.9 (4-6)).

2.4.3 Fabrication of µF devices from µCP silicon masters

As described in section 1.3.4, the features of µCP stamps were designed to align with each micro-electrode on the MEA. To save time, design and fabrication costs the µF device for patterning was fabricated by making a direct copy of the µCP silicon master.

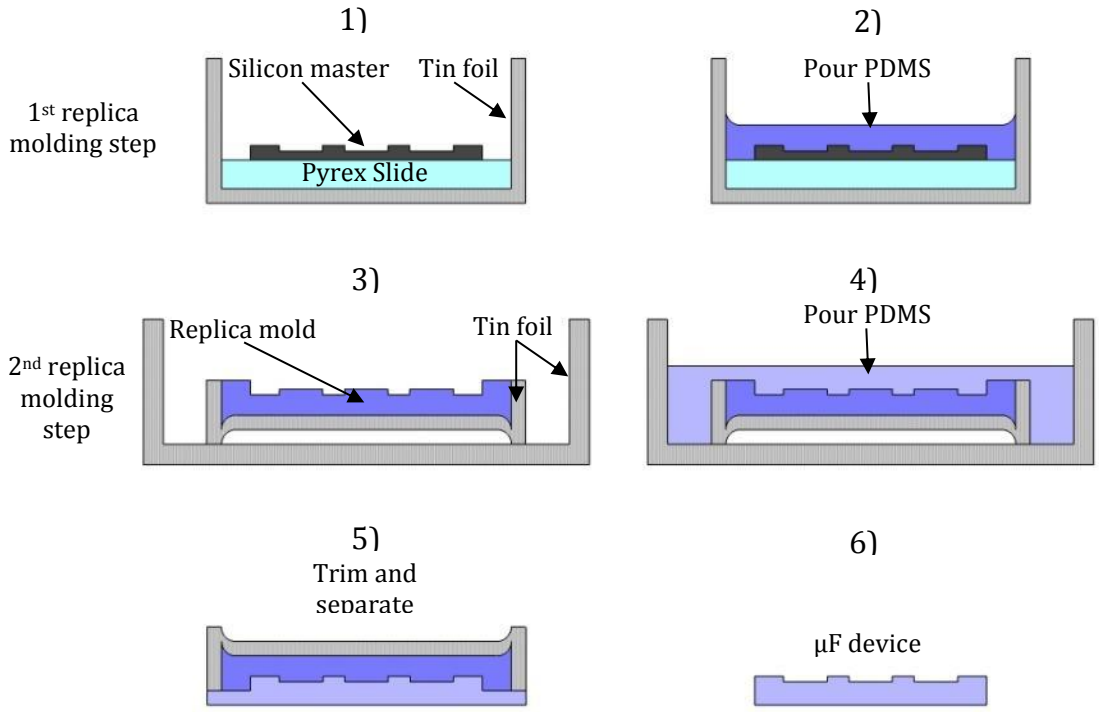


Figure 2.10: Basic schematic of fabrication of the μF devices using PDMS masters. 1) A silicon master was placed onto a Pyrex slide partially wrapped with tin foil. 2) 1st replica molding step. 3) A cured replica mold wrapped in tin foil. 4) The second replica molding step. 5) After PDMS is cured, the excess is trimmed using a razor blade and the mold is separated. 6) The fabricated μF device, a direct copy of silicon master.

In order to fabricate μF devices from the μCP masters, the replica molding was performed twice. The first step involved replica molding PDMS against the silicon master, essentially fabricating a μCP stamp. The second step involved replica molding PDMS against the μCP stamp fabricated in the first step. The final result of two molding steps was a direct copy of the silicon master. (Note: the first molding step produces a negative copy). TFOCS silicone masters were placed on a Pyrex slide inside a simple tinfoil container. The PDMS was then poured onto the masters, degassed and cured at 100 °C for 1 h. After an hour in the oven, the cured PDMS was peeled of the masters and trimmed to size. The newly cured replica molds were then placed into 10% solution of SDS in DI water for 10 min. After SDS soak, the molds were immediately dried with an air gun. SDS was used to aid with PDMS release after the next replica molding stage. The new PDMS masters were then wrapped in tinfoil, covering the back and the vertical walls. The tin foil wrapping was then trimmed with a razor blade, exposing master relief features. This ensured that the borders of the master could be seen after the second casting step. The tin foil allowed to distinguish between the PDMS master and the μF device. The PDMS master was then placed into another small tinfoil container, covered

with pre-polymerized PDMS, degassed and cured at 100 °C for 1 h. Once PDMS was cured, a scalpel was used to gently separate the newly cured PDMS from the master's borders. Then the PDMS master and the PDMS µF device were gently peeled apart (Figure 2.10).

2.4.4 Aligning µF devices to the substrates

The µF devices fabricated in section 2.3.2 are negative copies of µCP stamps, thus; also require alignment to the micro-electrodes prior to surface patterning. An old, in-house built MEA-computer interface was disassembled and repurposed to serve as a bench-top aligner for the µF devices (Figure 2.11). The alignment set up was relatively simple and consisted of a rectangular base and lid with an opening in the centre. When the setup was assembled, the lid was held up by coil springs positioned around four guide pins. The setup was placed under a microscope; the µF device was placed onto the fixed stage of the base, with the MEA hanging overhead, facing the µF device. The MEA was lowered until its surface was ~1 mm from the µF device. The MEA was then visually aligned with the µF device through the microscope. Once aligned, it was carefully lowered until in contact with the µF device.

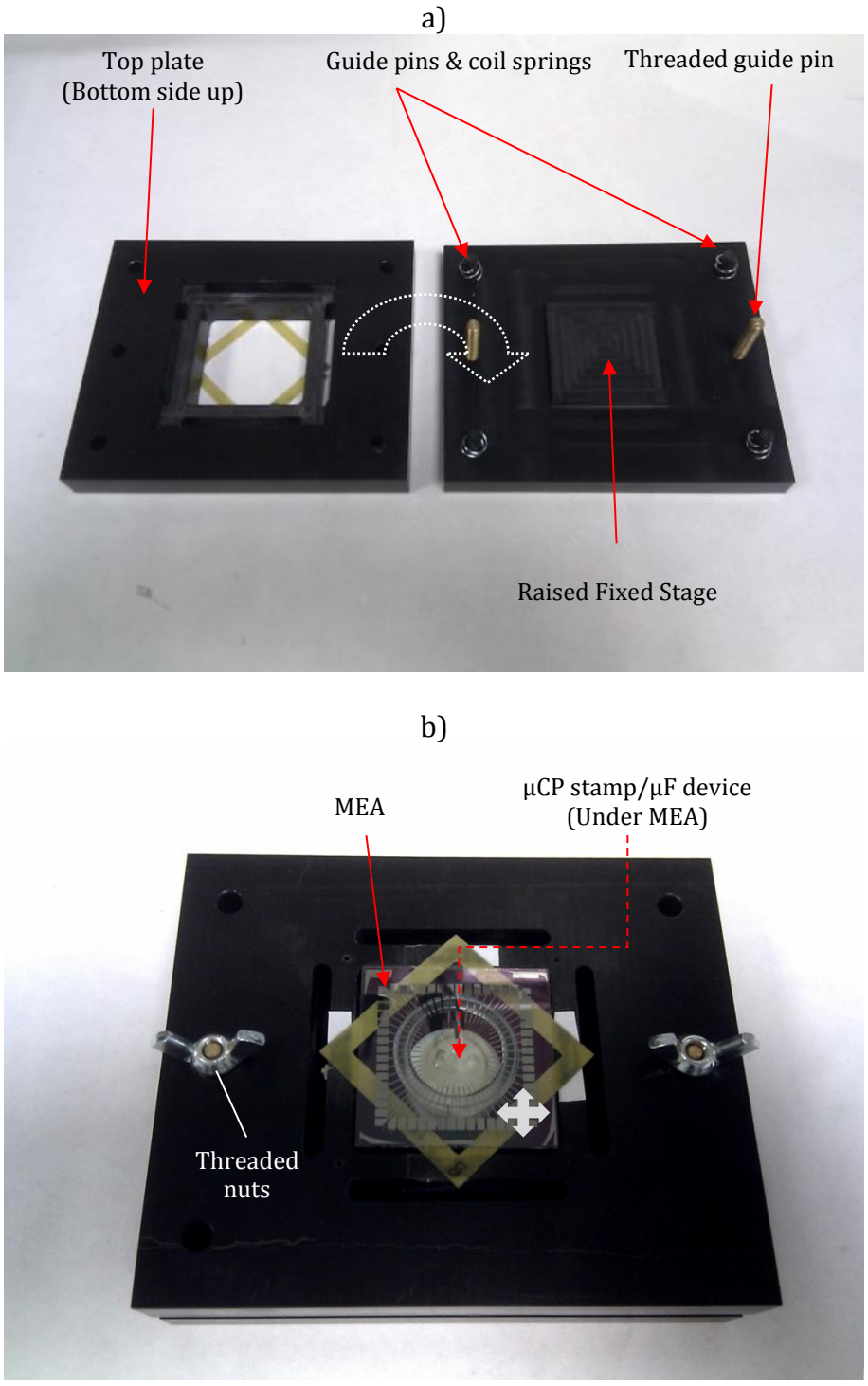


Figure 2.11: a) Photograph of disassembled, repurposed MEA-computer interface. The top plate is held over the raised stage by 4 coil springs located at each of the alignment pins. b) The assembled set up. Once the MEA is aligned with the μF device below it, the two nuts are tightened until the MEA comes into contact with the device. The white quad arrow represents the alignment of the MEA.

2.4.5 Methods of bonding the μF device to the surface

To find a suitable technique for integrating μF devices with MEAs, four methods of μF device attachment have been tested. The requirements included high bond strengths to allow manual handling as well as connection/disconnecting perfusion tubes. Specifically, in cases of patterned substrates or patterned MEAs, the bond had to be strong and simultaneously reversible to avoid damaging the MEA or the printed patterns.

2.4.5.1 Contact adhesion

This is the simplest method for temporary PDMS attachment. It involves placing the cured PDMS component on to the surface and gently pressing it down (Taylor et al., 2005). This method was used for MEA patterning via μF devices fabricated in section 2.4.3.

2.4.5.2 Plasma treatment

The μF devices were permanently plasma bonded to the substrates (Duffy et al., 1999). Briefly, the μF device and the substrate (MEA/Pyrex) were placed inside the oxygen plasma etcher and exposed to plasma for 30 sec at 900-950 mTorr and 32 W. After plasma treatment the μF device and the Pyrex substrate were brought into contact and bonded together by applying gentle pressure.

2.4.5.3 UV curable adhesives

It was attempted to bond PDMS to substrates using Dymax and NOA 68 UV adhesives. These adhesives are soluble in acetone and may be suitable for reversible attachment of μF devices. The procedure was carried out as follows; a drop of NOA 68 UV adhesive or Dymax UV adhesive was placed onto a Pyrex slide. A second Pyrex slide was used to spread the drop on the slide surface as evenly as possible creating a thin layer. After spreading the adhesive, the slide was left on a workbench for a few minutes to allow the adhesive to flow and even out. Then the μF device was carefully brought into contact with the thin layer of adhesive, removed and attached to the substrate surface. The UV adhesive was cured under a powerful UV lamp for 20 minutes. This method was used with cell culture experiments, but it proved unreliable because of bond failure after prolonged exposure to cell culture media.

2.4.5.4 Mechanical force

A method was devised where the µF device was temporarily clamped to the surface using mechanical force. This method required the use of flat top µF devices fabricated via the protocol described in section 2.2.1. To clamp the µF to the surface, first the PMMA/Nylon culture chamber was aligned and attached to the surface as described in section 2.1.1. The prefabricated µF device was then snugly inserted into culture ring and gently pushed down onto the surface. To clamp the µF device, the reservoir block (see section 2.2.4) was attached to the PMMA ring with four screws. Note: it was sometimes necessary to reduce the height of the PMMA ring to have a good seal between the surfaces and the µF device. This was achieved by sanding down the PMMA ring against a P100 abrasive sheet on a flat surface. This protocol was used for experiments requiring long term perfusion of the µF devices and cell cultures on patterned and non-patterned substrates.

2.5 Gravity driven passive perfusion device

Perfusion of µF devices can be achieved via motorized, electrically powered syringe or peristaltic pumps. These types of pumps are relatively large in comparison to the µF devices. To try and address this issue, an alternative, passive, gravity driven pump was built. A similar method of perfusion has been shown to work previously (Zhu et al., 2004). This device functioned on the principle of equalization of hydrostatic pressure. The difference in pressure was achieved by locating the source fluid reservoirs higher than the waste reservoir. There have been a number of publications detailing devices that work on this principle (see section 1.4.2).

The perfusion device for this project was made from a solid block of PMMA measuring 55 x 35 x 35 mm. The three cylindrical reservoirs (two supply and one waste) measured 20 mm long with ID of 5 mm. The reservoirs were made by simply drilling into PMMA block to the required depth. The two supply reservoirs were placed at the same distance from the top of the device, while the waste reservoir was placed 1-2 mm lower (Figure 2.12).

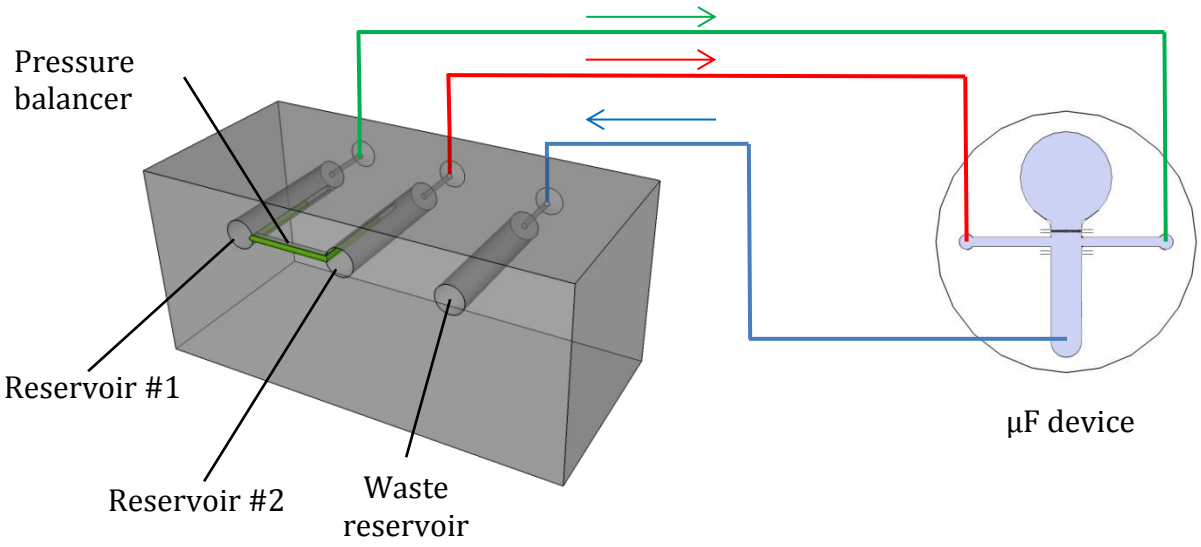


Figure 2.12: A schematic µF device perfusion using gravity. The reservoirs pictured are 5mm in diameter and 25mm long. The outlets are ~1 mm in diameter and 10 mm long. The coloured lines represent the Teflon tubing connecting the reservoirs with µF device inlets and waste outlet (see section 2.3.1). The coloured arrows represent the direction of fluid flow generated by difference of hydrostatic pressure between the reservoirs #1, 2 and the waste reservoir.

In addition, due to inevitable variation between the heights of the supply reservoirs with respect to each other, a pressure balancer was also integrated. The pressure balancer was made from a blunted G21 hypodermic syringe needle. To remove the leur, first the needle was scored then broken. This method ensured that the ends of the needle remained open. The drawback to the pressure balancer is that if there is a need to perfuse the µF device with liquid containing two different substances, eventually traces of one substance will start to appear in the other reservoir. The reservoir outlets were drilled using a 1.5 mm drill bit.

The reservoir block was then connected to the µF device using Teflon tubing with ID of 0.8 mm and OD of 1.6 mm. To ensure that there were no leaks, the ends of Teflon tubing were tapered. This was achieved by heating and gently pulling the tubes. The horizontal orientation of the reservoirs made the volumetric flow rate independent of volume. This orientation also ensured that the hydraulic balance was never reached and the only way that the perfusion would cease is either because the source reservoirs were empty or the waste reservoir was full.

2.6 Passive, vacuum driven filling of the µF channels

Vacuum driven filling of µF device was carried out as previously described (Cira et al., 2012). Briefly, two small inlets were punched into PDMS µF device using a 30G needle. The µF device was attached to a substrate and placed into a vacuum for 5 minutes. Immediately after vacuum exposure, two small drops of PDL, PEI or PDL-fibronectin solution were placed onto each inlet effectively blocking the access of air into the channels. This generated low pressure inside the channels as air was being drawn into the bulk of PDMS. As the pressure in the channels decreased, the drops of liquid were forced into the channels via ambient air pressure. This method was used for filling the relatively small µF devices, such as the ones used for µF patterning.

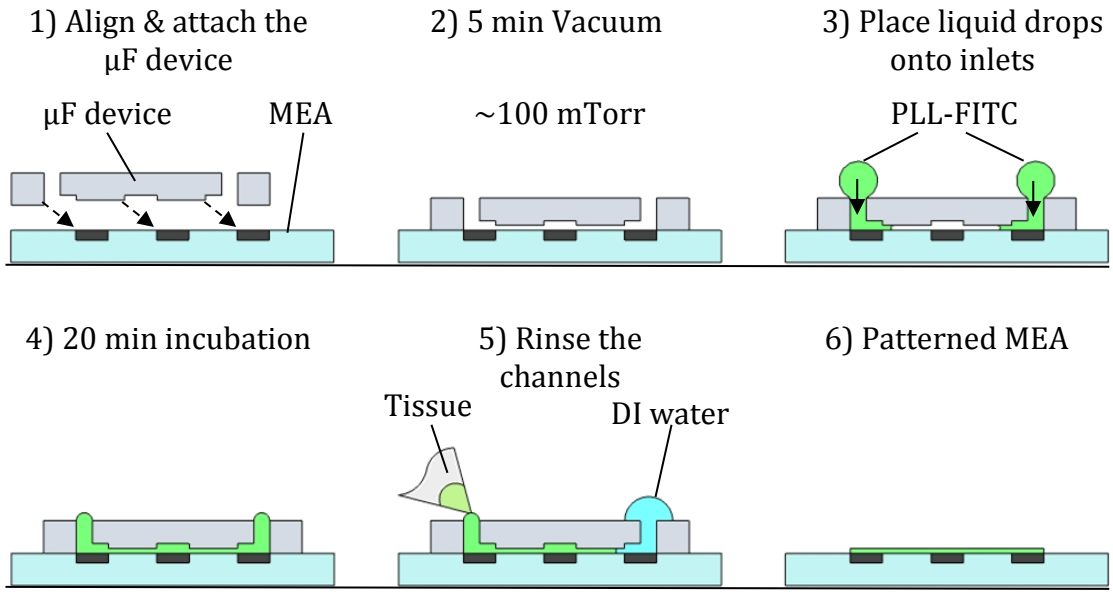


Figure 2.13: The schematic representing the basic steps of MEA patterning using an aligned µF device.

2.7 Cell Culture Protocols

2.7.1 Culturing of rat embryo cortical and spinal cord neurons

The neural cells were harvested from either the cortex or the spinal cord of Sprague Dawley rat embryos. The ages of the embryos used were: E12 (used once), E13 (used once), E14 (used regularly), E15 (used once), E18 (used 5-6 times) and E20 (used once). The neuronal tissue was acquired as described elsewhere (Streit et al., 2001). Briefly, a pregnant Sprague Dawley rat was anesthetized by inhalation of halogenated ether

vapor in a bell jar situated inside a biological fume hood. A tail pinch and an eye rub tests were performed to ensure that the rat was unresponsive and did not feel pain. The rat was then killed by decapitation and the embryos were extracted via a cesarean section. The embryo neuronal tissue was dissected under a microscope and suspended in sterile HBSS prior to dissociation. In cases when the tissue had to remain un-dissociated for more than 30 min, it was suspended in cool Neurobasal media instead of HBSS. To dissociate the nervous tissue, it was incubated in 5 mL of trypsin at 37 °C for 5 min. To stop the action of trypsin, 500 µL of trypsin inhibitor or 500 µL of FBS was added to the tissue suspension. The tissue was dissociated by trituration using a P1000 Gilson pipette. Following the trituration the cell suspension was spun in a centrifuge (Eppendorf 5810) for 5 min at 1100 rpm to separate the neuronal cells from the trypsin solution. After the spin, the supernatant was discarded and replaced with 1 mL of Neurobasal media. The pellet was gently triturated again for few minutes to re-suspend the cells in fresh media. To determine the cell count, 10 µL of the cell suspension was added to 990 µL of fresh Neurobasal media and gently mixed, creating a 1/100 dilution. Then 10 µL of 1/100 dilution was pipetted onto a haemocytometer and the cells were counted.

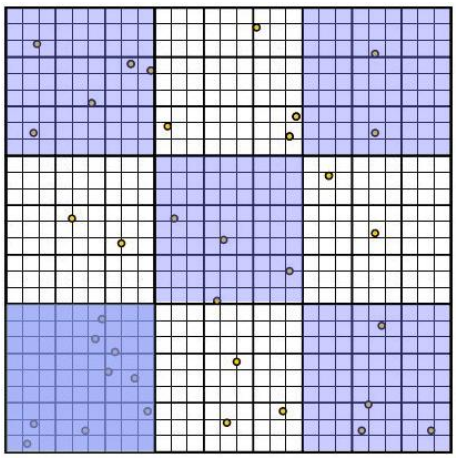


Figure 2.14: An illustration of the hemocytometer grid. The blue areas represent the areas that were used for counting cells. Yellow dots represent the cells.

The cells that were situated on the borders between the blue and white squares were not counted. The number of cells in the 1 mL of media suspension was determined by inserting the cell count into the following formula:

$$(Count/5) * (Dilution)*(1x10^4) = \#\ cells\ mL^{-1}.$$

Where, "Count/5" yields and average number of cells counted in each field. The "Dilution" adjusts the average cell count for the 1/100 dilution (10 µl in 990µl); hence the average cell count is multiplied by 100. Lastly, each large square area of the hemocytometer represents a volume of 100 nL, where multiplication by the "$1x10^4$" yields an average number of cells per 1000 µl (Figure 2.14). Neurons were plated at a density of $1*10^5$, $2*10^5$, $1*10^6$ and $2*10^6$ cells cm^{-2} in Neurobasal media supplemented with 7.5 µL mL^{-1} B 27, 10 µL mL^{-1} L-Glutamine, and 10 µL mL^{-1} Pen/Strep. The best plating density was determined to be between $1*10^5$-$1*10^6$ cells cm^{-2}.

2.7.2 Culturing protocol modification

To improve long term neuronal viability, the protocol in section 2.5.1 was modified as follows. Trypsin treatment was reduced from 5 min to 3 min to reduce possible negative effects of trypsinization on cell membrane and viability (Huang et al., 2010). L-Glutamine was entirely replaced with 10 µL mL^{-1} GlutaMAX. Removing L-Glutamine from culture was intended to reduce cytotoxic ammonia ion buildup due to its degradation (Invitrogen, 2013). Pen/Strep solution was only added to the 1 mL of cell suspension after dissociation, and was omitted from seeded cultures. The concentration of B27 was increased to 20 µL mL^{-1} (2%). In addition to increased concentration of B27, the culture media was supplemented with 10% FBS/FCS. Note: The addition of FBC/FCS also results in differentiation of part of neuronal population into glial cells (Ye and Sontheimer, 1998), as well as increased long term neuronal viability.

The specific culture protocol modifications are summarized by the Table 2.3 below.

Table 2.3: Table summarizing the modifications of neuronal culture protocol

Black=original concentration. Red=new, reduced concentration. Blue=new, increased concentration.

Protocol modifications	Media	B27 (µl mL^{-1})	L-Glutamine (µl mL^{-1})	Pen/Strep (µl mL^{-1})	GlutaMAX (µl mL^{-1})	FBS/FCS (%)	Trypsin (min)
1	Neurobasal	7.5	10	20	0	0	5
2	Neurobasal	7.5	5	20	2.5	0	5
3	Neurobasal	20	0	0	10	10	3

2.8 Electrophysiology

The electrophysiological recordings were performed using the Multi-Channel Systems MEA1600 Kit. First, the MEA Kit hotplate was preheated to 37 °C. Then, the MEA containing a 14 day in vitro (DIV) neuronal culture was placed onto the preheated hotplate and connected to the amplifier. The MEA was then grounded by designating the large "Ref" electrode as ground using MEA Select software. Alternatively, if the MEA did not have a large "Ref" electrode, a grounded Ag/AgCl wire was inserted directly into culture media (Figure 2.15). The sampling rate was set to 20 kHz. The recording was controlled and monitored in real time using MC rack software.

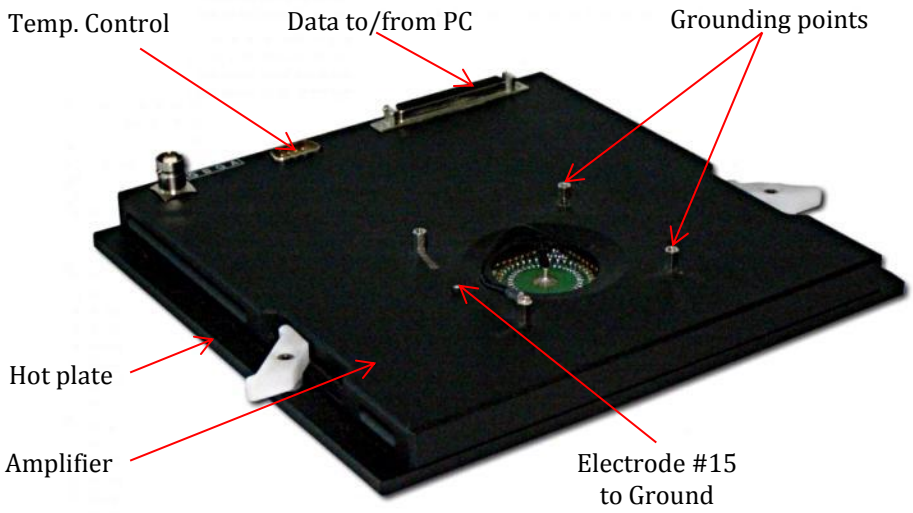


Figure 2.15: A photograph of Multi-Channel Systems MEA amplifier. Electrode #15 can be connected directly to ground using one of the grounding points (Multi-Channel-Systems, 2012).

In order to detect individual APs of the recorded signals, the MC Rack "spike sorter" tool was used. This digital tool allows the user to specify criteria that fits the observed AP. The tool provides two options for detection of APs, the first option is the detection using set threshold potential value, the second is more sophisticated and takes into account the minimum and maximum slopes of the AP signal as well as potential change (*-dV*). The detection using the first option requires a steady baseline, hence could only be performed in conjunction with the high pass filter set at 200 Hz. The second option was used for filtered and non-filtered signals. The criteria for this AP detection method were set as follows: minimum slope = -0.1, maximum slope = 0.9. The *-dV* criterion could only

be set after the visual examination of the signal. This criterion generally varied between -25 µV and -55 µV. It is important to note that any signal manipulation, such as filtering, was done off line. In addition to digital filtering, to reduce noise and mains hum (50 Hz noise); a small faraday cage was built to fit over the MEA during the recording session. The faraday cage consisted of a cardboard cylinder capped at one end by a plastic (polystyrene), circular lid. The entire cage was wrapped in aluminum foil and grounded using a woven cable.

2.9 MEA surface cleaning

2.9.1 Post tissue culture clean

Since the MEAs were recycled after each cell culture experiment it was important to clean the surface well to avoid contamination, infection, poor cell adhesion and noisy recordings. First, the MEAs were soaked in trypsin preheated to 37 °C for 5 min to remove any neurons still attached to the surface. After trypsin the MEAs were rinsed with water, isopropanol and 70% ethanol.

2.9.2 Removing PDMS residue from MEA surface

During µCP of the MEA surface, it was often observed that the MEA surface became fouled with PDMS residue (see section 3.2.4). In order to clean the surface and get rid of the PDMS contamination, the MEA surface was soaked in 1:14 solution of TBAF in DMF for 30 minutes at RT. The effectiveness of TBAF for dissolving PDMS was previously suggested elsewhere (Schnyder et al., 2003). After the soak, the MEA was rinsed with DMF, followed by a rinse with DCE, methanol, isopropanol and 70% ethanol. This procedure was repeated if necessary.

2.9.3 Removing silica (SiO_2) from MEA surface

The surface of the PDMS contaminant sometime oxidized to produce a thin layer of silica (SiO_2). The silica appeared as crystalline layer on the MEA surface resembling the pattern of the PDMS stamp. Once the PDMS oxidized and formed silica, the TBAF soak became ineffective because the PDMS was essentially masked. Hence in order to remove the masking layer of silica, the MEAs were suspended inside a beaker partially filled with hot NaOH solution and boiled for 30 min. After NaOH, the MEAs were rinsed with large volume of DI water (Table 2.4). The MEAs were then visually checked for presence of silica on the surface and soaked in TBAF as outlined in section 2.9.2.

Table 2.4: Table outlining the steps involved in cleaning the MEAs used as substrates for μCP and neuronal cultures.

Step	Post tissue culture	PDMS contamination	Silica contamination
1	Trypsin (5 min @ 35°C)	70% w/v TBAF	Hot 2M NaOH (30 min)
2	Rinse DI H_2O	Rinse DMF	3x Rinse DI H_2O
3	Rinse IPA	Rinse DCE	
4	Rinse 70% EtOH	Rinse MeOH	
5		Rinse IPA	

2.9.4 Updated and simplified MEA cleaning protocol

After each cell culture experiment the MEA were submerged overnight in 1% solution of Terg-a-zyme which removed any remnants of neural tissue from the surface (Multi-Channel-Systems, 2012). After Terg-a-zyme, the MEA was rinsed three times with DI water and dried using a nitrogen gun. Once dry the MEAs were places in plasma cleaner and exposed to plasma at 900 mTorr, 32 W for 5 minutes. The contaminations with PDMS and associated treatments with various solvents were avoided by improved PDMS casting, and pretreatment protocols.

2.10 Imaging

2.10.1 Image acquisition

The neuronal cultures where imaged every two to three days using an inverted microscope with a phase contrast capability. Surfaces, patterned with fluorescent inks such as PLL-FITC or Cy3-streptavidin were imaged using fluorescence microscopy. PLL-FITC patterns were imaged using excitation wavelengths of 495 nm (Blue). Cy3-streptavidin was imaged using excitation wavelengths of 550 nm (Green).

During each imaging session it was ensured that the microscope settings, e.g. ISO and exposure, remained consistent for each image recorded. The fixed settings allowed the images to be compared using fluorometric image analysis. It is important to note that the microscope settings were varied between sessions. The adjustment of exposure or ISO between sessions was necessary for recording images with optimal contrast. Because of these adjustments, fluorometric comparisons of images recorded during separate sessions were avoided.

2.10.2 Image processing

Ideally a fluorescent image should have a completely black background to ensure that any fluorescent signal seen is real. To perform fluorometric image analysis it was important to collect additional images such as background illumination and dark frame to try and increase the S/N of the images. Background illumination images were recorded to account for such phenomena as auto-fluorescence or un-even illumination or vignettes. The dark frame accounted for thermal noise generated by the camera and associated electronics. This image was always recorded with-out any illumination.

In essence, digital images are large matrices and image processing is a series of mathematical operations with these matrices. Hence, to reduce the thermal noise an averaged dark frame image was subtracted from a chosen fluorescence image.

The correction of background illumination required additional steps. First, the pixel values of a chosen image were inverted creating a negative. The background illumination was then added to the negative and the resultant image inverted again producing a positive image with corrected background illumination. Further processing, such as JPEG artifact removal, application of "Unsharp Mask" and adjustment of levels to further compensate for auto-fluorescence, was also performed as required. Measuring the intensity of fluorescence in images was performed using the combination of MATLAB, Origin 8, Paint Shop Pro and ImageJ software. For measuring fluorescence intensity of Fluorescein, FITC or Cy3, the processed images were imported into MATLAB. The imported images (if RGB) were converted into greyscale. The greyscale function assigned values ranging between 0 (Black) to 255 (White) to the pixels of the image. It also produced a matrix consisting of corresponding pixel values. However, if the imported images were already greyscale, this step was omitted. The MATLAB matrix was then imported into Origin 8.5 and the required profiles were plotted. The extraction of fluorescence profiles was also achieved using ImageJ software. This software has the dedicated function and greatly reduced the amount of time required to generate the fluorescence profiles.

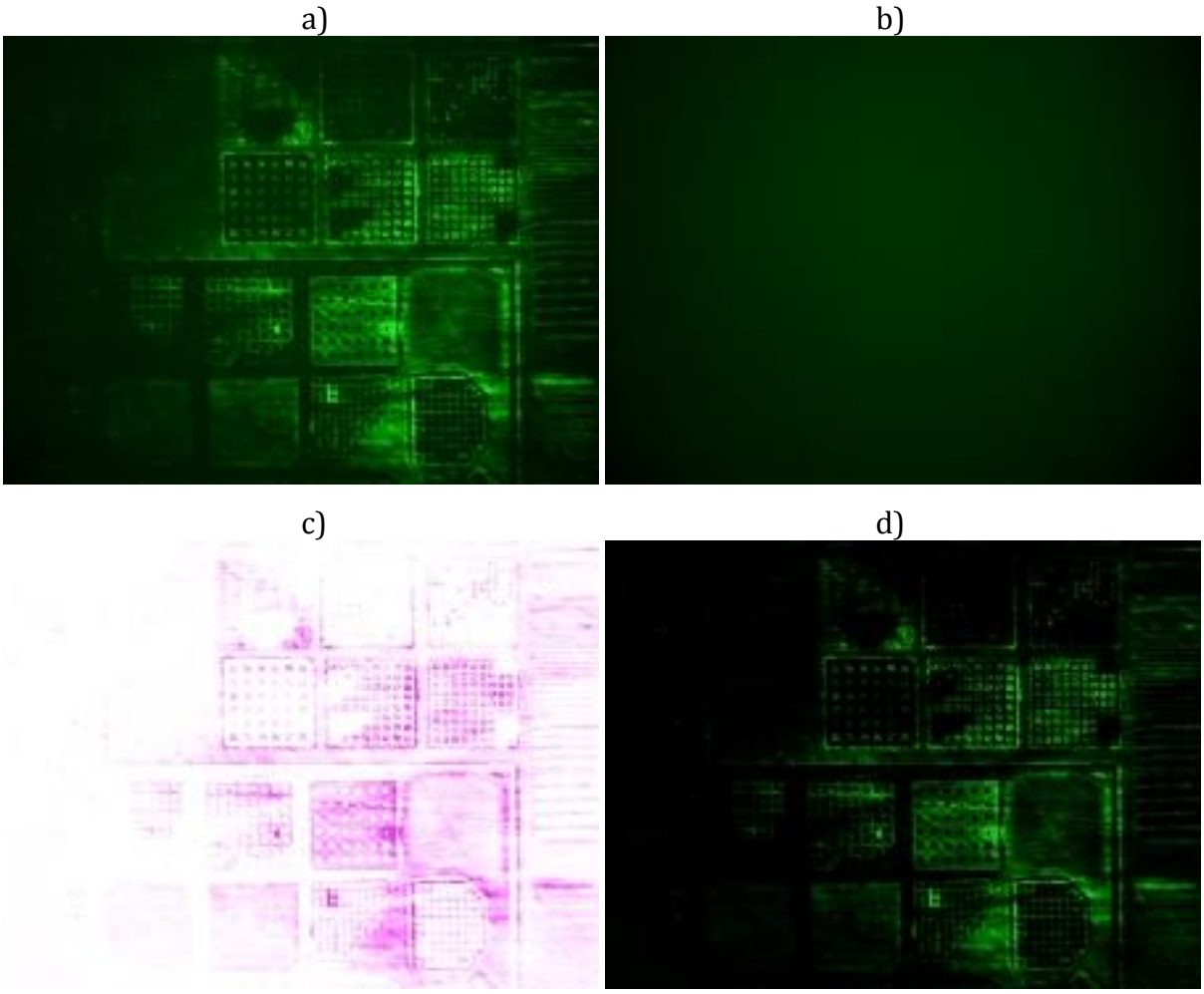


Figure 2.16: A series of fluorescent images at different stages of processing. a) Original fluorescent image. b) The background illumination image showing a vignette. c) The image that results from adding the background illumination to an inverted image of (a). d) Final, corrected image.

Chapter 3

3.0 Micro-contact printing and microfluidic devices

The viability and survival of neuronal cells in vitro is directly related to cell compatible surface chemistry and correct media composition. As described in section 1.2, the surface chemistry can be modified and controlled using μCP while the media composition can be controlled with microfluidic devices (μF) (Chang et al., 2001, Chang et al., 2003, Roth et al., 2004, Mourzina et al., 2006, Shim et al., 2007, Gross et al., 2007, Claverol-Tinturé et al., 2007, Kim et al., 2007, Wang et al., 2009, Jing et al., 2010). Thus, the aim of this chapter is to provide a detailed description of 1) design and fabrication of micro-stamps and micro-fluidic devices, 2) optimization of surface patterning and 3) optimization of micro-fluidic gradient formation.

The optimization of μCP was carried out on three types of substrates: Pyrex, Silicon Nitride (SiN) coated Pyrex and cyclic olefin co-polymer (Zeonor). The primary criterion for using these substrates was their compatibility with light/fluorescent microscopy and biocompatibility. Pyrex is a common substrate and has been extensively used for cell patterning (Vishwanathan et al., 2011, Liu et al., 2008, Corey et al., 1996). The SiN covered Pyrex substrates were chosen because this coating is used as passivation on commercially available MEAs (Multi-Channel-Systems, 2012). Lastly, Zeonor is of interest because of its potential for manufacturing relatively cheap devices such as sensors and MEAs (Illa et al., 2010, Raj et al., 2009). Hence, practicing and testing the surface modification techniques on this surface is essential.

In addition to fabrication and patterning techniques, this chapter will illustrate the fluorescent micro-printed patterns and compare their quality both visually and via fluorescence profiles and histograms. This chapter will also illustrate the formation of fluidic gradients inside microfluidic channels, and determine the most suitable method of perfusion (Wang et al., 2009, Gross et al., 2007, Claverol-Tinturé et al., 2007, Kim et al., 2007). The main reason behind the separate optimization of surface patterning and microfluidic perfusion was to try to achieve predictability and determine what practical issues are most prevalent with in each methodology.

3.1 Materials and Methods

3.1.1 Chemical reagents

Aminopropyl triethoxy saline (APTES) and Tridecafluoro-1,1,2,2-tetrahydrooctyl-1-trichlorosilane (TFOCS) were purchased from Flurochem Ltd, UK. Aminopropyl trimethoxy silane (APTMS) was purchased from ABCR GmbH & Co, Germany. Acetone, Cy3-streptavidin, 1,2 dichloroethane (DCE), hydrogen peroxide solution (30%), isopropanol (IPO), laminin, methanol (MeOH), poly-L-Lysine (PLL), poly-L-lysine FITC (PLL-FITC), sodium dodecyl sulphate (SDS), sodium hydroxide pellets and Tetra-n-butylammonium fluoride (TBAF) were all purchased from Sigma-Aldrich UK. Chondroitin 4 sulphate (used as a substitute for chondroitin sulphate proteoglycan), fluorescein, fluorescein sodium salt, hydrochloric acid, polyethylene(imine) (PEI), pyridine and sulphuric acid were all branded "Fluka Analytical" and purchased from Sigma-Aldrich, UK. Dimethylformamide (DMF) was purchased from Fischer Scientific, Ireland. Dymax UV curing adhesive was purchased from ECT Adhesive Solutions, Ireland. Dulbecco's modified eagle medium (DMEM) was purchased from Bio-Sciences, Ireland. NOA 68 UV curing adhesive was purchased from Norland, NJ, USA. Polydimethylsiloxane (PDMS) was purchased from Dow Corning, UK under trademark Sylgard 184. De-ionised water was purified using Elga water purification system (Veolia Water Systems, Ireland). The de-ionised water used throughout had resistivity of 18.2 MΩ·cm. Pyrex substrates and six well polystyrene culture plates were purchased from Corning via Sigma-Aldrich, UK. The biocompatible two part epoxy system Epo-Tek 353 ND was purchased from Epoxy Technology Inc. USA

Other hardware required for fabrication of micro-stamps was machined from poly(methylmethacrylate) (PMMA) or polytetrafluoroethylene (PTFE) in the Tyndall mechanical workshop. The etched silicon masters were fabricated in the Tyndall wafer fabrication facility.

3.1.2 Silicon masters

Three different silicon masters were used to optimize µCP, surface patterning via µF devices and fluidic gradient formation. Figure 3.1 illustrates the masters used.

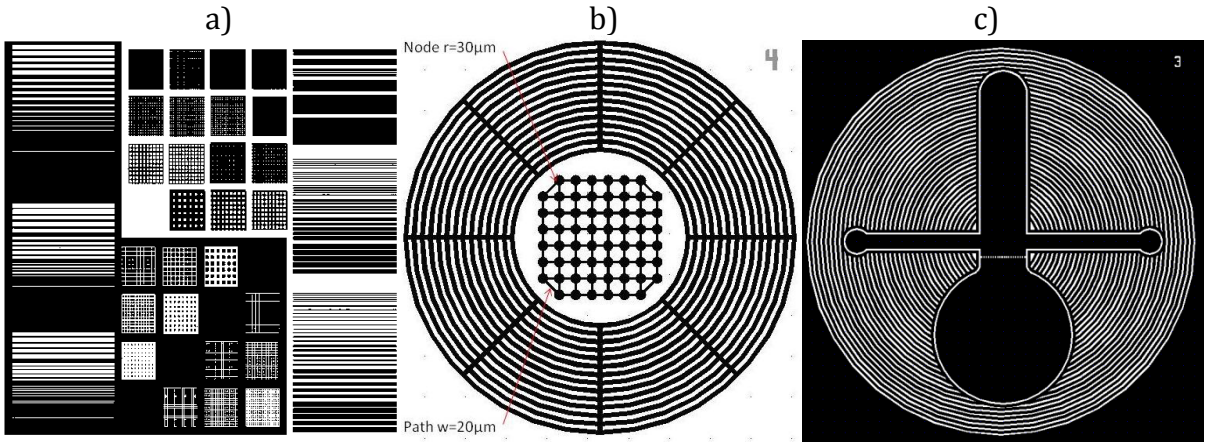


Figure 3.1: Illustration of silicon master designs used for optimization of a) µCP, b) µF patterning and c) µF gradients. The square features in (a) are 200µm². The circular areas in (b) have a diameter or 60µm. The vertical channel in(c) is 2000µm wide.

3.1.3 Surface chemistry modifications

The Pyrex coverslips were cleaned by immersion into 1:1 solution of Hydrochloric acid (HCl) and MeOH for 15 min followed by immersion into pure sulphuric acid for another 15 min. Following sulphuric acid soak, the coverslips were sequentially sonicated for 5 min in each of the following: acetone, MeOH and IPO. The substrates were then rinsed with DI water, dried with a nitrogen gun. Once dry, the µCP was carried out.

3.1.4 Micro-printing techniques

The µCP stamps were fabricated as described in section 2.3. The protocol for the stamp inking is an adaptation of previously published protocols (Jun et al., 2007, James et al., 2000) and was performed as follows. The surface of µCP stamps was plasma oxidized (~1 min, 900mTorr, 32W) to make the surface hydrophilic. Following the oxidation, 5 µl of Cy3 streptavidin (5 mg mL^{-1}) or fluorescein solution (3 mg mL^{-1}) was pipetted onto the stamp surface. After 20 min, the inking solution was simply dried using an air gun. The stamp was then dipped into DI water and then dried again. The inked stamps were placed into a dust free container prior to µCP. The substrates were patterned using

manual flip-chip bonder or a drill stand. The μCP via the drill stand was attempted to determine if this method was a feasible alternative to using the flip chip bonder.

3.1.4.1 μCP using the drill stand

The μCP was performed on Pyrex microscope slides or coverslips. Prior to μCP, the substrates were cleaned by 5 min sonication in each: acetone, methanol and isopropanol. The substrate was then places under the drill chuck. The inked stamp was inserted into the stamp holder (Figure 3.2); the holder was assembled and mounted in the chuck above the substrate.

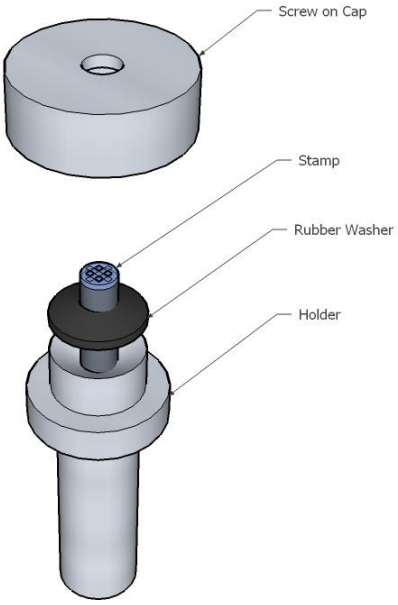


Figure 3.2: A custom made stamp holder. A stamp mounted onto a metal support rod is inserted into the holder. The rubber washer keeps the mounting rod in the holder during the lowering of the swing arm.

The stamp was carefully brought into contact with the substrate by lowering the drill. To control the amount of mass applied to the stamp; digital weighing scales were places under the substrate during printing. The mass applied to the stamp was ~ 714 g cm^{-2} (50 g/0.07 cm^{-2}). The stamp was held in contact with the substrate for 30 sec (Figure 3.3). Note: the mass applied to the stamp could not be controlled accurately because the spring-loaded drill stand had to be held down manually.

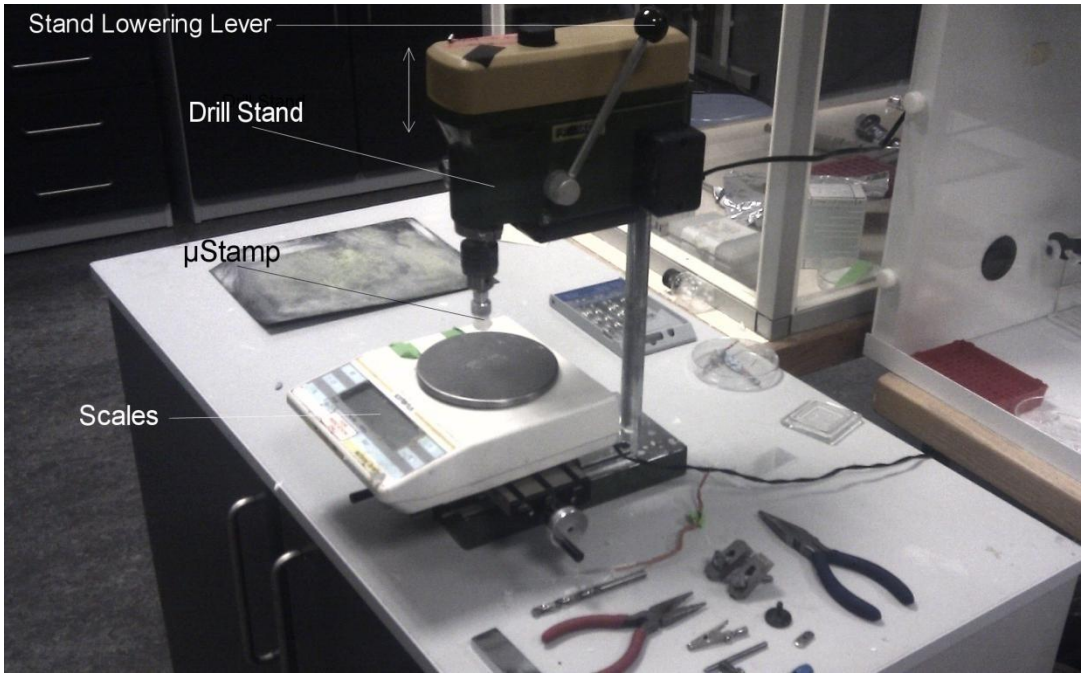


Figure 3.3: The photograph of the drill stand set up for micro-contact printing. The weighing scales were used as readout for the amount of mass applied to the stamp.

3.1.4.2 µCP using the flip chip bonder

The flip chip bonder is a precision device which is used for integration of small semiconductor devices with external printed circuit boards (PCB) (Figure 3.4). The contact pads of the semiconductor device to be bonded are first metalized to facilitate deposition of solder dots. Once the solder is deposited, the semiconductor device is mounted onto the swing arm of the flip chip bonder and aligned with the contact pads of PCB on the XY stage. The semiconductor device is brought into contact with the PCB. During the contact, a pre-determined amount of mechanical force is applied and the solder dots are melted either via a hot air stream or a hotplate.

The flip chip bonder was modified to suit µCP by replacing its pneumatic head with the machined stamp holder shown in Figure 3.2. The µCP of substrates was carried out as described previously (Lauer et al., 2001). Briefly, the stamp holder was assembled and attached to the swing arm of the flip chip bonder. A set of pincers was used to adjust the protrusion of the PDMS stamp to ensure that it was in focus and the correct distance from the substrate.

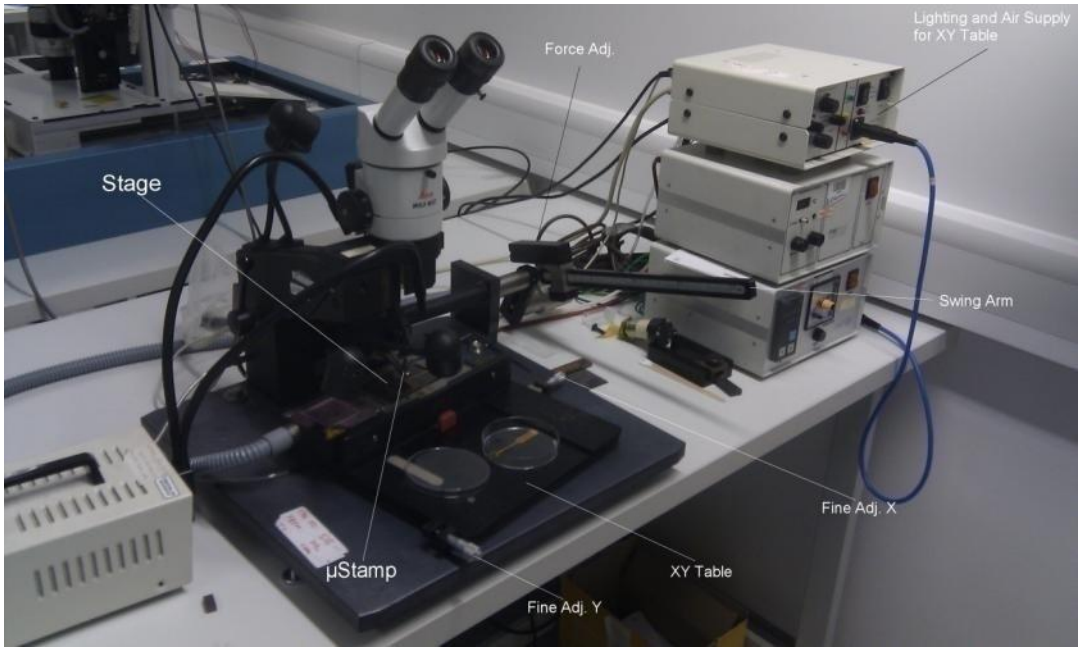


Figure 3.4: Flip chip bonder set up for μCP.

The substrates, either Pyrex slides or MEA, were placed on the XY table and aligned with the μCP stamp. The alignment was performed visually through the eyepiece and a prism. After alignment, the force of contact was set to the required magnitude and the stamp was brought into contact with the substrate for the period of 1 min. The forces tested were: 0.6 N-2.3 N. Following the μCP, the substrates were imaged using the fluorescent microscope. The quality of the patterns was determined visually. Image profiles and histograms were used to compare the patterns in terms of fluorescence intensity and distribution of pixel values. The fluorescence profiles and histograms both use the pixel values as a variable. The pixel value can range anywhere between 0-255, where black pixels are given the value of zero, while white pixels are given the value of 255. The pixel values above zero and below 255 are a range of grays. The fluorescence profiles show the pixel distribution along a set plane (profile) of the image, while the histogram shows the frequency distribution of pixel values. The fluorescence profiles were used to look at the specific areas of the image, while the histograms were used to compare the fluorescence levels of entire images.

3.1.5 Surface patterning using µF devises

Surface patterning via perfusion of the attached µF device was performed as described in section 2.6. The µF devices were aligned with the substrates (MEAs) using the setup described in section 2.4.4. For visualization purposes, the µF device was filled with a solution of red food dye. For the MEA patterning experiments, the µF device was filled with solution of fluorescein sodium salt in DI water.

3.1.6 µF gradients

3.1.6.1 The replica molding of µF device

The µF devices for perfusion and surface patterning were fabricated by replica molding PDMS as described in sections 2.4.2 and 2.4.3 respectively.

3.1.6.2 PDMS extraction

The un-polymerized short chain PDMS fragments were extracted from replica molded PDMS devices by a process of Soxhlet extraction as previously described elsewhere (Thibault et al., 2007). Since a commercial Soxhlet extractor was not available in our lab, simple, a simple extractor was built. The Soxhlet extractor consisted of 250 mL Pyrex bottle, screw-on cap, 5 mL Pyrex beaker, a generic small plastic screw on cap, a generic small 3 mL glass bottle and a 20 mL polystyrene sample tube.

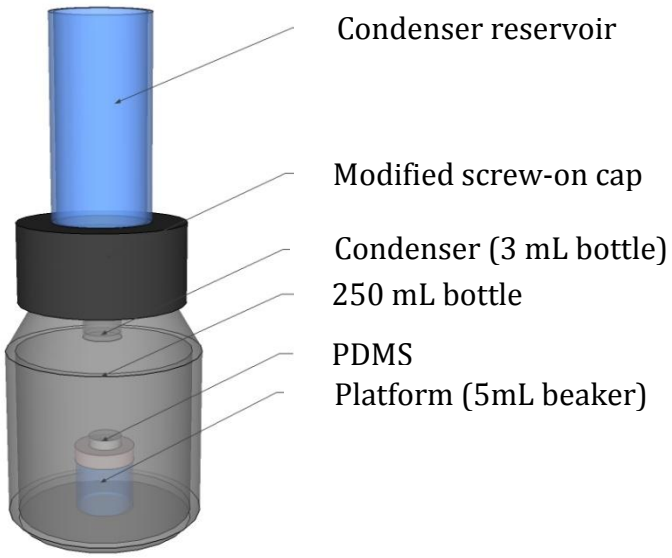


Figure 3.5: In house Soxhlet extractor schematic.

The schematic of the Soxhlet extractor is shown in (Figure 3.5). To make the condenser, the large plastic screw-on cap was modified by drilling a hole in its centre. The diameter of the hole was just large enough to fit the neck of the small bottle through it. The small bottle was then glued to the underside of the plastic cap using epoxy mixed at 10:1 as per instruction and cured in the oven at 40°C for 3-4 h. The water reservoir for the condenser was made from a 20 mL polystyrene sample tube. Using a hacksaw, the bottom of the tube was sawed off and the edge smoothed using an abrasive sheet. Using epoxy, the open ended tube was then glued into a recess on the top side of the plastic cap. A small plastic screw-on lid was fitted over the bottom of a 5 mL Pyrex beaker. This created a platform for the PDMS to sit on during the extraction. This platform was simply placed inside the 250 mL bottle, under the condenser.

Once all the parts were assembled and glued together, approximately 5-10 mL of absolute EtOH was poured into the 250 mL bottle. The PDMS device was weighed and positioned on the platform inside the bottle. The condenser reservoir and the condenser were filled with tap water and carefully screwed onto the 100 mL bottle. The condenser was screwed on just tight enough to remove any movement or play. The entire assembly was placed onto a hotplate. The heat supplied to the bottle was just enough to simmer the EtOH. The extraction was carried out for 3 h from the moment the extractor was placed onto the hotplate. After the extraction the µF device was dried on the bench overnight. The µF device was weighed the second time, to determine the amount of material removed from it. The reduction in PDMS mass post extraction was in the range of 0.7-2.8% (n=6). Using a blunt syringe needle, inlets were punched in the µF device before bonding.

3.1.6.3 Generating the micro-fluidic gradients

To determine the shape of the fluidic gradients, the µF device was plasma bonded to the Pyrex substrate as described in section 2.4.5.2 and then filled with DI water. The µF device was connected to a syringe pump through an intermediate section of tubing that was securely attached to the microscope stage together with the µF device (Figure 3.6). The intermediate stage consisted of a small polystyrene box, through which ran two input Teflon tubes, secured to the box with epoxy. Eighteen gauge needles (outer diameter equal to 1.27mm) were attached at the ends of the tubes. The needles were shortened and bent 90° in order for these to clear the lenses of the upright microscope.

This intermediate section eliminated any damage to the μF device by the needles when the stage was moved. Two syringes were used to perfuse the device. One syringe was filled with water and red food dye/fluorescein, while the second syringe contained just water. The waste was directed out of 3rd inlet port via a section of tube submerged in a small volume of water. The waste output had to be submerged to avoid the fluctuations of volumetric rates caused by the back pressure and the surface tension of the forming drop (see section 3.1.8). The device was perfused with the following volumetric rates: 1, 5, 10, 30, 60, 75, 100 and 500 μL hr^{-1}.

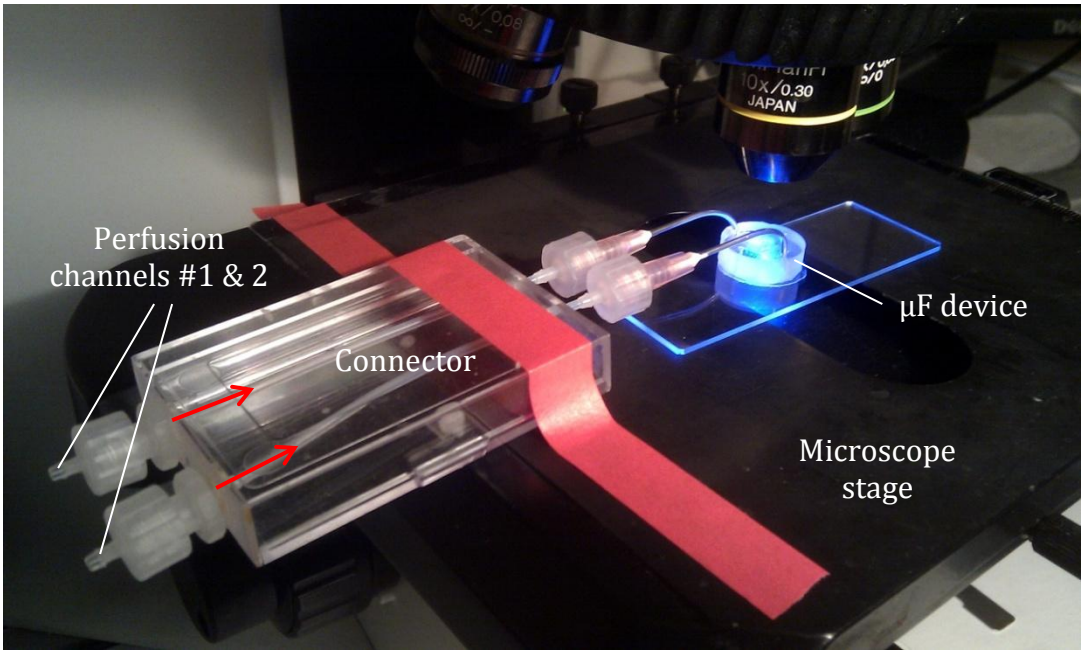


Figure 3.6: An image of the μF device-syringe pump connector. The connector allowed the pump to be connected and disconnected from the μF device without the potential to damage the device. Additionally, this connector removed any tension exerted on the μF device by the long perfusion lines. The direction of perfusion is indicated by the red arrows.

Additional to the syringe pump, a peristaltic pump was also used to perfuse the μF device. The volumetric rates were varied by controlling the speed of the revolving barrel. The speed settings tested were 0.01-0.09 revolutions per minute (RPM). Similarly to the syringe pump, the peristaltic pump perfused the μF device with two channels. To determine the volumetric rate at the given RPM, the pump was connected directly to a DI water source and a waste reservoir. The pump was switched on and let run for few minutes at a high RPM (2-4) to ensure that all air bubbles were removed from the tubing. Once the air bubbles were gone, the RPM was lowered to 0.01 and the

pump was switched off. Once the pump was off, the waste reservoir was weighed, and reconnected to the pump. The pump was then switched on for 10 min at 0.01 RPM. After 10 min the waste reservoir was weighed again to determine the mass of DI water pumped after 10 minutes. This procedure was repeated three times before working out the volumetric rate per minute.

3.1.7 Gravity driven passive perfusion

The gravity driven perfusion was performed using the PMMA reservoir block described in section 2.5. Briefly, the μF device attached to the substrate was prefilled with ethanol solution. Then the source reservoirs were filled with 2 mL of perfusing solution, while the waste reservoir was filled with approximately 500 μL perfusing solution. Teflon tubing was attached to the outlets and primed with fluid from the reservoirs. This was achieved by repeatedly applying pressure to the reservoir opening using a thumb. The reservoirs were then connected to a prefilled μF device thus making a fluidic connection between the source reservoirs and the waste reservoir. Care was taken to ensure that no bubbles got trapped inside either the tubing or the μF device channels.

3.1.8 Surface tension driven perfusion

This method of perfusion relies on the surface tension of the small drop of liquid sitting directly on top of an inlet (Xing et al., 2011, Berthier and Beebe, 2007). The flat top μF device was filled with DI water. A small 3-5μl drop of fluorescein solution was placed over one of the inlets. Two DI water drops were placed over the remaining inlets, ensuring that all the drops retained hemispherical shape. A larger drop (~10 μL) was placed over the waste outlet. The larger volume of this drop reduced the water surface tension and initiated the perfusion.

3.2 Results

3.2.1 µCP patterns generated using the drill stand.

Using the drill stand, Pyrex substrates were printed with fluorescent Cy3-conjugated streptavidin. The patterns generated without using the weighing scales showed that the stamp became excessively deformed when in contact with the substrate. This was indicated by the presence artefacts between the printed stamp features. The deformation was caused by excessive force applied during printing. With the introduction of the weighing scales under the substrate, it was possible to control the mass applied to the stamp. The patterns generated with the mass of up to 714 g cm^{-2} showed no artefacts associated with excessive stamp deformation or sagging (
Figure 3.7).

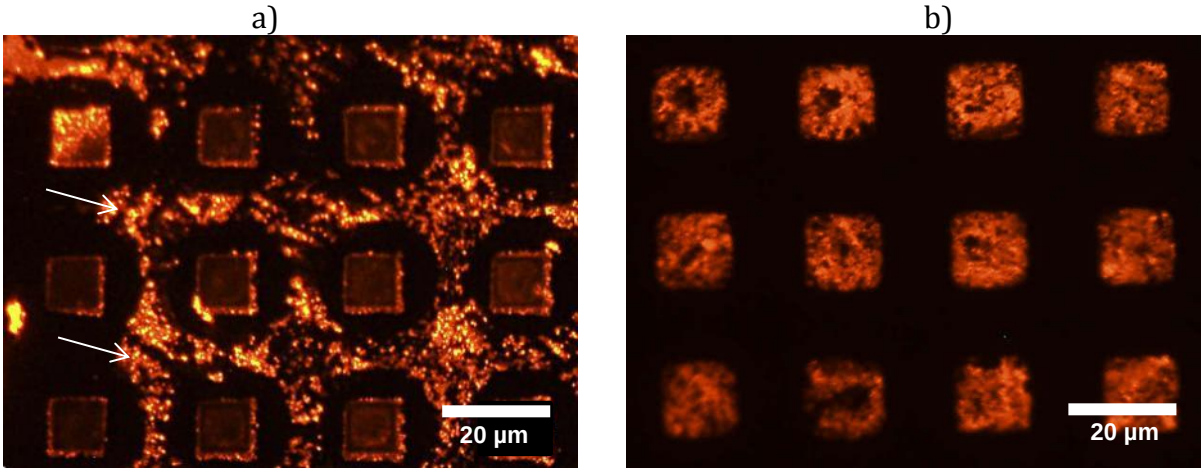


Figure 3.7: Fluorescent images of Cy-conjugated streptavidin printed on the Pyrex substrate. a) The patterns printed without the weighing scales show defects associated with stamp deformation and sagging. The white arrow indicates the artefacts produced by the ceiling of the stamp coming into contact with the substrate. b) The pattern printed with the aid of the weighing scales. The mass applied was ~50 g (714g cm^2).The patterns printed at this setting did not show stamp sagging artefacts.

It was observed that the design of the stamp and its features can influence the quality of the printed pattern. For example, high aspect ratio (long and narrow) cavities can pool the inking solution. The pooling resulted in excessive ink deposition in those areas during printing at optimal force (Figure 3.8(a)). Another artefact that was observed was associated with the Cy3-streptavidin slowly drying on the stamp surface. This process resulted in uneven deposition of Cy3-streptavidin on the stamp surface and consequently the substrate (Figure 3.8(b)).

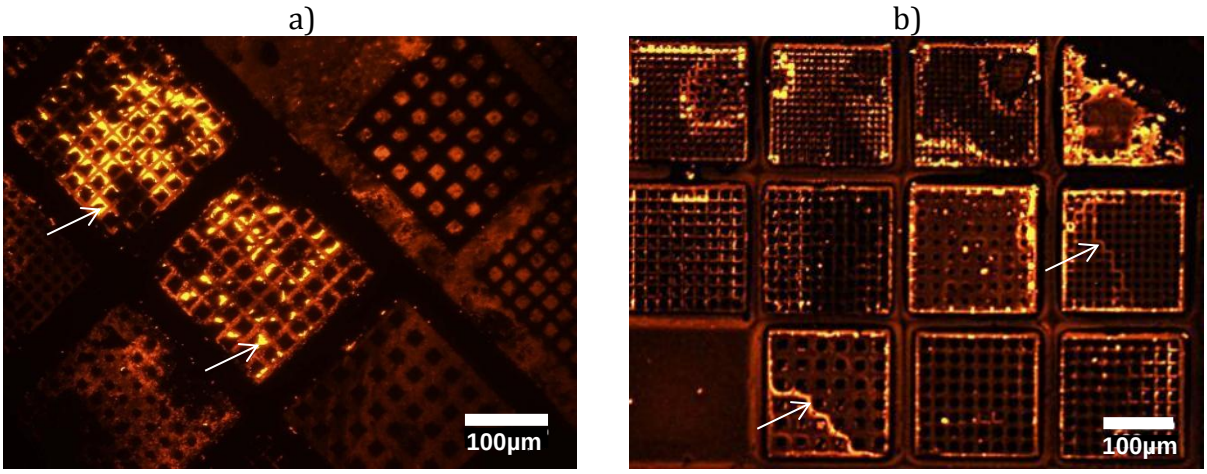


Figure 3.8: a) Image showing pattern artefacts associated with ink pooling in small stamp recesses. b) The pattern artifact associated with the drying of the Cy-3 streptavidin solution on the stamp surface (arrows).

3.2.2 µCP patterns generated using the flip-chip bonder

As shown above, the force applied to the stamp has a major influence on quality of the printed pattern. Excessive forces resulted in sagging and bringing the recessed surfaces into contact with the substrate, while insufficient force generally resulted in loss of features on the surface due to minute vertical stamp miss-alignments (see next subsection). Similar observations were made in numerous studies dealing with µCP using the PDMS stamp (Pla-Roca et al., 2007, Ruiz and Chen, 2007, Perl et al., 2009). Keeping the force magnitude consistent during printing steps was essential in order to produce consistent and high quality micro-patterns. In this respect the drill stand was at a disadvantage, because even though the presence of weighing scales under the stamp made it possible to monitor the applied force in real time, there was no way to keep the force at a constant magnitude. In this respect, the flip chip bonder was a superior tool because the force applied to the stamp was constant.

3.2.2.1 Printing force comparison

To determine the optimum force setting for µCP, patterns printed with increasing force settings where compared. The optimum force was considered to be of the maximum magnitude that did not induce the sagging of the stamp.

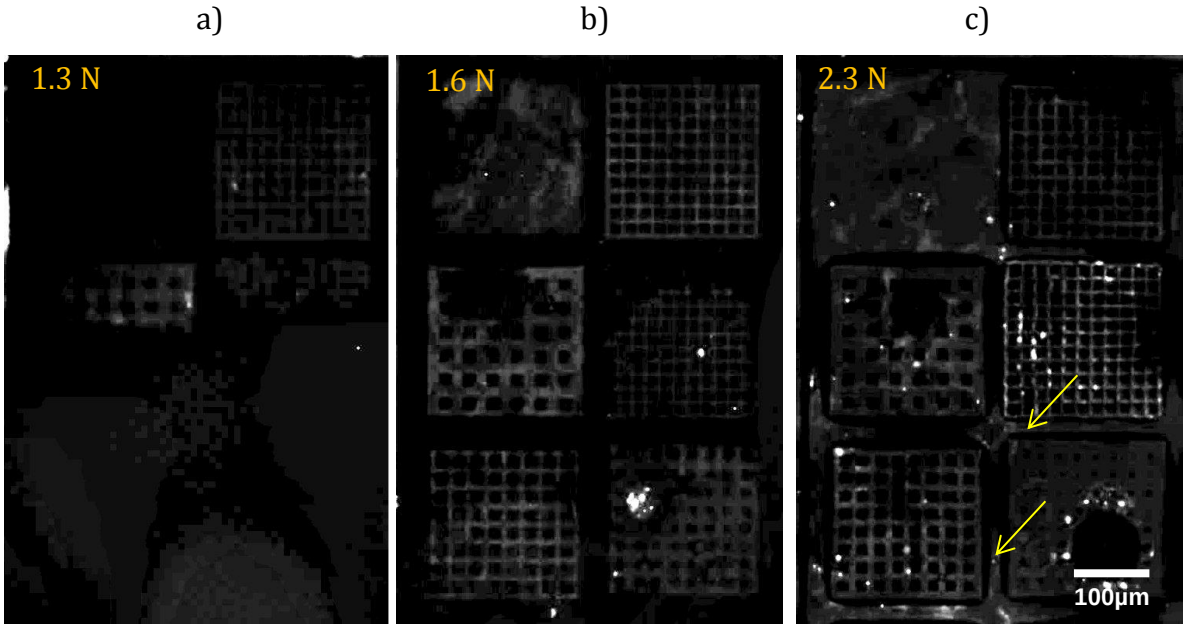


Figure 3.9: Grayscale fluorescent images of Cy3 Streptavidin on Pyrex substrate. Forces applied were a) 1.3 N, b) 1.6 N and c) 2.3N. The yellow arrows indicate the artefacts caused by stamp deformation and sag.

Using the flip chip bonder, the following force settings were tested: 0.6 N, 0.8 N, 1.0 N, 1.3 N, 1.5 N, 1.6 N, 2 N and 2.3 N (Table 3.1). No visible patterns were generated with setting below 1.3 N; hence, these images are not shown. Figure 3.9 shows three patterns on Pyrex printed with the force setting of 1.3, 1.6 and 2.3 N. The 1.3 N setting was insufficient because most of the features of the pattern were missing. The 1.6 N setting generated complete patterns without artifacts. Although some features were still missing from the surface. The pattern generated with the 2.3 N setting was complete. All the features of the stamp were present on the surface. However, this setting resulted in severe stamp sagging (Figure 3.9). The optimal force setting of the flip chip bonder was found to be 2.0 N. There is no evidence of stamp sagging between the large square features. At the same time there is no loss of features as seen in patterns generated with 1.3 or 1.6 N for example (Figure 3.10). Hence the force setting of 2.0 N and contact time of 1 min was used for all subsequent µCP investigations. Table 3.1 summarizes the forces and the equivalent pressures used to generate the fluorescent patterns.

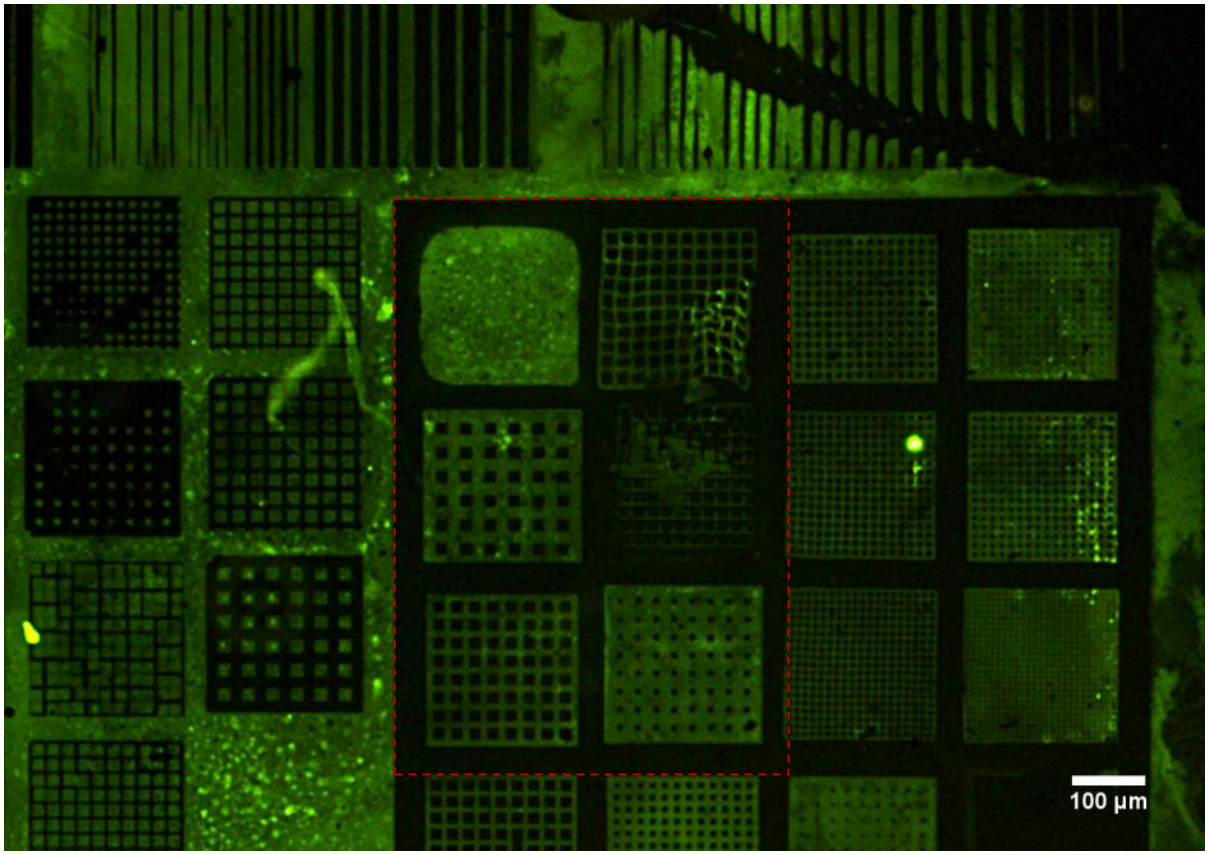


Figure 3.10: A fluorescent image of PLL-FITC pattern generated via µCP. The printing time was 1 minute and force applied 2.0N. This force setting is optimal and provides a pattern of good quality, where there was no stamp sag between large features. There is also no loss of features due to poor contact of the stamp with the surface. The red dashed box indicates the area of the pattern that was examined in Figure 3.9 and provides a good comparison of quality of patterns generated with increasing force.

Table 3.1: Table summarizing the force settings that were used during µCP. The pressure was calculated using the formula P=F/A. DS=Drill stand.

Force (N)	Stamp area (m^2)	Pressure (Pa)
0.5 (DS)	$7x10^{-6}$	$7x10^{4}$
1.3	$7x10^{-6}$	$1.85x10^{5}$
1.6	$7x10^{-6}$	$2.29x10^{5}$
2.0	$7x10^{-6}$	$2.86x10^{5}$
2.3	$7x10^{-6}$	$3.29x10^{5}$

3.2.2.2 *Relationship between the applied force and ink transfer*

Additionally to the effect of the mechanical deformation of the stamp, it was observed that the fluorescence intensity was also influenced by the magnitude of applied force. The patterns printed using higher force settings were brighter in comparison to patterns generated with weaker force settings (Figure 3.11). To the best knowledge of the author, this property of µCP has not been investigated directly. To determine if this relationship existed, the pixel value distribution of aligned images (n=9) was compared.

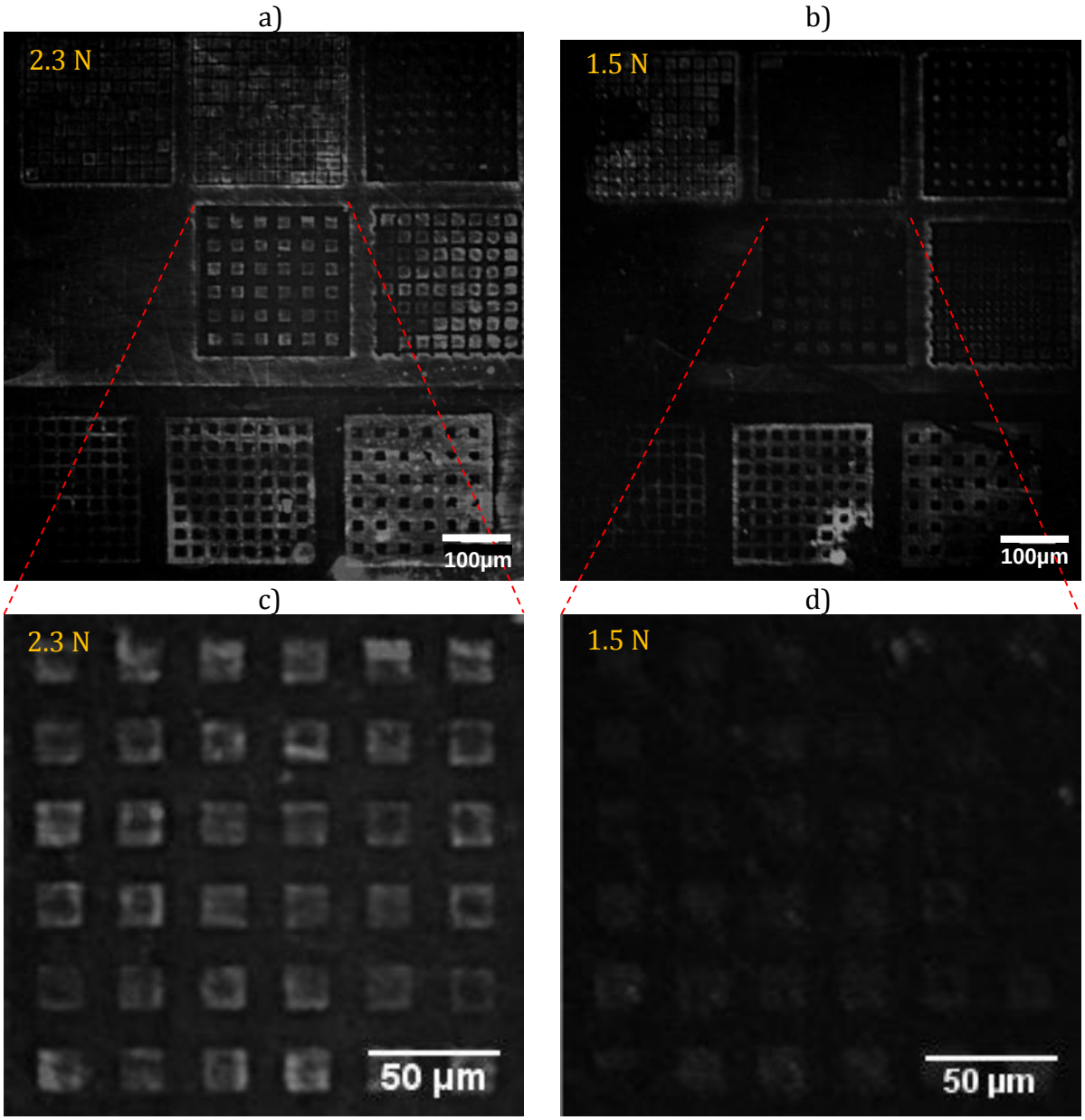


Figure 3.11: Comparison of µCP pattern quality generated with 2.3 N (a) and (b) and 1.5 N (c) and (d). Each image is an average of three separate images aligned using the common features of the printed patterns. Scale bars=50µm

The pixels in the image were assigned into one of three categories based on their value. Pixels with values between 171 and 255 were considered “bright”. Pixels with value between 86 and 170 were considered “gray” While, pixels with values below 85 were considered “dark”. The comparison indicated that increasing the contact force results in higher levels of pattern fluorescence (Figure 3.12). The patterns generated with higher contact force consistently had larger percentage of “bright” or “gray” pixels and lower percentage of “dark” pixels than those generated with weaker forces (Table 3.2).

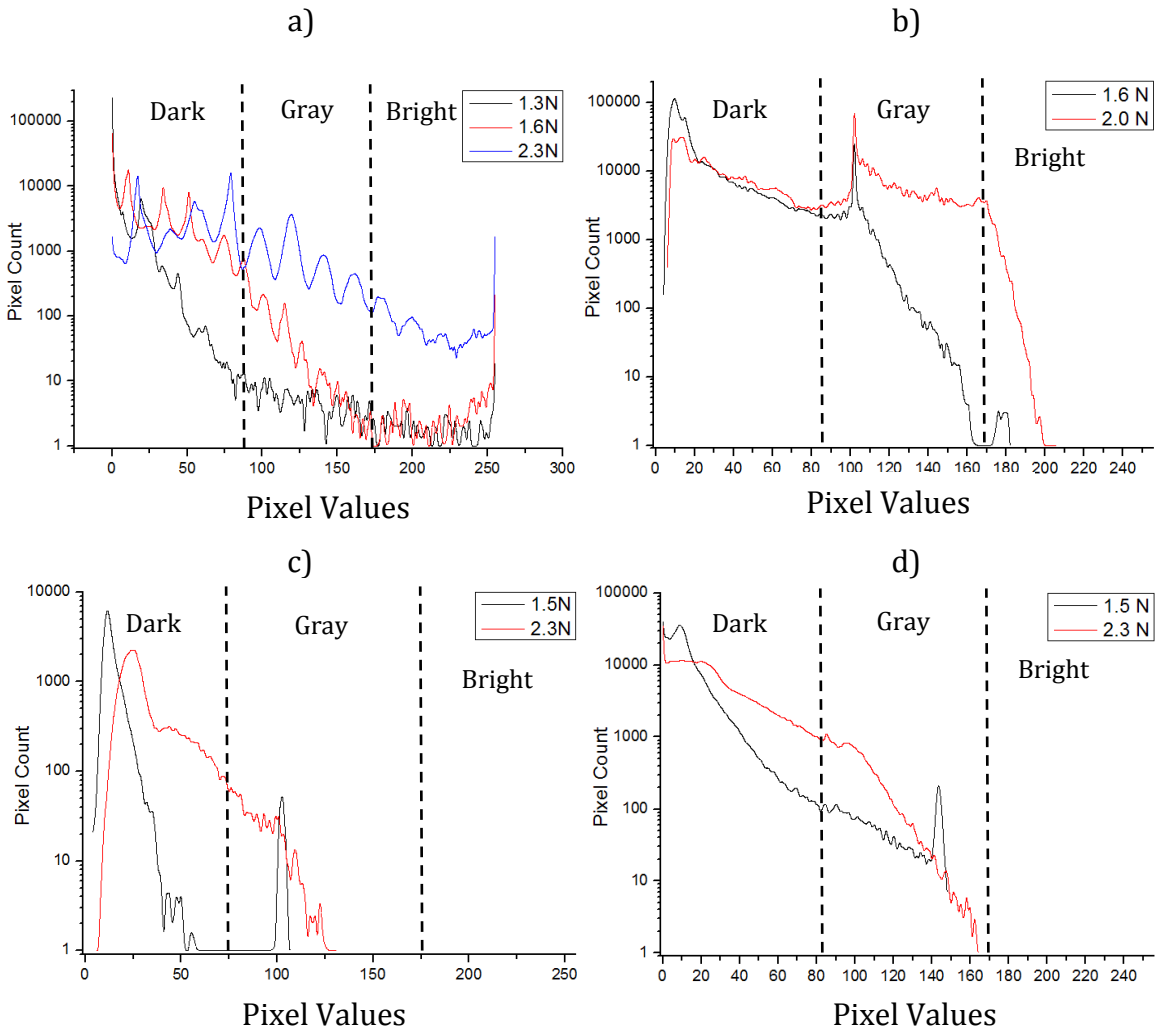


Figure 3.12: Histogram comparison of fluorescent patterns printed with increasing force settings. The pixels were assigned into categories based on their value. Pixels with values 0<x<85 were in “dark” category. Pixels with values 86<x<170 were in “gray” category. Pixels with values 171<x<255 were in the “bright” category.

These results indicate that the transfer of ink from the stamp to the surface can be improved by increasing the contact force. However, the application of higher force must be combined with tougher stamp material to reduce the stamp deformation and sagging.

Table 3.2: Table showing the total pixel counts of images and the corresponding percentages of "dark", "gray" and "bright" pixels. The letters a, b, c and d denote the associated histograms shown in Figure 3.12.

Force (N)	Total pixel #	Dark pixel %	Gray pixel %	Bright pixel %
1.3(a)	3.5×10^5	99.8	0.15	0.05
1.6(a)	3.6×10^5	97.6	2.3	0.1
2.0(a)	2.4×10^5	92.8	7.1	0.1
2.3(a)	3.5×10^5	75.5	22.2	0.3
1.6(b)	1.39×10^6	90.1	9.8	0.1
2.0(b)	1.39×10^6	54.1	44.9	1
1.5(c)	3.7×10^4	99.5	0.5	0
2.3(c)	3.7×10^4	98.2	1.8	0
1.5(d)	5.4×10^5	99.3	0.7	0
2.3(d)	5.1×10^5	96	4	0

3.2.2.3 Patterns generated using the thin µCP stamps

The previous section indicates that the fluorescence intensity is directly related to the force applied to the stamp. However, the potential excessive deformation of the stamp at forces above 2.0 N negates the benefit of increased ink transfer. Hence, to try and address this issue, µCP was performed using the thin stamps (see section 2.3.5). The results showed that decreasing the stamp thickness in an attempt to prevent sagging can result in oversensitivity to poor vertical alignment of the µCP stamps.

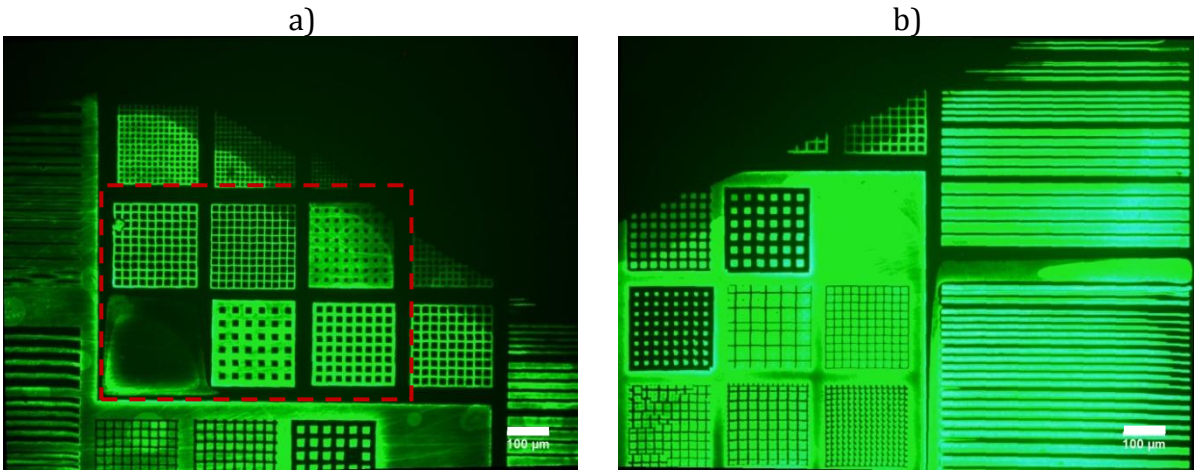


Figure 3.13: Problems and defects associated with µCP when using a thin stamp. a) 1.6 N b) 2.0 N. The slight vertical misalignment of a thin stamp prevents the stamp to fully conform to the surface resulting in poor pattern quality due to missing features. Scale bars = 100µm.

As one area of the stamp experienced the full applied force, the other side did not come into contact with the substrate at all. This resulted in an incomplete pattern that still presents sagging artifacts in some parts (Figure 3.11).

3.2.2.4 Feature edge artifacts

An interesting artifact associated with stamp deformation was the increased fluorescence intensity at the borders of the printed features (Figure 3.14). This artifact was likely caused by deformations of the vertical walls of the μCP stamp during printing (Figure 3.15). Chen et al, have used this property of PDMS features to print halos on the substrate (Chen et al., 2011).

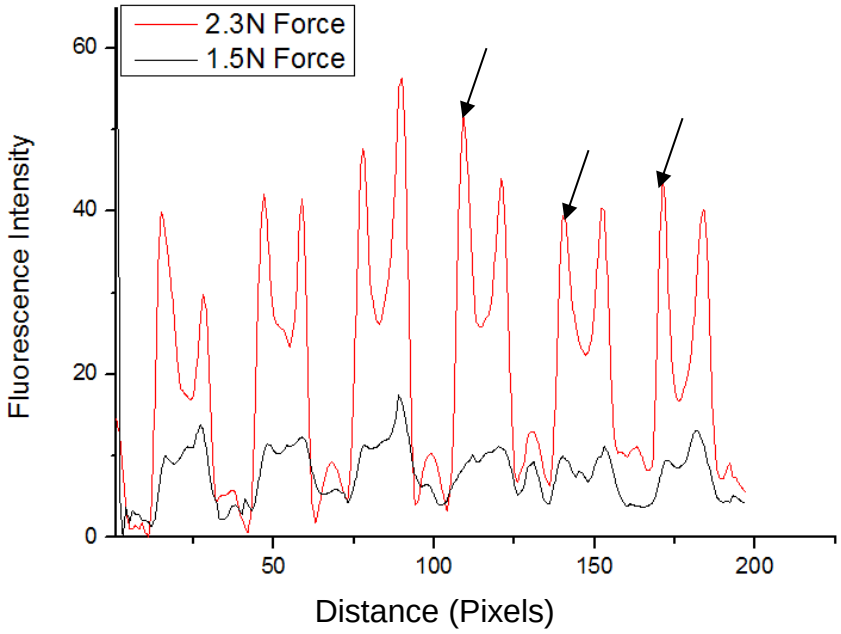


Figure 3.14: The average (n=10) fluorescence profile plots showing the relationship between the pressures applied to the stamp and the fluorescence intensity of individual features of the pattern. This profile comparison also shows the fluorescence spikes seen edges of printed patterns (balck arrows).

This property of PDMS μCP stamps can also be useful for directly printing chemical gradients on the substrate surfaces. This can be achieved by smoothing the transition between the horizontal and the vertical surfaces of the stamp features as shown previously (Choi and Zhang Newby, 2003).

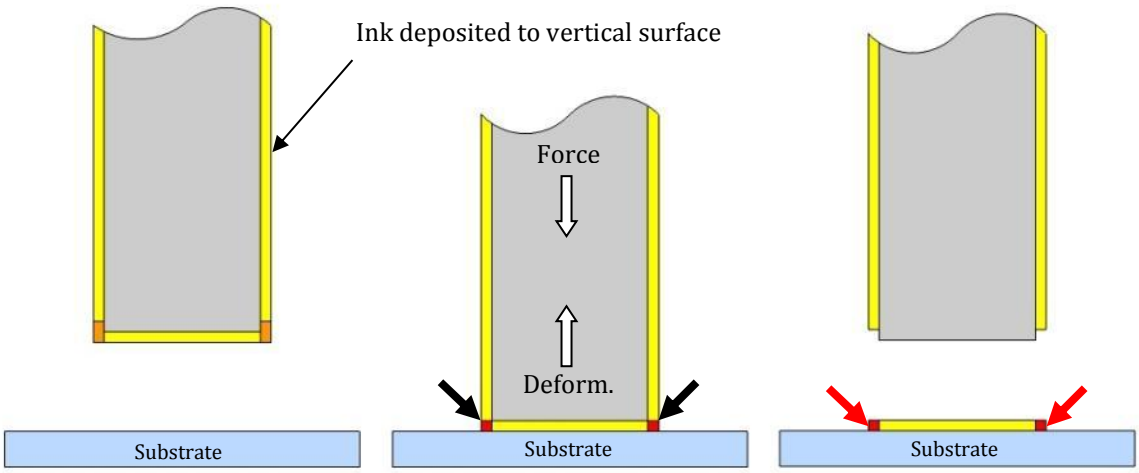


Figure 3.15: A schematic diagram representing the transfer of "ink" from the vertical surfaces of the stamp features onto the substrate. The thick black arrows (centre schematic) indicate the area of deformation and the increase in "ink" concentration per unit area. The red arrows (right schematic) indicate the areas of increased "ink" concentration per unit area of the substrate. The increased concentration of fluorescent molecules leads to increased fluorescence intensity in the fluorescent profile plots.

3.2.3 Defects and inconsistency of µCP

One of the major problems associated with µCP was the large variation in quality of printed patterns. It was observed that some patterns were of very good quality while other patterns printed on the same day using the stamps inked with the same protocol appeared either very dull, plagued with defects such as bright spots, misalignment or high background fluorescence (Figure 3.16). This variation may be linked to inconsistent surface chemistry of PDMS stamps. Due to high viscosity of PDMS, the homogenous mixing of the pre-polymer with hardener is hard to achieve. Hence, some stamps may be composed of PDMS with inconsistent mix ratio leading to variation in inking or ink transfer. The drying of the stamp post inking also had the potential to negatively influence the printed pattern. This step is relatively violent as it involves blowing off the inking solution using an air gun. Substituting this method with simply letting the stamp dry in the oven or at RT generally produced artifacts associated with particle precipitation in localized areas as the solution dried out. This was exacerbated if inks were dissolved in buffers such as PBS or Borate. In these cases the buffer salts would precipitate and form crystals on the stamp surface. Additional defects such as bright and dark areas on otherwise complete pattern might have been the result of random ink transfer from the stamp to the surface. Table 3.3 compares the "Dark", "Gray" and "Bright" pixel distributions and shows the large variations.

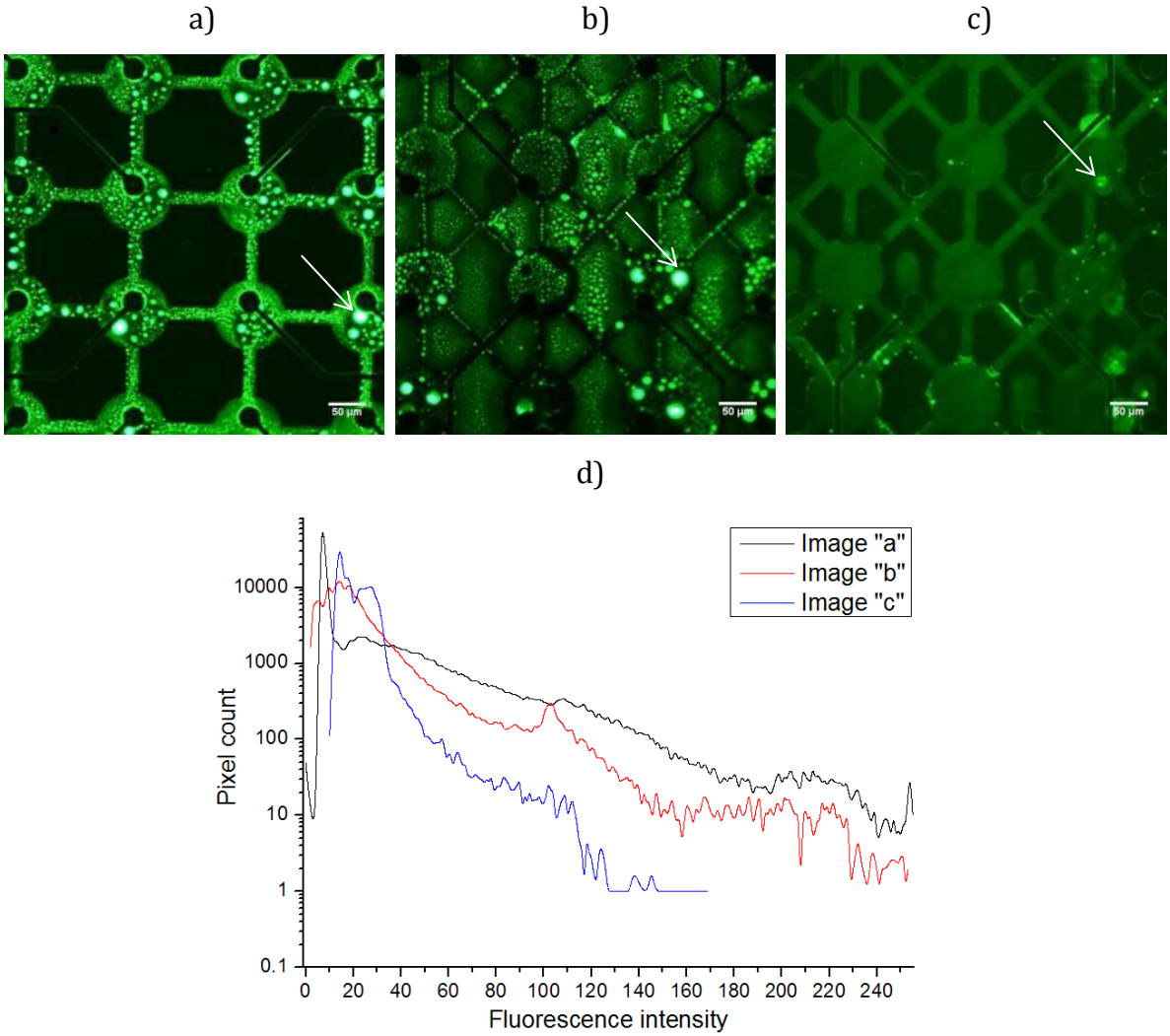


Figure 3.16: a) b) and c) Fluorescent images showing the variation of pattern quality when μCP is performed under the same conditions. The patterns seen in (a), (b) and(c) were all printed on MEA using the flip chip bonder and the force setting of 2.0 N. d) Histogram comparison of the three images showing variation of the pattern fluorescence intensities. The white arrows in (a), (b) and (c) indicate a defect related to non-uniform drying of PLL solution. Scale bars = 50μm

Table 3.3: Table stating the pixel distribution of fluorescent pattern images in Figure 3.16.

	Total pixel #	Dark pixel %	Gray pixel %	Bright pixel %
Image (a)	2.6×10^5	92.7	6.5	0.8
Image (b)	2.5×10^5	97	2.7	0.3
Image (c)	2.5×10^5	99.8	0.2	0

3.2.4 Effects of soak on quality of printed pattern

The μCP patterns were intended for patterning neurons on substrates; hence, they would be submerged in culture media for prolonged periods of time. It was important to investigate the effects of aqueous environment on the printed pattern. Since, Cy3 and FITC were chemically attached to streptavidin and polylysine respectively, the changes in fluorescence intensity (pixel values) were used to determine the percentage of printed material that re-dissolved back into the solution. The substrates printed with PLL-FITC were submerged in 1 mg mL^{-1} solution of Chondroitin 4 Sulphate (C4S) for 1 h. One set of substrates printed with Cy3-strep was submerged overnight in DI water and the second set was submerged in DMEM for six days. Following the soak, all the substrates were imaged again and compared.

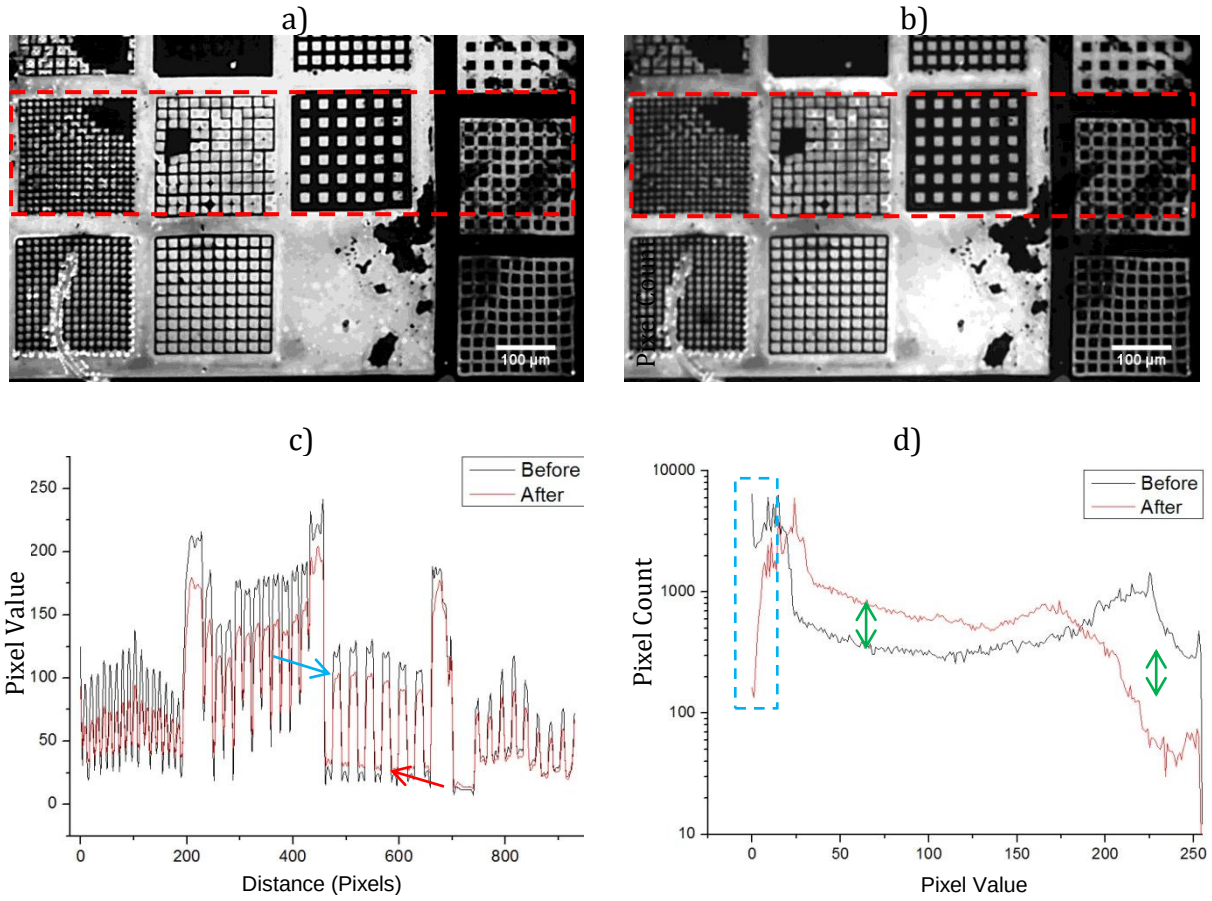


Figure 3.17:Fluorescent images of PLL-FITC pattern (a) before and (b) after 1 h soak in solution of C4S. c) Fluorescence profile comparison showing reduction of peak fluorescence and increase in background fluorescence. d) Histogram comparison showing the change of pixel value distribution. The red dashed boxes (a) and (b) indicate the area of image that was used for plotting the profiles and histograms. The blue dashed box in (d) highlights the sharp reduction pixel numbers with values below 15.

The effects of soaking the PLL-FITC pattern in solution of C4S for 1 h were the reduction in peak fluorescence and increase of background fluorescence. The increase of background fluorescence was evidenced by severe drop of number of black pixels (value=0) from 6419 to just 162 (Figure 3.17). This reduction in "black" pixel numbers may have occurred due to coating of background areas with PLL-FITC that has dissolved into the C4S solution from the printed patterns. The average fluorescence intensities of pre and post soak patterns were 90.9 and 77.9 respectively. This represents the 14.4 % drop in fluorescence intensity and consequently the amount of PLL-FITC on the printed surface. The overnight soak of Cy3-streptavidin in DI water resulted in the fluorescence drop of 72.5 % (Figure 3.18). While the six day soak in DMEM resulted in 92.75 % drop in fluorescence of Cy3 conjugated streptavidin (Figure 3.19). Table 3.4 shows the pixel value distribution of the three soak tests.

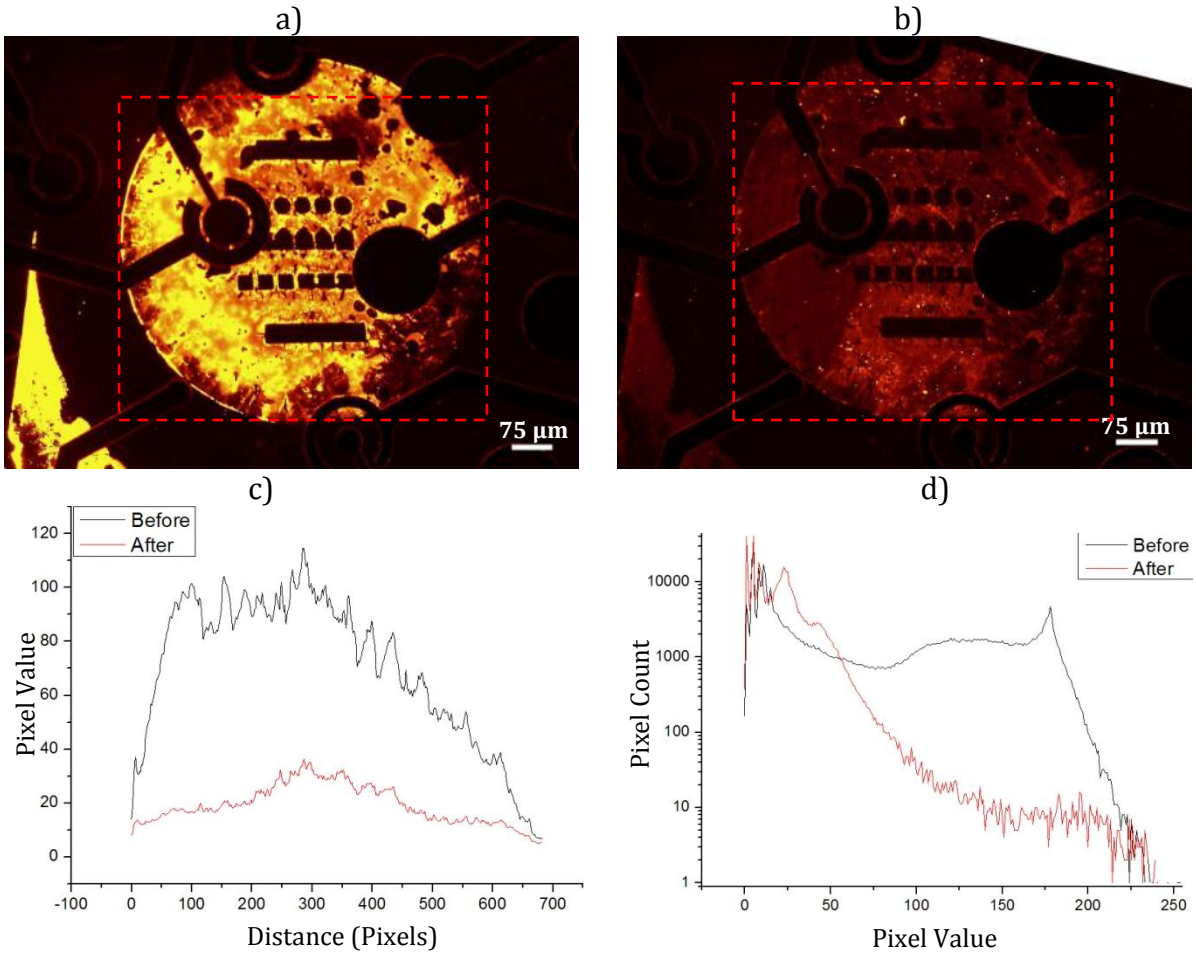


Figure 3.18: Fluorescent images showing the Cy3-strptavidin pattern (a) before and (b) after an overnight soak in DI water. c) Comparison of the fluorescence profiles from (a) and (b). d) Histogram comparison. The red dashed squares indicate the region that was represented in the profile and histogram comparisons.

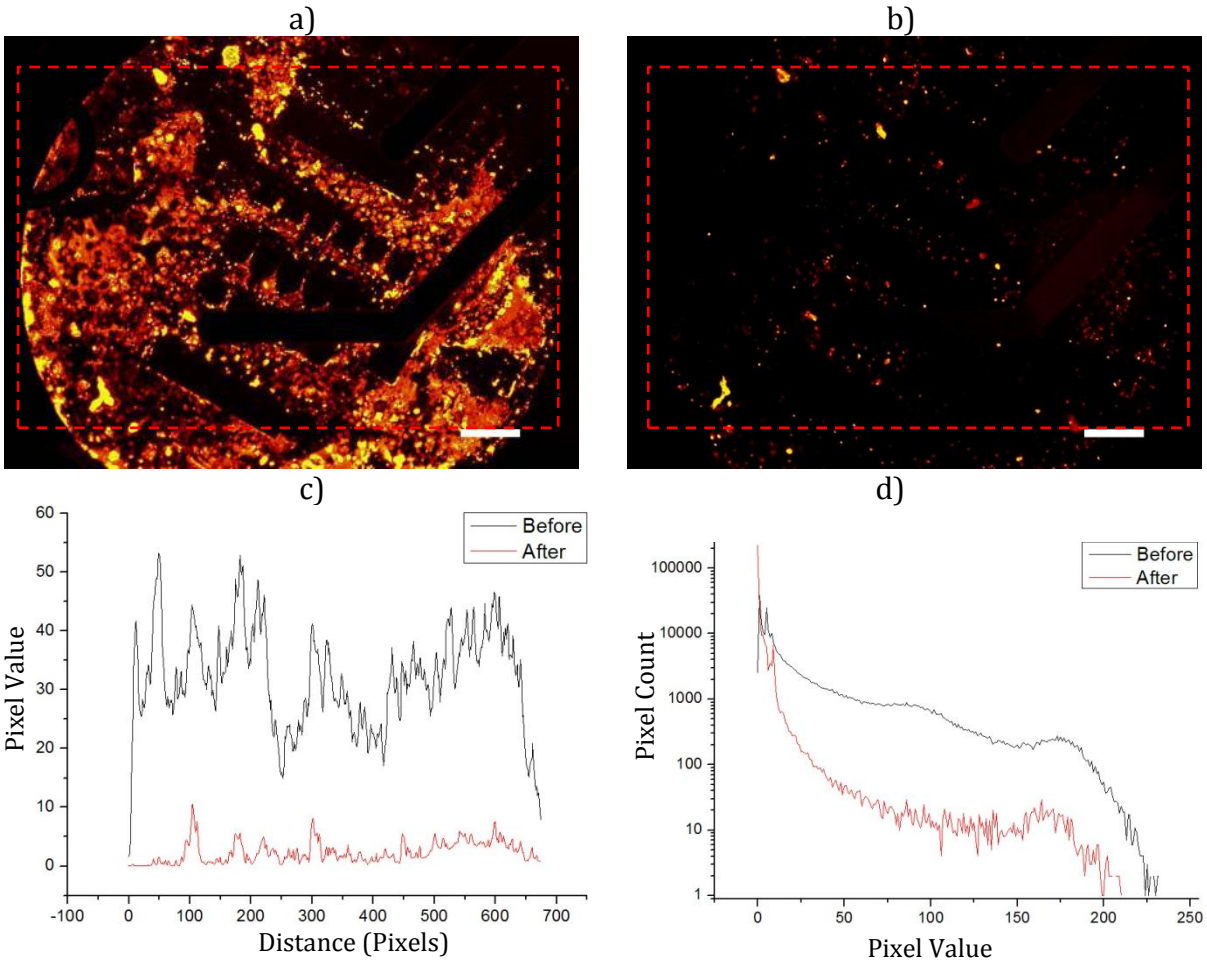


Figure 3.19: Fluorescent images showing the Cy3-strptavidin pattern (a) before and (b) after the six day soak in DMEM. c) Comparison of the fluorescence profiles from (a) and (b). d) Histogram comparison. The red dashed squares indicate the region that was represented in the profile and histogram comparisons.

Table 3.4: Table stating the pixel value distribution of all soak tests.

	Total pixel #	Dark pixel %	Gray pixel %	Bright pixel %
Before C4S	1.9×10^5	56.7	14.7	28.5
After C4S	1.9×10^5	61.8	26.3	11.9
Before DI	4.1×10^5	59.9	30.1	10
After DI	4.1×10^5	99.5	0.4	0.1
Before DMEM	3×10^5	87.5	10.7	1.8
After DMEM	3×10^5	99.5	0.4	0.1

3.2.5 Observed surface contamination with PDMS

During the experiments with μCP it was observed that a layer of residue sometimes remained on the substrate surface (section 2.10.2). The residue layer often resembled the μCP stamp features. The contaminating layer was also capable of trapping the fluorescent "ink" at the surface (Figure 3.20). This contamination became very obvious after the substrates were treated with oxygen plasma. The patterns became crystalline in appearance. This change in appearance was indicative of PDMS contamination because it turns into silica when oxidised as observed previously (Schnyder et al., 2003, Thibault et al., 2007). Washing or sonicating the substrates in ethanol, isopropanol, methanol or acetone was ineffective in removing the contamination. The only effective method to remove the PDMS contamination was soaking the surface in 1:14 solution of TBAF in DMF as suggested previously (Lee et al., 2003).

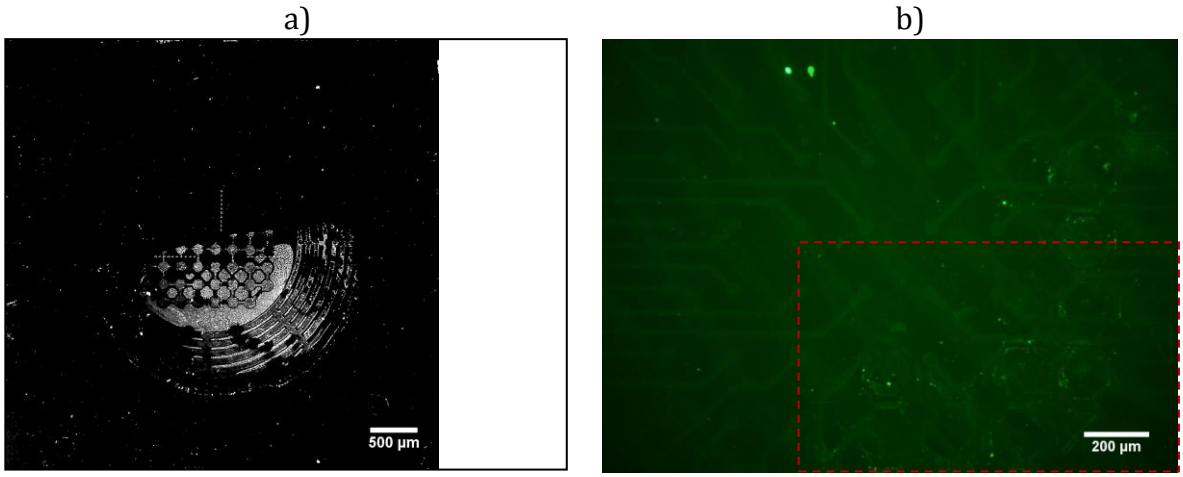


Figure 3.20: a) Inverted image of PDMS contamination of Pyrex surface. (No inking solution used). b) MEA surface contamination with PDMS that appears to be masking the printed fluorescent pattern.

3.2.6 Patterning substrates using microfluidics

In an attempt to avoid the issue of μCP described in sections 3.2.3 and 3.2.5, an alternative method of surface patterning was tested. Using a surface attached μF device, the substrate was patterned by perfusion of PLL-FITC of fluorescein solutions (Figure 3.21). This method of patterning removed the direct dependence of pattern quality on the stamp surface chemistry, inking protocol and printing technique. This method resulted in uniform deposition of "ink" on the substrate (Figure 3.22).

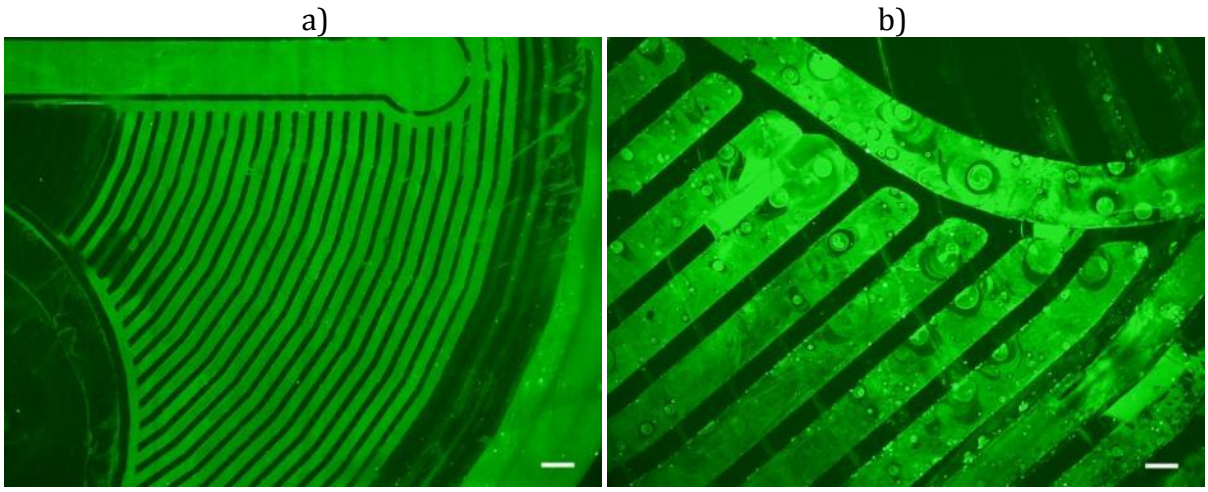


Figure 3.21: Fluorescence images showing the results of initial attempts of patterning fluorescein using the microfluidic device. Scale bars a) 150 μm b) 50 μm.

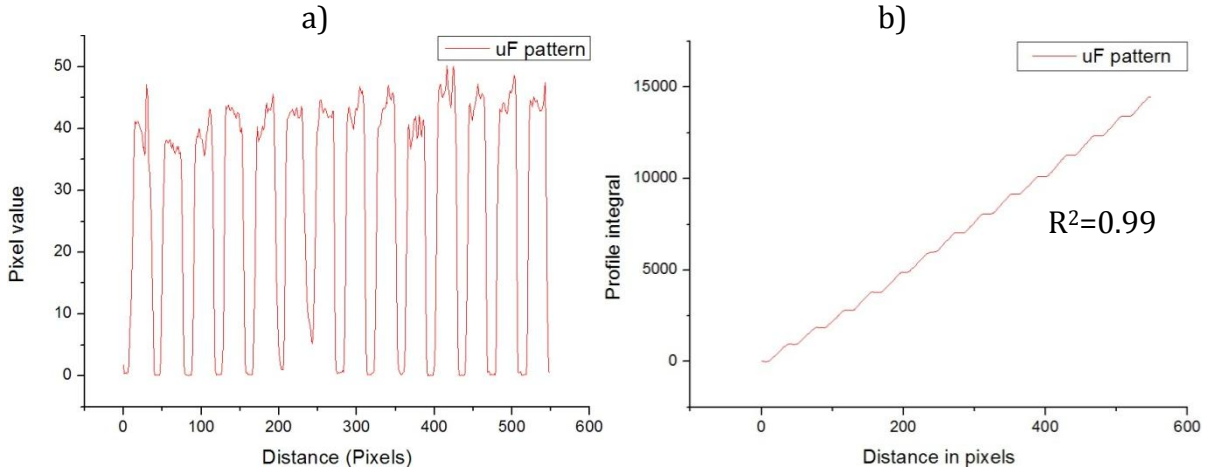


Figure 3.22: a) Fluorescence intensity profile if the pattern shown in Figure 3.21a. The fluorescent pattern was achieved by perfusion of fluorescein solution through the channels of μF device. b) Integrated fluorescence profile showing a linear increase or area under the profile in (a).

The above method of surface patterning was also performed using the μF devices fabricated in section 2.4.3. These devices were accurately aligned to the microelectrodes of the MEA as described in section 2.4.4. This sequence of steps resulted in an accurately

aligned, high quality and uniform fluorescent pattern on the surface of an MEA (Figure 3.23).

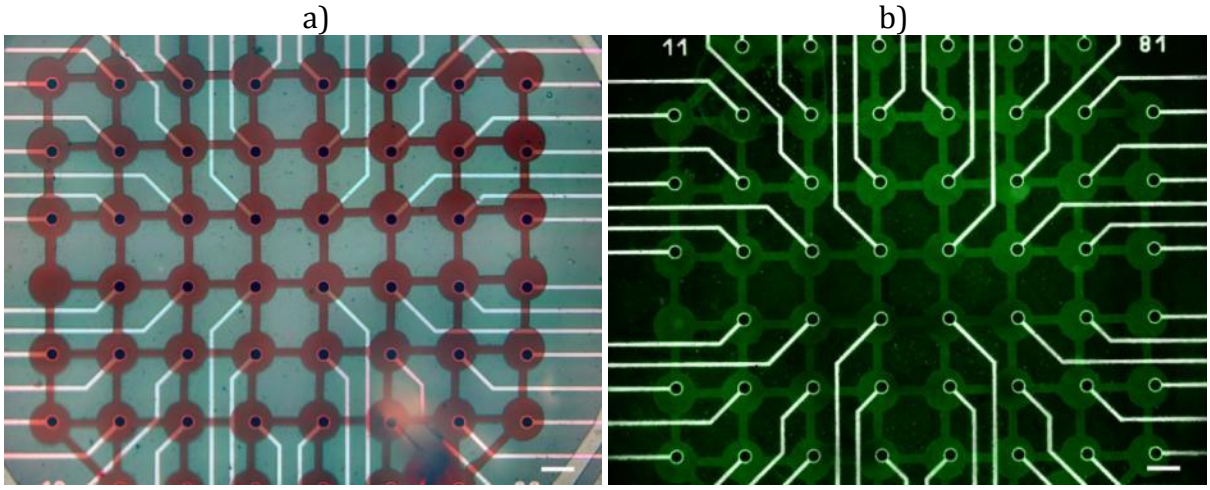


Figure 3.23: Aligned µF patterning on MEA. a) µF device filled with red food dye solution on MEA surface. b) 100µg/mL PLL-FITC pattern on MEA surface after the µF device was removed. Scale bars = 60 µm

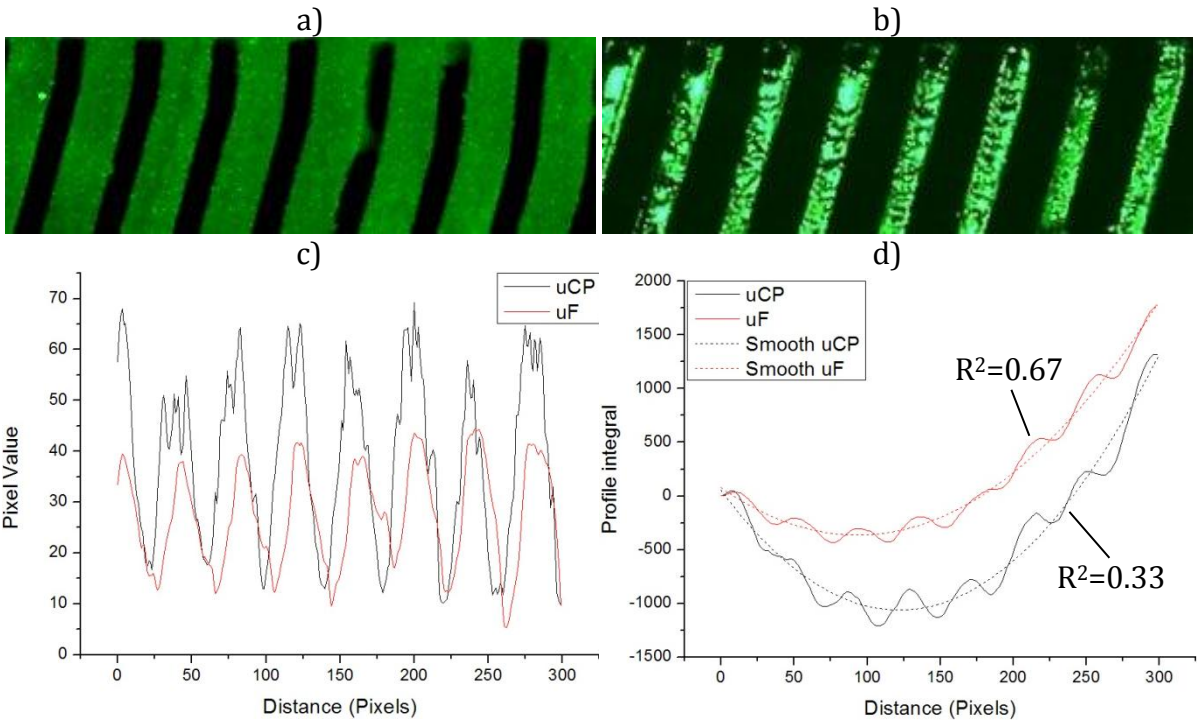


Figure 3.24: Direct comparison of a) µF pattern with identical b) µCP pattern. c) Fluorescence profile comparison plot. d) Integrated fluorescence data comparing the degree of feature recurrence (perfect recurrence: $R^2=1$).

The direct comparison showed that the variation of fluorescence was lower in patterns generated via µF devices. The fluorescent profiles where smoother and did not contain any random fluorescence spikes. Further comparison through integration and linear

fitting of fluorescence data showed that the μF patterns were more consistent (R^2=0.67) as compared to μCP patterns (R^2=0.33).

The combination of the device fabrication, alignment and surface patterning techniques resulted in a novel, improved and superior method of surface patterning compared to μCP. Because PDMS can be effectively used as an insulator, the major benefit of this methodology is the avoidance of PDMS contamination of areas such as the micro-electrodes (Maghribi et al., 2002). Additionally, the variation of ink deposition as seen in μCP is decreased. This is a direct benefit of ink adsorption from solution rather than from contacting surface. Overall, adaptation of this surface patterning method instead of μCP can be beneficial in experiments that require consistent surface patterning and uniform deposition of polymers on the surface.

3.2.7 Microfluidic gradients

The primary goal of integrating the microfluidic device was to create a concentration gradient of growth factors/inhibitors and provide neuronal culture with cues for direction of process growth. In essence, the microfluidic gradients are intended to make the growth and formation of neural networks in vitro less random.

Prior to fabricating the µF device described in section 2.3.1.2, a COMSOL simulation of gradient formation was performed with help from Dr Jorg Strutfolf (Life Science Interface Group, Tyndall National Institute, Cork, Ireland). The dimensions of µF device used in the simulation were identical to the envisioned device: main channel width=2000 µm, side input channel width=600 µm. The height of the channels was irrelevant because the concentration profiles in the vertical (z) axis were the same. The direction of fluid flow within the model is shown by red arrows. The wide 2 mm channel is perfused from one end. The gradient is generated by introducing a second fluidic channel (600 µm wide) perpendicular to the main channel and flow. Forcing the fluid from the side inlet into the main channel resulted in the final shape of the gradients (Figure 3.25). To visualize the gradients generated in practice, a microfluidic device was perfused using a syringe pump. Red food dye was added into one of two fluidic channels. The shape of the gradients generated in practice was in good agreement with the COMSOL simulation, although the simulated flow rates were higher, starting at 1.2 mL hr^{-1}, 2.4 mL $hr^{-1}$and 3.6 mL hr^{-1} (Figure 3.26). At these volumetric rates the diffusion is not noticeable in the µF channel because the rate of diffusion is relatively low. The diffusion can be observed either by looking at a longer channel or reducing the volumetric rate.

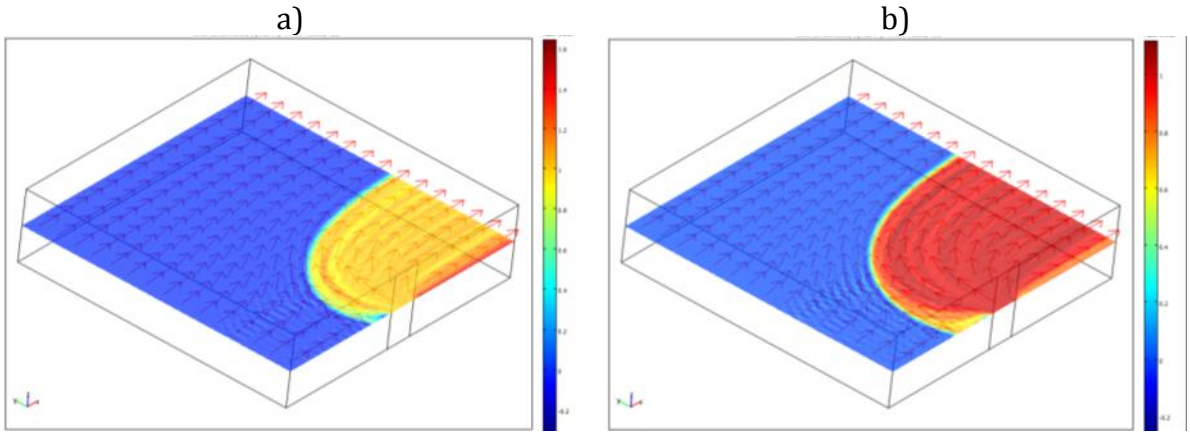


Figure 3.25: COMSOL simulation of gradient generated inside the µF device channel. Volumetric rate from the side inlet is simulated as a) 20µL min^{-1} (1.2 mL hr-1) and b) 60µl min^{-1} (3.6 mL hr-1).

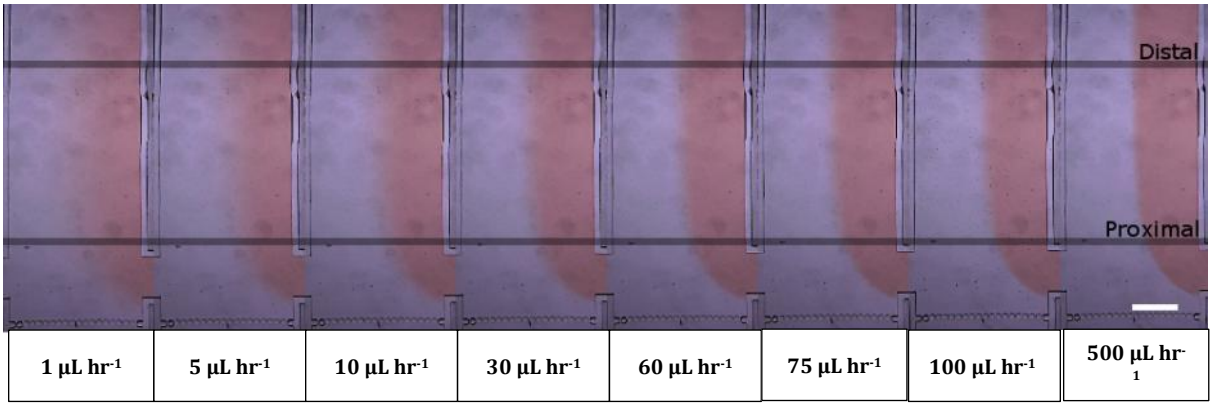


Figure 3.26: Sequential images of gradients generated by increasing volumetric rate. The dark horizontal lines indicate the 2 sections were luminescence intensity profiles of the gradients were measured (See Fig. Below) The measurements were taken from an average of 3 images of the same volumetric rate. Scale bar =650 µm.

Figure 3.26 shows the range of volumetric rates (1-500 µL hr^{-1}) as well as the associated gradients and degrees of diffusion. As can be seen from the figure, the diffusion becomes more prominent as the volumetric rates decrease.

The simulation rates of 1.2-3.6 mL hr^{-1} were deemed unpractical for use with neural cell culture due to excessive shear stresses; hence these rates were not tested in practice.

The volumetric rates directly determine the transverse concentration distribution of molecules within the channel, i.e. the concentration gradient from one wall to the other.

It was assumed that the luminescence intensity of the red food dye can be directly related to its concentration.

Thus, to determine the transverse concentration gradient, a series of luminescence profiles were collected from two parts of each image. One set of luminescence profiles were collected from a transverse plane close (proximal) to a side inlet, and the second set was collected approximately 2 mm downstream (distal) from the inlet.

Figure 3.27 shows the comparison of luminescence profiles for the range of volumetric rates. The high volumetric rates produce a steep sloped transition sections in luminescence profiles indicating that the red food dye is confined to one side of the channel, while gentle transitions are produced by low volumetric rates. Using these graphs it is possible to define the borders of fluidic environments that can be generated inside the channel as well as determining the concentration of various supplements in two sides of the channel. Similar gradient profiles were collected from gradients generated using passive means of perfusion such as gravity (hydrostatic pressure) and water surface tension as described in sections 3.1.7 and 3.1.8.

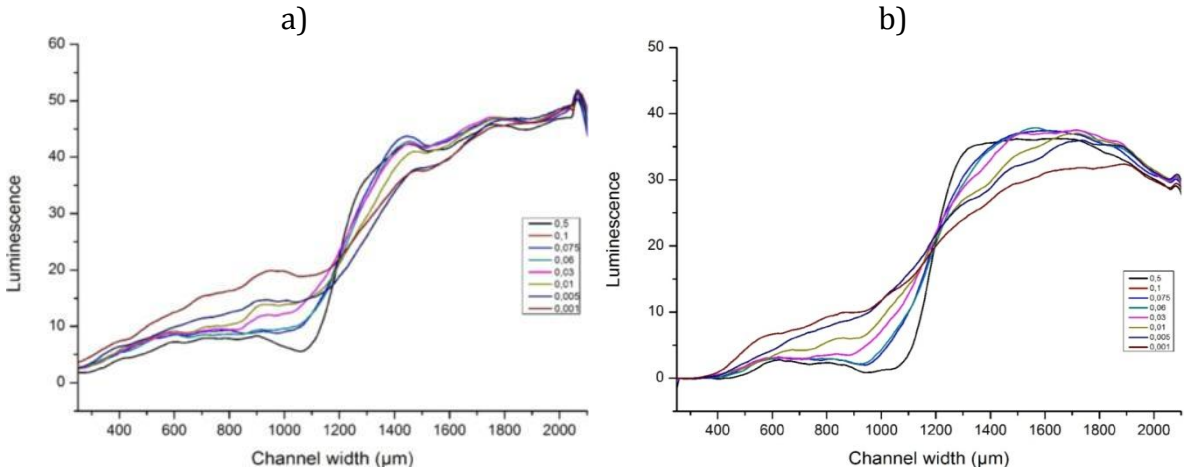


Figure 3.27: Graph of luminescence profiles of gradients generated using different volumetric rates. a) Measurement proximal to side channel inlet. b) Measurement distal (downstream) to the side channel inlet (See Fig. above). The graph represents the concentrations of red food dye in the channel.

These methods were tested to try and address the lack of space and a possibility of corrosion of electrical components of syringe or peristaltic pumps inside the biological incubators. Figure 3.28(a) shows the gradient generated using the gravity driven method.

The two reservoirs, one with DI water and the other with DI water and fluorescein, were connected to the two small opposing inlets of the µF device. This contrasts with the gradient generated in the previous experiment where one small side inlet was used to supply the food dye solution, while the clear DI water was fed into the µF from two additional inlets.

Figure 3.28(b) shows the gradient generated using the surface tension of the drops of DI water/Fluorescein solution placed on the inlets of µF device. The gradient seen in this figure takes up roughly a 1/3 of the channel width. This is because both the second opposing inlet and the inlet in the culture chamber were used for perfusion of the µF device. Since there was no direct or accurate way to determine the volumetric rates generated by the passive gradients, the slopes of the fluorescence profiles were used as an indicator of volumetric rates.

In order to determine the volumetric rates of passive gradients, the gradient slopes were compared with the slopes of gradients generated with syringe and peristaltic pumps. Figure 3.29(a) shows a sequence of fluorescence images of gradients generated via gravity, surface tension and the peristaltic pump. The revolutions per minute (RPM) setting on the peristaltic pump were sequentially increased from 0.01 RPM through to

0.09 RPM to generate a range of volumetric rates. All the images in Figure 3.30(a) were aligned with respect to each other and a broad (proximal/distal) fluorescence profile was collected. The width of the profile diminishes the influence of local variations in fluorescence and pixel values through averaging and is marked by the blue dashed box. The average fluorescence profiles are shown in Figure 3.29(b). The slopes of individual profiles are marked by red dashed lines.

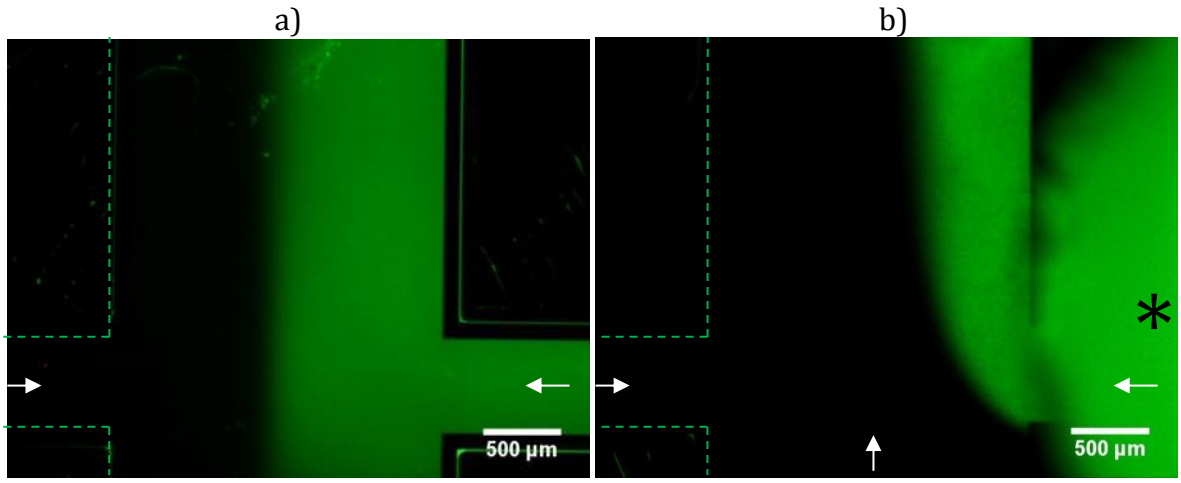


Figure 3.28: Fluorescent images showing the passively generated µF gradients. a) Gradient generated using gravity and difference in hydrostatic pressure between the source and the waste reservoirs. b) Fluidic gradient generated using droplet surface tension to drive the flow. Green dashed lines indicate position of the unseen channel borders of the µF device. The black asterisk indicates the fluorescent drop positioned over an inlet. The white arrows indicate the direction of flow from inlets.

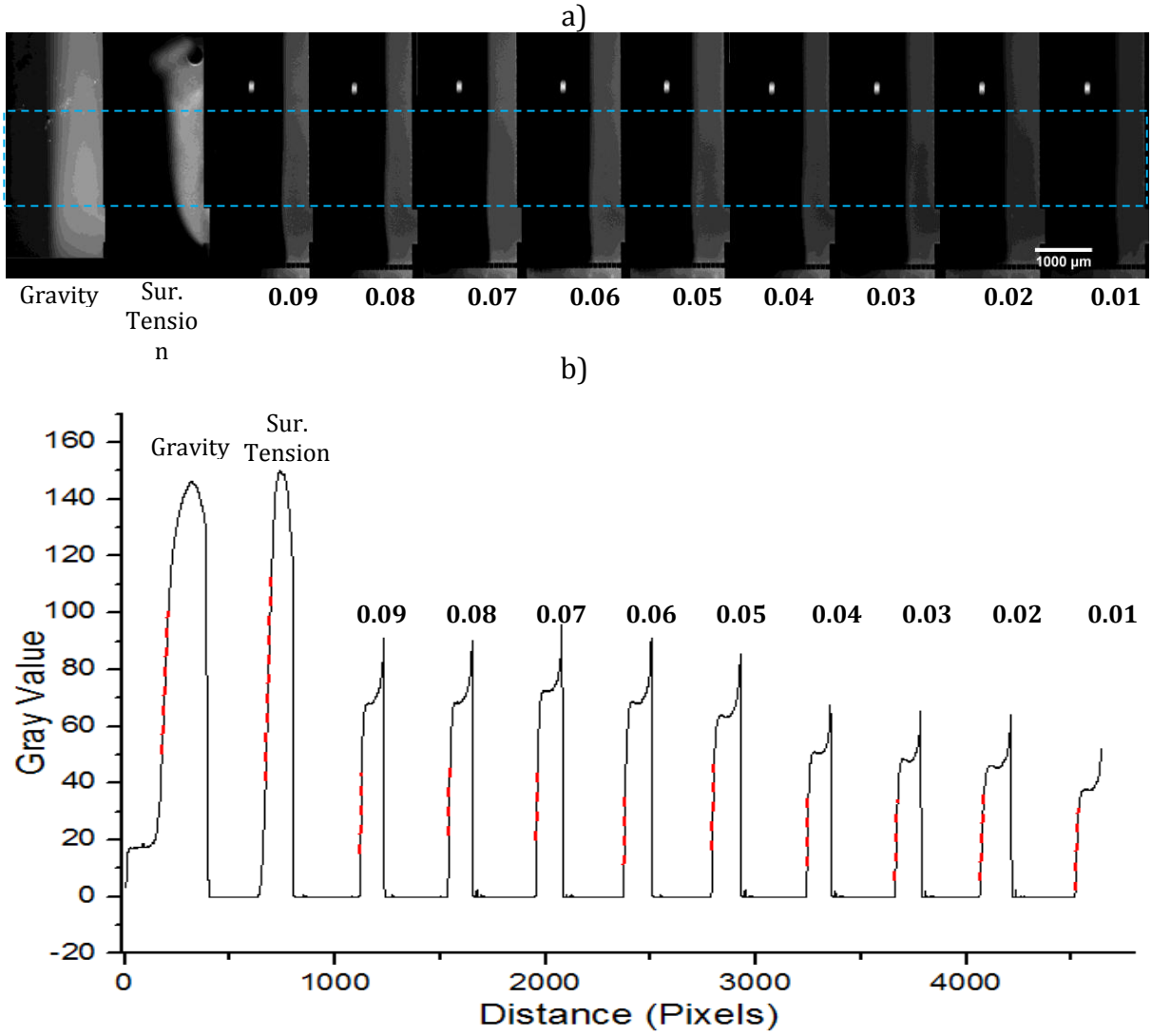


Figure 3.29: a) Sequence of grayscale fluorescence images of fluidic gradients generated using gravity, surface tension and a peristaltic pump. The numbers 0.01-0.09 indicate the RPM setting of the peristaltic pump when the particular image was taken. b) A broad cross-sectional fluorescence profile measured between the horizontal lines of the blue dashed box in a. Red dashed lines indicate the slopes of the gradient transitions and the lengths of the transition used to measure the slope.

Identical method of determining the slopes of gradients was applied to the inverted, grayscale image of Figure 3.30.

The gradient slopes of generated with gravity perfusion, surface tension, syringe and peristaltic pumps were compared (Figure 3.31). The comparison shows that the volumetric rates generated by the gravity perfusion lies between 0.001 and 0.005 ml hr^{-1} (0.02-0.08 µL min^{-1}) while the volumetric rate generated via surface tension lies between 0.06 and 0.075 ml hr^{-1} (1-1.25 µL min^{-1}). The minimum volumetric rate generated by the peristaltic pump, perfusing the µF device with two channels at 0.01

RPM was 0.093 ml hr^{-1} (1.55 µL min^{-1}) which is 4.5 X faster compared to the minimum tested perfusion rate of the syringe pump.

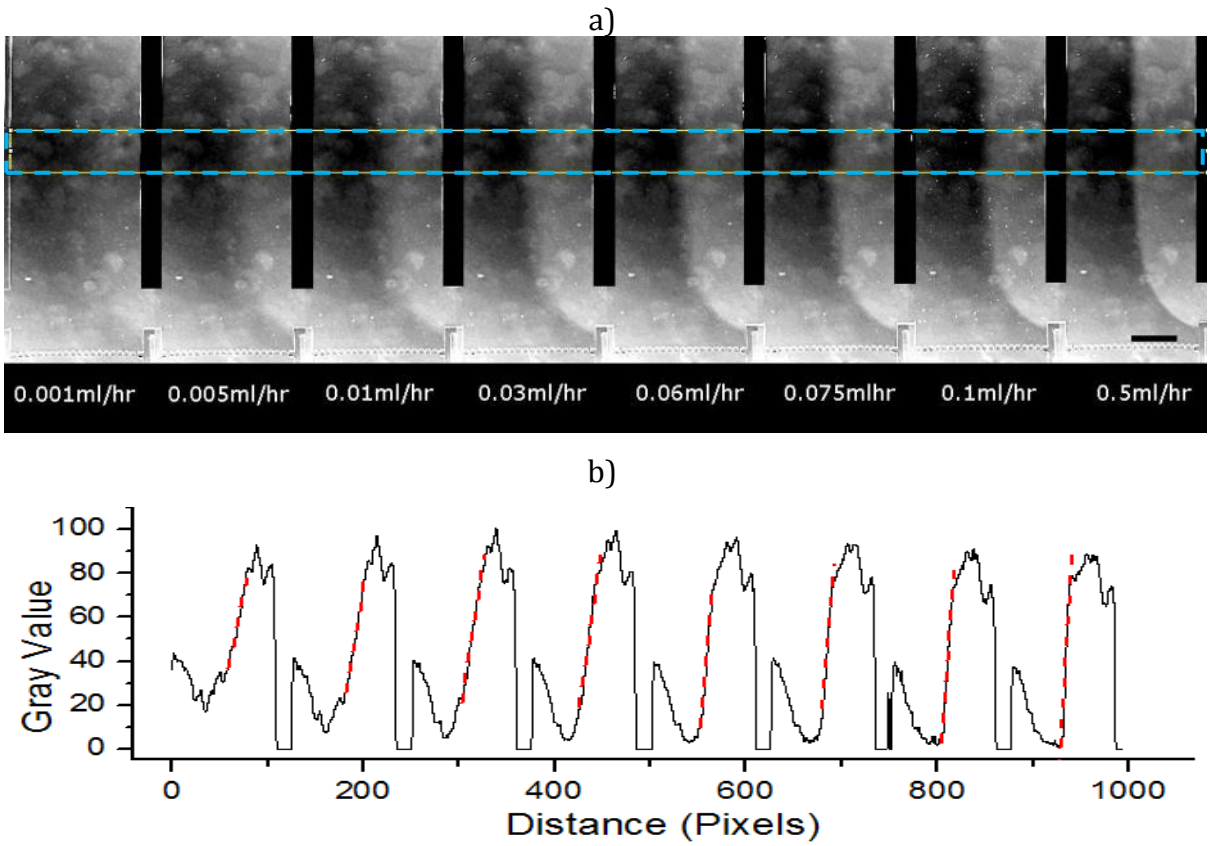


Figure 3.30: a) Sequence of inverted grayscale images of fluidic gradients generated using a syringe pump. b) A broad cross-sectional fluorescence profile measured between the horizontal lines of the blue dashed box in a. Red dashed lines indicate the slopes of the gradient transitions and the lengths of the transition used to measure the slope. Scale bar=650µm

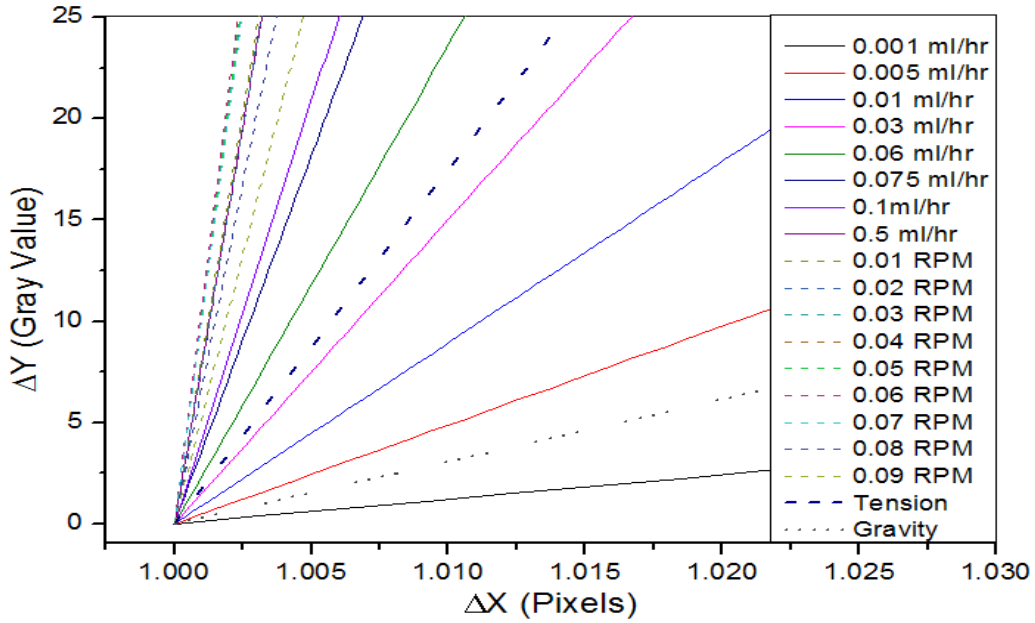


Figure 3.31: Graph of gradient slopes measured from the fluorescence and luminescence intensity profiles of fluidic gradients. Solid slopes represent gradients generated with a syringe pump; thin dashed lines represent the gradients generated with a peristaltic pump.

3.3 Discussion

The experiments described in this chapter were performed with the aim to optimise the methods and techniques intended to be used for culturing neural cells on chemically modified and patterned substrates. The specific challenges addressed in this chapter were fabrication of μCP stamps, the generation of good quality μCP patterns, integration of μF devices with the substrates and generation of microfluidic gradients using a number of perfusion methods. Additionally, this chapter attempted to explain the dependence of μCP on applied force and PDMS stamp feature deformation.

3.3.1 Fabrication of μCP stamps

The first technique that was optimised is the fabrication of the PDMS microstamps. The most common defects observed during the optimization of stamp fabrication were the air bubbles just under the stamp surface, separation of the PDMS stamp from the support rod and a complete failure due to tearing of the stamp when it was being removed from the master.

By placing the freshly mixed PDMS into a vacuum it was possible to remove any air bubbles from the mix. This step greatly reduced the amount of stamps fabricated with bubble defect. The rare occurrence of bubbles in all subsequent stamps was attributed to air being trapped when the PDMS pre-polymer came into contact with the silicon master. As the pre-polymer was heated, the air bubble expanded leaving defect in the stamp. To improve the stamp release from the master, the master was silanized by chemical vapour deposition (CVD) of TFOCS as previously described (Li et al., 2007, Qin et al., 2010). The SAM of TFOCS served as an effective release agent, allowing the stamp to be easily separated from the master. This treatment was also effective for masters containing deeper features of up to 100 μm as in case with μF devices. Once all masters were silanized the only problems encountered with regards to casting were associated with PDMS curing where on occasion parts of the stamp would fail to cure. This was attributed to water contamination of PDMS. Properly cleaned and dehydrated masters produced consistent results.

3.3.2 Generation of good quality μCP patterns

The primary technique for modifying and patterning substrates was the common method of μCP (Bernard et al., 1998). Using the flip-chip bonder, the optimal printing pressure was determined to be 2.0 N. At these pressures stamp sagging was rare but at

the same time it was possible to bring the entire surface of the stamp into contact with the substrate surface. Importantly, it was determined that the amount of ink transferred between the stamp and the substrate was directly related to the magnitude of applied force. This indicates that the μCP technique, and the patterns it generates, can be improved by substituting the PDMS with tougher elastomeric polymers and printing using higher contact forces. Alternatively, reducing the PDMS mix ratios from 10:1 down to 7:1 or 5:1 may prove to be sufficient for fabrication of stiff PDMS stamps capable of withstanding grater contact forces (Wang, 2011).

Despite all the optimization, the μCP proved to be a method that produced inconsistent results with regards to quality of the pattern on bare substrates. Quite often the batches of patterns that were printed on the same day using the stamps inked with the same protocol were notorious for displaying big variation in fluorescence intensities as well as pattern completeness. In addition to pattern variation, the μCP had the tendency to contaminate the printed pattern with PDMS residue. Additionally, the patterns were soak tested in DI water, solution of chondroitin 4 sulphate and cell culture media. The soak test showed the expected pattern degradation due to the material re-dissolving into the soaking solution. Despite this, the pattern was still observed indicating that there is a potential for long term surface modification without the need to chemically bind the pattern to the substrate surface.

3.3.3 Surface patterning using μF devices

To circumvent the issues of μCP discussed in the previous section, a novel, alternative method of aligned substrate patterning was tested. The novelty of this method is mainly in the combination and adaptation of previously described, simple techniques (Wang et al., 2010, Cira et al., 2012) into a surface patterning protocol superior to μCP. Provided that the design of the stamp is suitable, the PDMS μCP stamps can be used as masters for fabricating the μF devices. Thus, this technique can be implemented without any additional costs of micro-fabrication. There are a number of key advantages to this method of patterning over μCP. First, the μF device can be aligned to the features of the substrate i.e. the microelectrode using only an upright microscope; a flip chip bonder is not required. The μF can be detached and reattached if the alignment is poor. The second observed advantage is that the area of the surface that is being modified does not come into direct contact with PDMS; hence the chances of PDMS contamination are

greatly reduced. The third advantage observed during the experiments is the increased consistency of the patterns on the surface. The observed fluorescence levels were equal in all parts of the pattern. As an additional bonus, there is a reduction in the number of steps as compared to μCP.

There are a number of drawbacks to this method as well. The first drawback observed was the weak bond strengths between the μF device and the substrate. On occasion, the μF device detached from the surface during the patterning step. Since, these devices were cast from pliable PDMS devices, it was observed that a number of devices did not seal against the substrates. This was caused by the slight surface curvature introduced into the μF device during the molding step. Lastly, to ensure that the device remained on the surface, the physical contract had to be kept to a minimum. Overall the μF patterning is the preferred method because it is more consistent and once the μF devices are fabricated requires fewer steps to complete.

3.3.4 Microfluidic perfusion and gradients

The microfluidic device aimed at cell culture perfusion and generation of defined fluidic environments was designed and tested. A COMSOL simulation was performed to determine the shape of the fluidic gradients at specific flow rates. The practical tests showed a good agreement between COMSOL simulation and the experiments. The μF device, when perfused using a syringe pump, was able to generate stable fluidic gradients. When the flow rate was reduced sufficiently, a high degree of diffusive mixing occurred. Air bubbles did occur inside the device especially in the areas containing dead volume (liquid that is not moving) but there was no noticeable distortion of the fluidic gradients unless the bubbles were big enough to occupy a portion of the main channel.

Passive perfusion systems using surface tension and gravity were also tested. Both passive methods were able to generate similar gradients as the syringe pump; however, the gradients were only sustained for maximum of 15 min and 2 h for surface tension and gravity perfusion respectively. In these systems the air bubbles had much more influence on gradient generation. The flow of the fluid was easily blocked either in one channel or the entire device by small bubbles. To re-establish the flow, the entire device needed to be flushed. The surface tension method is also very sensitive to volume of liquid drops placed at the inlets and evaporation. In case of the gravity driven perfusion, the volumetric rates depended on the differences in height between the source and

waste reservoirs as well as the height difference between the two source reservoirs. This difference between the source reservoirs often led to domination of one source over the other, where the fluid from the dominant source would fill the main channel entirely.

Overall, even though the passive systems tried were much more compact, cheap and required no external power sources, they proved too unreliable and easily upset by the external environment.

3.4 Conclusion

In conclusion, this chapter looked at the method of μCP, surface patterning using μF devices as well as passive and motorized μF device perfusion. It was found that μF patterning of the surfaces is the preferred method over μCP as it produced patterns of more consistent quality as shown by fluorescence profile comparisons. The μF patterning also had practical advantages as it was less prone to alignment errors and generally more user friendly.

This chapter also looked at the different methods of μF device perfusion and their ability to generate and sustain microfluidic gradients inside the PDMS μF device. It was observed that the passive methods of μF device perfusion were able to generate comparable fluidic gradients as seen with perfusion pumps. However these methods severely lacked in reliability and were over-sensitive to surrounding environment. To achieve the comparable reliability of the passive perfusion would require a precise method of μF device and PMMA reservoir block fabrication coupled with stringent control of external environment. Specifically the passive perfusion devices need to be placed in an environment with controlled humidity to prevent evaporation of the reagent and perfectly flat horizontal surfaces to avoid imbalance in hydrostatic pressures between the reagent reservoirs.

Tables 3.1 and 3.2 summarize the positive and negative aspects of surface patterning and micro-fluidics methods discussed in this chapter.

Table 3.5 Table summarizing the positive and negative aspects of surface patterning techniques

Surface patterning methods	Positive aspects	Negative aspects
μCP with Drill Stand	V. Good vertical alignment Easily accessible	No XY alignment capability V. Poor control of applied force Final pattern quality is often poor
μCP with Hydraulic Rig	Cheap	V. Poor vertical alignment No XY alignment V. Poor control of applied force Final pattern quality is extremely poor
μCP with Flip Chip Bonder	Reasonably Good Vertical alignment Good XY alignment Controlled application of force Reasonably Consistent Pattern quality can be good	Speciality instrument Limited access Expensive Requires additional custom parts to integrate with μCP technique Pattern quality may suffer due to variations in vertical alignment
μF Patterning	Fundamentally very simple Reasonable XY alignment Possible to realign the μF if initial alignment was poor Consistent μCP stamps can be converted to μF device cheaply Pattern quality is often good	May initially require CAD design and silicon processing

Table 3.6: Table summarizing the positive and negative aspects of methods of μF device perfusion

Perfusion Method	Positive aspects	Negative aspects
Gravity Driven Perfusion	The setup is small, simple and cheap Requires no extra power supply Potential for long term perfusion (24 h) Potential for perfusion with multiple channels (more than 2) Low volumetric rate Large reservoir volumes Easy to set up Gradients easily imaged using the inverted microscope	Prone to spontaneous perfusion termination Prone to bubble formation Requires precise machining to fine tune the volumetric rates No control over the pre-set volumetric rates Difficult to load with perfusing solution Difficult to image using an upright microscope
Surface Tension Driven	Requires no extra	Prone to spontaneous perfusion termination

Perfusion	equipment Reasonably low volumetric rate Gradients easily imaged using upright and inverted microscopes	Prone to bubble formation V. Poor control over initiation of perfusion Incapable of long term perfusion due to low reservoir volumes Difficult to load the device with perfusing solution Requires steady hands and good dexterity
Syringe pump	Very good control of volumetric rate Can perfuse with very low volumetric rate Consistent Two channel perfusion Gradients easily imaged using an inverted microscope Large reservoir volume Long term perfusion (2-3 Days)	The setup is bulky and time consuming Requires an external power supply Limited to number of channels (depending on the unit). Hard to integrate with tissue culture
Peristaltic pump	Reasonably good control of volumetric rate Bi-directional perfusion Can use suction to draw fluid through μF device Less bulky than the syringe pump Two channel perfusion Gradients easily imaged using an inverted microscope Large reservoir volumes Long term perfusion (2-3 Days)	The minimum volumetric rate is high as compared to syringe pump. Requires an external power supply

Chapter 4

4.0 Electrophysiology and patterned neuronal networks

As discussed in the introduction chapter, most surfaces require some degree of modification to allow cells to adhere to these surfaces. The choice of modification can be influenced by the type of substrate used as well as other requirements such as solvent resistance or long term stability for example. Simple modification techniques that involve adsorption are advantageous because these can be performed quickly and are generally reversible. However, these types of modifications can degrade over time. More permanent modifications such as silanizations can also be used.

During this project, modified techniques such as adsorption and silanization were used on a range of surfaces to create localized patterns as described in detail in section 3.1. The modified, patterned surfaces were then used as substrates for culturing neuronal cell networks. Hence this chapter will focus on discussing long term culturing and patterning of neurons on a number of chemically modified surfaces including Pyrex, Cyclo-olefin, Silicon Nitride (SiN), Aluminium Nitride (AlN) and Polyimide.

The Pyrex and Cyclo-olefin surfaces were used as benchmarks since these surfaces are readily available and respond well to μCP or μF patterning. The SiN, AlN and polyimide are more specialized surfaces. These surfaces are specific to micro-electrode arrays (MEAs) where they are used as passivation for the conductive tracks (Multi-Channel-Systems, 2012). The reason behind cell patterning on all of the above surfaces is to attain control over localization of neuronal cell bodies. This is especially important when culturing and recording signals from neurons using MEAs. Due to low sensitivity of micro-electrodes, it is essential to minimize charge dissipation into the media; hence, close proximity of neurons to the electrodes is essential for good quality recording (Branch et al., 1998, Fejtl et al., 2006, Claverol-Tinturé et al., 2007). Additional to the neuron proximity, there are other factors affecting the quality of the recording. One of the main factors is the electrode impedance which contributes to background noise, reducing the S/N and making it more difficult to detect APs (section 1.3.3).

To date, a significant number of studies have been published demonstrating patterned neural cell cultures on MEA surfaces. These studies predominantly used dissociated hippocampal neurons on surfaces modified via adsorption, silanization or resist lift off (Chang et al., 2000, Nam et al., 2003, Chang et al., 2003, James et al., 2004, Liu et al., 2008). There is a small number of similar studies using the rat embryo spinal cord

neurons (Manos et al., 1999, Streit et al., 2001, Gramowski et al., 2004). However, specific studies utilizing *patterned* rat embryo spinal cord neurons on MEAs were not found. While hippocampal neurons are traditionally utilised for experiments involving memory and long term potentiation, the spinal cord neurons are more suitable for investigating the chemically controlled network formation. Patterning the spinal neurons has a direct link to the development and repair of the spinal cord.

Thus, the primary aims of the experiments described in this chapter are:

1) To use the surface patterning techniques described in section 3.2 for patterning E14 rat embryo spinal cord neurons on the surface of commercial and in-house built MEAs.

2) To use the MEAs and associated hardware to record the electrical activity of the patterned spinal cord neurons.

The specific aims associated with (2) are:

a) To achieve long term (14 days) neuronal viability on the MEA substrate,

b) To record individual neuronal action potential and

c) To record synchronized electrical activity of neurons located on separate micro-electrodes.

4.1 Materials and Methods

4.1.1 Chemical reagents and equipment

Aminopropyl triethoxy saline (APTES) and Tridecafluoro-1,1,2,2-tetrahydrooctyl-1-trichlorosilane (TFOCS) were purchased from Flurochem Ltd, UK. Aminopropyl trimethoxy silane (APTMS) was purchased from ABCR GmbH & Co, Germany. Acetone, Cy3-streptavidin, 1,2 dichloroethane (DCE), Dimethylformamide (DMF), foetal calf/bovine serum (FCS/FBS), hydrogen peroxide solution (30%), isopropanol (IPO), methanol (MeOH), penicillin/streptomycin solution (Pen/Strep), p-Phenylene diisothiocyanate (PDITC), poly-L-Lysine (PLL), poly-L-lysine FITC (PLL-FITC), sodium dodecyl sulphate (SDS), sodium hydroxide pellets, Terg-a-Zyme detergent and Tetra-n-butylammonium fluoride (TBAF) were all purchased from Sigma-Aldrich, UK. Chondroitin 4 sulphate (C4S), fluorescein, fluorescein sodium salt, hydrochloric acid, polyethylene(imine) (PEI), pyridine and sulphuric acid were all branded "Fluka Analytical" and purchased from Sigma-Aldrich, UK. Dymax UV curing adhesive was purchased from ECT Adhesive Solutions, Ireland. B 27 Supplement, Dulbecco's modified eagle medium (DMEM), Balanced Salt Solution (HBSS), GlutaMAX supplement were purchased from Invitrogen, CA, USA via Bio-Sciences, Ireland. NOA 68 UV curing adhesive was purchased from Norland, NJ, USA. Polydimethylsiloxane (PDMS) was purchased from Dow Corning under trademark Sylgard 184. De-ionised water was purified using Elga water purification system, Veolia Water Systems, Ireland. The de-ionised water used throughout had resistivity of 18.2 MΩ·cm. Pyrex substrates and 6 well polystyrene culture plates were purchased from Startsted. Biocompatible double sided adhesive tape was purchased from Orafol, Germany. Halogenated ether/Isoflow used for rodent anesthesia was supplied by Dept. of Anatomy, UCC with permission from the head of department.

Other hardware required for fabrication of micro-stamps was machined from poly(methylmethacrylate) (PMMA) or polytetrafluoroethylene (PTFE) in house. The etched silicon masters were also fabricated in house

4.1.2 Fabrication of micro-electrode arrays

As mentioned in section 4.0, the patterning of neurons was also attempted on in-house built MEAs. Fabricating the MEAs in-house allowed experimentation with neuronal growth on the alternative passivation layers. Three sets of MEAs were fabricated; one set passivated with silicon nitride (SiN), a set passivated with aluminium nitride (AlN) and a set passivated with polyimide. The design of the MEA layout was similar to the commercial devices with 60 microelectrodes of 30 µm diameter and 200 µm pitch (spacing between centres of electrodes).

The devices were fabricated using bi-layer metal lift off procedure (Figure 4.1) which was carried out as follows; first, 4" Pyrex wafers (1 mm thick) were spin-coated with Hexamethyldisilazane (HMDS) primer at 4000 RPM for 50 sec to improve photoresist adhesion followed by spin-coating of Polymethylglutarimide (PMGI) resist. The wafer was then baked on a hotplate at 170 °C for 3 min. Following the resist bake, HDMS was spin-coated onto PGMI at 4000 RPM for 50 sec followed by spin-coating of Microposit S1813 imaging resist at 4000 RPM for 50 sec. The wafer was then baked on a hotplate at 115 °C for 2 min.

The wafers were then exposed to metal level photo-mask (this mask defined the layout of the microelectrodes, conductive tracks and contact pads) in Karl Suss MA1006 mask aligner at 70mW cm^{-2}, developed in Microposit 319 developer, rinsed in running DI water and oven baked at 90 °C for 30 min.

Following the resist patterning, the wafers were treated with Ar plasma for 30 sec and $2x10^{-7}$ Torr in an evaporator to improve metal adhesion. Ti:Pt (10nm:100nm) was then evaporated onto the wafer at 80 °C.

The metal lift off was performed at 80 °C in Microposit R1165 resist stripper. The metal patterned wafers were then rinsed in DI water before deposition of passivation coatings.

Following the metal lift of, each device was coated with either: SiN, AlN or polyimide passivation. 500nm SiN passivation was deposited onto the devices by chemical vapour deposition (CVD) in STS310 PECVD system. AlN was deposited at the thickness of 650 nm by sputtering in Oxford Instruments Plasmalab 400 Magnetron Sputtering system. Polyimide was spin-coated onto the devices at thickness of 6 µm and cured in a vacuum oven at 250 °C.

The patterning of passivation coating was carried out as follows: The SiN and AlN passivation layers were patterned using the same procedure as described for metal deposition and patterning. However, the assisting layer of PGMI resist was omitted. An appropriate passivation level photo-mask was aligned with the metal features of the MEA. This photo-mask defined the areas that are free from passivation, i.e. the micro-electrodes and contact pads. Polyimide was patterned using 7 µm thick layer of AZ9260 photoresist instead of Microposit S1813 photoresist.

After resist patterning, SiN passivation was etched in STS Inductively Coupled Plasma (ICP) using CF_4/CHF_3 chemistry. AlN passivation was etched via reactive ion etching (RIE) in Oxford Instruments RIE Plasmalab System100 using BCl_3 chemistry. And finally, Polyimide was etched in ICP system using O_2/SF_6 chemistry. Following the passivation etch, the remaining resist was stripped using R1165 resist stripper and devices thoroughly rinsed in DI water.

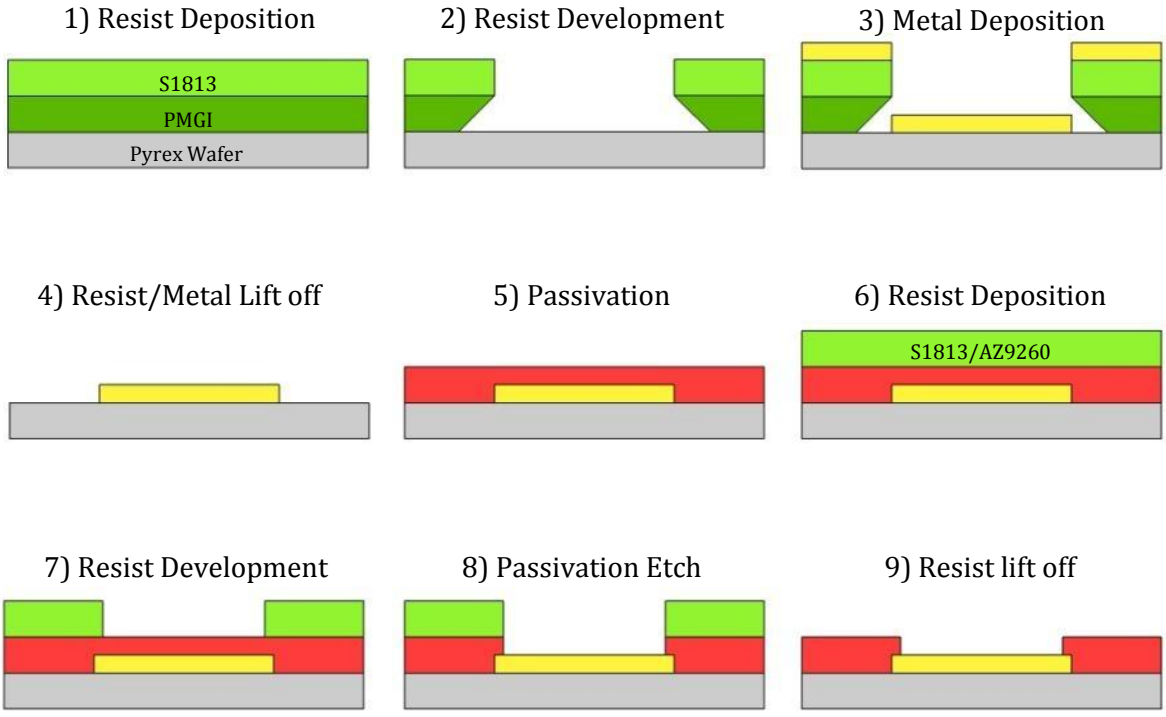


Figure 4.1: Schematic summarizing the bi-layer metal lift-off process. The bi-layer process ensures that the metal lift off is efficient and precise. This is achieved through creating an under-etch of S1813 resist (See step 2) so that the deposited metal on the glass does not form a continuous layer with the metal deposited on the resist. Thus, when resist/metal lift off is performed, the metal pattern is not affected by this process.

Following MEA fabrication, the microelectrode impedance was measured using an electrochemical workstation and three electrode method (Figure 4.2). The reference electrode was Ag/AgCl, the counter electrode was platinum while the working electrodes were the micro-electrodes on MEA surface. To measure the impedance of micro-electrodes, the culture chamber was filled with 1M solution of PBS. Voltage of ~5 mV and frequency range of 100 Hz-100 kHz was applied between the Ag/AgCl and one micro-electrode on the surface of the MEA. The AC voltage was superimposed over DC potential of 300mV. Using this method, the impedance of three out of 60 micro-electrodes on each type of MEA was determined. Additionally, the impedance of the large ground electrode was determined on the MEAs passivated with AlN and SiN.

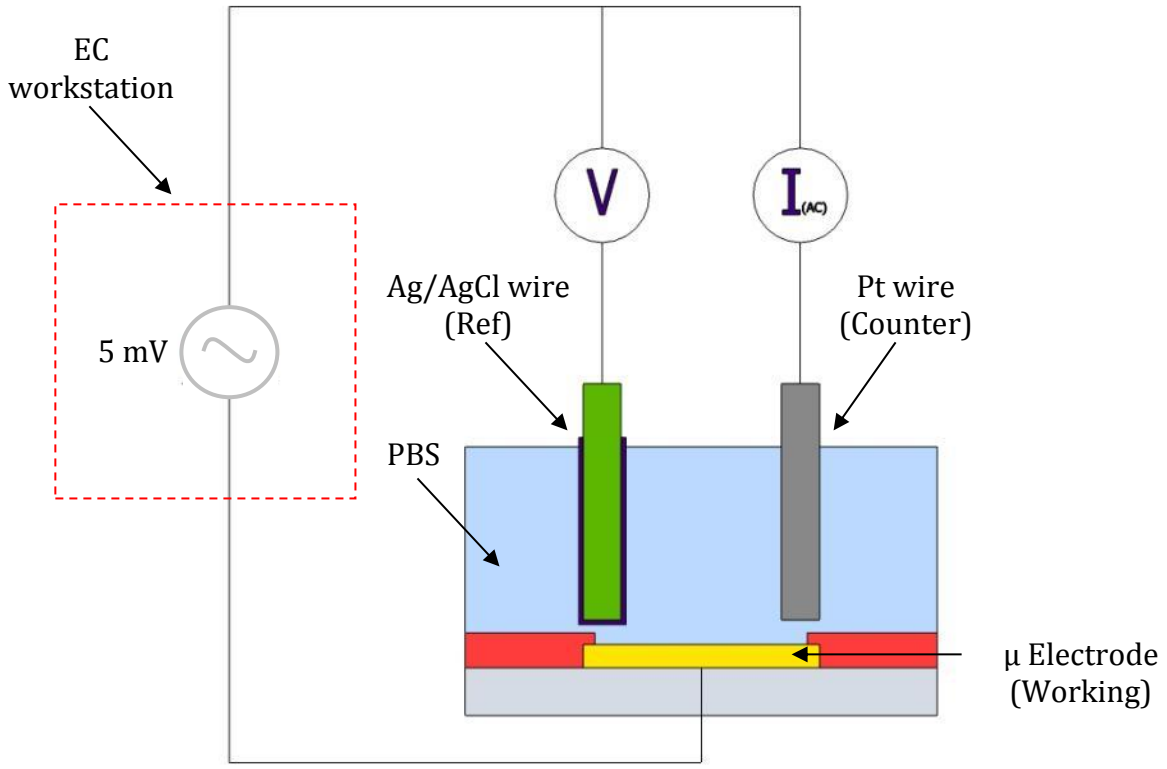


Figure 4.2: A schematic summarizing the EIS setup. The current is supplied to the system using an electrochemical work station. The counter electrode was a platinum wire, while the reference electrode was Ag/AgCl. The working electrode was the microelectrode of interest on the surface of MEA.

4.1.3 Surface pre-treatment and chemical modification

The surfaces used for chemical modifications and cell culture included Pyrex, Zeonor, SiN covered Pyrex, as well as MEAs with SiN, AlN and polyimide passivation layers. All

surfaces were modified via simple adsorption technique. Additionally Pyrex, Zeonor and SiN insulated MEA were also silanized with amino-silanes. Brand new surfaces did not undergo any surface cleaning prior to chemical surface modification, unless stated otherwise.

To achieve cellular adhesion to the substrate, PLL, PDL, PEI, Fibronectin and FBS, as well as the mixtures of these solutions, were used to modify both silanized and bare substrates. Additionally these substances were used for both non-patterned and patterned surface modification. The C4S was used as the cytophobic surface modifier mainly in conjunction with patterned cytophilic surfaces. This compound was used as a substitute for the chondroitin sulphate proteoglycan (CSPG), a protein widely regarded as one of the most effective inhibitors of axonal growth (Fawcett and Asher, 1999a, Bradbury et al., 2002).

The cell culture experiments were split into three sets:

1) Culture on patterned substrate to gain practical experience with basic surface modification, murine dissections and cell culturing. Optimize the substrate patterning techniques and modify the culturing protocols to suit the patterned substrate.

2) Culture on a non-patterned MEA to gain practical experience with gathering electrophysiological data from cell cultures, long term culture maintenance on MEA surface.

3) Culture on patterned MEA as a step towards the integration of the techniques performed in the previous experimental sets.

4.1.4 MEA surface coating

To test the electrophysiological performance of un-patterned neural cultures, the surfaces of the MEAs were coated with either PLL or PEI as previously described elsewhere (Chang et al., 2000). Briefly, to prepare the MEAs for adsorption of PLL/PEI the surface was first rinsed with DI water then dried with an air gun. Once dry, the MEA was exposed to plasma for <1 min at 32 W and 900 mTorr. After plasma treatment the MEAs were placed into the biological safety cabinet and filled with 70% ethanol and soaked for 20 min. The UV lamp of the cabinet was turned on for the period of the ethanol soak. These steps ensured that the MEA was sterile. The MEA surface was then soaked in 100 µg mL^{-1} solution of PLL or 1mg mL^{-1} solution of PEI for 1 h at RT. After

incubation, the polymer solution was aspirated and the MEAs were rinsed with DI water three times.

4.1.5 Substrate patterning

The MEAs, Pyrex and Zeonor slides were patterned via μCP and μF devices as described in sections 3.2.2 and 3.2.6 respectively. However, instead of Cy3-streptavidin or fluorescein, the PDMS stamps were inked with 100 μg mL^{-1} PLL/PLL-FITC or 1mg mL^{-1} PEI solution. The substrates were printed using the flip-chip bonder with 2.0 N contact force and 1 min contact time. An alternative μCP method was attempted where the substrate was first soaked in PLL, PDL or PDL : Fibronectin (100 μg mL^{-1} : 24 μg mL^{-1} respectively) solution overnight in a fridge (3 °C). After the soak, the substrates were rinsed with DI water, dried and patterned via μCP with C4S. This method provided the neural culture with the maximum surface for growth while restricting the cellular attachment only in small areas printed with C4S. The perceived advantage in doing this is better culture density and media conditioning.

Patterning the substrate using the μF device was also performed as described previously. Briefly, the sterile PDMS μF device was attached to the surface and filled with solution of PDL or PDL-fibronectin for 1 h at 37 °C. After incubation, the substrates were rinsed three times with cool, boiled DI water and placed into UV chamber for 20 min.

Note: The PEI solution was made up at a concentration of 1mg mL^{-1} by diluting 0.1 g of 50% (w/v) PEI in 50 mL of freshly prepared borate buffer. Borate buffer was made up by dissolving 3.09 g of 100 mM boric acid, 2.19 g of 75 mM NaCl and 4.77 g of 25 mM Borax in 1 L of molecular grade DI water. The solution was heated and stirred on a hotplate to help to dissolve the added chemicals. Then the pH was adjusted to 8.0 with HCl. The solution of PEI was then exposed to UV for 1 h to reduce the chances of infection during the cell culture step.

4.1.6 Substrate silanization

To try and enhance the longevity and cell compliance with the printed patterns, separate set of substrates (Pyrex, cyclo-olefin and a number of MEAs) were silanized. First, the substrates were plasma treated as describe in section 4.1.4. The plasma treated substrates were then silanized with 3% APTES and further modified with PDITC cross-linker as previously described (Wachter et al., 1973, Manning et al., 2003, Raj et

al., 2009). The silanized and cross-linked substrates were then patterned via μCP with PLL or PEI. The remaining free PDITC sites were blocked by incubation in 1 mg mL^{-1} solution of C4S. Note: PDITC is a homobifunctional crosslinker and was chosen because of its ability to bind amine groups present on APTES and PLL or PEI polymers (Raj et al., 2009).

Table 4.1: Table summarizing the types of surfaces and silanes used for surface modification

Substrate	Prep	Silane	Crosslinker	Patterning method	Patterned Polymer	Block
Pyrex	Plasma	APTES	PDITC	μCP	PEI/PLL	CSPG
	Plasma	APTMS	PDITC	μCP	PLL	
Zeonor	Plasma	APTES	PDITC	μCP	PEI/PLL	CSPG
MEA	Plasma	APTES	PDITC	μCP	PEI/PLL	CSPG
	DI water			μF	PDL/fibronec.	
SiN Pyrex	DI water			μF	PDL	

4.1.7 Neuronal culture and electrophysiology

The rat embryo spinal cord neurons were cultured on the modified substrates as described in section 2.7. The neurons were seeded at the density ranging between 1 x 10^5 - 1 x 10^6 cells cm^{-2}. Electrophysiological recording were performed on neuronal culture after minimum of 14DIV on the MEA surface as described in section 2.8. Each recording was kept to a maximum of two minutes to avoid excessive file sizes. The signal processing was performed off line on recorded signals.

4.2 Results

4.2.1 Neuronal culture optimization and patterning

4.2.1.1 Patterned neurons on Pyrex

Cell culture patterning was carried out on a number of substrates including Pyrex, Zeonor, and SiN coated Pyrex wafers. The aim of patterning the neuronal cells on these substrates was to optimize the protocol and to determine how it can be integrated with MEAs to produce electrically active patterned neuronal networks.

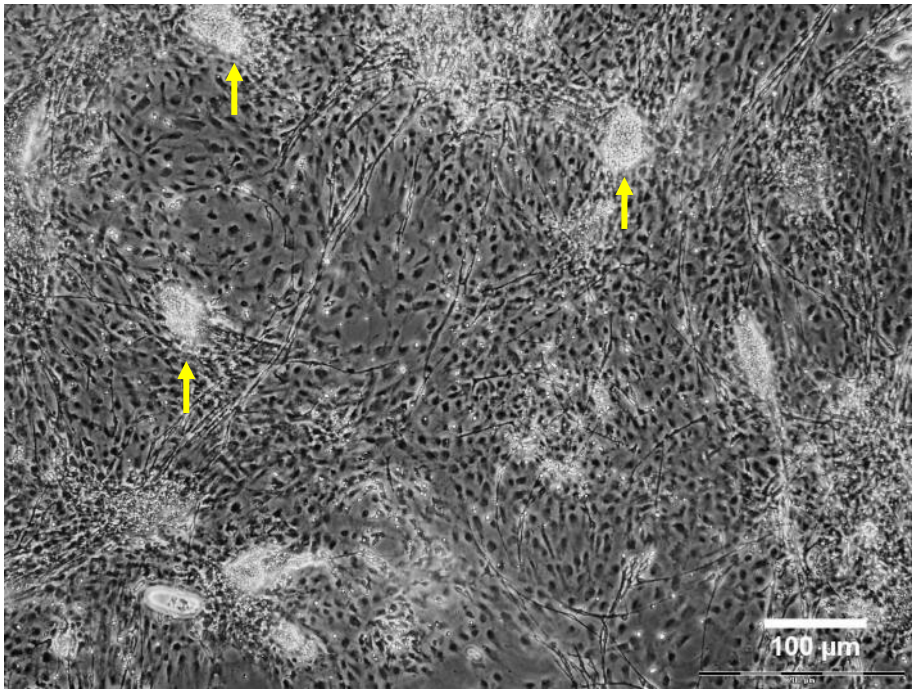
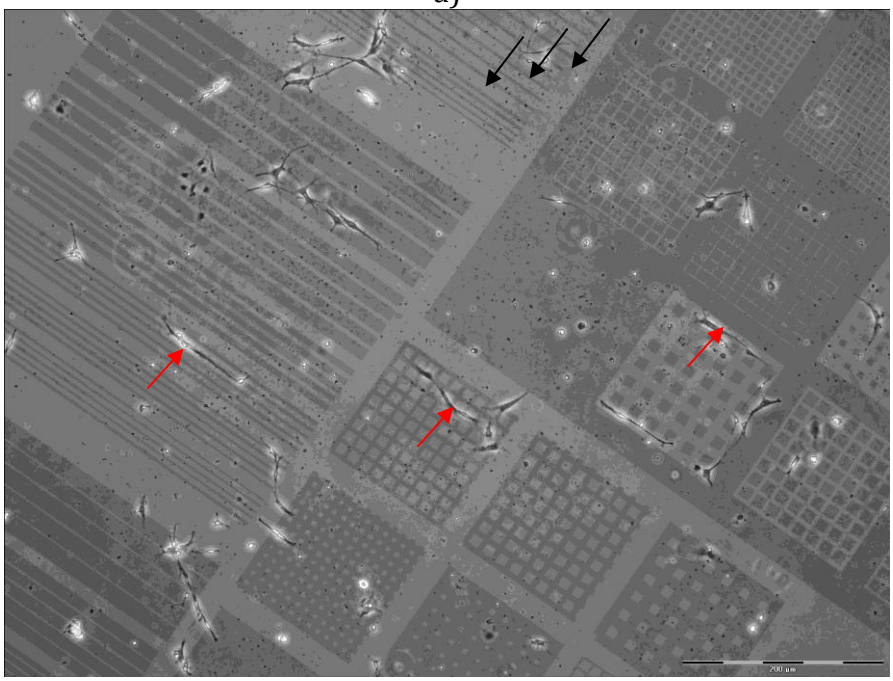


*Figure 4.3: Phase contrast image of un-patterned E14 spinal cord cells of Pyrex surface silanized with APTMS and patterned with PLL. No CSPG was used in this culture; the cells are adhering directly to PDITC crosslinker as well as PLL. Cell number = 1*10^{6} cm^{-2}. The culture seen is very dense and shows that cells were clumping together (yellow arrows).*

Figure 4.3 shows of E14 rat embryo spinal cord cells at ~5DIV on Pyrex substrate silanized with APTMS. The cells were seeded at a density of 1x10^{6} cm^{-2}. The substrate was patterned with PLL; however, no C4S was used to block the remaining amino groups of the PDITC crosslinker. Hence the cells were able to attach to both PLL and directly to PDITC thus yielding a non-patterned cell culture.

Figure 4.4(a) and (b) show patterned E 20 rat embryo spinal cord cells at 5 DIV and ~10 DIV respectively. The cells were cultured on Pyrex substrates silanized with APTMS, patterned with PLL and blocked with C4S.

a)



b)

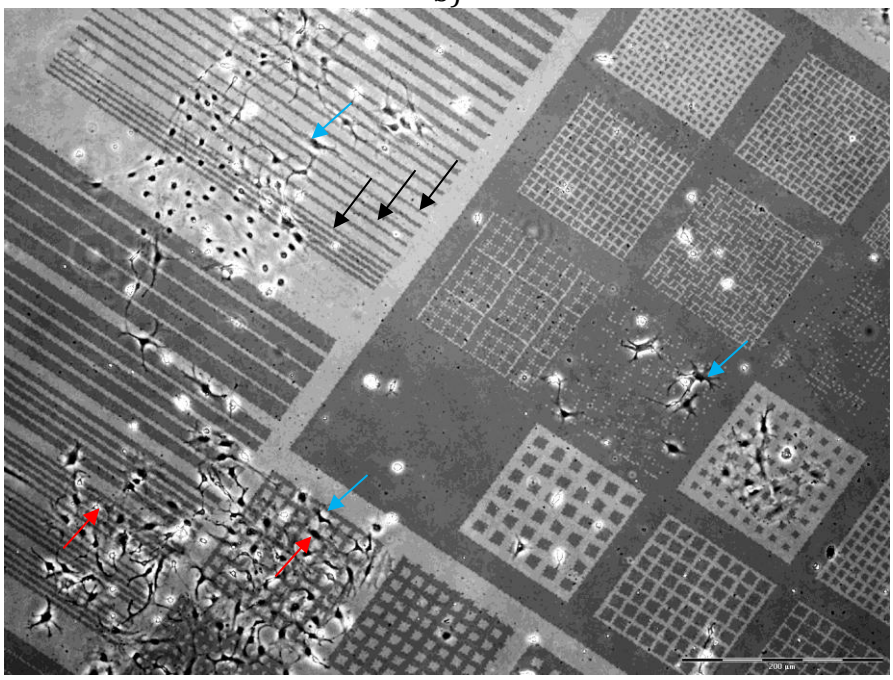


Figure 4.4: Phase contrast image showing patterned E20 rat embryo spinal cord cells on patterned Pyrex substrate at a) 5DIV and at b) ~10DIV). Examples of cells that appear to be aligned to the printed pattern are marked with red arrows. b) Evidence of significant rearrangement of cells on the surface. The black arrows indicate the position of visible pattern (as seen in (a)); red arrows indicate the positions of the patterned cells seen in (a). The blue arrows indicate some of the new positions of patterned cells. The red arrow point to cells resembling Type I astrocytes. Note: the visible pattern was digitally superimposed.

The difference between the positions of patterned cells seen in the two images is attributed to cellular migration to the desired areas of the printed pattern (Millet et al.,

2007). Another observation made is the difference in cell morphology. At the earlier time (5DIV) the cells resemble bipolar neurons with one cell body and 2-3 processes. However, at the later time (~10DIV), the cells resemble multi-polar neurons and astrocytes, sprouting numerous processes and taking up much more surface area as compared to the neurons at 5DIV. (Note: the actual cell type was not confirmed as this procedure required fixing the cells to the substrate and using fluorescently labeled antibodies to tag cell specific markers such as glial fibrillary acidic protein (GFAP) for glial cells and Neurofilament for neurons).

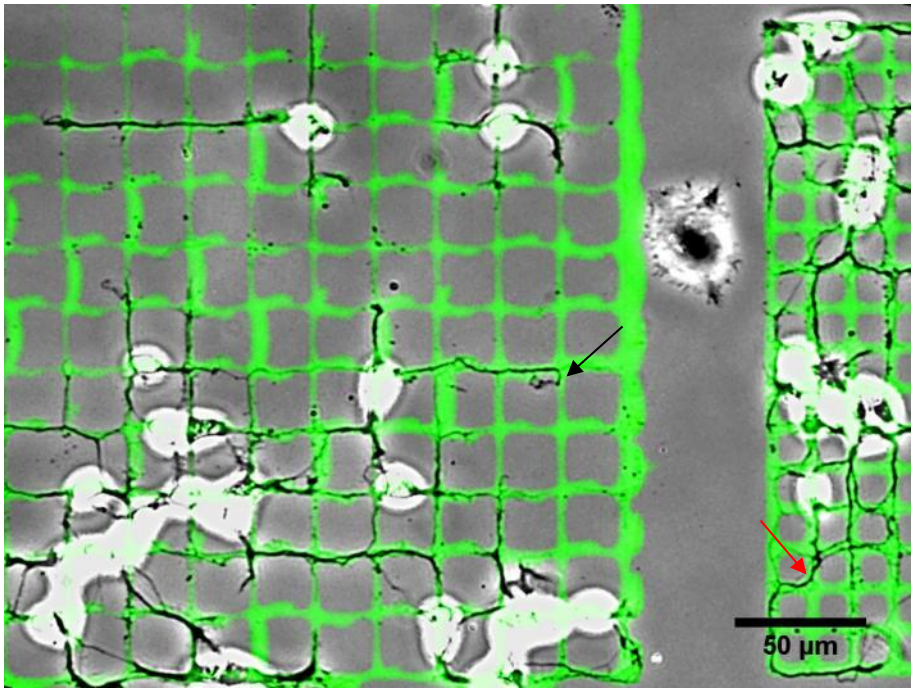


Figure 4.5: Combined fluorescence and phase contrast image of E17 rat embryo spinal cord cells on Pyrex surface patterned with PLL-FITC at 3DIV. Black arrow indicates a neuronal process that made a complete U-turn in under 6µm. The red arrow indicates a process that has changed the direction of growth multiple times.

To determine the quality of cell compliance to the PLL and to help visualize the cytophilic pattern, PLL tagged with FITC was used as ink for the µCP stamps. Figure 4.5 shows E17 rat embryo spinal cord cells forming a network on the PLL-FITC pattern at 3 DIV. The compliance of the cells to the PLL pattern in these images is very high because most of the cell bodies as well as associates processes are confined to the FITC tagged PLL. Although a small number of processes and cell bodied are found on the "background" areas of the surface. Additionally this figure also highlights the ability of

neuronal processes to change the direction of growth multiple times. Similar observations were also made previously (Jang and Nam, 2012).

4.2.1.2 Patterned neurons on Zeonor

Cyclic Olefin or Zeonor can be used as a foundation for MEA instead of Pyrex (Zou et al., 2007). It can also undergo similar surface chemistry modifications as Pyrex including silanizations with aminosilanes (Raj et al., 2009). Hence Zeonor was also investigated as a possible alternative substrate for culturing patterned neural networks. Although, Zeonor has been previously used as a substrate for patterning immortalized cells (Beaulieu et al., 2009), the results below represent the first recording of patterned primary neurons on this surface using wet silane chemistry. These results further highlight the potential of Zeonor to serve as a substrate for fabrication of cost effective micro-electrode devices suitable for electrophysiology of primary neuronal culture.

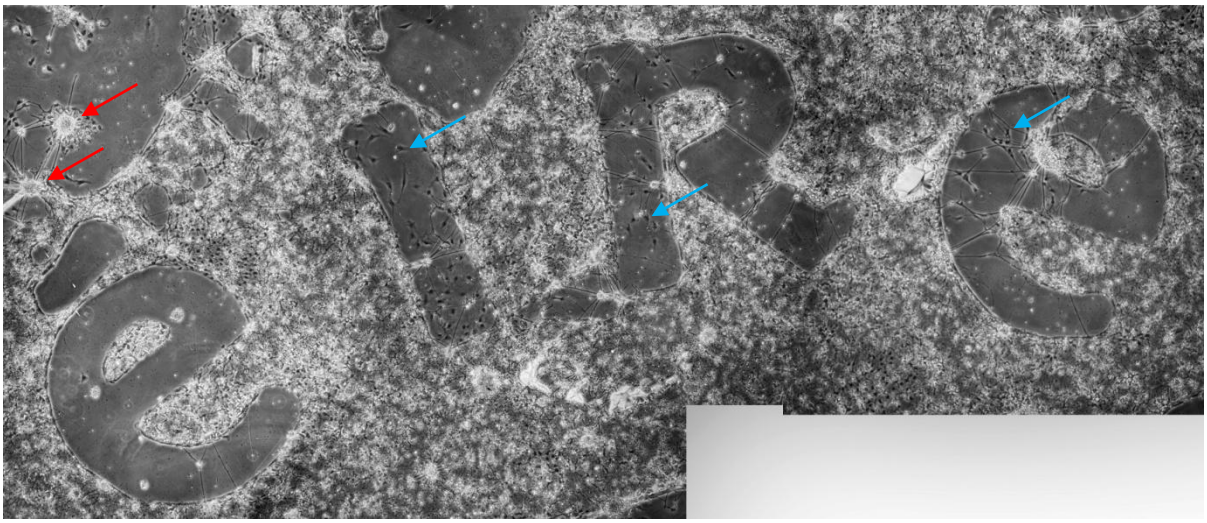


Figure 4.6: Patterned neuronal cell culture on Zeonor at 10DIV. The substrate was silanized as previously and patterned by μCP using a PDMS stamp.

Figure 4.6 shows a patterned culture at 10DIV. The presence of patterned growth is evident by the large areas of cell exclusion spelling "éire". The cells were seeded at a density of $1*10^6$ cm^{-2}. Zeonor was silanized using the same protocol as Pyrex and patterned with PEI via μCP using a stamp made from a 5 cent coin.

Figure 4.7(a) and (b) show patterned neuronal cell culture on Zeonor at 7 and 15 DIV respectively. At both stages of culture there a high degree of cell clumping was observed. This has been previously shown to occur at approximately 6 DIV on similar polymer coatings (Sun et al., 2012).

Despite the clumped cells, the culture shows compliance with the PEI pattern where directional growth and cell exclusion from defined areas is obvious. In addition to cell aggregation, a high degree of process fasciculation was also observed Figure 4.7(b). The fascicles observed were generally of two types, either attached to the surface or floating. The fascicles that were attached to the surface complied with the printed pattern.

The second type of fascicles radiated out of neuronal cell clumps in all directions. These fascicles appeared to be detached from the surface and under tension. If the substrate was lightly agitated while under a microscope it was possible to see the fascicles deform and return to their original position. This motion resembled that of a taut piece of string. The targets of the floating fascicles were other neuronal clumps which were either floating or anchored on the surface. The tension of the floating fascicles sometimes overcame the cell-surface adhesion force resulting in the cell bundle lifting off from the surface.

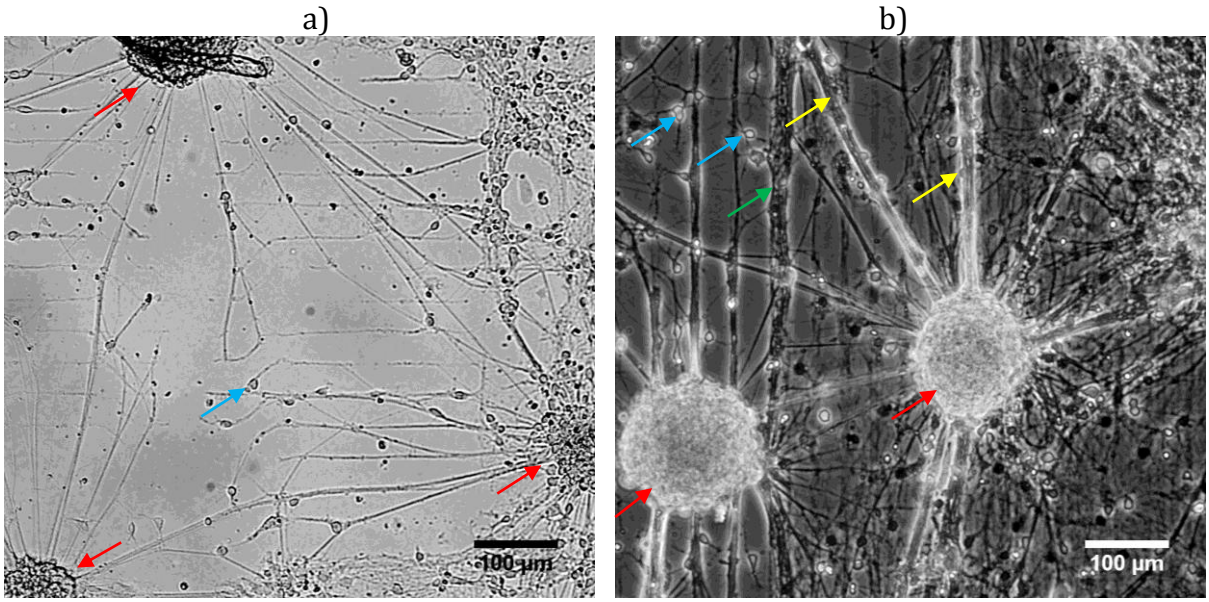


Figure 4.7: Phase contrast images of patterned neuronal culture on Zeonor at a) 7DIV and b) 15DIV. Zeonor was silanized with APTES and patterned by µCP using PEI as ink. The background was blocked using CSPG. The red arrows indicate neuron cell body clumps with radiating fascicles (yellow arrows). The fascicles emanating from the cell clumps were generally under tension yet detached from the surface. The blue arrow indicates the surface bound and pattern compliant fascicle of neuronal processes.

4.2.1.3 Patterned neural culture on SiN surface

Using µF patterning technique outlined in section 3.1.5, the E14 rat embryo spinal cord neurons were patterned on SiN surface (Figure 4.8). The surface was not plasma treated prior to patterning and thus remained hydrophobic and cytophobic off pattern.

Figure 4.8(a) and (b) show the patterned neurons at 2 DIV and 13 DIV respectively. These results show that the bare SiN surface with relatively high hydrophobicity can be used to confine the cells to a printed PDL pattern long term. These results are consistent with previous publications that used adsorbed PDL on bare SiN surface (Chang et al., 2001, Nam et al., 2003). Figure 4.8(b) shows that the cultured cells formed large aggregates similar to the cultured cells on Pyrex or Zeonor substrates. The formation of aggregates is linked to the initial presence of a large number of unbound cells during cell seeding, indicating that the initial seeding density may have been too high (Zeng et al., 2007).

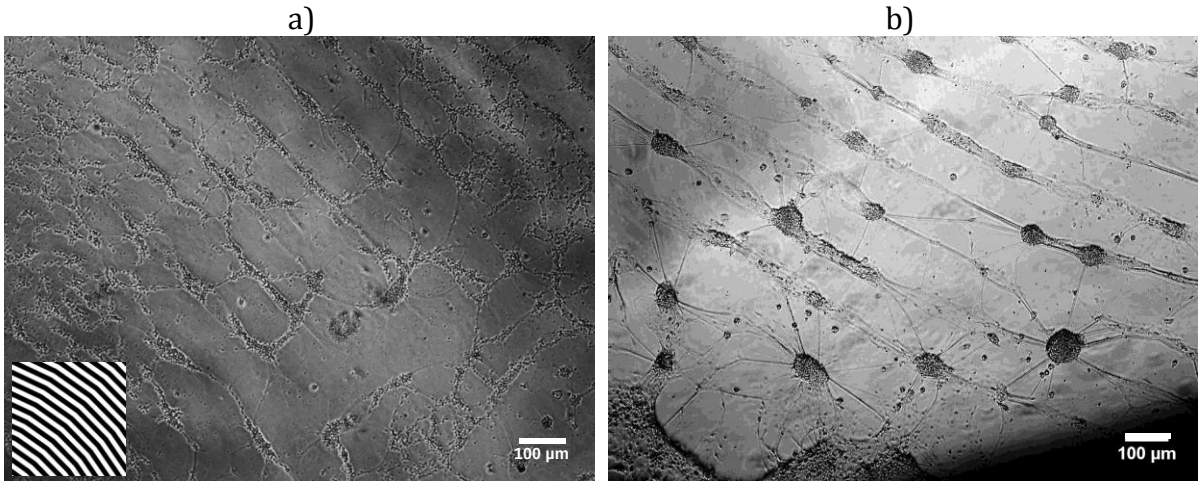


Figure 4.8: Phase contrast images of patterned neurons on SiN coated Pyrex wafer patterned with PDL via µF device perfusion. a) 2DIV and b) 13DIV. The inset in a shows the channel arrangement of the µF device. The channel width was 100 µm.

4.2.1.4 Patterned neurons on MEA

The aim of patterning neurons on the MEA was to define the neural network shape, the direction of process growth and cell body localization. In contrast to Pyrex or Zeonor, neuronal patterning was more difficult to achieve on the surface of the MEA.

The techniques such as µCP and µF applied to MEA did produce neuronal patterning aligned with microelectrodes (Figure 4.9). However, only short term cultures were obtained. Silanization of MEA with aminosilane produced better results in terms of cell viability, where small areas of surface were patterned and the cells remained attached to the surface for the required period of 14 DIV (Figure 4.10). Although some patterning has been observed, these patterns were mostly located between the micro-electrodes, and electrodes themselves appeared to be in contact with randomly placed neuronal cells or cell clumps. The biggest problem with achieving neuronal patterning through

silane deposition is that aminosilane raises the micro-electrode impedance to the detriment of the MEA (Chang and Wheeler, 2006). Moreover, because of repeated µCP on the MEA with non-extracted and under cured stamps, the surface became fouled with PDMS very quickly. Attempting to remove the PDMS contamination using TBAF made the fouling worse because it allowed the PDMS to be re-dissolved into TBAF, diffuse and adsorb to the rest of the MEA surface (Auvray et al., 1992). Consequently the MEA functionality was compromised due to insulating property of PDMS which could have increased the micro-electrode impedance (Nam et al., 2006).

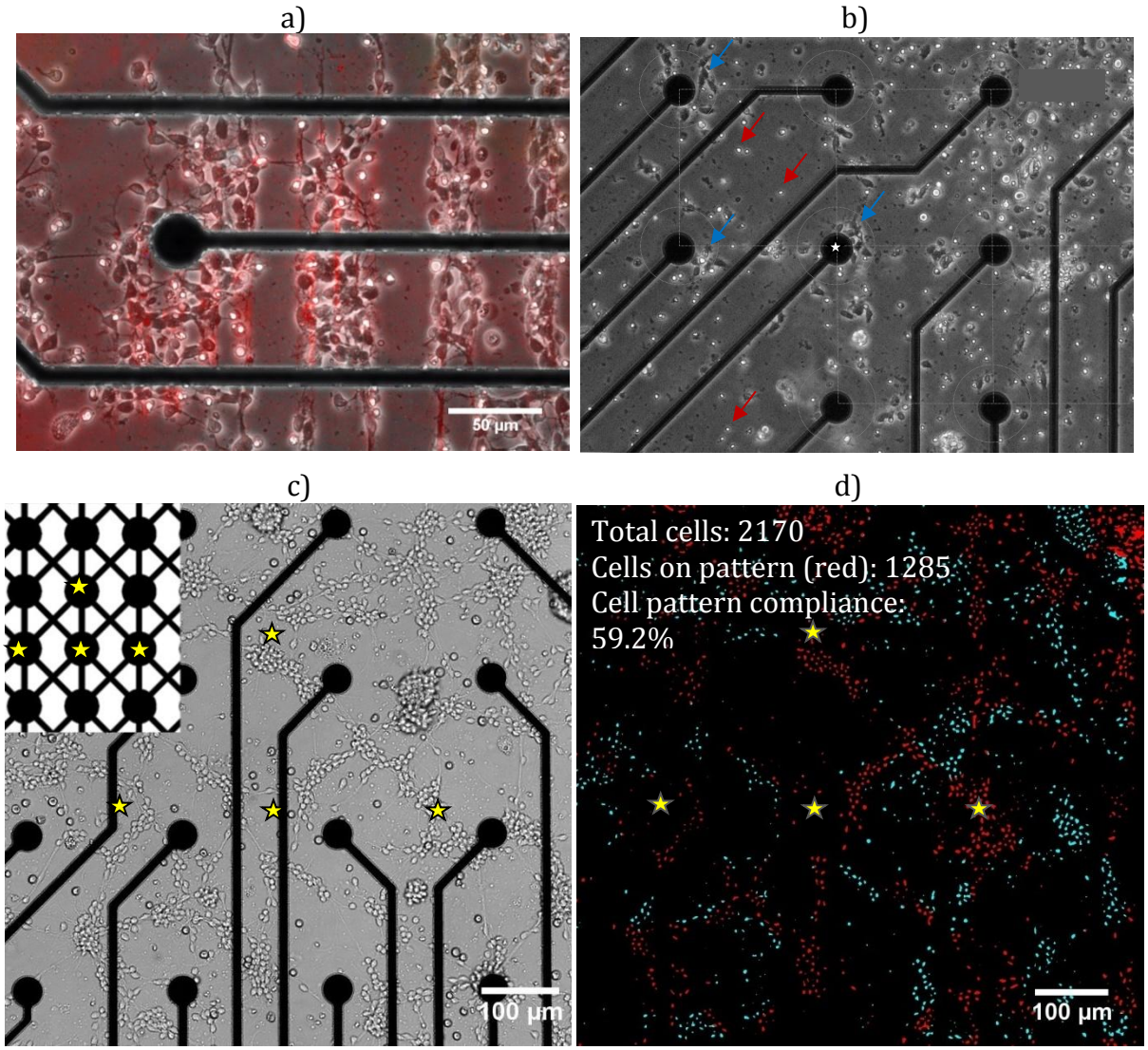


Figure 4.9: a) Image of E 14 rat embryo spinal cord neurons on MEA at ~2DIV. The MEA was patterned with PEI labeled with Cy3 streptavidin. b) Image of E 14 rat embryo spinal cord neurons on MEA patterned using µF perfusion of PDL and µCP of chondroitin 4 sulphate. c) Neurons on MEA, patterned via µCP using PEI. The inset shows the stamp layout used. The yellow stars indicate the approximate location of corresponding stamp features on the MEA surface. d) Digitally manipulated image seen in c) showing the neurons located on the printed pattern (red signal) and off pattern (blue signal). Overall 59.2% of cells in the image were located on PEI printed surface.

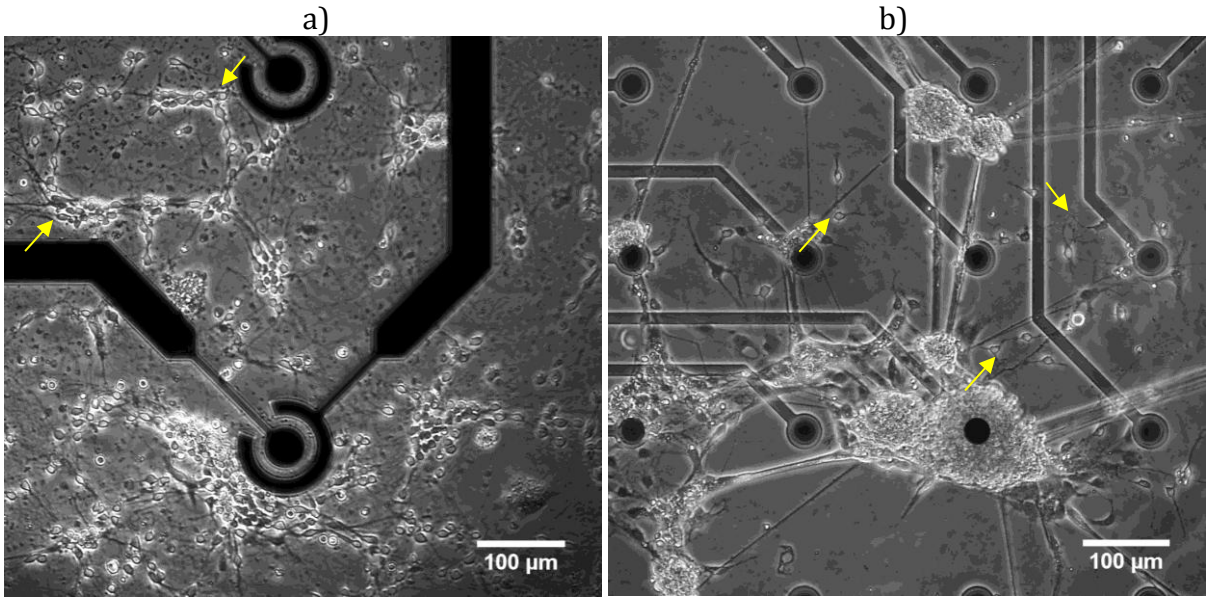


Figure 4.10: Phase contrast images of rat embryo E14 spinal cord cells on MEA surface silanized with APTMS and patterned via µCP at a) 7DIV and b) 15DIV. Very little patterned cell growth is observed in both images. Yellow arrows indicate the areas where patterned cell growth is observed.

Additionally, it was observed that neuronal attachment and cell viability on the MEA surface was greatly reduced after TBAF treatment. The failure of cell attachment and low viability may be linked to residual presence of TBAF on the MEA. TBAF is non-biocompatible, as its associated hazard codes are: flammable, corrosive and irritant (Chemical-Book, 2010).

Repeated treatments with cytophilic polymers such as PLL or PEI were ineffective at promoting cell attachment and survival. Further attempts to remove the PDMS residue using the plasma cleaner and oxidation resulted in formation of white silica-like layer on MEA surface (Schnyder et al., 2003). This silica-like layer was resistant to solvents such as acetone or methanol and could only be removed together with the SiN passivation by dipping the MEA into hot 2M solution of NaOH.

4.2.2 Electrochemical impedance spectroscopy

Electrochemical impedance spectroscopy was performed on three out of 60 TiN microelectrodes on three in-house built MEAs passivated with AlN, SiN and polyimide. Additionally the electrical impedance of the large ground electrodes was also measured on MEAs passivated with AlN and SiN. The impedance was measured at a frequency range of 100 Hz-100 kHz at a set voltage of 5 mV using AC current. The impedance measurements of interest are those that were recorded at 1 kHz. The electrode

impedance at this frequency is interesting because the AP's generated by neurons tend to be 1 ms long and thus are 1 kHz. Thus, the electrode impedance at this frequency can determine if the micro-electrodes on the MEA surface can be used to record APs.

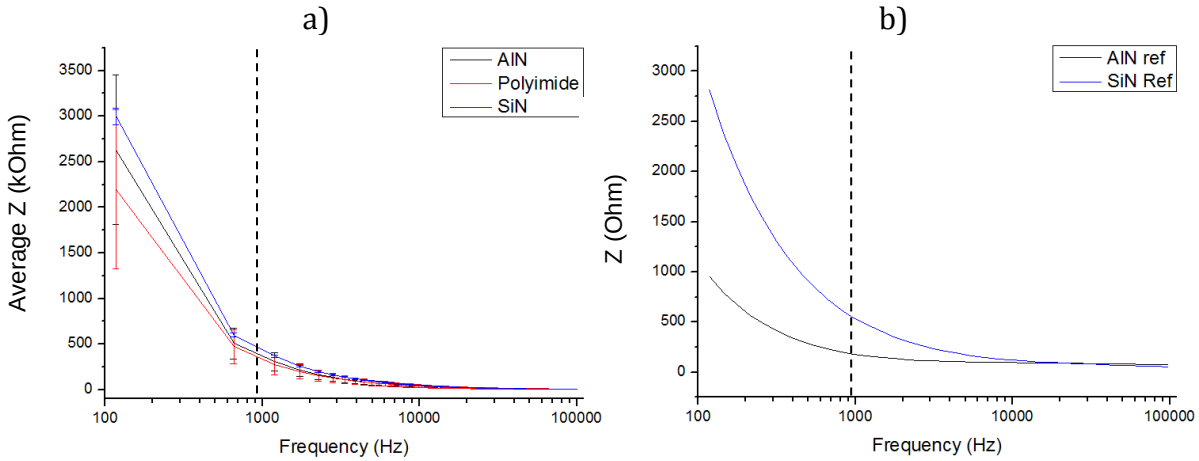


Figure 4.11: a) Average (n=3) impedance of 30 µm diameter microelectrodes on MEAs passivated with AlN (black trace) Polyimide (red trace) and SiN (blue trace). b) Impedance of large ground electrodes present on the MEA surface. The surface area of the ground electrodes is 10^3 times larger than that of the microelectrode. These electrodes show a significantly lower impedance at 1 kHz compared to the micro-electrodes. The impedance of micro-electrodes is frequency dependant where 1 kHz (dasheb black line) is of particular interest because neuronal APs occur at this frequency. Hence the impedance at this frequency determines if the device can be used to record cellular APs.

Figure 4.11 shows the plots of impedance against frequency for each type of MEA. Each plot in Figure 4.11(a) is the average of n=3 microelectrodes. The average impedances at ~1 kHz for MEAs passivated with AlN, Polyimide and SiN are 348 ± 88 kΩ, 330 ± 100 kΩ and 412 ± 10 kΩ respectively. The average impedance of all microelectrodes measured (n=9) is 364± 81 kΩ (Table 4.2). This value is 7-12 times greater than the quoted impedance of 30-50 kΩ for the commercial MEA (Multi-Channel-Systems, 2012). This difference was possibly caused by variations in the fabrication methods. It is possible that the surface area of the in-house built micro-electrodes was smaller as compared to the commercially available MEAs. The impedance at 1 kHz of the ground electrodes present on each of MEAs is nearly 1000 times smaller as compared to the microelectrodes. The impedance values for AlN and SiN ground electrodes (referred to as "Ref" in Fig 4.16) are 0.18 kΩ and 0.54 kΩ. Since the impedance is inversely proportional to surface area, these comparatively low impedance values can be explained by the relative large surface areas (7.44 mm^2) of the "Ref" electrodes. The area of the "Ref" electrode is roughly 1 x 10^4 larger than that of microelectrodes.

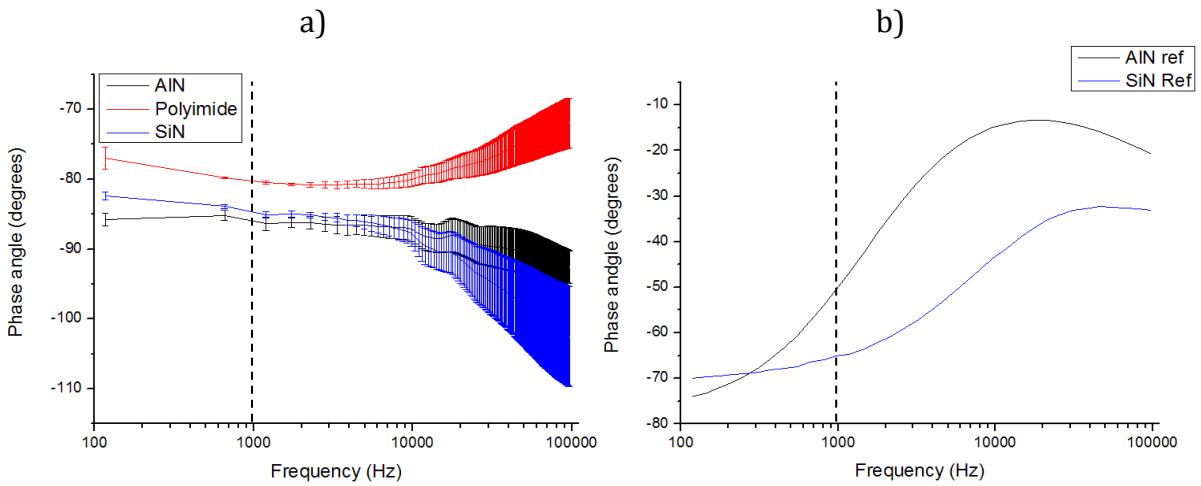


Figure 4.12: a) Phase angle of microelectrodes on MEAs passivated with AlN (black trace), Polyimide (red trace) and SiN (blue trace). b) Phase angle of the large ground electrodes on MEA surface. The phase angle gives the impedance composition in terms of capacitance and resistance. A phase angle of 90 ° indicates pure capacitive impedance, while 0° phase indicates a resistance based impedance.

The corresponding phase angles for MEAs passivated with AlN, Polyimide and SiN are -85° ± 0.5°, -80° ± 0.1° and -83° ± 0.1° respectively (Table 4.2). The phase angles indicate that the impedance of the electrodes is more capacitive that resistive where purely capacitive impedance would have a phase angle of -90° and purely resistive impedance has phase angle of 0° (Nelson et al., 2008). The capacitive impedance is preferable when using the microelectrodes for stimulation because up to certain voltage no oxidation/reduction reactions occur thus avoiding permanent damage to the electrode and the cells in the vicinity (Cogan, 2008).

As expected the electrode impedances and phase angles were not affected by the type of passivation used since the microelectrode material and surface area are the same on all in house built MEAs.

Table 4.2: Table showing the electrode impedances and phase angles on MEAs passivated with SiN, AlN and Polyimide. The average impedances do not include the ground ("Ref") electrode impedance due to difference in surface area.

MEA type	Impedance @ 966.8 Hz (kΩ)	Phase angle @ 966.8 Hz
AlN #1	422	-84.00°
AlN #2	216	-85.20°
AlN #3	407	-85.30°
Average AlN $_{123}$	348 ± 88	-85° ± 0.5°
AlN Ref.	0.180	-50.50°
Polyimide #1	243	-79.60°
Polyimide #2	481	-79.80°
Polyimide #3	267	-80°
Average Pi $_{123}$	330 ± 100	-79° ± 0.1°
SiN #1	407	-83.30°
SiN #2	402	-83.40°
SiN #3	428	-83.50°
Average SiN $_{123}$	412 ± 10	-83° ± 0.1°
SiN Ref.	0.544	-65.00°
Total Average (excl. Ref)	364± 81	-83° ± 2°

4.2.3 Electrophysiology of un-patterned neurons

To collect electrophysiological data from *in vitro* un-patterned neural networks, neurons were seeded onto MEAs coated with PLL or PEI. The most consistent results in terms of electrophysiological recordings were collected from neurons cultures on un-patterned PEI treated MEAs (Figure 4.13). After 14 DIV it was possible to observe spontaneous neuronal activity in multiple channels as well as multi-channel synchronized firing of neurons (Figure 4.14).

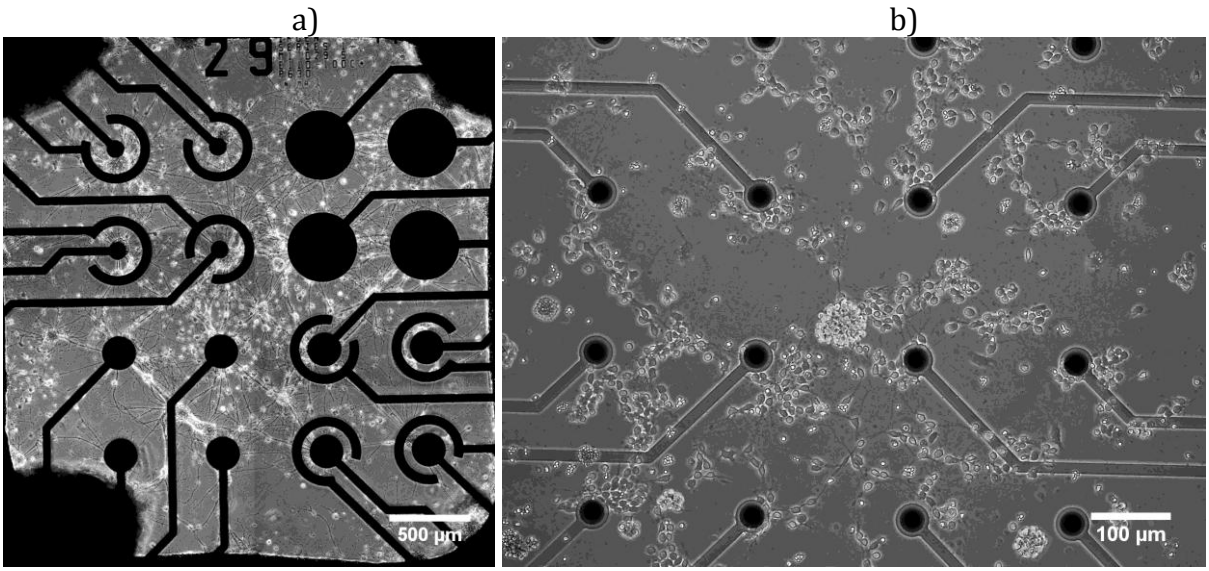


Figure 4.13: Phase contrast images of un-patterned neuronal cell culture on surface of a) (Old) Tyndall MEA and b) Commercial MEA. Seeding density 1x10^5 cells cm^{-2}.

The average amplitudes recorded during APs ranged between minimum and maximum of 26.6 µV and 59.9 µV respectively. The amplitude of high frequency noise varied between +/-5µV and +/-15µV. The application of the high pass filter set at 9.955 kHz produced a "flat-line", indicating that the maximum noise frequency present in the recordings is 9.9 kHz. Low frequency noise, below 200Hz, was also present during most recording sessions. Generally the amplitude of low frequency noise would shift the baseline by +/-30µV. This shift nearly always resulted in missed APs or detection of high frequency noise as an AP burst (Figure 4.14(a)).

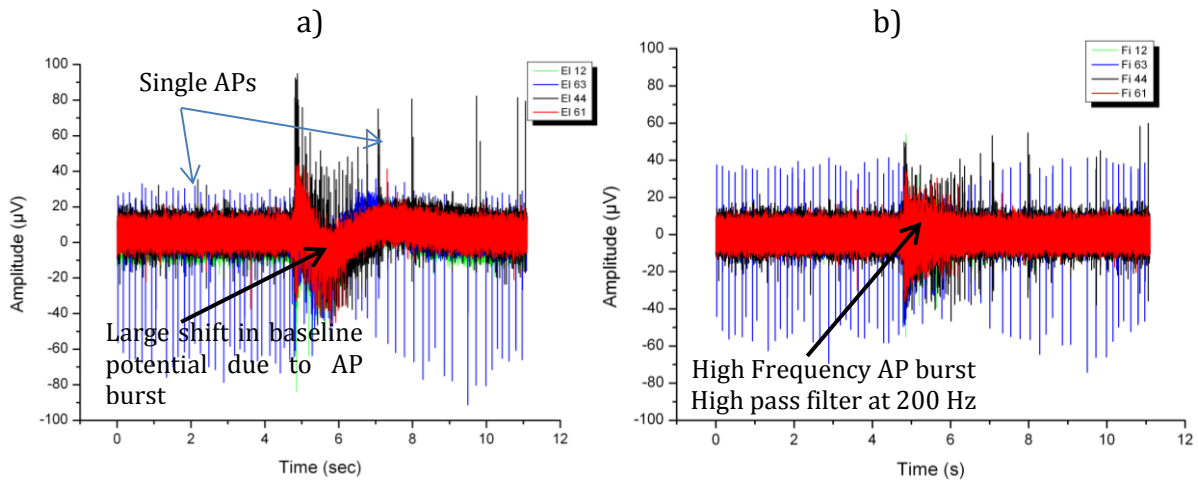


Figure 4.14: a) Raw, unfiltered recorded signal. b) Post-recording signal filtered using the 200Hz high pass filter (Data from recording session 2). Recorded using MCS MEA Kit

Using MC Rack high-pass filter set at 200Hz it was possible to achieve a steady baseline without slow potential deviations. The AP waveforms, fire rates (AP s^{-1} or Hz) and raster plots were all obtained from filtered signals in order to exclude any artefacts associated with low frequency noise and base-line drift. The neuronal activity observed during recording sessions consisted of AP bursts with fire rate up to 450Hz as well as standalone APs firing randomly or constantly. The recordings also regularly showed synchronized activity. The synchronization of the electrical activity of the neurons is indicative of network formation (Kamioka et al., 1996). Figure 4.15 shows the superimposed signals recorded from four separate channels of the MEA, 44, 55, 61 and 63. This figure shows that the electrical activity in channels 44 and 55 is synchronized because the AP bursts in both channels occur simultaneously. The activity or presence of AP in the other two channels is nearly invisible due to lower AP amplitude as compared to channels 44 and 55.

However, even though the amplitudes of AP recorded by channels 61 (Red trace) and 63 (Blue trace) are low, they were detected using the spike sorter tool of the MC Rack software. Figure 4.16 shows a raster plot of AP recorded seen in Figure 4.15. From the raster plot it can be seen that the APs recorded in channels 61 and 63 are also related to the AP busts in channel 44 and 55 although this relationship is less obvious because the number of APs is lower.

Figure 4.17 shows the AP fire rates of the four channels. This data was used to try and determine which neurons were responsible for initiation of this synchronous activity.

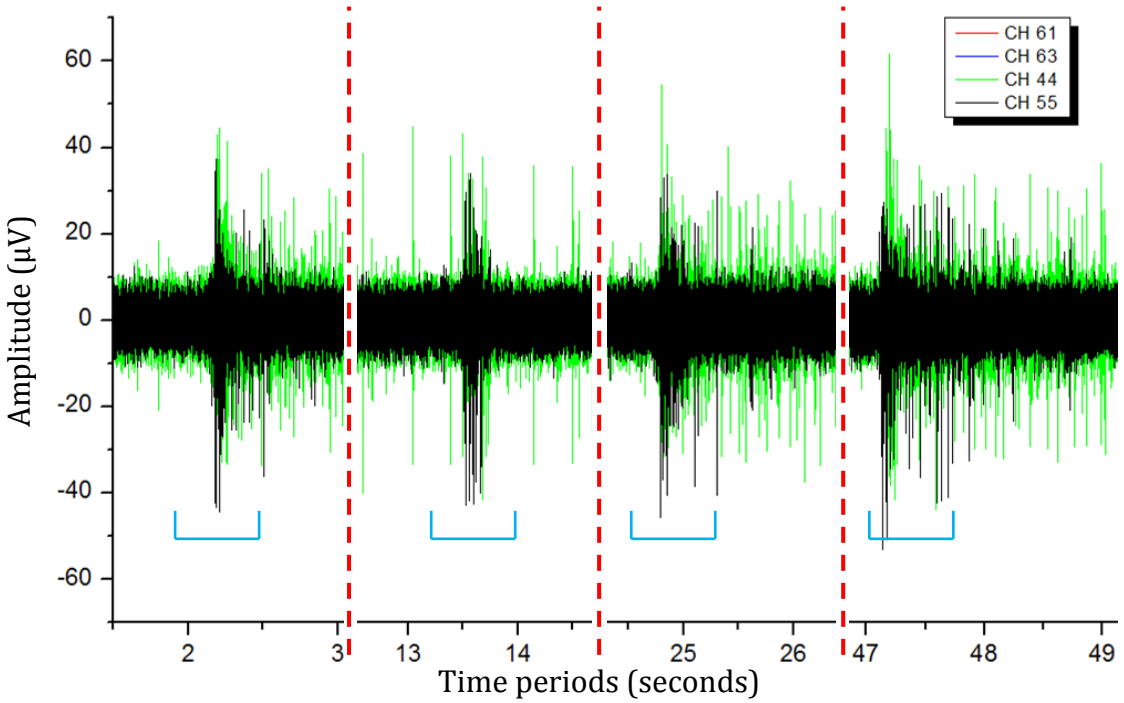


Figure 4.15:Recorded signals from E14 rat embryo spinal cord using the MEA kit. The figure shows the trace recorded during session #2. The recorded signals show good synchronization between channels 44 and 55. Note: Note: the signals shown were filtered using the 200Hz high pass filter. The red vertical lines separate the timeframes that show electrical synchronization (blue indicator).

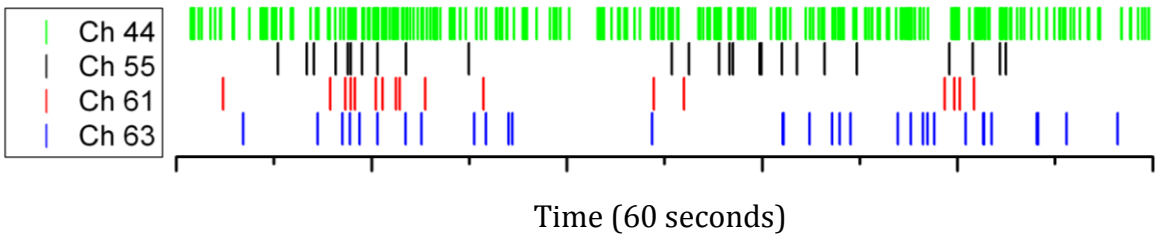


Figure 4.16: The raster plot showing the detected APs recorded in the 4 separate channels. Each dash represents 1 AP.

The fire rate comparison shows that synchronized bursting in all four channels only occurs when the fire rate in Ch 44 is in the region of 300 Hz, while other Ch 44 AP bursts with fire rates below 300 Hz are not accompanied by activity in any of the remaining channels. This indicates that Ch 44 is responsible for generation of activity in other channels but only when the threshold of 300 Hz is reached. Additional observation is that Ch 55 will not respond to Ch 44 AP burst every time, even though the 300 Hz threshold has been reached. This occurs when the AP bursts in Ch 44 occur close together indicating that neurons situated on the electrode #55 become desensitized to inputs from neurons on electrode #44 and require a certain recuperation period.

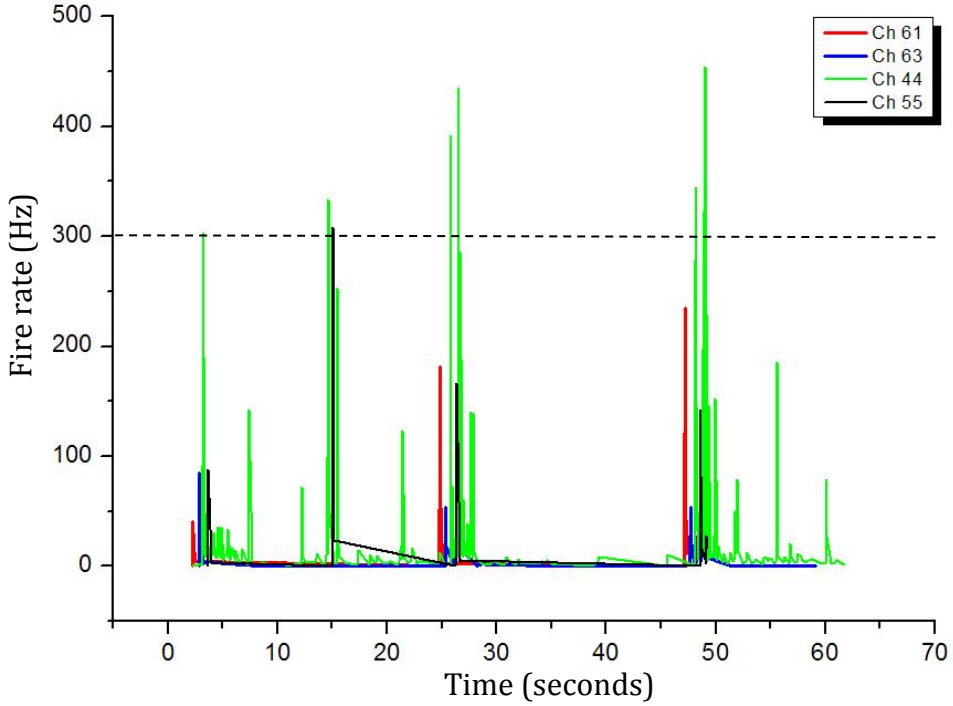


Figure 4.17: Graph showing AP fire rate comparison between 4 channels. There is evident synchronization of AP bursts between all four channels. Ch 44 has recorded 15 AP bursts, while Ch 55 recorded only 4. Note, for illustration, the each plot has been offset by 0.5 sec from one another. The dashed line indicated the 300 Hz threshold for synchronization.

Table 4.3: The descriptive statistics of AP fire rates illustrated in Figs 4.20-4.22.

	Mean (Hz)	**Standard Deviation**	**Minimum (Hz)**	**Maximum (Hz)**
Ch 44	50.95	69.42	0	307.69
Ch 55	38.82	78.83	0	454.55
Ch 61	12.04	19.46	0	85.11
Ch 63	61.15	73.10	0	235.29

4.2.3.1 AP waveforms

Using the spike sorter tool in MC Rack it was possible to isolate individual AP's from the recorded signals. As well as finding the AP's, the spike sorter also assigns the same time frame to all AP's making it possible to superimpose multiple AP's over each other and determine the average waveform and amplitude of the APs recorded by the specific channel. The waveform comparison in Fig 4.24(a) and (b) show that the AP's produced by neurons at different electrodes are mostly sinusoidal in shape.

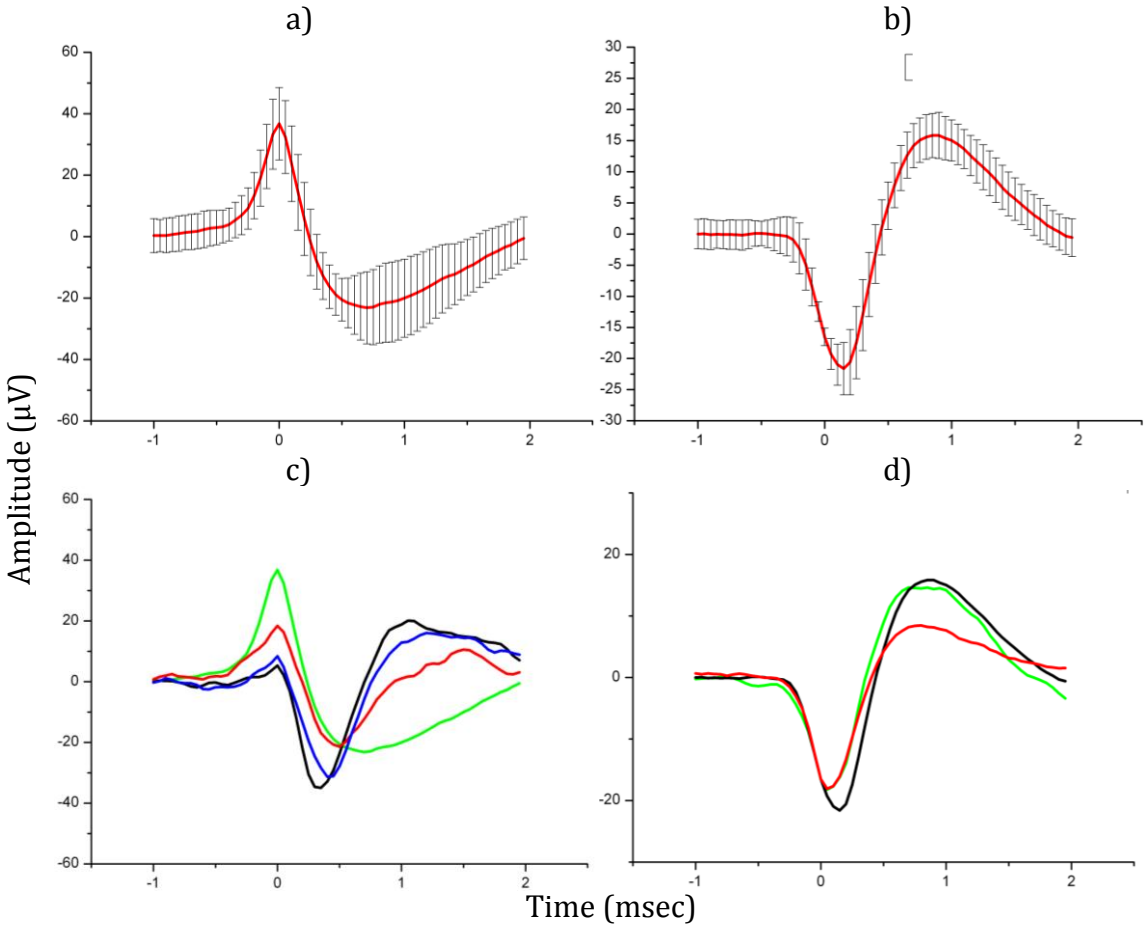


Figure 4.18: Waveform comparison between different channels of the MEA. a) and b) show the average waveform, amplitude and standard deviation of AP's. c) and d) are waveform comparisons between the AP recorded from different electrodes of the MEA (Note different scales between (a),(c) and(b),(d). Recorded using MCS MEA Kit

Although the shape does vary with regards to the amplitude of depolarization and repolarization (return to baseline potential), and neurons on the same MEA may produce APs that are different in shape (Fig. 4.24(c) and(d)). Provided that mechanism for generation of AP's by neurons is the same throughout neuronal population, the variation of the AP waveform might be the result of neuronal positioning relative to the recording electrode (Staveren van et al., 2002).

Table 4.4: The descriptive statistics of AP's shown in Fig 4.24 c.

	N APs	**Mean Amp. (µV)**	**Standard Deviation (µV)**	**Min. Potential (µV)**	**Max. Potential (µV)**	**AP Amp. (Max – Min)**
Ch 44	250	-3.92	15.05	-23.16	36.81	59.97
Ch 55	26	1.89	14.49	-34.98	20.05	55.04
Ch 61	17	1.19	9.39	-21.40	18.36	39.77
Ch 63	33	1.08	12.76	-31.27	16.06	47.33

4.3 Discussion

This chapter looked at neuronal growth on a range of substrates with surfaces modified using techniques such silanization, surface patterning via μCP and μF. Additionally this chapter looked at culturing neurons on commercial and in-house built MEAs. The scientific challenge of this chapter was to attempt and optimize individual techniques prior to their integration into one single experiment and device.

4.3.1 Neuronal patterning

The first step in optimization of techniques for integration was patterning primary neurons on Pyrex, Zeonor and SiN surfaces. The most consistent results were obtained with a silanized Pyrex substrate. Cells cultured on Pyrex permanently modified with aminosilane and micro-printed with PLL or PEI were consistent with regards to patterned growth, pattern compliance and culture longevity. These results are consistent with previous publications dealing with neurons on patterned aminosilane substrates (Corey et al., 1996, Chang and Wheeler, 2006). Using the well-established silanization and μCP techniques it was possible to demonstrate long term patterned neuronal growth on Zeonor, a biocompatible, amorphous polymer with excellent optical properties. To the best knowledge of the author, this is the first demonstration of patterned, primary neuronal growth on this substrate. The growth and viability of neurons on this substrate was comparable to that of Pyrex substrates. This result indicates that Zeonor may be used instead of Pyrex in fabrication of MEMS devices aimed at neuro-biological experiments. Zeonor surface can be modified chemically or structurally via hot embossing, direct injection molding and metal deposition as shown previously (Mönkkönen et al., 2002, Raj et al., 2009, Illa et al., 2010). As current state of the art, commercially available MEAs are sensitive to surface chemistry modifications as well as being relatively expensive (ca. 500 euro/MEA), they are limited in their applicability to electrophysiological experiments. Using Zeonor for fabrication of micro-devices however, has the potential to be a cost effective method of performing various surface chemistry modifications in combination with electrical characterization or electrophysiological recordings.

Patterning the SiN coated Pyrex via perfusion of PDL through μF device did produce long term neuronal cultures that remained viable for 13 DIV. Neuronal patterning has been previously documented on PDL coated Pyrex substrate micro-fluidically patterned

with cell repulsive CSPG (Wang et al., 2009). The success of μF patterning is important because this particular method of surface patterning, when applied to MEA, avoids direct contact with the fragile micro-electrodes. The lack of direct contact between PDMS and the micro-electrodes circumvents the issues of electrode fouling through PDMS deposition and the resultant increases in noise and impedance. Avoiding the deposition of PDMS on individual electrodes is very important because PDMS has been previously shown to function as a viable inter-electrode insulation layer (Park et al., 2012).

Patterning neurons on MEAs using μCP proved to be more difficult to achieve and far less consistent. Patterning this substrate using PLL or PEI via μCP produced neuronal patterns that remained viable for maximum of 2DIV. It was noticed that the best results with regards to cell pattern compliance were achieved on the MEAs that were brand new and unused. This indicated that previous coatings made it difficult for neurons to differentiate between the background and the newly printed pattern. No previous direct investigations of cell growth on recycled, patterned substrates have been found.

A number of MEAs were silanized with aminosilane to try and replicate the patterning achieved on Pyrex and Zeonor substrates and in previous publications (Chang and Wheeler, 2006). However, the patterning achieved on silanized MEA was poor. Importantly, the silanization irreversibly damaged the micro-electrodes of the MEA. The deposited APTES increased the electrode impedance drastically. The result was that the electrodes were showing baseline noise level of +/- 80 μV. In contrast, the baseline noise of brand new electrode was in the region of +/- 5 μV. The observed increased noise levels are consistent with previous publications (Chang et al., 2001). This point further highlights the need for inexpensive, electrophysiological micro-devices that can be used to test the effects of surface chemistry modifications on electrode impedance without carrying a great financial cost.

4.3.2 Substrate recycling

Since the substrates are submerged in culture media for prolonged periods of time at raised temperature (37 °C), it is possible that the cleaning techniques were insufficient, leading to poor patterning. Plasma treatment of the surface might have exacerbated the neuronal non-compliance to the pattern on the surface. Because plasma treated SiN is hydrophilic, the un-patterned areas of the substrate might have been just as cytophilic

as the patterned areas. Achieving long term (14 DIV) patterned culture using patterns of PLL-FITC, PDL, PEI or Fibronectin was difficult and results were very inconsistent. The main problem observed was the very low cell viability where the entire population would die, as early as 1DIV. Longer surviving cultures showed only hints of cell patterning. Interestingly, in cases where cell patterning was achieved on MEA surface, the patterns could be observed as early as one hour post seeding. This most often occurred on MEA patterned with PEI, although one instance of this also occurred when the MEA was patterned with a FBS and PDL.

4.3.3 Practical issues

In addition to observed problems that seemingly relate to neuronal environment, another set of practical problems associated with complexity of the device further reduced the amount of data collected (Flachsbart et al., 2006).

The problem that occurred most often was a complete detachment of culture chamber from the MEA. These failures randomly occurred at various stages of MEA preparation and cell culture. It was observed that when using UV adhesive to attach the chambers, the failures mainly occurred after the device has been seeded with neurons and placed in an incubator for a number of days. The chambers tended to simply slip off the surface when attempting to feed the cultures were made. Similar difficulties were observed when using two part biocompatible thermosetting epoxy. But, even though the number of instances of bond failures after seeding where drastically reduced, the epoxy presented another, terminal problem. The MEAs (especially with 1 mm thick Pyrex base) integrated with nylon or PMMA culture rings using epoxy tended to crack, especially when placed in a fridge for storage. The reason for the destruction of MEA seems to be the combination of increased bond strengths of the epoxy and different thermal expansion coefficients of plastic culture chambers and the substrate. Because the epoxy was cured at 90 °C, the plastic culture rings would heat up, expand and bond to the substrate in their thermally expanded state. However, as the assembly cooled, the rings would contract, distort and apply tension to the epoxy and the substrate. Furthermore, after the substrates were patterned and placed into the fridge for storage, the rings would contract further distorting and bending the Pyrex substrate resulting in its fracture. Thus, to avoid further costly mistakes, the epoxy was cured at RT for two days and once patterned the substrates were not placed into cool environments to

minimize the thermal expansions and contractions. This however is at odds with recommended storage guidelines that ensure the effectiveness of the chemically modified surface.

The ultimate solution to this problem is to use a silicone based biocompatible adhesive as these types of adhesives generally maintain elasticity and very high bond strengths through a range of temperatures.

Despite the poor reproducibility and short cell survival period, the patterned cell culture on MEA has been achieved using μCP and μF device perfusion. The poor reproducibility, cell viability, pattern compliance and substrate recycling will require further optimization to tease out the details of surface chemistry, cytophilic coatings, and their integration with various parts of the modified MEA to achieve long term culture that can be used for electrophysiological recordings. The possible solution to the problems could lie in simplification of surface modification, chamber bonding and substrate cleaning. Reducing the number of steps between dirty and culture ready substrates should also reduce the number of potential failures. Removing plasma treatments may be advantageous in that the natural hydrophobic state of the surface can be used as a deterrent to cells while cell adhesive areas may be patterned by using only fetal calf serum as described in Multichannel Systems literature (Multi-Channel-Systems, 2012). This step may potentially remove buildup of cytotoxic polylysine and increase cell viability past 2-3 DIV.

4.3.4 Neuronal electrophysiology and electrode characterization

The purpose of culturing neurons on MEAs is to record the electrical activity of the neurons on and in close proximity to the microelectrodes. The success of the recording also depends on the properties of microelectrodes, specifically its impedance at 1 kHz. The electrical impedance of 30 μm electrodes on commercial MEA was specified to be in the region of 30-50 kΩ at 1 kHz. The stated impedance level was acceptable as shown by successful recordings of electrical activity of five separate cultures. The four out of five aims stated in the beginning of this chapter were achieved: the long term neuronal culture on MEA surface, the recording of individual action potential, the recording of synchronous neuronal electrical activity and lastly patterning the neurons on the MEA surface.

To ensure that in-house MEA were suitable for recording APs, the electrode impedance of all three types of MEAs was characterized using EIS. The type of MEA was determined solely by the type of passivation used since the layouts of all MEA were identical. The passivation coatings used were AlN, SiN and Polyimide. SiN is a common type of passivation found on commercial MEA devices, while AlN and Polyimide are not widely used (Fejtl et al., 2006, Multi-Channel-Systems, 2012). Hence, building the additional MEA passivated with alternative coatings was aimed at providing more information on the biocompatibility of the coatings as well as any other practical issues. The impedance of the electrodes was found to be 7-12 times greater than that of commercial MEAs supplied by Multi Channel Systems. This implies that the in-house built MEAs are noisier and less sensitive to neuronal APs. It was not possible to test if the impedance levels of the in-house built MEA were sufficiently low to detect APs because the signal recording and processing hardware (MC card) was not accessible. There was no significant difference in impedance magnitude between the arrays passivated with different coatings.

During non-patterned cell culture tests, the cell viability on SiN and AlN coatings was comparable. However both types of in-house build MEAs exhibited the same low viability problems discussed previously. In case of Polyimide passivated MEAs, no long term cell cultures were cultured because the Polyimide coating separated from the Pyrex substrate after 1-2 day incubation. This indicated that there was an issue with bonding of Polyimide to Pyrex, especially when submerged in aqueous solutions such as HBSS or Neurobasal Media. Hence no actual electrophysiological recordings were performed using the in house built MEAs at this time.

4.4 Conclusion

This chapter has highlighted a number of practical issues that influence the viability, patterning and electrophysiology of *in vitro* neuronal cultures. Despite the poor neuronal viability, five out of six stated goals were accomplished. First, this chapter demonstrated long term neuronal culture on the MEA surface. Second, it was possible to record the neuronal electrical activity from these long term cultures. Third it was possible to record, analyze and compare individual action potentials generated by neurons on multiple electrodes. Fourth, it was possible to observe and record the synchronization of neuronal electrical activity, a hallmark of the maturing neuronal

network. Lastly, using the well-established surface patterning techniques, it was possible to align and pattern rat embryo spinal cord neurons on the surfaces of MEAs. This is a significant result because, to the best knowledge of the author, this cell type has not been patterned on the MEA previously. The optimization of patterning on the MEA also highlighted the need for more cost effective micro-fabricated substrates which can be used for surface modification experiments. As it has been previously integrated with microelectrodes, Zeonor has the potential to be a suitable substrate for fabrication of such devices. This chapter demonstrated that Zeonor is also highly compatible with primary neuronal culture indicating that it may be suitable for fabrication of cost-effective MEAs.

Chapter 5

5.0 Integration of MEA with neuronal patterning and microfluidics

As discussed in section 1.4.1, the permanent attachment of PDMS μF devices to substrates such as Pyrex or polystyrene, requires surface oxidation. The permanency of the bond between the PDMS μF device and its substrate is generally desired because it ensures a watertight seal. Due to the relative low cost of the components, if the device succumbs to fouling or wear and tear, a replacement can be made quickly. However, the permanent bonding of the μF device becomes a limiting factor when used with expensive, complex substrates such as the micro-electrode arrays (MEAs). Their cost prohibits these devices to be single-use. MEAs generally consist of a planar substrate that supports various metal macro/micro-electrodes and corresponding passivation coatings. These devices undergo a series of design and fabrication procedures which drive up their cost. In addition to the high cost, these devices are fragile. Their proper functionality can be drastically degraded by fouling of the electrode surfaces thereby raising their impedance (Chang and Wheeler, 2006). The permanently attached μF device has the potential to exacerbate surface fouling by trapping cell debris on the electrode surfaces. In addition, the enclosed, limited volume of the channel can reduce the effectiveness of detergents in removing stubborn debris or contaminants (Guo et al., 1996).

The second problem occurs when the permanently attached PDMS μF fails and detaches from the surface. When the PDMS-substrate bond fails in this way, it leaves the surface contaminated with chunks of PDMS. This prevents attachment of a new μF device to the surface. Removing the PDMS contaminant using a solvent such as TBAF may instead coat the electrodes with PDMS by simple adsorption (De Gennes, 1981, Auvray et al., 1992, Park et al., 2009). Due to the electrical insulating property, the adsorbed layer of PDMS has the potential to raise the micro-electrode impedance (Maghribi et al., 2002, Park et al., 2009).

In an attempt to integrate additional functionality into the neuro test platform, this chapter will also describe a technique of using the MEA for selective cell electroporation. Electroporation is a technique that involves creating temporary pores in the cell membrane, making it permeable to solutions in extracellular space.

Traditionally, electroporation is achieved via exposure of cells in suspension to a series of square voltage pulses of predetermined magnitude and duration.

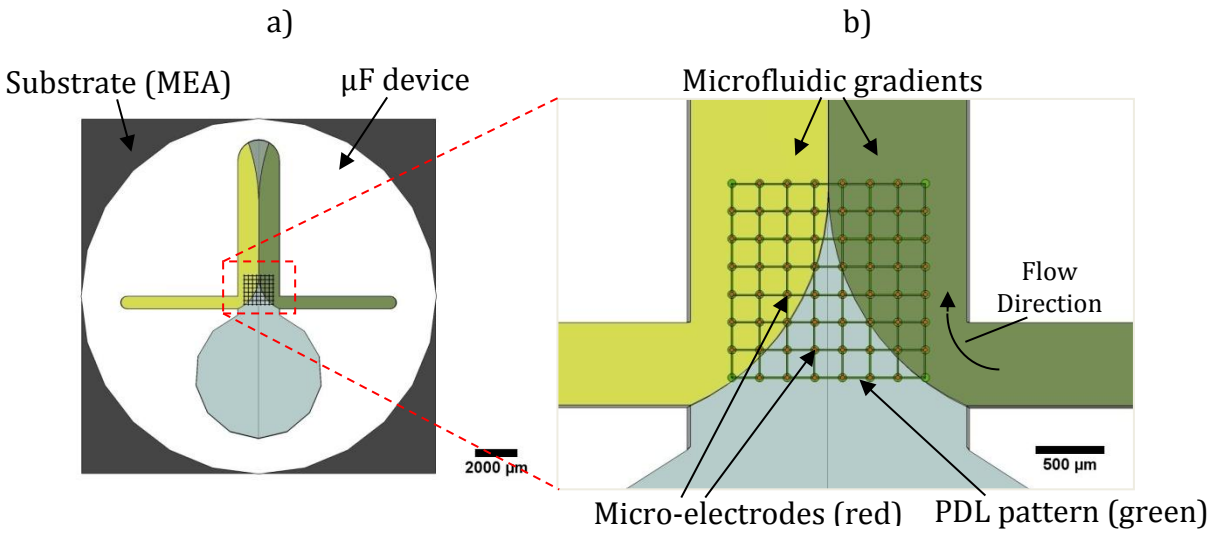


Figure 5.1: a) Schematic of intended μF device attachment to the surface of an MEA (top view). The μF device will be aligned to the micro-electrodes on the surface. b) Close up of the micro-electrodes and features of μF device. The μF device will generate fluidic gradients (yellow and green) that will flow over the micro-electrode (red dots). In addition to the μF, the MEA will be patterned with cytophilic polymers such as PDL (green) to achieve neuronal attachment. The pattern will be aligned to the microelectrodes.

Since the cell membrane is non-conductive in its resting state, it functions like a capacitor with a small potential across it. This naturally existing potential is termed the resting membrane potential. When external voltage pulses are combined with the resting membrane potential, the membrane capacitance can be exceeded leading to a transient membrane fracture. The fractured membrane exposes the hydrophobic interior of the membrane which is quickly covered up by lipid rearrangement, forming hydrophilic pores. The formation of pores allows the cell to be stained using a dye or transfected with DNA plasmids (Gehl, 2003). Whereas conventional electroporation method, described above, aim to transfect as many suspended cells as possible, the MEA should be able to focally transfect specific cells that are adhering in the vicinity of positive and negative voltage source electrodes (Jain and Muthuswamy, 2007a, Jain and Muthuswamy, 2007b, Xu et al., 2011). The benefit of this method is the ability to focally dye or transfect cells at various locations on the MEA with different dyes/plasmids. Additionally it may be possible to transfect select cells with different dyes/plasmids simultaneously using the specially defined microfluidic gradients.

Thus, this chapter will demonstrate:

1) A novel, alternative method of reversibly attaching the μF device to polystyrene, Pyrex and MEA substrates.

2) How these µF-substrate assemblies can be used to grow and control cell cultures in dynamic and static fluidic environments (Kim et al., 2007).
3) The novel method of simultaneously integrating an MEA with a patterned neuronal culture and a functional µF device to build the proposed neuro test platform outlined in section 1.5 (Figure 5.1).
4) Using the microelectrodes of the MEA for focal cell electroporation and staining with non-fluorescent dye.

5.1 Materials and methods

5.1.1 Materials

Acetone, fibronectin, foetal calf/bovine serum (FCS/FBS), Brilliant Blue G (BBG), isopropanol (IPO), methanol (MeOH), penicillin-streptomycin solution (Pen/Strep) poly-D-lysine (PDL), poly-L-lysine (PLL) and Terg-a-zyme were purchased from Sigma-Aldrich, U.K. Reagents for cell culture: B-27 supplement (B27), GlutaMAX, Hank's balanced salt solution (HBSS) and Neurobasal media were all purchased from Invitrogen, USA via Bio-Sciences, Ireland. Adhesive polymerase chain reaction (PCR) film was purchased from Thermo Scientific, Germany. Polydimethylsiloxane and hardener (PDMS) was purchased from Dow Corning, UK. Biocompatible double-sided pressure sensitive adhesive tape was purchased from Orafol, Germany. De-ionised water was purified using Elga water purification system (Veolia Water Systems, Ireland). The de-ionised water used throughout had resistivity of 18.2 MΩ·cm. Halogenated ether/Isoflow used for rodent anesthesia was supplied by Dept. of Anatomy, UCC with permission from the head of department. To ensure personal safety, the rat anesthesia was carried out inside a glass bell jar located in a biological fume hood in the designated laboratory with permission from the Dept. of Anatomy.
The microelectrode arrays (MEAs) used for neuronal electroporation, MEA interface, PMMA and Nylon culture rings were all fabricated in Tyndall fabrication facility and mechanical workshop respectively.

5.1.2 Substrates and cell types

Polystyrene, Pyrex, SiN coated Pyrex and AlN passivated MEAs (see section 4.1.2) were used for optimization and testing of µF integration and neuronal cell culture. In addition to primary neuronal cultures, BALB and A549 cell lines were also used for a number of

experiments. The BALB are the immortalized strain of mouse embryo fibroblast cells. The A549s are adenocarcinomic human alveolar basal epithelial cells. These cell lines were used because they were easily accessible, more robust than primary neurons and most importantly reduced the number rat sacrifices and dissections.

Polystyrene substrates were used for culturing controls as well as testing the performance of µF devices with long term neuronal cultures. The SiN coated Pyrex substrates were divided into two groups

1) Substrates with permanently attached PDMS µF device.

2) Substrates with detachable µF device.

These substrates were used instead of SiN passivated MEAs for culturing cells in perfused and non-perfused environments. The AlN passivated MEAs were used for electroporation of neurons and A549 cells as well as culturing of patterned neurons in conjunction with fully functional µF device.

5.1.3 Microfluidic assembly

The silicon masters and the µF devices were fabricated as described in detail in section 2.2. The fabricated µF devices were placed in acetone for 2-3 days to extract unbound short siloxane chains. To achieve temporary µF integration, the substrates (e.g. Pyrex, SiN and MEA) were modified by attaching a PMMA culture ring. This ring had the exactly the same dimentions (internal diameter and depth) as the µF device.

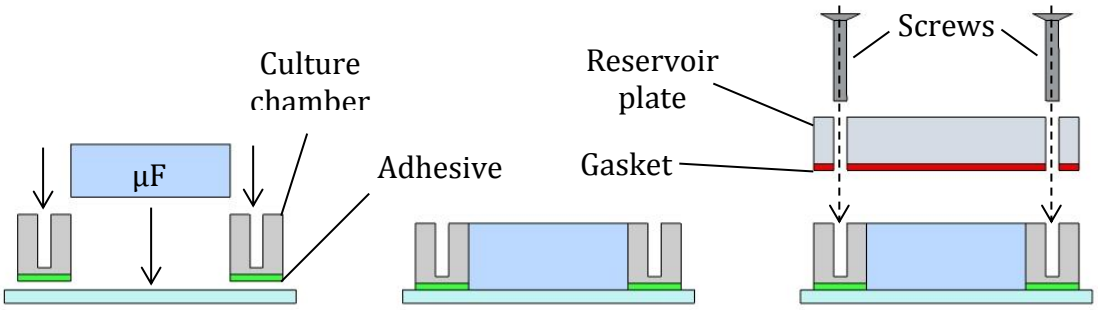


Figure 5.2: Schematic of reversible µF device attachment to the substrate. The adhesive (green) used was the Orafol double sided tape. The gasket (red) was fabricated from adhesive PCR film (see section 2.2.4) .

It was attached to the surface via biocompatible double sided, pressure sensative adhesive tape. Instead of permenantly binding the µF device to the substrate, the device was mechanically pressed onto the surface via an overlying PMMA reservoir plate (Figure 5.2).

5.1.4 Fabrication of the reservoir plates

This reservoir plate was fabricated as follows; first, three reservoirs were drilled in locations matching those of the µF device fluidic inlets. A fourth opening was drilled in the location of the waste outlet. The waste outlet on the reservoir plate was then widened to allow for integration of the Omni-Lok Inverted Cone Ferrule to function as an interface between the µF device and the vacuum/perfusion systems such as peristaltic or syringe pumps. The ID of the ferrule opening fits the most commonly used 1.6 mm outer diameter (OD) Teflon tubbing. Following the integration of ferrule, a 1 mm thick PMMA cover was glued onto the reservoir plate on the same side as the ferrule using double sided tape.

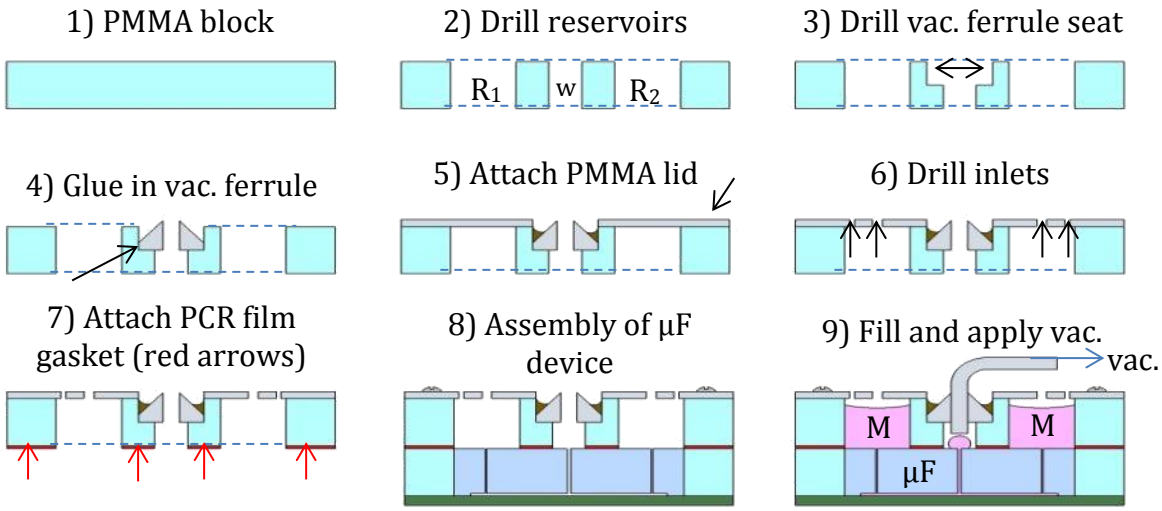


Figure 5.3: Schematic representing fabrication of µF reservoir plate and its integration with PDMS µF device. 1) A 5mm thick PMMA block is cut to size. 2) The media reservoirs (R1 and R2) and waste outlet (w) drilled out. 3) The waste outlet is widened and 4) the vacuum coupler is glued in using epoxy. 5) A 1mm thick PMMA cover is attached to the reservoir plate using transfer tape. 6) Small inlets are drilled in PMMA cover (2 per reservoir). 7) PCR film is attached to the bottom of the reservoir plate to serve as a gasket (red arrows). 8) The reservoir plate is attached to the PMMA ring on the substrate surface housing the PDMS µF device. Screws are used to hold the assembly together. 9) The reservoirs are then filled with cell culture media (M), the waste outlet is connected to a vacuum source (peristaltic or syringe pump) and the media is drawn from the reservoirs into the µF device and out to waste outlet.

The other side of a reservoir plate was then covered with PCR film which functioned as a gasket between the plate and the culture ring. Using a scalpel, the PCR film was carefully cut to open the reservoirs (Figure 5.3). The second simplified version of the reservoir plate consisted of just the PMMA block and the PCR film gasket. The 1mm PMMA lid as well as the vacuum ferule were not needed. Due to elimination of the

various layers, the simpler version had the benefits of faster fabrication and enhanced optical clarity at the expense of reduced reservoir volumes (Figure 5.4).

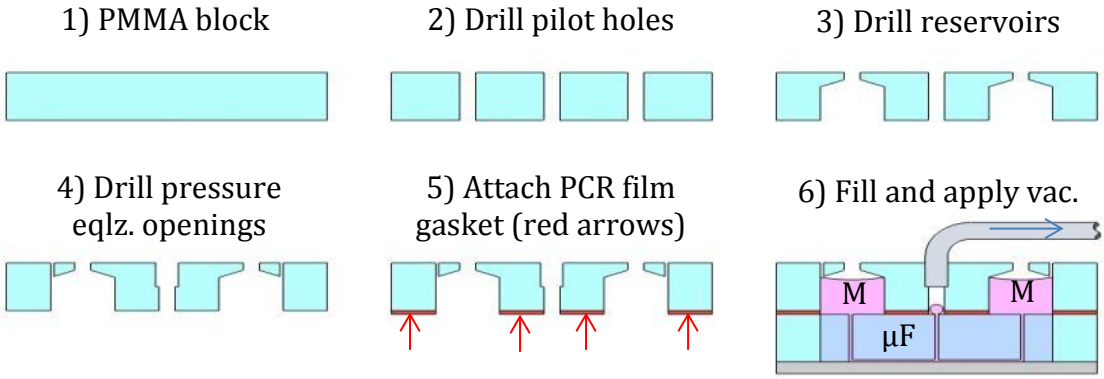


Figure 5.4: Schematic representing simplified fabrication of µF reservoir plate and its integration with PDMS µF device. This method of fabrication greatly reduces the number of steps and components required.

5.1.5 Surface modification for cell adhesion

To ensure cell adhesion, polystyrene and SiN coated Pyrex were incubated with 100 µg mL^{-1} solution of PDL in DI water at 37°C for 1 h as described in section 4.1.4 (Chang et al., 2000). The substrates permanently integrated with a µF device were coated with PDL solution only after the µF device was attached to ensure that the oxidative plasma treatment (required for adhesion of PDMS µF device to the substrate, section 2.5.5.1) did not negatively affect polymer coating. The PDL adsorption inside the µF channel was carried out as soon as possible after the integration of the µF device to take advantage of the hydrophilic Pyrex and µF device surfaces. The permanently attached µF devices were filled with PDL solution via vacuum as described in section 2.6.

The AlN MEAs and plain Pyrex substrates were coated with a combination of PDL and fibronectin. The fibronectin was added to the coating procedure to further improve neuronal adhesion by providing the RGD sites (Huang et al., 2009, Thompson et al., 2013). The surface modification was carried out as follows; PBS buffer was made up by dissolving a PBS pellet in 200 mL of DI water. The measured pH was 7.5. 1 mg of Fibronectin was diluted in 40 ml of PBS to yield 25 µg mL^{-1} fibronectin solution. The pH of remaining 160 mL of PBS buffer was adjusted to 11.0 using NaOH. 5mg of PDL (mol. weight 70000-150000 g mol^{-1}) was then diluted in 50 mL of PBS to yield 100 µg mL^{-1} solution. Clean AlN or Pyrex substrates were first incubated with PDL for 1 h at 37 °C. The PDL solution was the aspirated and substrates rinsed twice with cool boiled DI water. Following the rinse the substrates were incubated with fibronectin for 1 h at 37

°C. After the incubation, the solution was aspirated and the substrates were rinsed three times with DI water as described for PDL incubation. The substrates were then submerged in Neurobasal media supplemented with 2% B 27, 10 % FCS and 2.5 µl mL^{-1} GlutaMAX and placed in biological incubator in preparation for cell culture the next day. (Note: the PBS pH was adjusted to aid with PDL adsorption to the surface (Richert et al., 2004, Sigma-Aldrich, 2013)). The types of substrates and coatings used are summarized in Table 5.1.

Table 5.1: Table stating the types of surfaces and coatings used for cell culture experiments.

Substrate	Coating	(µg mL^{-1})	°C	Time (h)
Polystyrene	PDL	100	37	1
SiN-Pyrex	PDL	100	37	1
Pyrex	PDL & Fibronectin	100 & 25	37	1+1
AlN MEA	PDL & Fibronectin	100 & 25	37	1+1

5.1.6 Cell culture

5.1.6.1 Culture using permanently attached µF devices

To provide a media reservoir, a polystyrene culture well was first attached to the substrate using epoxy (sections 2.2.1 & 2.3.1). Newly fabricated and extracted µF devices were plasma bonded to the substrate inside the culture well (section 2.5.5). The channels of the µF device were coated with PDL and filled with Neurobasal media as described above (section 5.1.5). After the µF device was filled and free of bubbles, $5.4x10^4$ neuronal cells suspended in small volume (<5 µL) of Neurobasal media were carefully pipetted into the µF device. This cell number yielded a final cell concentration of $1x10^5$ cells cm^{-2} inside the device. Once the device was loaded with cells, 2 mL of Neurobasal media was added to the well, completely submerging the attached µF device.

5.1.6.2 Culture using detachable µF devices

The following procedure was carried out to test the long term neuronal viability inside a perfused µF device and to determine the effects of media supplements on A549 cell culture. Prior to cell culture, the substrates such as SiN coated Pyrex wafers, polystyrene substrates or MEAs were modified by attaching a PMMA or Nylon culture rings as

described in section 2.1.1. The substrates were then coated with PDL and fibronectin as described in section 5.1.2. The neurons were seeded onto the substrate at a density of $1x10^5$ or $2x10^5$ cells cm^{-2}. The A549 cells were seeded at a density of ~$3.5x10^5$ cells mL^{-1}. After seeding, the A549 cells were transferred to an incubator for 1 h, while the neuronal culture was incubated overnight. Following the incubation, 600 µL of media was removed from the cell culture chamber and the µF device was inserted. The µF device was pre-soaked in HBSS for 2-3 days at 37 °C. The pre-soaking of µF device reduced the probability of trapping air bubbles in the channels during the perfusion period (Wang et al., 2012). The µF device was secured to the substrate with the overlying reservoir plate and reservoirs filled with cell type specific media. Neurobasal (10% FBS, 2% B27 and 1% GlutaMAX) media was used for neurons whereas DMEM (10% FBS and 1% GlutaMAX) was used for A549 cells (Figure 5.4). For the experiments attempting to determine the effects of media supplements on A549 cells, two reservoirs were filled with DMED supplemented with 10% FBS and 2.5 µL mL^{-1} GlutaMAX. One well was filled with DMEM without any supplements or Growth factors.

(Note: the Neurobasal media used for µF perfusion was mixed 1:1 with preconditioned media, collected from a separate neuronal culture.)

5.1.6.3 Cell culture perfusion

The µF device and the cell cultures were perfused by connecting the waste outlet of the µF device to a peristaltic pump at the "suction" end. The peristaltic pump barrel rotation speed was set to its minimum value of 0.01 RPM (93 µL hr^{-1}). Alternatively a syringe pump with a "withdraw" function was used. The withdraw rate was set to 5 µl h^{-1}. The syringe pump was a preferred method of perfusion because it allowed for 24 h perfusion period before the µF device required attention due to media depletion.

5.1.7 Electroporation using MEAs

Electroporation was tested on A549 cells because of their robust viability as compared to primary neurons. The experiment was carried out as follows. The A549 cells were grown inside a T75 flask for up to three days to 70-80% confluency (cell surface area coverage). The media was discarded; cells were rinsed with HBSS and incubated with 4 mL of Trypsin for 5 min. Trypsin detached the cells from the flask surface. 6 mL of DMEM supplemented with 10% FBS was added to the cell suspension to stop the action of Trypsin. The suspension was then centrifuged for 5 min at 1000RPM, Trypsin/DMEM

mix was discarded and the pellet was re-suspended in 5 mL of fresh DMEM. 1 mL ($7x10^5$ cells mL^{-1}) of stock cell suspension was then pipetted onto PDL/fibronectin coated MEA and placed into incubator for 1 h. After incubation, the MEA and A549 cells were imaged to determine which electrode pairs (total of 5 pairs) can be used for electroporation. The media was aspirated and pipetted into a 1 mL micro-centrifuge tube for the duration of electroporation. 1 mL of 0.025 % solution of Brilliant Blue G in HBSS was added to the MEA well and the chosen electrode pairs were connected to a signal generator (Awad et al., 2011). Each electrode pair delivered a single 10 ms voltage pulse to the surrounding A549 cells. The magnitude of the first voltage pulse was 3 V, and was increased by 1 V for each subsequent electrode pair. The maximum amplitude tested was 7 V. After a total of 5 min, the dye solution was aspirated and discarded, culture was washed twice with HBSS. The 1 mL of media stored in the micro-centrifuge tube was pipetted back into the MEA well. The cells were then imaged to determine if any BBG uptake occurred. A second round of electroporation using the same electrodes and voltage pulses was performed 48 h later.

(Note: When dissolving the Brilliant Blue G, the HBSS was heated in a microwave for 5 sec. This step ensured dissolution of the dye).

5.1.8 Biocompatibility testing

It was attempted to determine if the washing of the substrates with 1 % Terg-a-zyme had a negative effect on the subsequent cell cultures. Since primary neurons were previously observed to be sensitive to substrate recycling (section 4.3.2), they were substituted with a more robust, BALB cell line. The biocompatibility testing was carried out as follows. Six polystyrene culture wells were attached to three Pyrex slides (two each) and the substrates were incubated with FBS overnight. The BALB cells were cultured to confluency (90-100 % surface coverage) in DMEM supplemented with 10 % FBS inside a T-75 tissue culture flask. Once the confluency was reached, the DMEM was discarded; the cells were washed twice with HBSS and detached from the surface via 5 min incubation with 4 mL of Trypsin at 37 °C. The action of trypsin was then stopped by adding 6 mL of culture media (DMEM+10 % FBS). The BALB cells were separated from the trypsin/DMEM solution by centrifugation (1000 RPM, 5 min), the supernatant was discarded and the cells were re-suspended in 5 mL of fresh culture media. 4 mL of cell suspension was seeded into a new T-75 flask, while the remaining cell suspension was

equally divided (160 µL) and added into the wells on the Pyrex substrates. The wells were then filled with 2 mL of culture media. After two day in culture, one well on each Pyrex slide was washed with DI water while the second well was washed with 1 % Terg-a-zyme (12h at RT). Once the substrates were clean, the cell culture was repeated. The BALB culture inside the T-75 flask was used as the healthy control.

5.2 Results

5.2.1 Biocompatibility trends of integrated MEAs

One of the most challenging aspects of building the neuro test platform was achieving a satisfactory level of biocompatibility with primary neuronal cells. The most consistent observation was that the biocompatibility of the surfaces or devices tended to decline progressively each time the substrate was recycled. Similar trends were observed with new substrates integrated with recycled culture rings, or recycled substrates integrated with new culture rings. Figure 5.5 qualitatively compares health of neuronal cultures on brand new MEA with that on an MEA that has been recycled two to three times, and an MEA that has been recycled more than five times. The poor biocompatibility is evidenced by presence of dead neurons (white circles in Figure 5.5b and c) either attached to the substrate or floating freely in the media. Similar low viability was also observed on patterned substrates where the cells remain viable long enough to adhere to the pattern on the surface, but die shortly afterwards (Figure 5.6).

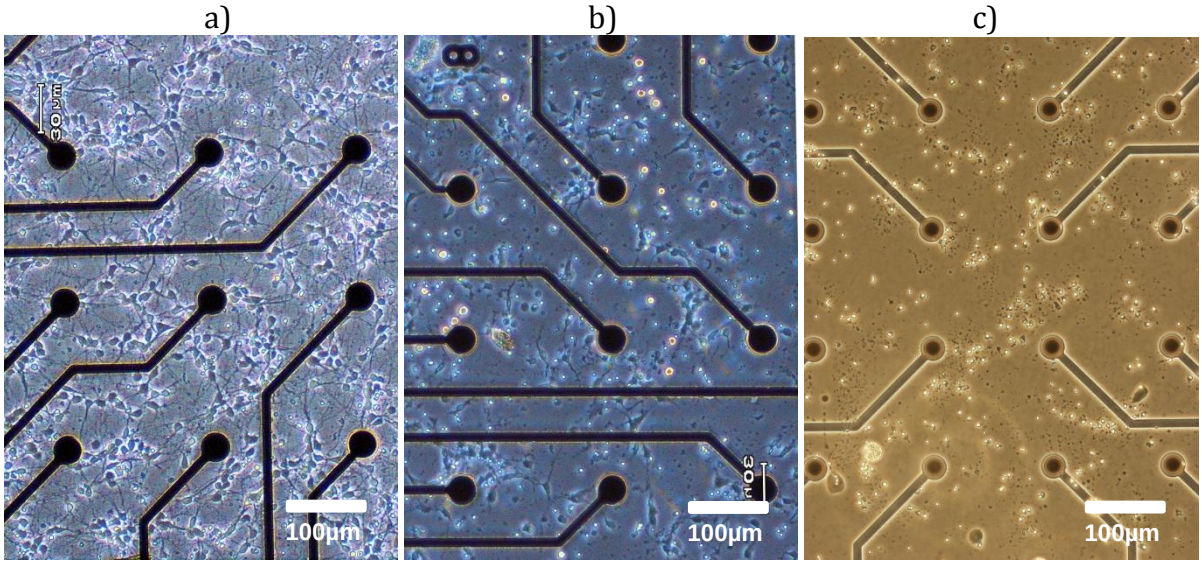


Figure 5.5: Images representing the decline of MEA biocompatibility with repeated use. The cultures in the images are 2-3 DIV. a) Neuronal culture on brand new MEA. b) neuronal culture on recycled MEA. c) Neuronal death on MEA recycled over 5 times.

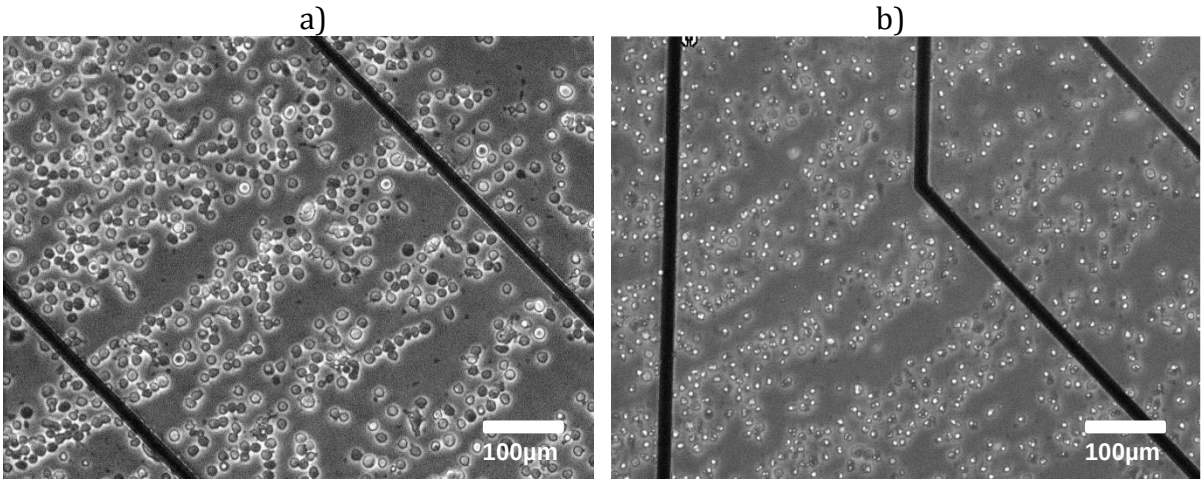


Figure 5.6: a) Evidence of patterned cell localization 1 hour after seeding on SiN passivated MEA. b) Dead patterned cells at 1DIV.

5.2.2 Biocompatibility test

Since the average treatment with Terg-a-zyme lasts approximately 12 hours (overnight), it is possible that this detergent could adsorb to the multiple surfaces of the integrated components or seep into micro-cracks in the MEA passivation and the well material (PMMA/polystyrene)(Nam et al., 2012). In addition, epoxy showed the tendency to absorb solutions (including detergents) into its bulk. This was consistently observed after incubation with DMEM, where the epoxy turned red. This staining has likely occurred due to presence of phenol red, a pH indicator present in the media. This is a direct indication that the culture media penetrated the epoxy matrix (Figure 5.7).

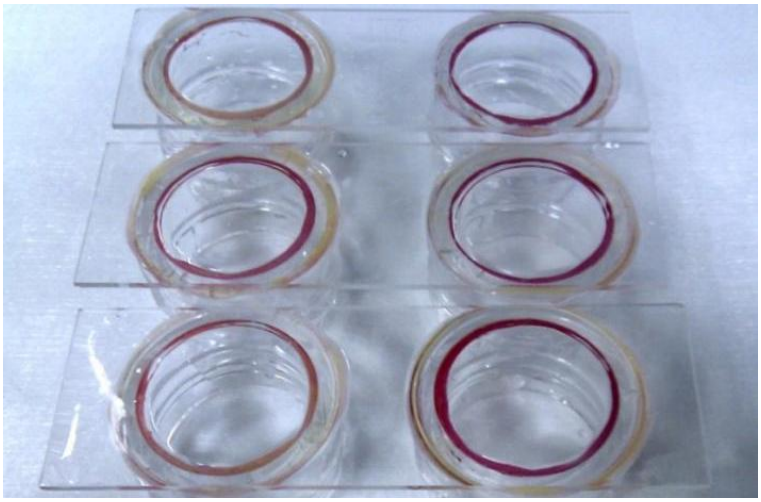


Figure 5.7: Image showing the epoxy staining with phenol red (red circles). The epoxy was submerged in media for 2 days. The staining of epoxy indicates that cured epoxy may adsorb or absorb other solutions such as polylysine or detergents and slowly leaching these back into culture media during culturing resulting in poor neuronal viability.

Thus, the effects of repeated exposure of substrate to Terg-a-zyme were tested on the BALB cell line. It was found that even after four washing cycles, there was no obvious decline of cell viability in Terg-a-zyme treated wells compared to DI water washed wells. The BALB viability in both wells was also comparable to the BALB cells grown inside a T75 flask (Figure 5.8). These observations indicate that Terg-a-zyme treatment had no observable effect on viability of BALB cells. Unfortunately, this result does not indicate that Terg-a-zyme has no negative effects on device biocompatibility. This result only shows that the BALB cell line is not affected by the cytophobic conditions induced by substrate recycling.

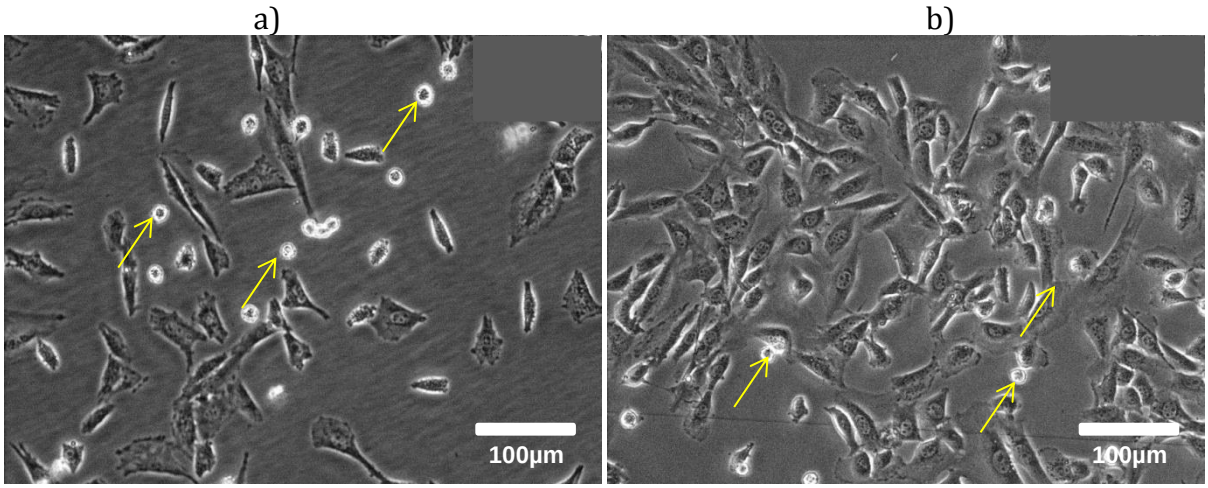


Figure 5.8: a) BALB cells in T75 flask at 2DIV after passage. b) BALB cells on Pyrex substrate coated with FBS. The substrate has been recycled and washed with 1 % Terg-a-zyme four times. Although some dead cells are present, the number of these is similar to the control flask and can be attributed to reduced viability due to high passage number. Dead cells are indicated with yellow arrows.

5.2.3 Electroporation and cell staining

In addition to electrophysiological capabilities of the neuro-test platform, the AlN passivated Tyndall fabricated MEAs were used for focal electroporation of adherent cells. The integration of electroporation into this platform was aimed at increasing the range of its capabilities and ensuring multi-functionality. At the same time it was also attempted to simplify and improve the detection of the electroporated cells by using an alternative non-fluorescent BBG stain. At non-toxic levels of 0.025% w/v this stain has deep blue appearance in solution (Awad et al., 2011). To determine if this stain could not pass through the un-electroporated membrane, solution of BBG in HBSS was added to a neuronal cell culture for 5 min. As expected, no BBG uptake into viable neurons

occurred. However, BBG was able to clearly stain the dead neurons on the surface (Figure 5.9(b)). After two days, BBG diffused back out of the cells into the media giving it a blue hue as seen in Figure 5.9(c).

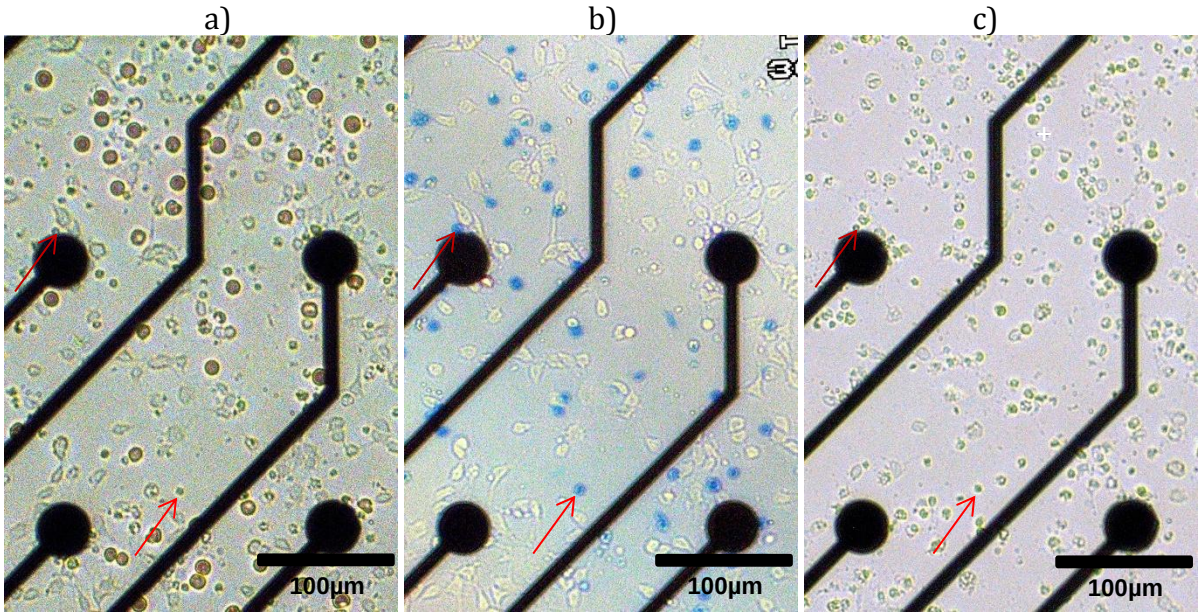


Figure 5.9: a) Brightfield image of neurons on MEA prior to staining with BBG. b) Image showing BBG staining of dead neuronal cells (blue circles). The viable neurons remain unstained. c) 2DIV after BBG staining. The BBG within dead cells has diffused back into the media. Also note that at 2DIV most of the neurons are dead. (Note the staining occurred in the absence of electroporation).The red arrows indicates examples of dead neurons that were stained and de-stained after two day incubation.

Due to persistent difficulties with neuronal viability, the electroporation was tested on the A549 cell line. Following the first round of electroporation, no viable BBG stained A549 cells were observed near any of the electrode pairs. Only dead cells showed BBG uptake (Figure 5.10). However, there was clear evidence of BBG staining after the second round of electroporation (Figure 5.10(b) and (c)). This shows that the staining efficiency is directly related to the timeframe of membrane permeability. The second round of electroporation effectively doubled the "open" pore timeframes allowing more BBG to diffuse into the A549 cells. Similar observations were made previously with spatially electroporated HeLA cell culture (He et al., 2007). This indicates that to achieve efficient staining of A549 cells with BBG, additional optimization of the electroporating pulses needs to be carried out.

The cells clustered around the 4 V electrode pair showed signs of staining only around the positive terminal/electrode. While cells clustered around 5, 6 and 7 V pairs showed

signs of staining around both, positive and negative electrodes. No staining was observed around the 3 V electrode pair (Figure 5.11).

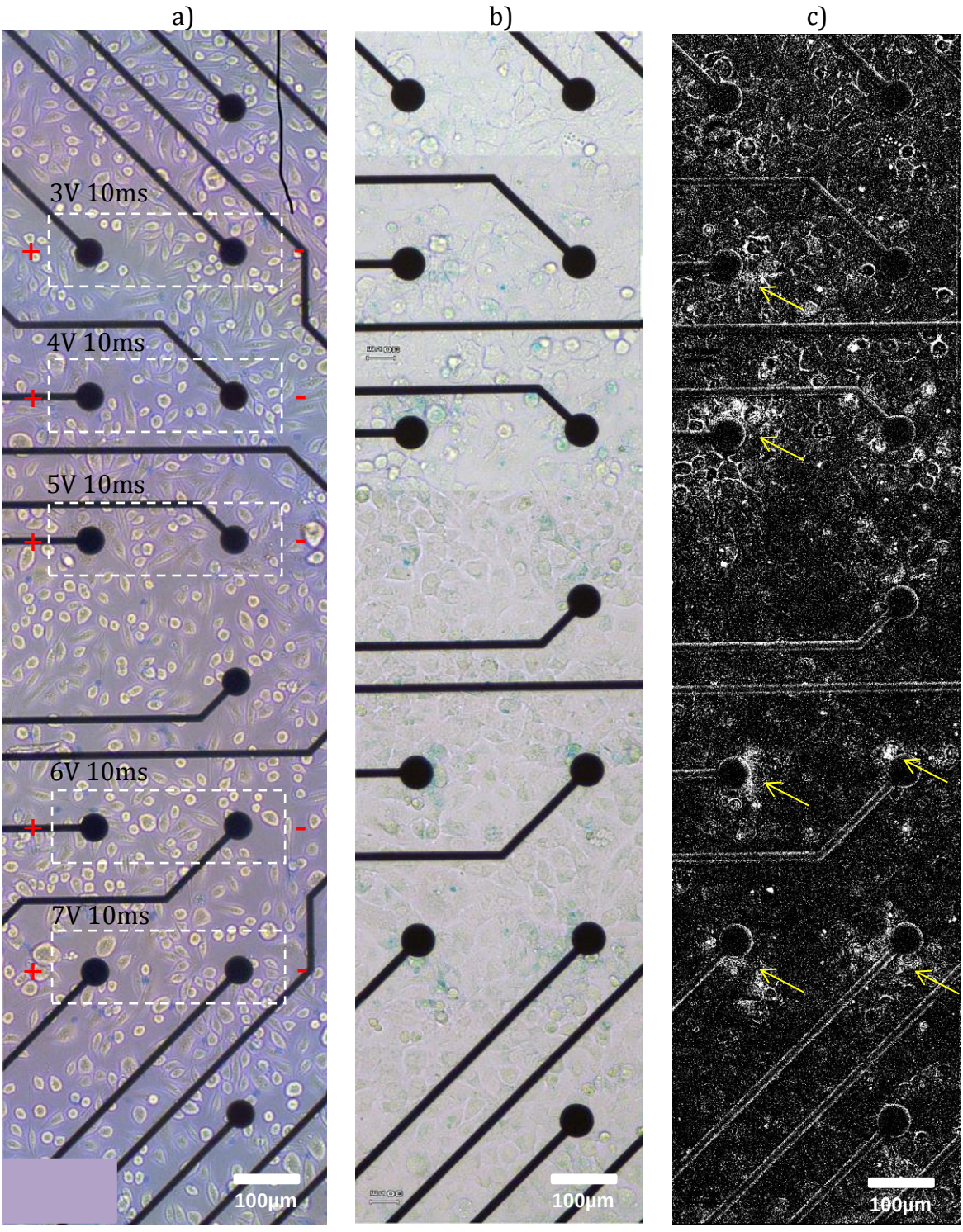


Figure 5.10: Images of A549 cells after electroporation. Progressively higher voltages were applied to designated electrode pairs (dashed boxes). The pulses were 10 msec long. a) A549 cell after 1st electroporation experiment. b) A549 after 2nd electroporation experiment, 48 h later. c) Cyan channel of b showing the BBG staining more clearly. Yellow arrows indicate the BBG stained A549 cells.

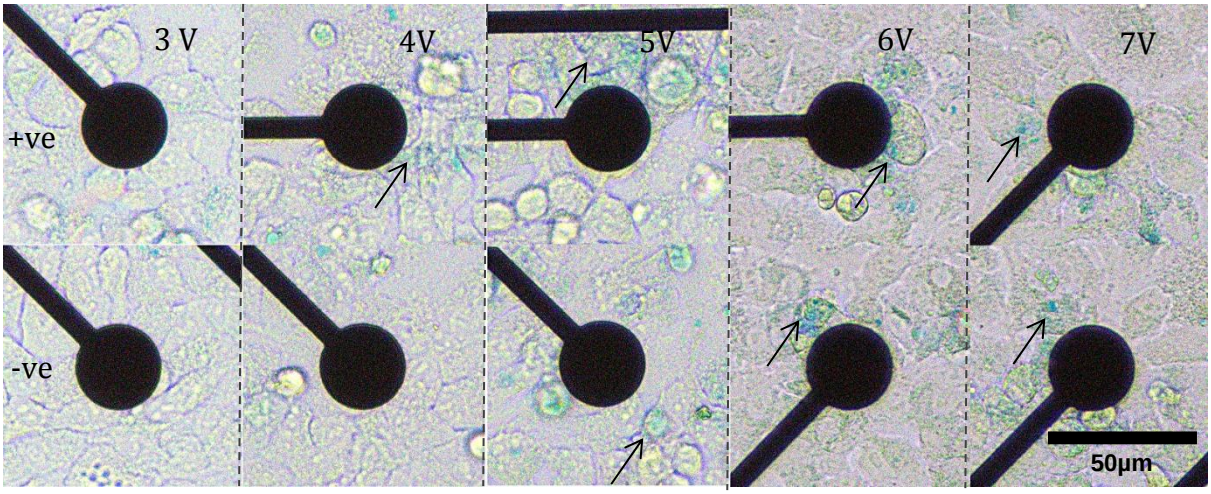


Figure 5.11: Magnified images of individual microelectrodes used for electroporation of A549 cells. The images show that the BBG staining is confined to small circular areas inside the A549 cells (Black arrows).

The staining of A549 cells (Figure 5.11) appears relatively mild in comparison to that of dead neurons seen in Figure 5.9(b). Since the degree of staining is directly related to the permeability timeframe of the cell membrane. The highly permeable membranes of the dead neurons provided sufficient time for maximum diffusion of the stain into the cell. Figure 5.12 shows the comparison between the BBG staining of dead neurons after 3 min versus 15 min exposure. The staining after 3 min exposure appears to be mild as the intensity of the BBG is low. In contrast the 15 minute BBG exposure produces a very vibrant and intense blue stain. These timeframes are significantly longer than those of electroporated A549 cells leading to the noticeable difference in the degree of staining.

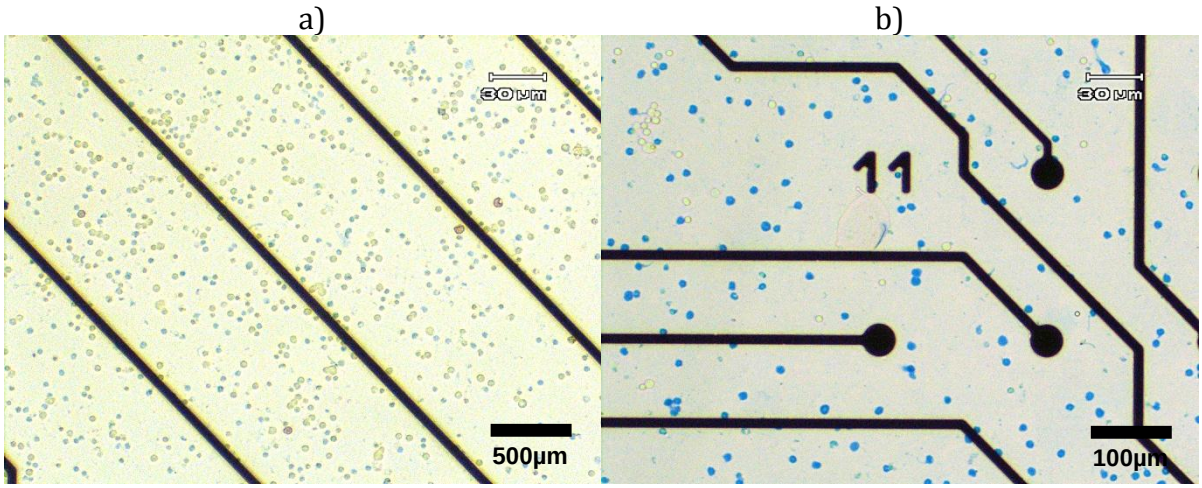


Figure 5.12: Brightfield images showing dead, BBG stained neurons. The intensity of BBG stain is directly related to the lengths of dead cell exposure to the stain. a) 3 min exposure to BBG b) 15 min exposure to BBG. (Note: as in Figure 5.9, staining of dead neurons does not require electroporation)

5.2.4 Neurons cultured inside microfluidic device

5.2.4.1 Permanent µF device assemblies

Culturing of the neurons inside the µF device was attempted in a static environment where there was no perfusion. The major technical issues that arose with culturing neurons in these devices were failure of µF device because of detachment, introduction of air bubbles into channels, blocked inlets and bubble formation inside the channel which is an especially well known issue with gas permeable hydrophobic surfaces (Kim et al., 2007). At 1 DIV, in the centre of µF device, there was some evidence of neuronal cell growth. However, by 5 DIV there were no viable neurons inside the µF device channel (Figure 5.13).

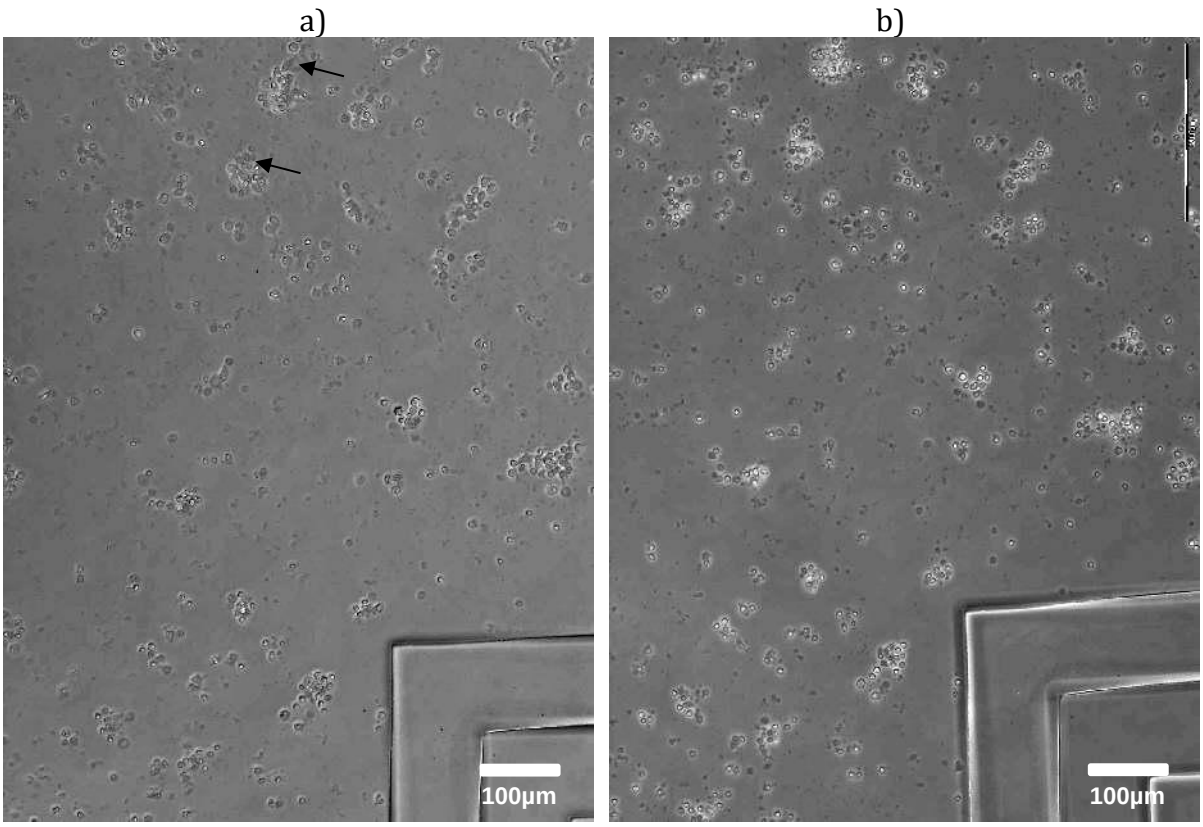


Figure 5.13: Phase contrast images of E14 rat embryo spinal cord cells seeded inside a µF device on SiN coated Pyrex after a) 1 DIV and b) 5 DIV. The black arrows in (a) indicate a small number of cells that have extended short processes. However, in (b) at 5 DIV there is no observable neuronal growth or network formation

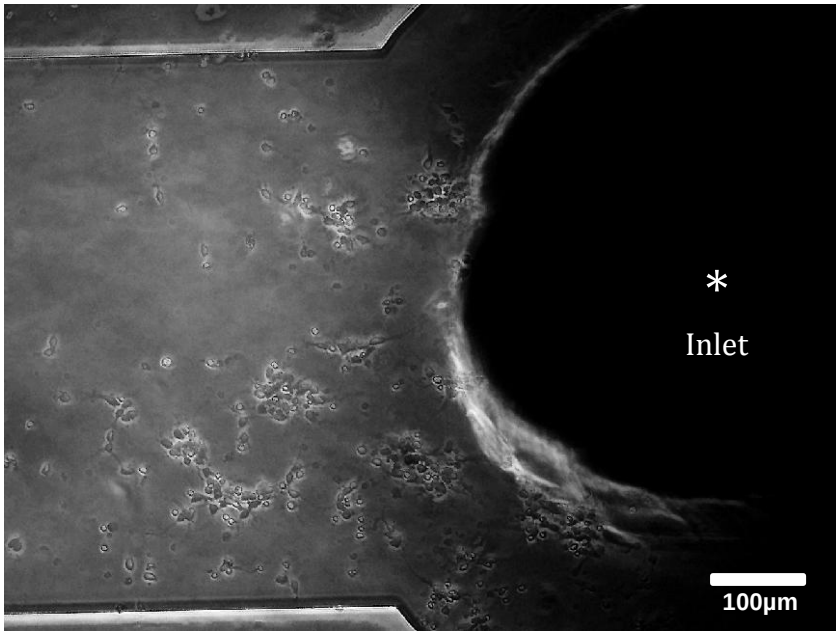


Figure 5.14: Phase contrast image of E 14 rat embryo spinal cord cells inside a µF channel. The close proximity of the cells to the channel inlet allowed long term culturing as compared to the areas of the µF device that are further away. This long term viability can be explained by higher rates of diffusion due to large inlet diameter and close proximity to the fresh media reservoir.

However, the neurons that were positioned near the fluidic inlet showed good viability, growth and network formation (Figure 5.14). The inlet had an approximate cross-sectional (CS) area of 0.28 mm^2 while the CS areas of the µF channels are 0.2 mm^2 (main large channel) and 0.06 mm^2 (small side channels). The larger CS area of the inlet allows for higher diffusion rates, while the shorter distance from the fresh media reservoir further reduces the time required for sufficient nutrient diffusion and gas exchange. Hence the poor long term viability of cells positioned far away from the inlets can be explained by poor nutrient diffusion, gas exchange and waste build up (Kim et al., 2007). This result established that this particular design of µF device can only sustain viable neurons near inlets and requires fluidic perfusion to achieve good neuronal viability throughout the micro-channels network.

5.2.4.2 Assemblies with detachable µF device

In order to avoid the practical difficulties of loading the neurons into the µF device (see previous section), the experimental procedure was revised where the µF device was added after the neurons were seeded on to the surface. This method eliminated the issues associated with the µF device failure due to detachment and ensured that correct number of cells per unit area was present inside the µF channel. Additionally the bubble formation issue was overcome by soaking the µF devices in HBSS at 37°C for 2-3 days as previously described (Biffi et al., 2012). However, this also made the µF device hazy and more difficult to image the cells.

The efficient mass transport of nutrients was achieved by perfusion with a syringe pump with a withdraw function. After overnight perfusion at 5 µL h^{-1}, a small number of viable neurons were observed inside the channel (Figure 5.15(a)). The initial low number of viable cells in the channels indicated that the culture would not survive. Interestingly, the culture was able to survive a further 72 h inside the channel without any mechanical perfusion (Figure 5.15(b)). It was observed that after 72 h, three large cell aggregates appeared in the channel, each extending a number of fascicles in random directions. At this point the perfusion was resumed. As the time passed, more and more individual cells were observed inside the channel at different distances from the cell aggregates (Figure 5.15(c))

At 6 DIV it was attempted to add new primary neurons to the existing culture by adding the cell suspension into the main reservoir and drawing the cells into the channels. This however did not result in an immediate increase of cell numbers inside the channel. The highest numbers of cells in the channel was observed at 11DIV (Figure 5.15(d)) and the culture remained healthy up to 13DIV. At 14 DIV, the viability of the culture was starting to decrease as indicated by a change in cell morphology and appearance of floating debris (Figure 5.15(e)). Similar changes were observed in the control culture seeded on polystyrene culture dish without the integrated µF device (Figure 5.15(f)).

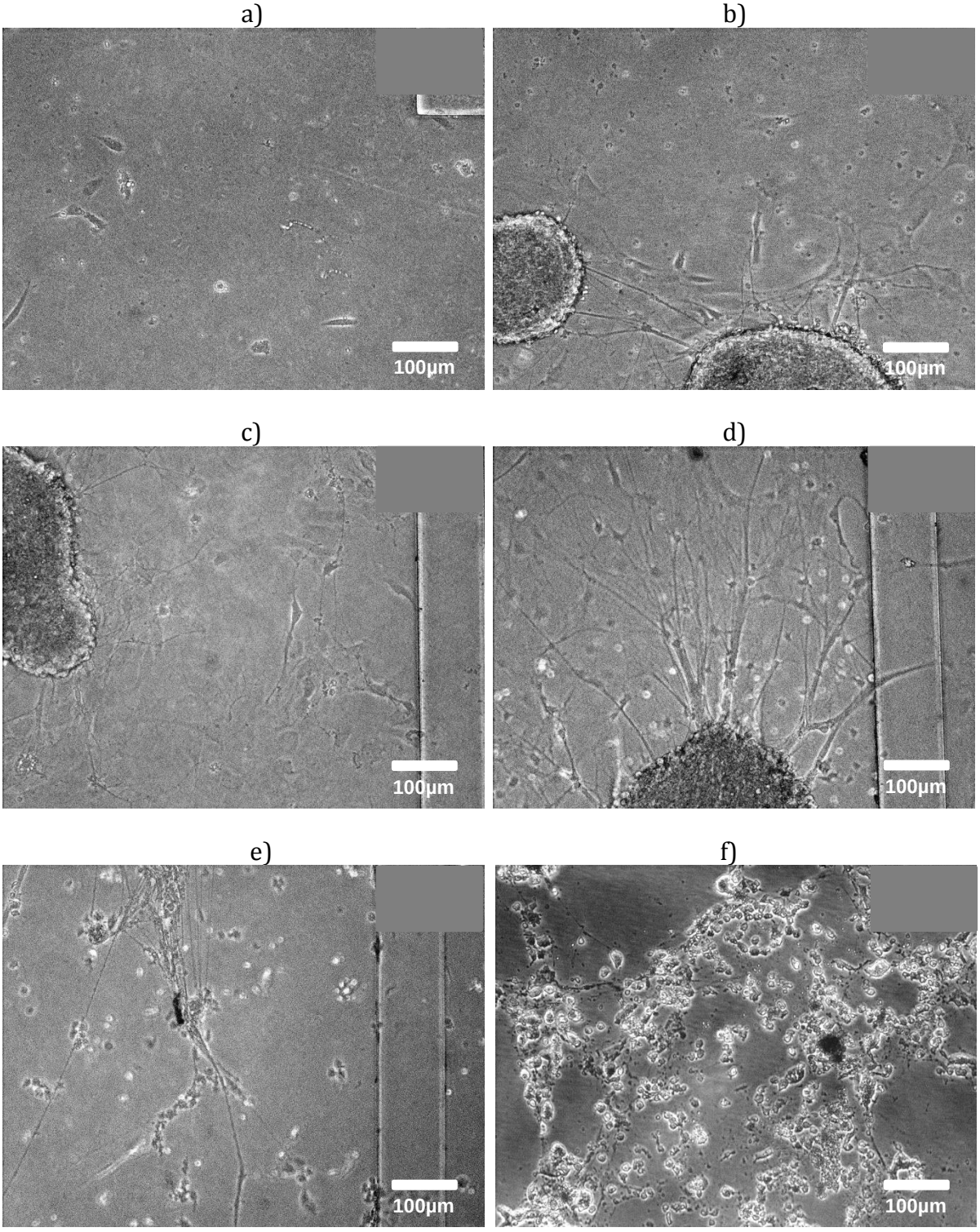


Figure 5.15: Phase contrast image of surviving neuronal cells on polystyrene surface with integrated µF device. a) µF perfused overnight. Minimal cell numbers inside the channel at 1 DIV b) Neurons at 4 DIV, device was not perfused for 72h. c) Increased neuronal cell number in channel at 6 DIV. d) Robust neuronal culture at 13 DIV. e) Decreased neuronal viability at 14 DIV. f) Control neuronal culture at 14 DIV on polystyrene surface showing a similar viability drop as neurons inside the µF device.

5.2.5 Aggregate migration

Figure 5.16 shows the neuronal cell aggregates between 100 µm PDMS features of µF device. The particular cell aggregate was split in two when the µF device was introduced to the culture. The evidence for this are what appear to be torn processes between the aggregates under PDMS (Figure 5.16(a)). It was observed that the damaged cell aggregates migrated towards one another down the narrow channels eventually joining together via a thick fascicle (Figure 5.16(a-d)). This a significant result because it indicates that the cell aggregates were releasing growth factors into the surrounding media which led to establishment of growth factor gradient and induced migration of the cell aggregates towards one another.

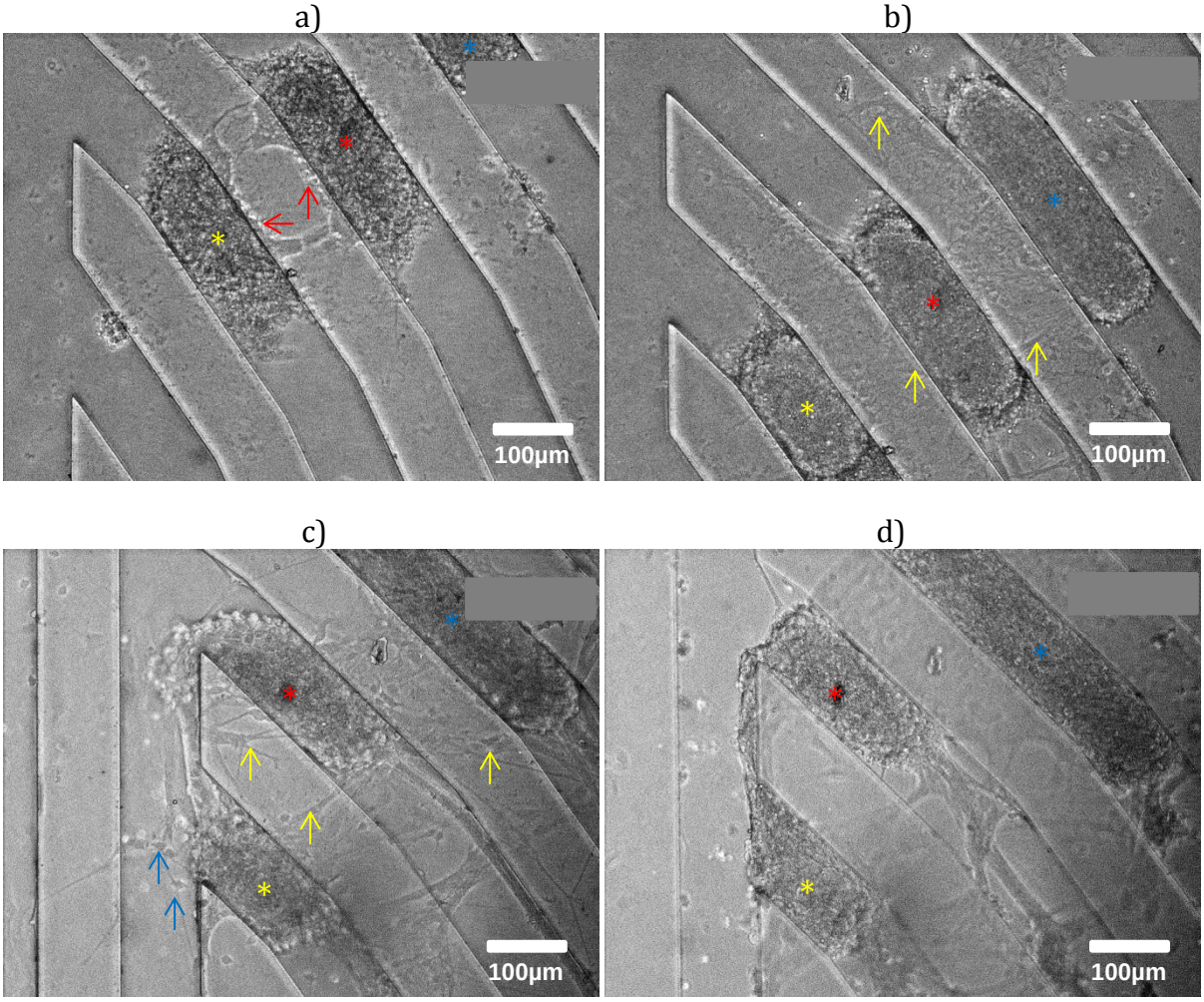


Figure 5.16: Neuronal aggregation in areas separate from the main channel (colour stars). a) Neuronal cell aggregate after physical split by the PDMS wall. b) The neuronal aggregates regrow processes under the PDMS wall (yellow arrows). c) The aggregate migration towards one another. d) The decline of neuronal viability. Blue arrows indicate single neurons growing separately from the aggregates

This result reaffirms that the formation of neuronal networks can be controlled via diffusive fluidic gradients inside MEMS devices. As the ability of the neuronal cells to re-establish their connectivity after controlled damage *in vitro* has been previously demonstrated (Hellman et al., 2010), this result highlights the potential of using the controlled aggregate lesions for guiding neuronal growth inside the enclosed µF environment.

Another interesting observation made during the 14 day culture was the survival of cell aggregates in areas separate from the main perfusion channel. The neuronal survival in the un-perfused areas of the µF device can be explained by the poor seal between the µF device and the surface. The lack of an adequate mechanical seal is evidenced by the growth of neuronal processes under the PDMS features as indicated by yellow arrows in Figure 5.16(b) and (c). The gap between PDMS and the substrate appears to be sufficiently large to allow fresh media to seep into the un-perfused areas of the µF device and sustain the neurons and the aggregates. At 4 DIV there is evident regrowth of the processes between the cell aggregates. These processes grew under the PDMS wall (Figure 5.16(b)). The viability of the cell aggregates mirrored that of the aggregates and neurons in the main channel and remained healthy up to 13 DIV (Figure 5.16(c)) but by 14 DIV (Figure 5.16(d)) the culture started showing similar signs of decline.

5.2.6 Controlled distribution of cells in µF channels

The controlling of the cell distribution inside microfluidic channels has been previously demonstrated using trypsin or SDS fluidic gradients (Nie et al., 2007, Villa-Diaz et al., 2009, Lee et al., 2013). Rather than using potent detergents, it was demonstrated that the distribution of A549 cells can also be controlled via exclusion of growth factors (FBS/FCS and GlutaMAX) from a perfusing gradient (Figure 5.17). After 24 h, on one side of the channel, the population of A549 cells that were perfused with un-supplemented media was reduced by 85 % (cell count drop of 62) while the cells perfused with normally supplemented media recorded a population reduction of only 13% (cell count drop of 33). This result shows that the integration of the µF device with the neuro test platform can be used to control cell distribution as well as free up additional culture area. In turn, this additional space could be used for seeding other cell types to produce hybrid, *in vitro* co-cultures on a chemically patterned, micro-fabricated device.

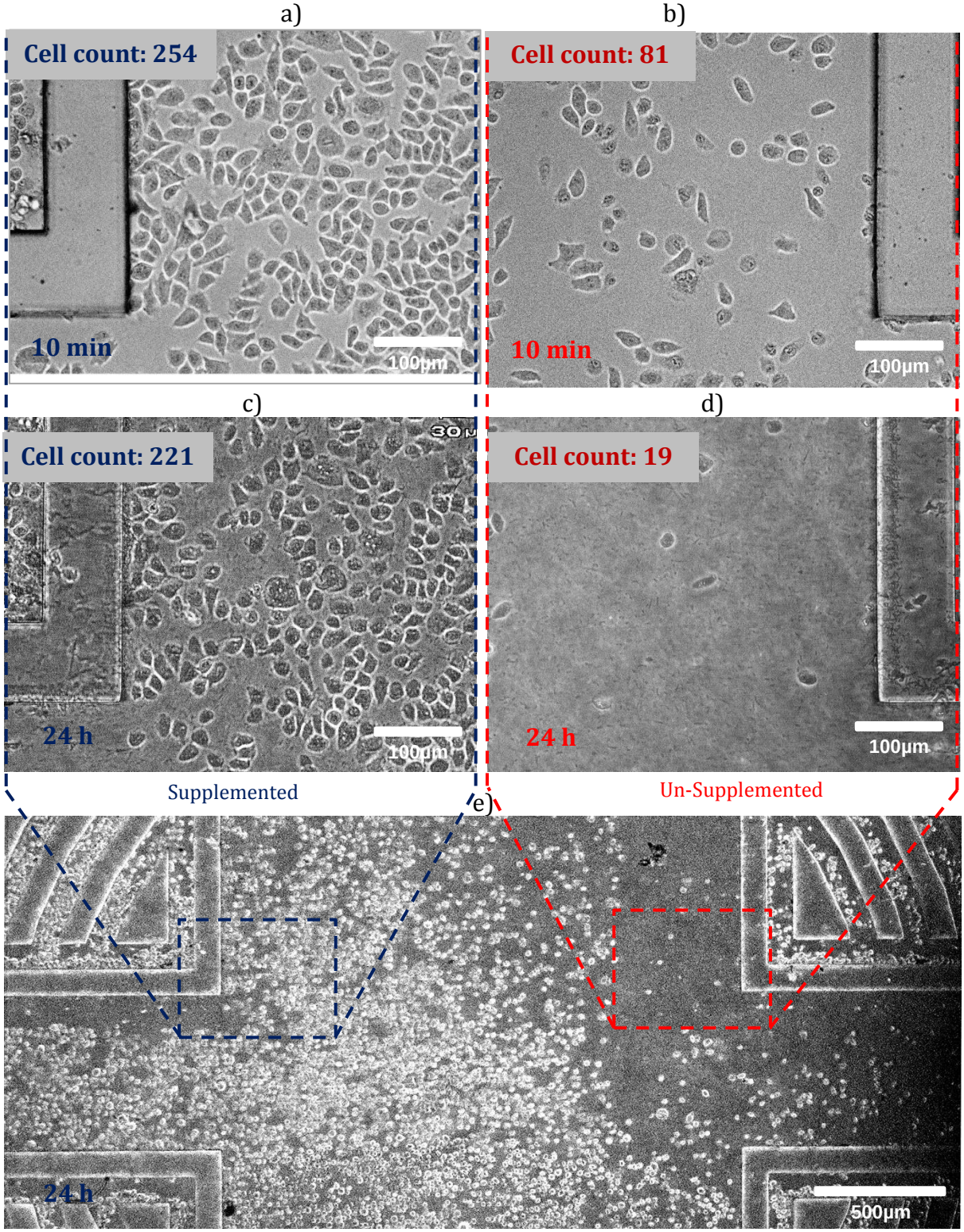


Figure 5.17: Phase contrast images of A549 cell line growing in differential environment inside a µF device. a) A549s at 0DIV in fully supplemented media. b) A549s at 0DIV in media without any supplements. Both images, (a) and (b) were taken after 10 min perfusion. c) A549s on supplemented side after 24 h perfusion. d) A549 on un-supplemented side after 24 h perfusion. e) Image showing the difference in A549 cell density relative to fluidic inlets.

Table 5.2: Table showing the A549 cell counts in different regions of the μF device channel after 10min and 24 h perfusion periods.

	Supplemented media	Un-supplemented media
10 min	254	81
24 h	221	19
% difference	13%	85%

5.2.7 The neurobiological test platform

The functional integrated neurobiological test platform is shown in Figure 5.18. This result represents the first demonstration of an MEA simultaneously integrated with a functional μF device and chemically patterned neuronal network. This result shows that the neuronal network can be successfully patterned via μF perfusion on the MEA substrate and integrated with the μF device at a later stage without negatively affecting the seeded neuronal culture. The ability to attach or remove the μF device as needed allows this device to sustain the culture in potentially more favorable static environment without sacrificing the ability to perform μF cell culture experiments.

The combination of the ability to record electrical activity with spatial control of cell distribution and fluidic environment has produced a powerful, flexible, multifunctional research tool and allows this device to be used for experiments involving electrophysiology, neuronal guidance or drug screening etc.

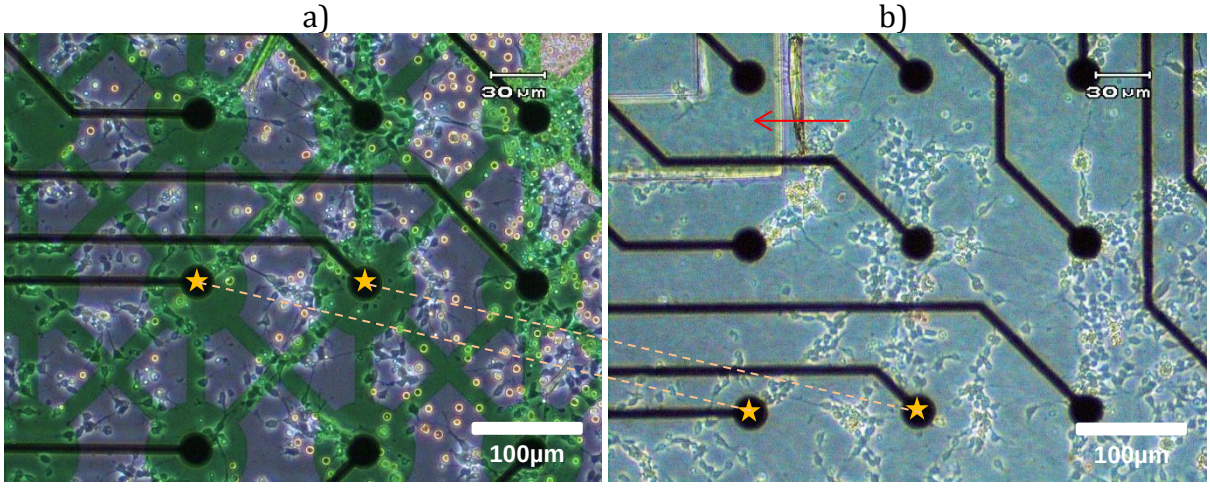


Figure 5.18: a) Patterned neuronal network on recycled MEA surface. b) Neurons seen in (a) but with an integrated μF device. Note: images (a) and (b) show the same neuronal pattern. The yellow stars indicate the same electrodes. The red arrow indicates the μF channel wall.

Overall, this final result shows that the aim of building an integrated neurobiological test platform has been achieved and it validates the methods and techniques used to achieve this level of integration. This result also provides a solid foundation for

optimizing the neuronal environment to achieve a long term culture capable of spontaneous electrical activity.

5.3 Discussion

The experiments described in this chapter were aimed at achieving functional integration between MEAs, substrate patterning, patterned neuronal culture and µF device. As stated in the introduction, the aim of the research was to build a multifunctional platform capable of guiding the formation of the neural network through combined influence of surface chemistry and micro-fluidic gradients, sustaining a viable patterned neuronal culture and recording neuronal electrical activity.

5.3.1 Biocompatibility and device recycling

Direct comparison of patterned neurons on a re-used MEA with the patterns on new Pyrex substrates shows that the neurons on new substrates are much more pattern-compliant. This has been observed after numerous experiments that used recycled MEAs for neuronal patterning. The conclusion that can be drawn from this is that best neuronal patterning can be achieved on brand new MEAs. A small degree of neuronal patterning can be achieved on MEAs that have been used and recycled once or twice. However, it is unlikely that neuronal patterning can be achieved on MEAs that have been extensively re-coated and recycled unless effective surface cleaning methods are used (Suzuki et al., 2013). This suggests that single-use devices may have an advantage with regards to producing consistent neuronal patterns. Single-use devices however, would be highly impractical if they were based on the high cost commercial MEA. Thus, the successful and consistent neuronal patterning on MEA may require either a fabrication of cost-effective single-use MEAs or a more stringent patterning and recycling approaches. For example, repeat patterning needs to be aligned as accurately as possible with the previous pattern to avoid creating any additional cytophilic areas. These types of measures should decrease the chances of neuronal attachment to the background areas. Although, it is important to point out that due to protein adsorption, the cell compliance with the pattern will continue to fall each time the MEA is recycled due to protein adsorption from culture media (Ni et al., 2009). The ideal solution may require permanently patterning the MEA with anti-fouling coatings to stop protein adsorption and cell attachment on areas between the micro-electrodes (Guo et al., 1996, Roach et al., 2010, Ricoult et al., 2012). Combining the anti-fouling coatings with the

stringent patterning techniques should yield an MEA that can be used for growing the patterned neuronal cultures time after time (Suzuki et al., 2013).

5.3.2 Neuronal electrophysiology and electroporation

The ability to record neuronal electrophysiological activity was a key requirement that dictated the integration of MEA into the neuro test platform. The successful recordings of neuronal electrical activity have been described in some detail in Chapter 4 and in numerous studies (Fejtl et al., 2006, Pine, 2006, Potter et al., 2006, Ruffini et al., 2006, Whitson J. et al., 2006, Claverol-Tinturé et al., 2007).

To demonstrate the additional benefits of the integrated MEA, its circular electrodes were successfully used for electroporation of A549 cells. This method of electroporation was demonstrated previously using an MEA with square micro-electrodes, 100 μm apart (Jain and Muthuswamy, 2007b) as well as 3D electrodes (He et al., 2007). It was attempted to improve upon the previous work by simplifying the protocol. First, the dependence on fluorescent microscopes for signal detection was eliminated by using a non-fluorescent Brilliant Blue G (Coomassie blue) dye. This concept has been demonstrated previously *in vivo* (Pinault, 1996). Secondly, this method was further simplified by adapting it to the commonly used MEAs with 60 circular electrodes and 200 μm spacing (Wheeler and Brewer, 2010, Biffi et al., 2012). Because of the difference in electrode shape (square vs. circle) and distance (100 vs. 200 μm) the electroporation settings specified in the study by Jain and Muthuswamy could not be used. The reasons for this are as follows; the square electrodes generate variable current densities due to the edge effect, where the electrode's corners produce higher current densities compared to the straight side (Jain and Muthuswamy, 2007a). The circular electrode in contrast produces a uniform current density at its edge. Because of this difference, the applied potential has to be adjusted to achieve the current density equivalent to that of the square electrode corners. Additional potential adjustments had to be incorporated to account for the increased distance between the cathode and anode electrodes. It is important to point out though that, unlike in the previously published studies, the cell staining was observed only after the second round of electroporation. This indicates that the period between pore formation and closing is insufficient to allow the detectable amount of BBG to diffuse into the cell. Doubling the "open" period however, produced a positive result. The BBG staining has the potential to be improved by further

optimizing the applied potentials. For example, the multistage, variable amplitude potentials have been shown to enhance the cell uptake of fluorescent dyes (He et al., 2007).

5.3.3 Integration of the µF device

Due to the fragile nature of the MEAs, an alternative method of temporary µF attachment was investigated. Instead of permanently plasma bonding the µF device to the substrate, the µF device was held against the surface using a custom machined chamber and a lid. The method of reversible µF device integration proved to be far superior to the traditional methods published in the literature (Morin et al., 2006, Wu et al., 2008, Xu et al., 2010). Only one publication detailing an alternative method of reversible µF attachment to an MEA was found (Biffi et al., 2012). The benefits of the reversible µF integration are as follows:

1) The strengths of the µF device attachment to the surface was dependent on the strengths of adhesive used to bond the culture ring to the substrate. The adhesive bond strengths can far supersede the bond strengths between PDMS and substrate (Pyrex or SiN). Hence it made it much easier to attach and more importantly detach perfusion lines.

2) This setup eliminated the need to bond the µF to the substrate prior to culturing, removing the potential for introduction of air bubbles into the µF channels during cell loading (Kim et al., 2007). Unlike the traditional methods e.g. (Thiébaud et al., 2002, Taylor et al., 2003), the µF device could simply be attached after the cells have adhered to the surface.

3) This method simplified the process of culturing the neurons inside µF device. The cell density per area of the substrate could be more easily controlled during cell seeding and would not change after the addition of the µF device.

4) Finally, provided that an MEA can be efficiently recycled, this method allows an expensive MEA to be integrated with µF devices of multiple designs in reversible manner.

Reversible µF device attachment also has its drawbacks which are associated with the increased complexity. The culture media tended to leak between the faces of the reservoir plate and the culture ring thus requiring the use of vacuum grease, or gaskets (PCR film) further adding to the number of steps required to assemble the device.

5.3.4 Cell cultures using µF devices

Despite the increased complexity of the reversible µF integration, this method proved to be reliable and suitable for long term culturing and multi-channel perfusion of primary neurons. An interesting result was the restoration of neuronal connectivity following the mechanical dissection of a neuronal aggregate when attaching the µF device. After the initial split, the two aggregates started sending neuronal processes to one another under the dividing PDMS wall. Similar behaviour has been previously observed with damaged fascicles of neuronal processes (Hellman et al., 2010). The process growth was shortly followed by the aggregate migration towards one another along the channel walls. This uni-directional migration strongly indicates the presence of a growth factor gradient in the vicinity of the neuronal aggregates. This observation demonstrates that the growth and development of neuronal networks can be controlled via static, diffusive fluidic gradients inside the µF devices. This observed phenomenon has a number of potentially useful applications. First, it may be possible to harvest the growth factor supplemented media by intentionally damaging the neuronal aggregates, perfusing the channel and collecting the "waste" media. Alternatively, the controlled damage to the aggregates may be used for in vitro cell guidance inside purpose designed MEMS devices.

5.3.5 Control of cell distribution with dynamic µF gradients

One of the aims of this project was to control neuronal growth and distribution using the micro-fluidic gradients and supplements (Nie et al., 2007, Villa-Diaz et al., 2009). A very recent publication showed that it is possible to apply micro-fluidic control on a single cell level (Lee et al., 2013). Unfortunately, during this project, it was not possible to directly demonstrate the influence of dynamic gradients on the neuronal cell culture due to persistent issues with biocompatibility and contamination. Instead, this concept was successfully demonstrated by controlling the distribution of the A549 cell population inside the fluidic channel. This result was consistent with the previous publications and showed a marked decrease of cell numbers in the region of the µF channel perfused with DMEM un-supplemented with growth factors (10 % FBS and 0.1 % GlutaMAX).

5.3.6 Integrated platform for neurobiological applications

After numerous optimization experiments described in this project, the architectural integration of MEA with patterned neuronal cell culture and μF device has been achieved. It was possible to perfuse the patterned culture for 24 h demonstrating that the patterned neuronal cultures can withstand a dynamic microfluidic environment and remain attached to the surface of the MEA. This result further validates the use of μF surface patterning and the method of reversible μF device integration and provides some additional clues with regards neuronal patterning on MEAs. However, the most important result of this research and integration is the fabrication of a multifunctional integrated platform, geared toward multiple types of experiments. The list of the simultaneous device capabilities is as follows.

1) The integrated MEA enables the device to record or stimulate neuronal electrical activity as well as focally electroporate the cells on the surface.

2) The surface chemistry can be modified using μF patterning to suit the experimental demands.

3) The integrated, detachable μF device provides the capability to control the cell culture environment. This environment can be made static or dynamic, uniform or consisting of multiple fluidic gradients with different supplements. Importantly, the attachment of the μF device does not directly depend on the device surface chemistry.

4) In addition, this test platform is not limited by integration with single μF device design. Because the μF device can be detached from the surface, multiple channel layouts can be tested.

5) This architecture also allows the addition of the μF device at any stage of the experiment.

6) Lastly, this neuro test platform architecture is compatible with common microscopy techniques.

The combination of the above capabilities enables this platform to be used for different experiments involving any combination of the following: cell culture, cell types, electrophysiology, transfection, cell staining, surface chemistry, micro-fluidics and microscopy. The current state of the art MEMS and lab on chip devices can be very complex and highly engineered (Vulto et al., 2013, Lin et al., 2013, Schimek et al., 2013) as compared to the device built during this project. However, the complexity of the device does not specifically allow it to perform multiple functions. Instead, most state of

the art devices are geared towards performing one, complex task (El-Ali et al., 2006). Thus, the multi-functionality is what differentiates the integrated neurobiological test platform built during this project from large numbers of previously described devices. Although it is important to point out that multifunctional MEMS devices such as a multifunctional pipette have been previously described (Ainla et al., 2012, Gavin, 2012). The integrated neurobiological platform of this type has the potential to be applied to research in the field of, for example, regenerative neuroscience or spinal cord injury. The ability to control the surface and fluidic environment of the neuronal culture is very useful because it is closely related to the *in vivo* models of neuronal growth through damaged areas and scar tissue of the spinal cord. The additional capability of this platform to record the neuronal electrical activity can be utilised to determine if the anatomical regeneration was accompanied by functional connectivity between severed neurons. Alternatively, this platform can be applied to experiments involving neuromodulation. The added benefit is that the modulatory effects of various compounds can be focused on the selected parts of the neuronal culture using the microfluidic gradients. The effects of focal neuromodulation can then be measured by comparing the electrophysiological data.

5.4 Conclusion

The experiments described in this chapter were aimed at reaching the goal of fabricating an integrated, multifunctional, micro-fabricated test platform that can be used for neurobiological research. This chapter successfully demonstrated that the cell culture populations can be controlled through static or dynamic fluidic gradients, and are able to survive in such environment for up to 14 days. Additionally, this chapter demonstrated the multi-functionality of the neuro test platform through successful focal, electroporation of A549 cells using an MEA capable of electrophysiological recordings. Through integration, optimization and modification of established techniques, this chapter demonstrated for the first time the patterned growth of rat embryo spinal cord neurons on the surface of an MEA, integrated with perfused microfluidic device. This final result marked the achievement of the fundamental aims set out in the beginning of this project.

Chapter 6

6.0 Conclusion

In the initial stages of this project, the focus of research was to build a multifunctional neuro test platform and use it for gathering data relating to neuronal electrophysiology, patterning and studying the effects of different fluidic environments on the neuronal population. This device was intended to be simply a tool to determine if the growth of neuronal culture can be controlled more precisely through combination of surface chemistry and microfluidic gradients *in vitro.* At the same time, to determine if such neuronal culture remained functional, this platform was also tasked with recording the electrical activity of patterned neurons on its surface. As the experiments were performed and basic integration was attempted, it became very clear that the main research challenges lay in integration of every single constituent part and not in using this device for its final purposed as a data gathering tool. This shift in focus towards more fundamental aspects is a necessity if the goals of studying neuronal network formation using this device are to be achieved. The optimization and integration performed in this project resulted in a multifunctional platform potentially more capable and versatile than previously published devices. As the final integrated neuro test platform is a combination of techniques and physical components, this chapter will discuss the most important and influential integrated techniques.

6.1 Surface patterning

The first aspect that this project investigated was: chemically patterning substrates with cytophilic polymers using micro-contact printing (μCP) (Bernard et al., 1998). The results of investigations with regards to pattern quality and patterning neurons can be found in sections 3.2 and 4.2 respectively.

In the literature, the technique of μCP is generally regarded as one of the simplest methods for generating chemical patterns on surfaces. Many published studies have produced high quality fluorescent micro-printed patterns with impeccable edge definition and uniformity (Csucs et al., 2003, Vogt et al., 2004, Chen et al., 2011, Ricoult et al., 2012, Ruiz et al., 2013). This project was also successful in generating patterns of comparable quality on different surfaces as well as using these for cell culture. However, because μCP is not a simple process, it did require a lot of optimization to achieve these results. The most problematic aspect of μCP was the un-even transfer of ink from the

stamp to the surface. This is thought to be caused by the ink drying process where, as the volume decreases, the solutes precipitate at the edges of receding drops, leaving the distinct areas of concentrated ink. This results in a poor pattern quality on the substrate. The evidence for this can be seen in Figure 3.16, section 3.2.2. Similar evidence comes from studies that imaged the printed patterns with the atomic force microscope (AFM). These measurements showed a thickness variation of the printed pattern indicating non-uniform deposition of the ink (Oliva et al., 2003, Ruiz et al., 2008). The solution to this issue may lie in more sophisticated and controlled methods of stamp inking. Dry inking, where the stamp is pressed against a loaded inkpad, has produced uniform single layer patterns in nanometer range (Libioulle et al., 1998). An alternative stamp manufacturing method that bypasses the soft lithography may prove even more practical and consistent. For example, microstamps have been fabricated via a solid state, commercial printer where the required pattern was printed on a flat, featureless stamp and then transferred onto the surface of interest (Xing et al., 2012). The advantage of this method is the high degree of control over the amount of ink deposited onto the stamp leading to a more controlled printing process.

It is important to point out that other characteristics of μCP are also related to the chemical and physical properties of Polydimethylsiloxane (PDMS). An undesirable feature of PDMS is the presence of short, unbound PDMS chains in the PDMS matrix. As described in section 3.2.4, these short chains tend contaminate the printed substrate (Thibault et al., 2007). These unbound chains also make it difficult to achieve any long term modifications of the PDMS surface for the same reasons (Zhou et al., 2010). It is possible that the observed inconsistency of the μCP was compounded by the masking of ink from the target surface by leaching of the unbound short chains.

Overall, the widespread use of μCP is necessitated by lack of simple alternatives and a need for sub-micrometer resolution (Mukhopadhyay, 2007). Even though surface patterning can be achieved through a vast array of different methodologies such as laser ablation and resist lift off, these techniques require specialized equipment such as lasers, spin-coaters, photomasks etc. and thus may be unavailable to many researchers.

Thus, to try and address the above issues and keep the methodology simple, a different approach was tested. The chosen solution was to use μF devices to pattern substrates (Delamarche et al., 1997). The existing PDMS micro-stamps were adapted into masters for casting microfluidic devices with identical pattern layout to μCP (Wang et al., 2010).

This solution proved superior because, compared to μCP, the microfluidic devices consistently produced patterns of higher quality and uniform ink distribution. In addition, because patterned areas did not come into direct contact with PDMS, this method was immune to pattern masking or surface fouling (Thibault et al., 2007). Other advantages are: simplification of patterning procedure, multiple alignments of the μF device with the substrate, independence from the flip chip bonder and better integration with MEAs due to reduced surface fouling.

6.2 Integration of microfluidics

The optimization of μCP and engineering of solutions to circumvent the drawbacks associated with PDMS resulted in a relatively reliable surface patterning method using the μF approach. Importantly the lessons related to PDMS replica molding and surface fouling were applied to μF perfusion and μF device integration with substrates and MEAs. Similarly to μCP, the literature described the integration of μF devices with substrates as a trivial matter. The common consensus is that for secure attachments of PDMS μF devices to Pyrex or polystyrene substrates, it is enough to simply treat both surfaces with plasma (Zhu et al., 2004, Bhattacharya et al., 2005). This is true as long as the PDMS surface is free from unbound short chains, a requirement rarely mentioned in literature. Numerous attempts to bond PDMS to various substrates were performed during this project with varying degrees of success. The main observation was that most PDMS devices attached to Pyrex only partially, some areas were strongly attached while other areas failed to attach completely. On the occasions when a secure bond was achieved, it was possible to use the μF device to generate μF gradients. Despite the secure μF attachment, these μF device assemblies were found to be impractical, especially if the device was to be viewed under a fluorescent microscope. The Teflon tubing would cause problems when accidentally coming in contact with the microscope lens during imaging, either tearing or detaching the μF device. This problem was compounded by multi-channel perfusion, since each channel required a separate Teflon tube.

After a number of trials it became clear that to fabricate a reliable and practical test platform, it had to be made physically robust. The PDMS μF device is simply too weak to structurally support stiff components, such as Teflon tubing. The solution involved using alternative means of securing the μF device against the surface. As described in

sections 2.3.4 and 5.1.4, this was achieved by pressing the μF device against the substrate using a number of ridged, machined components. Only one other MEA relevant publication outlining an alternative method of μF attachment was found (Biffi et al., 2012). Despite the increased fabrication complexity, the assembly proved to be robust and able to easily withstand numerous long term perfusions, physical handling and temperature cycling. This method proved suitable for integration and multi-channel perfusion of primary neuronal cell culture for a period of 14 days, the optimal cited timeframe for detection of synchronized electrophysiological activity (Kamioka et al., 1996, Chang and Wheeler, 2006, Biffi et al., 2012).

This method of μF integration opens up a number of additional opportunities. First, because this method uses suction to draw the fluid through the μF device, there is a potential for increasing the number of perfusion channels without increasing the number of connections to the pump. One vacuum line can be used to draw fluid from any number of on-chip reservoirs, thus avoiding the overcomplicated reservoir-to-chip setups seen elsewhere (Cooksey et al., 2009). Second, this method opens up the possibility to reversibly attach a μF device to surfaces other than Pyrex, polystyrene or Zeonor. Bare, chemically unmodified surfaces such as stainless steel, gold or various structural polymers can be integrated with a PDMS μF device. Moreover, the surface chemistry can be modified to suit the experimental requirements rather than PDMS-substrate bond, allowing for greater experimental flexibility (Lee and Ram, 2009).

6.3 PDMS alternatives

Since, the issues encountered during optimization of μF perfusion and surface patterning were associated with PDMS, using an alternative material could be of benefit. For example, a material such as photo-curable perfluoropolyether (PFPE) shows great potential. This material is similar in terms of flexibility, transparency and can be replica molded against a master just like PDMS. The biggest advantage of PFPE is its resistance to solvents such as toluene and dichloromethane (Rolland et al., 2004). However, it is yet to be investigated if this alternative material has any issues with surface fouling or surface chemistry that may restrict its integration with cell culture or MEAs.

6.4 Primary neuronal cell cultures

As stated previously, control over formation of neuronal networks was one of the main goals behind the integration of above techniques with the MEAs. However, the culturing

of primary neurons in a setting with just one integrated aspect proved extremely challenging. In cases of cell surface patterning, two most common outcomes were either neuronal death at early stages of culture (1-2 days), or that healthy neuronal population showed minimal signs of patterning. Neurons cultured inside µF devices showed similar inconsistency.

Eventually, the issues with neuronal viability were attributed to a serum free environment. This environment was used to maintain a high ratio of neurons versus glial cells to ensure that only neurons attached to the micro-electrodes (Manos et al., 1999). However, recent publications suggest that presence of glial cells can have a positive effect on neuronal electrical activity (Wheeler and Brewer, 2010, Shi et al., 2013). The neuronal viability in serum free environment was supposed to be maintained by the B-27 supplement instead of glial cells (Brewer et al., 1993). It was observed that this supplement did function very well when used with well-established culture protocols on commercial culture plates. However, it was also observed that B-27 on its own was not sufficient for long term neuronal cultures on in-house built devices. On these substrates, better viability was achieved in media supplemented with both, B27 and Fetal Calf Serum (FCS). Similar observations were made in other studies investigating neuronal viability and toxicity (Ye and Sontheimer, 1998, Carrier et al., 2006). An additional effect of the presence of FCS is the differentiation of some neurons into glial cells. It has been shown that this cell type does not directly influence the neuronal viability, but instead improves the synaptic connectivity (Pfrieger and Barres, 1997). It is important to point out that although, the addition of FBS improved neuronal viability, it was not a perfect solution. On a number of occasions, extremely low neuronal viability was observed with FCS and B27 supplemented media.

6.5 Biocompatibility and integration

As pointed out above, the addition of serum to the neuronal cultures was relatively effective in increasing the neuronal viability. However, this did not solve the viability issue completely as, on number of occasions, low viability was still observed. These observations indicate involvement of other factors. The likely reason for poor viability is low biocompatibility of the assembled device (Kotzar et al., 2002). Notably, neuronal viability got progressively worse each time the platform was reused indicating that the recycling method was also a factor. Though individual components are considered bio-

compatible, their integration and notably recycling was often incompatible with primary neurons.

The anti-bacterial soap or active enzyme detergent such as Terg-a-zyme, used to remove cells and debris from the device's surface, are not biocompatible. In fact, it has been recently shown that detergents such as SDS will damage primary neurons within seconds after exposure (Lee et al., 2013). The substrates are required to be thoroughly rinsed after cleaning with detergents. It is possible that the rinse step was insufficient or too short (~10 min) allowing small quantities of detergent to remain in the culture well. Micro-cracks in PMMA or MEA passivation studied previously may have contributed to this issue by providing additional surface area and volume for detergent adsorption and lodgement (Nam et al., 2012). The lodged detergent may have leached back into culture media resulting in neuronal death. Interestingly, it has been recently shown that very strong detergent or bleach can be used successfully to restore the MEA surface to pre-culture condition provided that the device is soaked in water for up to 24 h (Suzuki et al., 2013).

The issue of poor biocompatibility was also complicated by cell specificity. Primary neurons were found to be the most fragile and died very quickly while cell lines like BALB and A549 were robust and insensitive to repeated device recycling.

The most important conclusions that can be made with respect to reusability are:

1) Biocompatibility cannot be used as a single criterion that determines if a material is suitable for integration with biological cell cultures. The suitable material needs to be both biocompatible and unaltered by the culture and recycling processes.

2) The process of device cleaning and recycling has to be optimized to ensure that no residual detergent has remained in the culture well.

6.6 Culturing patterned neurons in the neuro test platform

To date, there has been a large variety of MEA-based micro-devices (Corey et al., 1996, Maher et al., 1999, Pearce et al., 2005, Morin et al., 2005, Dworak and Wheeler, 2009, Xu et al., 2011, Suzuki et al., 2013). In these assemblies, the MEAs were generally combined with either cell patterning or µF devices. Other related studies that did not use an MEA, integrated µF devices with patterned cells on traditional substrates instead (Thiébaud et al., 2002, Taylor et al., 2003, Rhee et al., 2004). The devices described in the above studies were limited in their applicability because they were designed for a single

purpose. In an attempt to improve upon the existing MEMS devices, the research and optimization described in this project resulted in fabrication of a multi-functional micro-fabricated neuro test platform suitable for electrophysiological, micro-fluidic and surface chemistry experiments with primary or immortalized cells.

The achievements of this project are as follows.

1) Through integration of cell patterning, micro-fluidic devices with MEAs, it was possible to build a novel, multifunctional MEMS device capable of recording and stimulating neuronal electrical activity, electroporating targeted cells and controlling the *in vitro* environment via dynamic microfluidic gradients.

2) The second achievement was the successful implementation of an alternative, reversible μF device bonding technique. This method is superior to the well-established plasma based bonding because it can be applied to a larger variety of substrates. In turn, the substrate chemistry can be modified to suit the experiment rather than the substrate-μF device bond. This method also allows the substrate to be more easily cleaned and reused, this is especially important in experiments that use MEAs or other planar micro-fabricated devices.

3) The third achievement of this project is patterning the E14 rat embryo spinal cord neurons on the MEA perfused with the integrated μF device.

Overall, this project has achieved a significant number of its goals in designing and building a multifunctional platform that has the potential to be used as a multi-disciplinary research tool. During the optimization stages, this project was also able to improve upon a number of traditional methodologies such as surface patterning and microfluidics.

6.7 Future work

To achieve the maximum potential of this neuro test platform, further work is needed in a number of areas. First, the surface modification and patterning may be improved further by incorporating antifouling coatings with more robust protein/polymer surface grafting (Suzuki et al., 2013). Second, the materials chosen for integration with the MEA must be more compatible with primary neurons and the recycling/cleaning procedures. This is essential to achieve consistent, long term neuronal viability. Third, the overall platform assembly needs to be further simplified to reduce the number of components required for μF device attachment and perfusion. The optimization of these areas can

yield a powerful, adaptable tool for neuroscience, surface chemistry and micro-fluidics research. And lastly, there is a need for cost effective micro-fabricated devices such as MEAs. Hence, additional research and characterization of alternative polymer substrates for micro-devices has to be carried out to allow electrophysiological experiments on surfaces with alternative chemistries.

7.0 Acknowledgements

First, I wish to thank Damien Arrigan, John Alderman and Kieran McDermott for providing me with this opportunity nearly five years ago. Their dedication and practical advice greatly contributed to this multidisciplinary research. I would also like to thank Grégoire Herzog and Paul Galvin for taking on roles as my supervisors, their ideas and securing much needed, additional funding. In this respect I would also like to thank Vladimir Ogurtsov who made a significant contribution. I would like to thank James Rohan for his input at the review meetings. Special thanks to Eileen Hurley for dealing with orders, maintaining equipment and generally having my back. Thanks to Nathan Jackson for advice and help with electrophysiology, electroporation, EIS and MEAs. Also thanks to Matthias Gerhardt for training on MEA kit. Big thanks to Michelle Fitzgerald, Patricia Fitzpatrick, Eve McLoughlin and Eric Moore for granting me access to cell culture and designating an incubator. Thanks to Lynette Keeney, Jacqueline Wrench and Karen Twomey for the IR thermometer, advice on thesis write-up and imparting general wisdom. Thanks to Walter Messina for sharing transfer tapes and generally knowing the locations of obscure tools and components. I would like to thank Dan O'Connell and Alan Blake for BOE of wafers and fabrication of MEAs using non-standard methods. Also thanks to Richard Murphy and Jim Scully for advising on design of masters and devices.
Thanks to Donal O'Sullivan for fabrication and machining of high quality custom parts. Thanks to Conor Delaney for dealing with the finances and fees. Thanks to Don Lynch and Brian Walsh in IT for their help with various software.
I would also like to thank my friends and staff in Biosciences Institute in UCC. First, huge thanks to Louise Collins for looking out for me, her dedicated involvement with our team "Rodent doom" and sharing her dissecting tools. Also thanks to Shane Hegarty, Ian O'Brien and Sean Crampton for sharing their rats. Big thanks to Tara Enright for her advice and help with injections. Thanks to Suzanne Crotty for microscope training. Thanks to Sinead Ryan, Sinead Walsh, Janelle Parkan and Elaine O'Loughlin for general banter and lending me their access cards. Huge thanks to all my friends, especially Kieran Giller and Grace Collins and my family in Ukraine for their support and active interest. I wish to sincerely thank my dad Michael for his unwavering support for me, my family and my career path. Lastly I wish to thank my wife Kira for all her love, patience, strengths and ability to singlehandedly raise our three children.

8.0 References

AINLA, A., JEFFRIES, G. D., BRUNE, R., ORWAR, O. & JESORKA, A. 2012. A multifunctional pipette. *Lab on a Chip,* 12**,** 1255-1261.

ANDERSON, J. R., CHIU, D. T., JACKMAN, R. J., CHERNIAVSKAYA, O., MCDONALD, J. C., WU, H., WHITESIDES, S. H. & WHITESIDES, G. M. 2000. Fabrication of Topologically Complex Three-Dimensional Microfluidic Systems in PDMS by Rapid Prototyping. *Analytical Chemistry,* 72**,** 3158-3164.

ANDRES-BARQUIN, P. J. 2001. Ramón y Cajal: a century after the publication of his masterpiece. *Endeavour,* 25**,** 13-17.

ASANUMA, H. & ROSEN, I. 1972. Topographical organization of cortical efferent zones projecting to distal forelimb muscles in the monkey. *Experimental Brain Research* 14**,** 243-256.

AUVRAY, L., CRUZ, M. & AUROY, P. 1992. Irreversible adsorption from concentrated polymer solutions. *J. Phys. II France,* 2**,** 1133-1140.

AWAD, D., SCHRADER, I., BARTOK, M., MOHR, A. & GABEL, D. 2011. Comparative toxicology of trypan blue, brilliant blue G, and their combination together with polyethylene glycol on human pigment epithelial cells. *Investigative ophthalmology & visual science,* 52**,** 4085-4090.

BEAULIEU, I., GEISSLER, M. & MAUZEROLL, J. 2009. Oxygen Plasma Treatment of Polystyrene and Zeonor: Substrates for Adhesion of Patterned Cells. *Langmuir,* 25**,** 7169-7176.

BEEBE, D. J., MENSING, G. A. & WALKER, G. M. 2002. Physics and applications of microfluidics in biology. *Annual review of biomedical engineering,* 4**,** 261-286.

BEH, W. S., KIM, I. T., QIN, D., XIA, Y. & WHITESIDES, G. M. 1999. Formation of Patterned Microstructures of Conducting Polymers by Soft Lithography, and Applications in Microelectronic Device Fabrication. *Advanced Materials,* 11**,** 1038-1041.

BERNARD, A., DELAMARCHE, E., SCHMID, H., MICHEL, B., BOSSHARD, H. R. & BIEBUYCK, H. 1998. Printing patterns of proteins. *Langmuir,* 14**,** 2225-2229.

BERTHIER, E. & BEEBE, D. J. 2007. Flow rate analysis of a surface tension driven passive micropump. *Lab on a Chip,* 7**,** 1475-1478.

BHATTACHARYA, S., DATTA, A., BERG, J. & GANGOPADHYAY, S. 2005. Studies on surface wettability of poly (dimethyl) siloxane (PDMS) and glass under oxygen-plasma treatment and correlation with bond strength. *Microelectromechanical Systems, Journal of,* 14**,** 590-597.

BIFFI, E., MENEGON, A., PIRAINO, F., PEDROCCHI, A., FIORE, G. B. & RASPONI, M. 2012. Validation of long-term primary neuronal cultures and network activity through the integration of reversibly bonded microbioreactors and MEA substrates. *Biotechnology and Bioengineering,* 109**,** 166-175.

BRADBURY, E., MOON, L., POPAT, R., KING, V., BENNETT, G., PATEL, P., FAWCETT, J. & MCMAHON, S. 2002. Chondroitinase ABC promotes functional recovery after spinal cord injury. *Nature,* 416**,** 636-640.

BRANCH, D. W., COREY, J. M., WEYHENMEYER, J. A., BREWER, G. J. & WHEELER, B. C. 1998. Microstamp patterns of biomolecules for high-resolution neuronal networks. *Medical and Biological Engineering and Computing* 36**,** 135-141.

BREWER, G. J., TORRICELLI, J. R., EVEGE, E. K. & PRICE, P. J. 1993. Optimized survival of hippocampal neurons in B27-supplemented neurobasal™, a new serum-free medium combination. *Journal of Neuroscience Research,* 35**,** 567-576.

BRODAL, P. 2004. *The central nervous system: structure and function,* Oxford University Press, USA.

BULLOCK, T. H., HORRIDGE, G. A. & BERN, H. A. 1965. *Structure and function in the nervous systems of invertebrates,* WH Freeman San Francisco.

CALVERT, P. 2001. Inkjet Printing for Materials and Devices. *Chemistry of Materials,* 13**,** 3299-3305.

CANTY, A. & MURPHY, M. 2008. Molecular mechanisms of axon guidance in the developing corticospinal tract. *Progress in Neurobiology,* 85**,** 214-235.

CARRIER, R. L., MA, T. C., OBRIETAN, K. & HOYT, K. R. 2006. A sensitive and selective assay of neuronal degeneration in cell culture. *Journal of Neuroscience Methods,* 154**,** 239-244.

CASTRO-ALAMANCOS, M. A. & BORRELL, J. 1995. Functional recovery of forelimb response capacity after forelimb primary motor cortex damage in the rat is due to the reorganization of adjacent areas of cortex. *Neuroscience,* 68**,** 793-805.

CECH, V., PRIKRYL, R., BALKOVA, R., GRYCOVA, A. & VANEK, J. 2002. Plasma surface treatment and modification of glass fibers. *Composites Part A: Applied Science and Manufacturing,* 33**,** 1367-1372.

CHANDRASEKARAN, A., ACHARYA, A., YOU, J. L., SOO, K. Y., PACKIRISAMY, M., STIHARU, I. & DARVEAU, A. 2007. Hybrid integrated silicon microfluidic platform for fluorescence based biodetection. *Sensors,* 7**,** 1901-1915.

CHANG, J., BREWER, G. & WHEELER, B. 2000. Microelectrode array recordings of patterned hippocampal neurons for four weeks. *Biomedical Microdevices,* 2**,** 245-253.

CHANG, J. C., BREWER, G. J. & WHEELER, B. C. 2001. Modulation of neural network activity by patterning. *Biosensors and Bioelectronics,* 16**,** 527-533.

CHANG, J. C., BREWER, G. J. & WHEELER, B. C. 2003. A modified microstamping technique enhances polylysine transfer and neuronal cell patterning. *Biomaterials,* 24**,** 2863-2870.

CHANG, J. C. & WHEELER, B. C. 2006. Pattern Technologies for Structuring Neuronal Networks on MEAs. 153-189.

CHEMICAL-BOOK. 2010. *Tetrabutylammonium fluoride* [Online]. www.chemicalbook.com. Available: http://www.chemicalbook.com/ChemicalProductProperty_EN_CB8740854.htm [Accessed 18 June 2013 2013].

CHEN, T., JORDAN, R. & ZAUSCHER, S. 2011. Extending micro-contact printing for patterning complex polymer brush microstructures. *Polymer,* 52**,** 2461-2467.

CHENG, J.-Y., YEN, M.-H., KUO, C.-T. & YOUNG, T.-H. 2008. A transparent cell-culture microchamber with a variably controlled concentration gradient generator and flow field rectifier. *Biomicrofluidics,* 2**,** 024105-12.

CHOI, S.-H. & ZHANG NEWBY, B.-M. 2003. Micrometer-scaled gradient surfaces generated using contact printing of octadecyltrichlorosilane. *Langmuir,* 19**,** 7427-7435.

CHUNG, B. G., FLANAGAN, L. A., RHEE, S. W., SCHWARTZ, P. H., LEE, A. P., MONUKI, E. S. & JEON, N. L. 2005. Human neural stem cell growth and differentiation in a gradient-generating microfluidic device. *Lab Chip,* 5**,** 401-406.

CIRA, N. J., HO, J. Y., DUECK, M. E. & WEIBEL, D. B. 2012. A self-loading microfluidic device for determining the minimum inhibitory concentration of antibiotics. *Lab on a Chip*.

CLAVEROL-TINTURE, E. & PINE, J. 2002. Extracellular potentials in low-density dissociated neuronal cultures. *Journal of Neuroscience Methods,* 117**,** 13-21.

CLAVEROL-TINTURÉ, E., ROSELL, X. & CABESTANY, J. 2007. Technical steps towards one-to-one electrode-neuron interfacing with neural circuits reconstructed in vitro. *Neurocomputing,* 70**,** 2716-2722.

COGAN, S. F. 2008. Neural Stimulation and Recording Electrodes. *Annual review of biomedical engineering,* 10**,** 275-309.

COOKSEY, G. A., PLANT, A. L. & ATENCIA, J. 2009. A vacuum manifold for rapid world-to-chip connectivity of complex PDMS microdevices. *Lab on a Chip,* 9**,** 1298-1300.

COREY, J., WHEELER, B. & BREWER, G. 1996. Micrometer resolution silane-based patterning of hippocampal neurons: Critical variables in photoresist and laser ablation processes for substrate fabrication. *IEEE transactions on biomedical engineering,* 43**,** 944-955.

CSUCS, G., MICHEL, R., LUSSI, J. W., TEXTOR, M. & DANUSER, G. 2003. Microcontact printing of novel co-polymers in combination with proteins for cell-biological applications. *Biomaterials,* 24**,** 1713-1720.

DARBY, C. 2013. *Lab on a Chip* [Online]. www.rcs.org: RCS Publishing. Available: http://www.rsc.org/Publishing/Journals/guidelines/AuthorGuidelines/JournalPolicy/Journals/LC.asp [Accessed 04 April 2013 2013].

DE GENNES, P. G. 1981. Polymer solutions near an interface. Adsorption and depletion layers. *Macromolecules,* 14**,** 1637-1644.

DELAMARCHE, E., BERNARD, A., SCHMID, H., MICHEL, B. & BIEBUYCK, H. 1997. Patterned delivery of immunoglobulins to surfaces using microfluidic networks. *Science,* 276**,** 779-781.

DRÖSCHER, A. 1998. Camillo Golgi and the discovery of the Golgi apparatus. *Histochemistry and cell biology,* 109**,** 425-430.

DUFFY, D. C., SCHUELLER, O. J., BRITTAIN, S. T. & WHITESIDES, G. M. 1999. Rapid prototyping of microfluidic switches in poly (dimethyl siloxane) and their actuation by electro-osmotic flow. *Journal of Micromechanics and Microengineering,* 9**,** 211.

DWORAK, B. J. & WHEELER, B. C. 2009. Novel MEA platform with PDMS microtunnels enables the detection of action potential propagation from isolated axons in culture. *Lab on a Chip,* 9**,** 404-410.

ECCLES, J. C. 1964. *The physiology of synapses,* Springer.

EDGERTON, V. R., TILLAKARATNE, N. J. K., BIGBEE, A. J., DE LEON, R. D. & ROY, R. R. 2004. Plasticity of the spinal neural circuitry after injury*. *Annual Review of Neuroscience*.

EL-ALI, J., SORGER, P. & JENSEN, K. 2006. Cells on chips. *Nature,* 442**,** 403-411.

FAN, Y. W., CUI, F. Z., HOU, S. P., XU, Q. Y., CHEN, L. N. & LEE, I. S. 2002. Culture of neural cells on silicon wafers with nano-scale surface topograph. *Journal of Neuroscience Methods,* 120**,** 17-23.

FAWCETT, J. & ASHER, R. 1999a. The glial scar and central nervous system repair. *Brain Research Bulletin,* 49**,** 377-391.

FAWCETT, J. W. & ASHER, R. A. 1999b. The glial scar and central nervous system repair. *Brain Research Bulletin,* 49**,** 377-391.

FEJTL, M., STETT, A., NISCH, W., BOVEN, K. & MOLLER, A. 2006. On Micro-Electrode Array Revival: Its Development, Sophistication of Recording, and Stimulation. *Advances in Network Electrophysiology: Using Multi-Electrode Arrays***,** 24-38.

FLACHSBART, B. R., WONG, K., IANNACONE, J. M., ABANTE, E. N., VLACH, R. L., RAUCHFUSS, P. A., BOHN, P. W., SWEEDLER, J. V. & SHANNON, M. A. 2006. Design and fabrication of a multilayered polymer microfluidic chip with nanofluidic interconnects via adhesive contact printing. *Lab on a Chip,* 6**,** 667-674.

FLINK, S., VEGGEL, F. C. J. M. V. & REINHOUDT, D. N. 2001. Functionalization of self-assembled monolayers on glass and oxidized silicon wafers by surface reactions. *Journal of Physical Organic Chemistry,* 14**,** 407-415.

FOLCH, A. & TONER, M. 2000. Microengineering of cellular interactions. Annual Reviews 4139 El Camino Way, PO Box 10139, Palo Alto, CA 94303-0139, USA.

GAVIN, D. 2012. Single-cell electroporation using a multifunctional pipette. *Lab on a Chip,* 12**,** 4605-4609.

GEHL, J. 2003. Electroporation: theory and methods, perspectives for drug delivery, gene therapy and research. *Acta Physiologica Scandinavica,* 177**,** 437-447.

GESTELAND, R. C., HOWLAND, B., LETTVIN, J. Y. & PITTS, W. H. 1959. Comments on Microelectrodes. *Proceedings of the IRE,* 47**,** 1856-1862.

GETTING, P. A. 1989. Emerging principles governing the operation of neural networks. *Annual Review of Neuroscience,* 12**,** 185-204.

GETTING, P. A. & DEKIN, M. S. 1985. Mechanisms of pattern generation underlying swimming in Tritonia. IV. Gating of central pattern generator. *Journal of neurophysiology,* 53**,** 466-480.

GRAMOWSKI, A., JÜGELT, K., WEISS, D. G. & GROSS, G. W. 2004. Substance identification by quantitative characterization of oscillatory activity in murine spinal cord networks on microelectrode arrays. *European Journal of Neuroscience,* 19**,** 2815-2825.

GROSS, P. G., KARTALOV, E. P., SCHERER, A. & WEINER, L. P. 2007. Applications of microfluidics for neuronal studies. *Journal of the Neurological Sciences,* 252**,** 135-143.

GU, W., ZHU, X., FUTAI, N., CHO, B. S. & TAKAYAMA, S. 2004. Computerized microfluidic cell culture using elastomeric channels and Braille displays. *Proceedings of the National Academy of Sciences of the United States of America,* 101**,** 15861.

GUO, B., ANZAI, J.-I. & OSA, T. 1996. Modification of a glassy carbon electrode with diols for the suppression of electrode fouling in biological fluids. *CHEMICAL AND PHARMACEUTICAL BULLETIN-TOKYO-,* 44**,** 860-862.

HAMILL, O. P., MARTY, A., NEHER, E., SAKMANN, B. & SIGWORTH, F. 1981. Improved patch-clamp techniques for high-resolution current recording from cells and cell-free membrane patches. *Pflügers Archiv European Journal of Physiology,* 391**,** 85-100.

HARRICK-PLASMA. 2011. *PLASMA APPLICATIONS: Surface Activation and Modification* [Online]. Harrick Plasma. Available: http://www.harrickplasma.com/applications_activation.php [Accessed 12 March 2013 2013].

HAY, E. D. 1991. *Cell biology of extracellular matrix,* Springer.

HAYKIN, S. 2008. *Neural networks: a comprehensive foundation,* Prentice Hall.

HE, H., CHANG, D. C. & LEE, Y.-K. 2007. Using a micro electroporation chip to determine the optimal physical parameters in the uptake of biomolecules in HeLa cells. *Bioelectrochemistry,* 70**,** 363-368.

HELLMAN, A. N., VAHIDI, B., KIM, H. J., MISMAR, W., STEWARD, O., JEON, N. L. & VENUGOPALAN, V. 2010. Examination of axonal injury and regeneration in micropatterned neuronal culture using pulsed laser microbeam dissection. *Lab on a Chip***,** -.

HODGKIN, A. L., HUXLEY, A. & KATZ, B. 1952a. Measurement of current-voltage relations in the membrane of the giant axon of Loligo. *The Journal of physiology,* 116**,** 424.

HODGKIN, A. L. & HUXLEY, A. F. 1952. A quantitative description of membrane current and its application to conduction and excitation in nerve. *Bulletin of Mathematical Biology,* 117**,** 500-544.

HUANG, H.-L., HSING, H.-W., LAI, T.-C., CHEN, Y.-W., LEE, T.-R., CHAN, H.-T., LYU, P.-C., WU, C.-L., LU, Y.-C., LIN, S.-T., LIN, C.-W., LAI, C.-H., CHANG, H.-T., CHOU, H.-C. & CHAN, H.-L. 2010. Trypsin-induced proteome alteration during cell subculture in mammalian cells. *Journal of Biomedical Science,* 17**,** 36.

HUANG, J., GRATER, S. V., CORBELLINI, F., RINCK, S., BOCK, E., KEMKEMER, R., KESSLER, H., DING, J. & SPATZ, J. P. 2009. Impact of Order and Disorder in RGD Nanopatterns on Cell Adhesion. *Nano Letters,* 9**,** 1111-1116.

ILLA, X., ORDEIG, O., SNAKENBORG, D., ROMANO-RODRIGUEZ, A., COMPTON, R. G. & KUTTER, J. P. 2010. A cyclo olefin polymer microfluidic chip with integrated gold microelectrodes for aqueous and non-aqueous electrochemistry. *Lab on a Chip,* 10**,** 1254-1261.

INVITROGEN. 2013. *GlutaMAX™ vs. Glutamine* [Online]. www.invitrogen.com. Available: http://www.invitrogen.com/site/us/en/home/Products-and-Services/Applications/Cell-Culture/Mammalian-Cell-Culture/media-supplements/GlutaMAX-Media/glutamax-vs-glutamine.html [Accessed 4 June 2013 2013].

JACOBSON, M. 1993. *Foundations of neuroscience,* Plenum Pub Corp.

JAIN, T. & MUTHUSWAMY, J. 2007a. Bio-chip for spatially controlled transfection of nucleic acid payloads into cells in a culture. *Lab Chip,* 7**,** 1004-1011.

JAIN, T. & MUTHUSWAMY, J. 2007b. Microsystem for transfection of exogenous molecules with spatio-temporal control into adherent cells. *Biosensors and Bioelectronics,* 22**,** 863-870.

JAMES, C., DAVIS, R., MEYER, M., TURNER, A., TURNER, S., WITHERS, G., KAM, L., BANKER, G., CRAIGHEAD, H. & ISSACSON, M. 2000. Aligned microcontact printing of micrometer-scale poly-L-lysine structures for controlled growth of cultured neurons on planar microelectrode arrays. *Biomedical Engineering, IEEE Transactions on,* 47**,** 17-21.

JAMES, C. D., SPENCE, A. J. H., DOWELL-MESFIN, N. M., HUSSAIN, R. J., SMITH, K. L., CRAIGHEAD, H. G., ISAACSON, M. S., SHAIN, W. & TURNER, J. N. 2004. Extracellular recordings from patterned neuronal networks using planar microelectrode arrays. *Biomedical Engineering, IEEE Transactions on,* 51**,** 1640-1648.

JANG, M. J. & NAM, Y. 2012. Geometric effect of cell adhesive polygonal micropatterns on neuritogenesis and axon guidance. *JOURNAL OF NEURAL ENGINEERING,* 9**,** 046019.

JING, G., PERRY, S. & TATIC-LUCIC, S. 2010. Precise cell patterning using cytophobic self-assembled monolayer deposited on top of semi-transparent gold. *Biomedical Microdevices,* 12**,** 935-948.

JUN, S. B., HYND, M. R., DOWELL-MESFIN, N., SMITH, K. L., TURNER, J. N., SHAIN, W. & KIM, S. J. 2007. Low-density neuronal networks cultured using patterned poly-l-lysine on microelectrode arrays. *Journal of Neuroscience Methods,* 160**,** 317-326.

KAMHOLZ, A., WEIGL, B., FINLAYSON, B. & YAGER, P. 1999. Quantitative analysis of molecular interaction in a microfluidic channel: the T-sensor. *Anal. Chem,* 71**,** 5340-5347.

KAMIOKA, H., MAEDA, E., JIMBO, Y., ROBINSON, H. P. C. & KAWANA, A. 1996. Spontaneous periodic synchronized bursting during formation of mature patterns of connections in cortical cultures. *Neuroscience Letters,* 206**,** 109-112.

KATZ, B. 1966. *Nerve, muscle, and synapse*, McGraw-Hill.

KEEFER, E. W., BOTTERMAN, B. R., ROMERO, M. I., ROSSI, A. F. & GROSS, G. W. 2008. Carbon nanotube coating improves neuronal recordings. *Nat Nano,* 3**,** 434-439.

KERN, W. 1970. Cleaning solutions based on hydrogen peroxide for use in silicon semiconductor technology. *RCA review,* 31**,** 187-206.

KIM, L., TOH, Y. C., VOLDMAN, J. & YU, H. 2007. A practical guide to microfluidic perfusion culture of adherent mammalian cells. *Lab Chip,* 7**,** 681-694.

KIM, S.-J., LIM, Y. T., YANG, H., SHIN, Y. B., KIM, K., LEE, D.-S., PARK, S. H. & KIM, Y. T. 2005. Passive Microfluidic Control of Two Merging Streams by Capillarity and Relative Flow Resistance. *Analytical Chemistry,* 77**,** 6494-6499.

KOTZAR, G., FREAS, M., ABEL, P., FLEISCHMAN, A., ROY, S., ZORMAN, C., MORAN, J. M. & MELZAK, J. 2002. Evaluation of MEMS materials of construction for implantable medical devices. *Biomaterials,* 23**,** 2737-2750.

LAERMER, F. & SCHILP, A. 2003. *Method of anisotropic etching of silicon*. USA patent application 09/328019.

LANGSTON, J. W., FORNO, L. S., TETRUD, J., REEVES, A. G., KAPLAN, J. A. & KARLUK, D. 1999. Evidence of active nerve cell degeneration in the substantia nigra of humans years after 1-methyl-4-phenyl-1,2,3,6-tetrahydropyridine exposure. *Annals of neurology,* 46**,** 598-605.

LAUER, L., INGEBRANDT, S., SCHOLL, K. & OFFENHAUER, A. 2001. Aligned microcontact printing of biomolecules on microelectronicdevice surfaces. *IEEE TRANSACTIONS ON BIOMEDICAL ENGINEERING,,* 48**,** 838-842.

LE SAUX, G., MAGENAU, A., BÖCKING, T., GAUS, K. & GOODING, J. J. 2011. The Relative Importance of Topography and RGD Ligand Density for Endothelial Cell Adhesion. *PLoS ONE,* 6**,** e21869.

LEACH, W. M. 1994. Fundamentals of low-noise analog circuit design. *Proceedings of the IEEE,* 82**,** 1515-1538.

LEE, C. Y., ROMANOVA, E. V. & SWEEDLER, J. V. 2013. Laminar stream of detergents for subcellular neurite damage in a microfluidic device: a simple tool for the study of neuroregeneration. *JOURNAL OF NEURAL ENGINEERING,* 10**,** 036020.

LEE, J. N., PARK, C. & WHITESIDES, G. M. 2003. Solvent Compatibility of Poly(dimethylsiloxane)-Based Microfluidic Devices. *Analytical Chemistry,* 75**,** 6544-6554.

LEE, K. S. & RAM, R. J. 2009. Plastic–PDMS bonding for high pressure hydrolytically stable active microfluidics. *Lab on a Chip,* 9**,** 1618-1624.

LI, N., SIP, C. & FOLCH, A. 2007. Microfluidic chips controlled with elastomeric microvalve arrays. *Journal of visualized experiments: JoVE*.

LIBIOULLE, L., BIETSCH, A., SCHMID, H., MICHEL, B. & DELAMARCHE, E. 1998. Contact-Inking Stamps for Microcontact Printing of Alkanethiols on Gold. *Langmuir,* 15**,** 300-304.

LIN, S.-C., LU, J.-C., SUNG, Y.-L., LIN, C.-T. & TUNG, Y.-C. 2013. A low sample volume particle separation device with electrokinetic pumping based on circular travelling-wave electroosmosis. *Lab on a Chip*.

LIU, B., MA, J., GAO, E., HE, Y., CUI, F. & XU, Q. 2008. Development of an artificial neuronal network with post-mitotic rat fetal hippocampal cells by polyethylenimine. *Biosensors & Bioelectronics,* 23**,** 1221-1228.

MAGHRIBI, M., HAMILTON, J., POLLA, D., ROSE, K., WILSON, T. & KRULEVITCH, P. Stretchable micro-electrode array [for retinal prosthesis]. Microtechnologies in Medicine; Biology 2nd Annual International IEEE-EMB Special Topic Conference on, 2002 2002. 80-83.

MAHER, M. P., PINE, J., WRIGHT, J. & TAI, Y. C. 1999. The neurochip: a new multielectrode device for stimulating and recording from cultured neurons. *Journal of Neuroscience Methods,* 87**,** 45-56.

MAKAMBA, H., KIM, J. H., LIM, K., PARK, N. & HAHN, J. H. 2003. Surface modification of poly(dimethylsiloxane) microchannels. *Electrophoresis,* 24**,** 3607-3619.

MALMIVUO, J. & PLONSEY, R. 1995. *Bioelectromagnetism: principles and applications of bioelectric and biomagnetic fields*, Oxford University Press, USA.

MANNING, M., HARVEY, S., GALVIN, P. & REDMOND, G. 2003. A versatile multi-platform biochip surface attachment chemistry. *Materials Science and Engineering: C,* 23**,** 347-351.

MANOS, P., PANCRAZIO, J. J., COULOMBE, M. G., MA, W. & STENGER, D. A. 1999. Characterization of rat spinal cord neurons cultured in defined media on microelectrode arrays. *Neuroscience Letters,* 271**,** 179-182.

MASSEY, J. M., AMPS, J., VIAPIANO, M. S., MATTHEWS, R. T., WAGONER, M. R., WHITAKER, C. M., ALILAIN, W., YONKOF, A. L., KHALYFA, A. & COOPER, N. G. F. 2008. Increased chondroitin sulfate proteoglycan expression in denervated brainstem targets following spinal cord injury creates a barrier to axonal regeneration overcome by chondroitinase ABC and neurotrophin-3. *Experimental neurology* 209**,** 426-445.

MELLORS, J. S., GORBOUNOV, V., RAMSEY, R. S. & RAMSEY, J. M. 2008. Fully Integrated Glass Microfluidic Device for Performing High-Efficiency Capillary Electrophoresis and Electrospray Ionization Mass Spectrometry. *Analytical Chemistry,* 80**,** 6881-6887.

MILEV, P., FRIEDLANDER, D. R., SAKURAI, T., KARTHIKEYAN, L., FLAD, M., MARGOLIS, R. K., GRUMET, M. & MARGOLIS, R. U. 1994. Interactions of the chondroitin sulfate proteoglycan phosphacan, the extracellular domain of a receptor-type protein tyrosine phosphatase, with neurons, glia, and neural cell adhesion molecules. *The Journal of Cell Biology,* 127**,** 1703-1715.

MILLET, L. J., STEWART, M. E., SWEEDLER, J. V., NUZZO, R. G. & GILLETTE, M. U. 2007. Microfluidic devices for culturing primary mammalian neurons at low densities. *Lab on a Chip,* 7**,** 987-994.

MÖNKKÖNEN, K., PAKKANEN, T. T., HIETALA, J., PÄÄKKÖNEN, E. J., PÄÄKKÖNEN, P., JÄÄSKELÄINEN, T. & KAIKURANTA, T. 2002. Replication of sub-micron features using amorphous thermoplastics. *Polymer Engineering & Science,* 42**,** 1600-1608.

MORIN, F., NISHIMURA, N., GRISCOM, L., LEPIOUFLE, B., FUJITA, H., TAKAMURA, Y. & TAMIYA, E. 2006. Constraining the connectivity of neuronal networks cultured on microelectrode arrays with microfluidic techniques: a step towards neuron-based functional chips. *Biosensors & Bioelectronics,* 21**,** 1093-1100.

MORIN, F. O., TAKAMURA, Y. & TAMIYA, E. 2005. Investigating neuronal activity with planar microelectrode arrays: achievements and new perspectives. *Journal of bioscience and bioengineering,* 100**,** 131-143.

MOURZINA, Y., KALIAGUINE, D., SCHULTE, P. & OFFENHÄUSSER, A. 2006. Patterning chemical stimulation of reconstructed neuronal networks. *Analytica Chimica Acta,* 575**,** 281-289.

MUKHOPADHYAY, R. 2007. When PDMS isn't the best. *Analytical Chemistry,* 79**,** 3248-3253.

MULTI-CHANNEL-SYSTEMS. 2012. *MEA Manual* [Online]. Reutlingen, Germany: Multi Channel Systems MCS GmbH. Available: http://www.multichannelsystems.com/sites/multichannelsystems.com/files/documents/manuals/MEA_Manual.pdf [Accessed 29/06 2012].

NAM, K. H., PARK, I. H. & KO, S. H. 2012. Patterning by controlled cracking. *Nature,* 485**,** 221-224.

NAM, Y., KHATAMI, D., WHEELER, B. C. & BREWER, G. J. Electrical stimulation of patterned neuronal networks in vitro. Engineering in Medicine and Biology Society, 2003. Proceedings of the 25th Annual International Conference of the IEEE, 2003. 2246-2248 Vol.3.

NAM, Y., MUSICK, K. & WHEELER, B. 2006. Application of a PDMS microstencil as a replaceable insulator toward a single-use planar microelectrode array. *Biomedical Microdevices,* 8**,** 375-381.

NAUNDORF, B. R., WOLF, F. & VOLGUSHEV, M. 2006. Unique features of action potential initiation in cortical neurons. *Nature,* 440**,** 1060-1063.

NEHER, E., SAKMANN, B. & STEINBACH, J. H. 1978. The extracellular patch clamp: a method for resolving currents through individual open channels in biological membranes. *Pflügers Archiv European Journal of Physiology,* 375**,** 219-228.

NELSON, M. J., POUGET, P., NILSEN, E. A., PATTEN, C. D. & SCHALL, J. D. 2008. Review of signal distortion through metal microelectrode recording circuits and filters. *Journal of Neuroscience Methods,* 169**,** 141-157.

NGALIM, S. H., MAGENAU, A., LE SAUX, G., GOODING, J. J. & GAUS, K. 2010. How do cells make decisions: engineering micro-and nanoenvironments for cell migration. *Journal of oncology,* 2010.

NI, M., TONG, W. H., CHOUDHURY, D., RAHIM, N. A. A., ILIESCU, C. & YU, H. 2009. Cell Culture on MEMS Platforms: A Review. *International Journal of Molecular Sciences,* 10**,** 5411-5441.

NIE, F.-Q., YAMADA, M., KOBAYASHI, J., YAMATO, M., KIKUCHI, A. & OKANO, T. 2007. On-chip cell migration assay using microfluidic channels. *Biomaterials,* 28**,** 4017-4022.

NUDO, R., PLAUTZ, E. & FROST, S. 2001. Role of adaptive plasticity in recovery of function after damage to motor cortex. *Muscle and Nerve,* 24**,** 1000-1019.

ODORIZZI, L., RESS, C., COLLINI, C., MORGANTI, E., LORENZELLI, L., COPPEDÉ, N., ALABI, A. B., IANNOTTA, S., VIDALINO, L. & MACCHI, P. 2010. An enhanced platform for cell electroporation: controlled delivery and electrodes functionalization. *Procedia Engineering,* 5**,** 45-48.

OLIVA, A., JR., JAMES, C., KINGMAN, C., CRAIGHEAD, H. & BANKER, G. 2003. Patterning Axonal Guidance Molecules Using a Novel Strategy for Microcontact Printing. *Neurochemical Research,* 28**,** 1639-1648.

PARK, J., KIM, H. S. & HAN, A. 2009. Micropatterning of poly (dimethylsiloxane) using a photoresist lift-off technique for selective electrical insulation of microelectrode arrays. *Journal of Micromechanics and Microengineering,* 19**,** 065016.

PARK, J., KOITO, H., LI, J. & HAN, A. 2012. Multi-compartment neuron-glia co-culture platform for localized CNS axon-glia interaction study. *Lab on a Chip*.

PEARCE, T. M., WILSON, J. A., OAKES, S. G., CHIU, S. Y. & WILLIAMS, J. C. 2005. Integrated microelectrode array and microfluidics for temperature clamp of sensory neurons in culture. *Lab on a Chip,* 5**,** 97-101.

PERL, A., REINHOUDT, D. N. & HUSKENS, J. 2009. Microcontact Printing: Limitations and Achievements. *Advanced Materials,* 21**,** 2257-2268.

PFRIEGER, F. W. & BARRES, B. A. 1997. Synaptic Efficacy Enhanced by Glial Cells in Vitro. *Science,* 277**,** 1684-1687.

PINAULT, D. 1996. A novel single-cell staining procedure performed in vivo under electrophysiological control: morpho-functional features of juxtacellularly labeled thalamic cells and other central neurons with biocytin or Neurobiotin. *Journal of Neuroscience Methods,* 65**,** 113-136.

PINE, J. 2006. A History of MEA Development. *Advances in Network Electrophysiology: Using Multi-Electrode Arrays***,** 3-24.

PLA-ROCA, M., FERNANDEZ, J. G., MILLS, C. A., MARTÍNEZ, E. & SAMITIER, J. 2007. Micro/Nanopatterning of Proteins via Contact Printing Using High Aspect Ratio PMMA Stamps and NanoImprint Apparatus. *Langmuir,* 23**,** 8614-8618.

POTTER, S. M., WAGENAAR, D. A. & DEMARSE, T. B. 2006. *Closing the loop: stimulation feedback systems for embodied MEA cultures*, Springer.

QIN, D., XIA, Y. & WHITESIDES, G. M. 2010. Soft lithography for micro- and nanoscale patterning. *Nat. Protocols,* 5**,** 491-502.

RAJ, J., HERZOG, G., MANNING, M., VOLCKE, C., MACCRAITH, B. D., BALLANTYNE, S., THOMPSON, M. & ARRIGAN, D. W. M. 2009. Surface immobilisation of antibody on cyclic olefin copolymer for sandwich immunoassay. *Biosensors and Bioelectronics,* 24**,** 2654-2658.

RHEE, S. W., TAYLOR, A. M., TU, C. H., CRIBBS, D. H., COTMAN, C. W. & JEON, N. L. 2004. Patterned cell culture inside microfluidic devices. *Lab on a Chip,* 5**,** 102-107.

RICHERT, L., ARNTZ, Y., SCHAAF, P., VOEGEL, J.-C. & PICART, C. 2004. pH dependent growth of poly (L-lysine)/poly (L-glutamic) acid multilayer films and their cell adhesion properties. *Surface science,* 570**,** 13-29.

RICOULT, S. G., GOLDMAN, J. S., STELLWAGEN, D., JUNCKER, D. & KENNEDY, T. E. 2012. Generation of microisland cultures using microcontact printing to pattern protein substrates. *Journal of Neuroscience Methods,* 208**,** 10-17.

ROACH, P., PARKER, T., GADEGAARD, N. & ALEXANDER, M. R. 2010. Surface strategies for control of neuronal cell adhesion: A review. *Surface Science Reports,* 65**,** 145-173.

ROBINSON, D. A. 1968. The electrical properties of metal microelectrodes. *Proceedings of the IEEE,* 56**,** 1065-1071.

ROLLAND, J., VAN DAM, R. M., HAGBERG, E. C., CARTER, K. R., QUAKE, S. R. & DESIMONE, J. 2004. Functional perfluoropolyethers as novel materials for microfluidics and soft lithography. *POLYMER PREPRINTS-AMERICA-*, 45**,** 106-107.

ROSS, J. D., O'CONNOR, S. M., BLUM, R. A., BROWN, E. A. & DEWEERTH, S. P. 2004. Multielectrode impedance tuning: reducing noise and improving stimulation efficacy. *Engineering in Medicine and Biology Society,* 2.

ROTH, E. A., XU, T., DAS, M., GREGORY, C., HICKMAN, J. J. & BOLAND, T. 2004. Inkjet printing for high-throughput cell patterning. *Biomaterials,* 25**,** 3707-3715.

RUFFINI, G., DUNNE, S., FARRÉS, E., MARCO-PALLARÉS, J., RAY, C., MENDOZA, E., SILVA, R. & GRAU, C. 2006. A dry electrophysiology electrode using CNT arrays. *Sensors and Actuators A: Physical,* 132**,** 34-41.

RUIZ, A., BUZANSKA, L., GILLILAND, D., RAUSCHER, H., SIRGHI, L., SOBANSKI, T., ZYCHOWICZ, M., CERIOTTI, L., BRETAGNOL, F., COECKE, S., COLPO, P. & ROSSI, F. 2008. Micro-stamped surfaces for the patterned growth of neural stem cells. *Biomaterials,* 29**,** 4766-4774.

RUIZ, A., ZYCHOWICZ, M., CERIOTTI, L., MEHN, D., SIRGHI, L., RAUSCHER, H., MANNELLI, I., COLPO, P., BUZANSKA, L. & ROSSI, F. 2013. Microcontact printing and microspotting as methods for direct protein patterning on plasma deposited polyethylene oxide: application to stem cell patterning. *Biomedical Microdevices*, 1-13.

RUIZ, S. A. & CHEN, C. S. 2007. Microcontact printing: A tool to pattern. *Soft Matter*, 3, 168-177.

SCHIMEK, K., BUSEK, M., BRINCKER, S., GROTH, B., HOFFMANN, S., LAUSTER, R., LINDNER, G., LORENZ, A., MENZEL, U., SONNTAG, F., WALLES, H., MARX, U. & HORLAND, R. 2013. Integrating biological vasculature into a multi-organ-chip microsystem. *Lab on a Chip*.

SCHNYDER, B., LIPPERT, T., KÖTZ, R., WOKAUN, A., GRAUBNER, V. M. & NUYKEN, O. 2003. UV-irradiation induced modification of PDMS films investigated by XPS and spectroscopic ellipsometry. *Surface science*, 532, 1067-1071.

SCHOLL, M., SPRÖSSLER, C., DENYER, M., KRAUSE, M., NAKAJIMA, K., MAELICKE, A., KNOLL, W. & OFFENHÄUSSER, A. 2000. Ordered networks of rat hippocampal neurons attached to silicon oxide surfaces. *Journal of Neuroscience Methods*, 104, 65-75.

SHI, M., MAJUMDAR, D., GAO, Y., BREWER, B., GOODWIN, C., MCLEAN, J. A., LI, D. & WEBB, D. J. 2013. Glia Co-Culture with Neurons in Microfluidic Platforms Promotes the Formation and Stabilization of Synaptic Contacts. *Lab on a Chip*.

SHIM, H.-W., LEE, J.-H., HWANG, T.-S., RHEE, Y. W., BAE, Y. M., CHOI, J. S., HAN, J. & LEE, C.-S. 2007. Patterning of proteins and cells on functionalized surfaces prepared by polyelectrolyte multilayers and micromolding in capillaries. *Biosensors and Bioelectronics*, 22, 3188-3195.

SIGMA-ALDRICH. 2013. *Poly-D-Lysine product information* [Online]. www.sigmaaldrich.com. Available: http://www.sigmaaldrich.com/etc/medialib/docs/Sigma/Product_Information_Sheet/1/p0171pis.Par.0001.File.tmp/p0171pis.pdf [Accessed 8/5/13 2013].

SIRRINGHAUS, H., KAWASE, T., FRIEND, R. H., SHIMODA, T., INBASEKARAN, M., WU, W. & WOO, E. P. 2000. High-Resolution Inkjet Printing of All-Polymer Transistor Circuits. *Science*, 290, 2123-2126.

SORRIBAS, H., PADESTE, C. & TIEFENAUER, L. 2002. Photolithographic generation of protein micropatterns for neuron culture applications. *Biomaterials*, 23, 893-900.

SQUIRE, L. R., BLOOM, F. E. & SPITZER, N. C. 2008. *Fundamental neuroscience*.

SRINIVASAN, R. & BRAREN, B. 1989. Ultraviolet laser ablation of organic polymers. *Chemical Reviews*, 89, 1303-1316.

STAVEREN VAN, G. W., BUITENWEG, J. R., HEIDA, T. & RUTTEN, W. L. C. 2002. Wave shape classification of spontaneous neuronal activity in cortical cultures on micro-electrode arrays. *Second Joint EMBS/BMES Conference, 2002.* Houston, Texas, USA: IEEE-EMBS/BMES.

STREIT, J., TSCHERTER, A., HEUSCHKEL, M. O. & RENAUD, P. 2001. The generation of rhythmic activity in dissociated cultures of rat spinal cord. *European Journal of Neuroscience*, 14, 191-202.

STUART, G., SPRUSTON, N., SAKMANN, B. & HÄUSSER, M. 1997. Action potential initiation and backpropagation in neurons of the mammalian CNS. *Trends in Neurosciences*, 20, 125-131.

STUART, G. J., DODT, H. & SAKMANN, B. 1993. Patch-clamp recordings from the soma and dendrites of neurons in brain slices using infrared video microscopy. *Pflügers Archiv European Journal of Physiology*, 423, 511-518.

SUN, Y., HUANG, Z., LIU, W., YANG, K., SUN, K., XING, S., WANG, D., ZHANG, W. & JIANG, X. 2012. Surface Coating as a Key Parameter in Engineering Neuronal Network Structures In Vitro. *Biointerphases,* 7**,** 1-14.

SUZUKI, M., IKEDA, K., YAMAGUCHI, M., KUDOH, S. N., YOKOYAMA, K., SATOH, R., ITO, D., NAGAYAMA, M., UCHIDA, T. & GOHARA, K. 2013. Neuronal cell patterning on a multi-electrode array for a network analysis platform. *Biomaterials,* 34**,** 5210-5217.

TANK, D. 1989. Sealing cultured invertebrate neurons to embedded dish electrodes facilitates long-term stimulation and recording. *Journal of Neurosctence Methods*, 30**,** 91-106.

TAYLOR, A. M., BLURTON-JONES, M., RHEE, S. W., CRIBBS, D. H., COTMAN, C. W. & JEON, N. L. 2005. A microfluidic culture platform for CNS axonal injury, regeneration and transport. *Nature Methods,* 2**,** 599-605.

TAYLOR, A. M., RHEE, S. W., TU, C. H., CRIBBS, D. H., COTMAN, C. W. & JEON, N. L. 2003. Microfluidic Multicompartment Device for Neuroscience Research. *Langmuir,* 19**,** 1551-1556.

THIBAULT, C., SÉVERAC, C., MINGOTAUD, A.-F., VIEU, C. & MAUZAC, M. 2007. Poly(dimethylsiloxane) Contamination in Microcontact Printing and Its Influence on Patterning Oligonucleotides. *Langmuir,* 23**,** 10706-10714.

THIÉBAUD, P., LAUER, L., KNOLL, W. & OFFENHÄUSSER, A. 2002. PDMS device for patterned application of microfluids to neuronal cells arranged by microcontact printing. *Biosensors and Bioelectronics,* 17**,** 87-93.

THOMAS JR, C., SPRINGER, P., LOEB, G., BERWALD-NETTER, Y. & OKUN, L. 1972. A miniature microelectrode array to monitor the bioelectric activity of cultured cells. *Experimental Cell Research,* 74**,** 61.

THOMPSON, M., CHERAN, L.-E. & SADEGHI, S. 2013. CHAPTER 2 The Cell-Substrate Surface Interaction. *Sensor Technology in Neuroscience.* The Royal Society of Chemistry.

UNGER, M. A., CHOU, H.-P., THORSEN, T., SCHERER, A. & QUAKE, S. R. 2000. Monolithic Microfabricated Valves and Pumps by Multilayer Soft Lithography. *Science,* 288**,** 113-116.

VAHIDI, B., PARK, J. W., KIM, H. J. & JEON, N. L. 2008. Microfluidic-based strip assay for testing the effects of various surface-bound inhibitors in spinal cord injury. *Journal of Neuroscience Methods,* 170**,** 188-196.

VARSHNEY, M., LI, Y., SRINIVASAN, B. & TUNG, S. 2007. A label-free, microfluidics and interdigitated array microelectrode-based impedance biosensor in combination with nanoparticles immunoseparation for detection of Escherichia coli O157:H7 in food samples. *Sensors and Actuators B: Chemical,* 128**,** 99-107.

VICKERS, J. C., DICKSON, T. C., A. ADLARD, P., SAUNDERS, H. L., KING, C. E. & MCCORMACK, G. 2000. The cause of neuronal degeneration in Alzheimer's disease. *Progress in Neurobiology,* 60**,** 139-165.

VILLA-DIAZ, L. G., TORISAWA, Y.-S., UCHIDA, T., DING, J., NOGUEIRA-DE-SOUZA, N. C., O'SHEA, K. S., TAKAYAMA, S. & SMITH, G. D. 2009. Microfluidic culture of single human embryonic stem cell colonies. *Lab on a Chip,* 9**,** 1749-1755.

VISHWANATHAN, A., BI, G.-Q. & ZERINGUE, H. C. 2011. Ring-shaped neuronal networks: a platform to study persistent activity. *Lab on a Chip*.

VOGT, A. K., STEFANI, F. D., BEST, A., NELLES, G., YASUDA, A., KNOLL, W. & OFFENHÄUSSER, A. 2004. Impact of micropatterned surfaces on neuronal polarity. *Journal of Neuroscience Methods,* 134**,** 191-198.

VULTO, P., KUHN, P. & URBAN, G. A. 2013. Bubble-free electrode actuation for micro-preparative scale electrophoresis of RNA. *Lab on a Chip*.

WACHTER, E., MACHLEIDT, W., HOFNER, H. & OTTO, J. 1973. Aminopropyl glass and its p-phenylene diisothiocyanate derivative, a new support in solid-phase Edman degradation of peptides and proteins. *FEBS Letters,* 35**,** 97-102.

WANG, C. J., LI, X., LIN, B., SHIM, S., MING, G. & LEVCHENKO, A. 2008. A microfluidics-based turning assay reveals complex growth cone responses to integrated gradients of substrate-bound ECM molecules and diffusible guidance cues. *Lab on a Chip,* 8**,** 227-237.

WANG, J., REN, L., LI, L., LIU, W., ZHOU, J., YU, W., TONG, D. & CHEN, S. 2009. Microfluidics: A new cosset for neurobiology. *Lab on a Chip,* 9**,** 644-652.

WANG, J., ZHENG, M., WANG, W. & LI, Z. 2010. Optimal protocol for moulding PDMS with a PDMS master. Available from: http://blogs.rsc.org/chipsandtips/2010/07/06/optimal-protocol-for-moulding-pdms-with-a-pdms-master/ 2012].

WANG, Y., LEE, D., ZHANG, L., JEON, H., MENDOZA-ELIAS, J., HARVAT, T., HASSAN, S., ZHOU, A., EDDINGTON, D. & OBERHOLZER, J. 2012. Systematic prevention of bubble formation and accumulation for long-term culture of pancreatic islet cells in microfluidic device. *Biomedical Microdevices,* 14**,** 419-426.

WANG, Z. 2011. *Polydimethylsiloxane Mechanical Properties Measured by Macroscopic Compression and Nanoindentation Techniques.* University of South Florida.

WEBER, S. G. 1989. Signal-to-noise ratio in microelectrode-array-based electrochemical detectors. *Analytical Chemistry,* 61**,** 295-302.

WHEELER, B. C. & BREWER, G. J. 2010. Designing Neural Networks in Culture. *PROCEEDINGS OF THE IEEE,* 98**,** 398-406.

WHITESIDES, G. M. 2006. The origins and the future of microfluidics. *Nature,* 442**,** 368-373.

WHITSON J., KUBOTA D., SHIMONO K., JIA Y & M., T. 2006. Multi-Electrode Arrays: Enhansing Traditional Methods and Enabling Network Physiology. *Advances in Network Electrophysiology: Using Multi-Electrode Arrays***,** 38-69.

WONG, I., ATSUMI, S., HUANG, W.-C., WU, T.-Y., HANAI, T., LAM, M.-L., TANG, P., YANG, J., LIAO, J. C. & HO, C.-M. 2010. An agar gel membrane-PDMS hybrid microfluidic device for long term single cell dynamic study. *Lab on a Chip,* 10**,** 2710-2719.

WU, M.-H., HUANG, S.-B., CUI, Z., CUI, Z. & LEE, G.-B. 2008. A high throughput perfusion-based microbioreactor platform integrated with pneumatic micropumps for three-dimensional cell culture. *Biomedical Microdevices,* 10**,** 309-319.

XIA, Y. & WHITESIDES, G. M. 1998. Soft lithography. *Materials Science,* 28**,** 153-184.

XIANG, G., PAN, L., HUANG, L., YU, Z., SONG, X., CHENG, J., XING, W. & ZHOU, Y. 2007. Microelectrode array-based system for neuropharmacological applications with cortical neurons cultured in vitro. *Biosensors & Bioelectronics,* 22**,** 2478-2484.

XING, S., HARAKE, R. S. & PAN, T. 2011. Droplet-driven transports on superhydrophobic-patterned surface microfluidics. *Lab Chip*.

XING, S., ZHAO, S. & PAN, T. 2012. Print-to-print: a facile multi-object micro-patterning technique. *Biomedical Microdevices***,** 1-8.

XU, Y., YAO, H., WANG, L., XING, W. & CHENG, J. 2011. The construction of an individually addressable cell array for selective patterning and electroporation. *Lab on a Chip,* 11**,** 2417-2423.

XU, Z.-R., YANG, C.-G., LIU, C.-H., ZHOU, Z., FANG, J. & WANG, J.-H. 2010. An osmotic micro-pump integrated on a microfluidic chip for perfusion cell culture. *Talanta,* 80**,** 1088-1093.

YE, Z.-C. & SONTHEIMER, H. 1998. Astrocytes protect neurons from neurotoxic injury by serum glutamate. *Glia,* 22**,** 237-248.

ZENG, H. C., HO, Y. C., CHEN, S. T., WU, H. I., TUNG, H. W., FANG, W. L. & CHANG, Y. C. 2007. Studying the formation of large cell aggregates in patterned neuronal cultures. *Journal of Neuroscience Methods,* 165**,** 72-82.

ZHOU, J., ELLIS, A. V. & VOELCKER, N. H. 2010. Recent developments in PDMS surface modification for microfluidic devices. *Electrophoresis,* 31**,** 2-16.

ZHU, X., YI CHU, L., CHUEH, B.-H., SHEN, M., HAZARIKA, B., PHADKE, N. & TAKAYAMA, S. 2004. Arrays of horizontally-oriented mini-reservoirs generate steady microfluidic flows for continuous perfusion cell culture and gradient generation. *Analyst,* 129.

ZIAIE, B., BALDI, A., LEI, M., GU, Y. & SIEGEL, R. A. 2004. Hard and soft micromachining for BioMEMS: review of techniques and examples of applications in microfluidics and drug delivery. *Advanced Drug Delivery Reviews,* 56**,** 145-172.

ZOU, Z., KAI, J., RUST, M. J., HAN, J. & AHN, C. H. 2007. Functionalized nano interdigitated electrodes arrays on polymer with integrated microfluidics for direct bio-affinity sensing using impedimetric measurement. *Sensors and Actuators A: Physical,* 136**,** 518-526.